Loughborough University

This item was submitted to Loughborough's Institutional Repository (https://dspace.lboro.ac.uk/) by the author and is made available under the following Creative Commons Licence conditions.

creative commons

COMMONS DEED

Attribution-NonCommercial-NoDerivs 2.5

You are free:

- to copy, distribute, display, and perform the work

Under the following conditions:

Attribution. You must attribute the work in the manner specified by the author or licensor.

Noncommercial. You may not use this work for commercial purposes.

No Derivative Works. You may not alter, transform, or build upon this work.

- For any reuse or distribution, you must make clear to others the license terms of this work.
- Any of these conditions can be waived if you get permission from the copyright holder.

Your fair use and other rights are in no way affected by the above.

This is a human-readable summary of the Legal Code (the full license).

Disclaimer

For the full text of this licence, please go to:
http://creativecommons.org/licenses/by-nc-nd/2.5/

Measurement System for Fast Power and Energy Rating of Photovoltaic Devices

Martin Bliss

Doctoral Thesis

Submitted in partial fulfilment of the requirements for the award of
Doctor of Philosophy of Loughborough University

February 2011

© by Martin Bliss 2011

Loughborough University

CERTIFICATE OF ORIGINALITY

This is to certify that I am responsible for the work submitted in this thesis, that the original work is my own except as specified in acknowledgments or in footnotes, and that neither the thesis nor the original work contained therein has been submitted to this or any other institution for a degree.

……Martin Bliss…….. (Signed)

……28.04.2011…….. (Date)

Abstract

This thesis presents a new type of solar simulator and new measurement methods that allow for fast power rating of photovoltaic devices and for fast performance measurements for energy rating and energy yield predictions indoors under controlled, and more realistically simulated outdoor conditions.

A novel indoor measurement system for photovoltaic device characterisation based on light emitting diodes (LEDs) as the light sources is described. The solar simulator is capable of reproducing spectral changes seen in natural sunlight, with its intricacies of variable air mass and weather conditions, to a better match than previously possible. Furthermore, it allows measurements under varying light intensity and device temperature.

The prototype LED-based solar simulator developed is characterised and its measurement quality is analysed. The system achieves a class BAA solar simulator classification with a class B spectral match, class A light intensity uniformity and a class A temporal stability. It is the first system of its kind that meets the standards of a solar simulator in spectral match to the standard sunlight spectrum and in terms of minimum light intensity. An uncertainty analysis shows that calibration uncertainty for crystalline silicon solar cells is 5% in maximum power with a 95.45% level of confidence. Recommendations for further versions of the solar simulator are given and show potential of reducing this uncertainty down to 2.9% across all measurement spectra (1.8% with a primary calibrated reference cell).

A new method for automated power-rating of single- and multi-junction devices is developed. The method uses a unique spectral response measurement and fitting method. It eliminates the need of external measurement equipment for determining spectral response. A simulated characterisation of an amorphous silicon single- and double-junction solar cell show accuracy of better than 0.5% in maximum power. First measurements on the LED-based solar simulator show a measurement error

of 4.5% in maximum power, which is due to a lack of measurement feedback of spectral output and measurement irradiance.

The first three-dimensional performance matrix for use in photovoltaic energy rating is reported, utilising the LED-based solar simulator. Device characteristics are measured indoors under varying irradiance, temperature and spectrum. A measurement method is detailed and utilised on a crystalline and amorphous silicon solar cell. It allows for the first time a direct investigation of spectral effects on photovoltaic devices under controlled conditions. Results show that amorphous silicon devices are very sensitive to changes in spectrum. Thus, spectral effects should not be neglected in energy yield predictions for such devices.

Acknowledgements

First, I would like to thank the Engineering and Physical Sciences Research Council (EPSRC) for funding this project, as without it this work would have been impossible. Very special thanks go to my supervisors Professor Ralph Gottschalg and Dr. Thomas Betts for their invaluable support, motivations and advice throughout my PhD studies and writing of my thesis and for their confidence in my abilities to carry out this work which I enjoyed to the last day.

For their great support, special thanks are due to all current and previous members of the Applied Photovoltaics group in CREST including Mike Parker, Michal Krawczynski, Ian Cole, Foteini Plyta, Hassan Qasem, Dr. Chris Hibberd, Jyotirmoy Roy, Brian Goss, Ira Sara, Ketut Astawa, Jiang Zhu, Dr. Sheryl Williams, Dr. Pongpan Vorasayan, Dr. Christos Monokroussos, Dr. Matthias Strobel and Dr. Yingning Qiu. This does not go without special thanks to all members in the complete CREST team.

I like to thank the electrical workshop for their good advice and printing of PCBs. Furthermore, I thank the entire mechanical workshop for constructing many mechanical parts and for their advice in design. Thanks go also to Alan Jones in stores for his support in ordering countless parts. Further thanks go to Roger Tomlinson, Dr. Matt Little, Ramesh Pancholi and Mahendra Pancholi for valuable advice in discussions on electronics and hardware development.

And last but not least I would like to express my sincere thanks to my parents, grandpa, grandma, sister and brother who supported me greatly during my studies. Finally, I thank Marie Stack, my Sweety whom is brightening up every day and the next day, for the support all along and the countless tasty lunches and dinners that surely kept me from starvation.

Contents

1 Introduction

Photovoltaic (PV) devices are normally characterised in a solar simulator. This measurement is carried predominantly under standard test conditions (STC) at a defined device temperature of 25°C, a light spectrum as defined in the IEC90604-3 standard (air mass 1.5 global) [1] at 1000W/m^2 intensity and normal incidence. This so called “power rating” can give a fast and simple indication of how a device performs under standardised conditions and is thus useful for a quick comparison between different devices.

The simplicity of a standardised condition has made STC module efficiency and power output the principal driving factors on the solar photovoltaic market. The field is, however, moving into a different direction, as real operation conditions of PV devices are different and varying. For example, STC conditions were found to make up less than 0.3% of all recorded outdoor measurement data in 2003 at CREST in Loughborough [2] without even considering the angle of incidence. Considering this reduces recorded data to a few measurements a year. The fact that STC conditions are almost unrelated to realistic outdoor operation is resulting in operating efficiencies of PV devices outdoors which typically are lower than the STC efficiency. Nevertheless, the actual performance outdoors is very much dependent on the device type, material and structure, which means that there is no easy translation from STC to outdoor behaviour. Therefore, power rating can mislead the PV system designer in making the best choice between different PV module types, which can cost the system owner if an inappropriate choice was made. This is an additional risk, i.e. it adds uncertainty, and thus will affect financing.

The only way to minimise the uncertainty in these decisions is to give a value of energy production at the location rather than a power rating at STC. A PV module’s value of predicted energy output requires the input of many environmental factors such as temperature, light intensity and light spectrum. The predicted energy yield is usually given as a yearly value at a certain

location. With this information the PV system designer can compare the performance of different technologies at the location of the power plant and can maximise energy delivery of the plant in relation to costs. This does support the market as the end user and investor are much more interested in the actual financial return and energy production (measured in kWh) of their PV technology of choice. The mismatch between the performance indicators of manufacturer (maximum power at STC measured in kWp) and user results in energy yield prediction of PV devices gaining in importance. The incentive for the PV industry to change to an energy predictive price driving factor for their products lies in energy rating, which is very similar to energy yield prediction, but one made for standardised meteorological data sets.

Solar modules are variable-output devices and it is necessary to understand their behaviour in various environments before it is possible to improve the device structures for higher efficiency, overall energy production and for reduction of costs. The behaviour in different environments is, especially for thin film solar cells, not well understood and typically can only be derived from direct field data, because realistic conditions as seen outdoors cannot be re-produced indoors. If measured accurately, research of PV device performance outdoors can take a long time span from weeks to several months, because many environmental factors such as temperature and sunlight spectra vary with the seasons. Additionally, large amounts of data are needed, for example, to extract temperature coefficients of photovoltaic devices because data of the same light intensity, light spectrum and incident angle at different device temperatures is needed. Yet, this data is rarely available because device temperature is very much dependent on sunlight intensity and other weather conditions that cannot be controlled outdoors.

Most solar simulators today are only capable of varying PV device temperature and, to a degree, irradiance level. Very few simulators, with more than one light source type or with filters, can change the light spectrum to some extent. This is not enough for a full performance characterisation of a PV device, which means that to date solar simulators do not provide the required variability of environmental conditions to give a clear answer of how a PV device will perform outdoors. Therefore a module's yearly energy output

can only be measured and predicted accurately from outdoor measurements, which at the current rate of technology developments simply takes too long. To greatly improve the situation one would need to measure indoors under controlled conditions, which requires a measurement system that can reproduce outdoor conditions more accurately.

In all aspects, multi-junction devices are problematic to characterise. These devices have led to record efficiencies in solar energy conversion by utilising a wider range of the incident solar spectrum. This is achieved by stacking multiple solar cells, each responding to different spectral ranges of the incident irradiance. This increased device complexity has made them difficult to calibrate, especially at production relevant speeds. Measurements with commonly used single-lamp solar simulators are associated with large uncertainties, even when the simulator is classified spectrally as meeting the most stringent requirements. Uncertainties occur because the accuracy of the calibration depends to a large extent on the agreement of the test spectrum to the one prescribed by the testing standard. This agreement defines the matching of the junctions within the device and thus the calibration quality. To properly characterise multi-junction solar cells one needs to operate a multi-source or by other means spectrally adjustable solar simulator (i.e. with filters). By adjusting the spectral distribution of the solar simulator stacked cells can be current matched or current balanced to a given reference spectrum. However, the available methods are somewhat slow and cannot be used in production, as they require additional measurement of spectral response. Methods are difficult to operate and small mistakes can already lead to significant uncertainties in the measurement. A method that eliminates the need of spectral response measurements and can run automated in one measurement system has the potential to greatly reduce problems in this area and could prove useful in production lines.

Within this work a new type of solar simulator was developed that is able to measure power rating as well as measurements required for energy rating and energy yield predictions of single-junction and multi-junction solar cells. The first measurement system of its kind, based on light emitting diodes (LEDs) as main light sources, has the ability to reproduce more realistic

outdoor conditions with varying spectral irradiance, light intensity and device temperature. It has opened the possibility to carry out measurements required for energy yield prediction of PV devices of different materials and structures within a much-reduced measurement time-span, which is demonstrated throughout this work. Furthermore, the developed system has enabled a new way to fully automatically characterise multi-junction as well as single-junction solar cells without the need of additional spectral response measurement equipment, potentially reducing measurement time and costs. A measurement method, delivering photovoltaic test device's spectral response and current-voltage (I-V) characteristic at any given reference spectrum has been developed and is demonstrated within this work.

A description of the performance indicators and characteristics of solar cells can be found in chapter 2. This chapter also provides information on the performance influencing effects such as temperature, light intensity and irradiance spectrum. Device performance measurements are described and the basic aspects of PV device measurement technologies are reviewed.

Chapter 3 concentrates on the LED-based solar simulator prototype developed within this work. This includes a review of measurement systems and a detailed hardware and software description of the solar simulator.

The classification and characterisation results of the solar simulator testing are detailed in chapter 4. The first device characterisation results and a measurement uncertainty analysis are also included. Furthermore, a detailed list of improvements for the full version is given.

The automated device characterisation method is explained in detail in chapter 5 and a simulated measurement demonstrates that the method works. Initial device characterisation results from the LED simulator are analysed and discussed.

Device performance measurements under varying spectral irradiance, light intensity and device temperature for energy yield prediction are demonstrated in chapter 6 on two different types of solar cell. Measurements are analysed and show a good agreement to reported outdoor behaviour of

the device types and underline the importance of performance measurements that include spectral variations.

The conclusions drawn from the work in this thesis can be found in chapter 7. This chapter also provides recommendations for future work and proposals. A list of conference and journal publications relating to this work is given thereafter.

2 Photovoltaic device performance factors and characterisation

This chapter provides an overview of the fundamental concepts used in this thesis. It identifies and links together the three key research areas identified in chapter 1. A detailed review specific to the areas of research can be found in the first sections of each of the following chapters. This chapter will introduce the issues of global importance.

Firstly, different performance indicators of photovoltaic devices as well as their dependence on outdoor operating environment are reviewed in more detail. This is done in section 2.1 and 2.2. Section 2.3 concentrates on the differences between the two photovoltaic performance characterisation methods: Power rating and energy rating. Section 2.4 provides an overview of measurement technology used to characterise the performance of solar devices with emphasis on areas of improvement this thesis is concentrating on.

2.1 Photovoltaic device characteristics and performance indicators

2.1.1 Solar cells and Current-Voltage characteristic

The performance of photovoltaic devices is measured by the current and voltage generated in the device from the incidence light. The generated electrical power is dependent on many factors as such as the material type, quality and structure of solar cell, the operating environment and the actual electrical load applied to the device. The behaviour under different loads is described with the current-voltage characteristic or “I-V curve”.

Behaviour of an ideal solar cell:

In the dark, the solar cell's current-voltage characteristic behaves similarly to a diode. In illuminated conditions, a current generator is added in parallel to the diode. It is a common convention to use negative currents, i.e. all currents are taken against their physical direction. The advantage of this is that the produced power is positive in operation. This can then be described as in equation (2.1). Where I is the current, V stands for voltage, I_0 is the diode saturation current, q is the elementary charge, n is the ideality factor of the diode, k is Boltzmann's constant and T is the absolute temperature in Kelvin. I_{Ph} is the photocurrent, i.e. the current generated from the incident light.

$$I = I_{Ph} - I_0\left[\exp\left(\frac{qV}{nkT}\right) - 1\right] \tag{2.1}$$

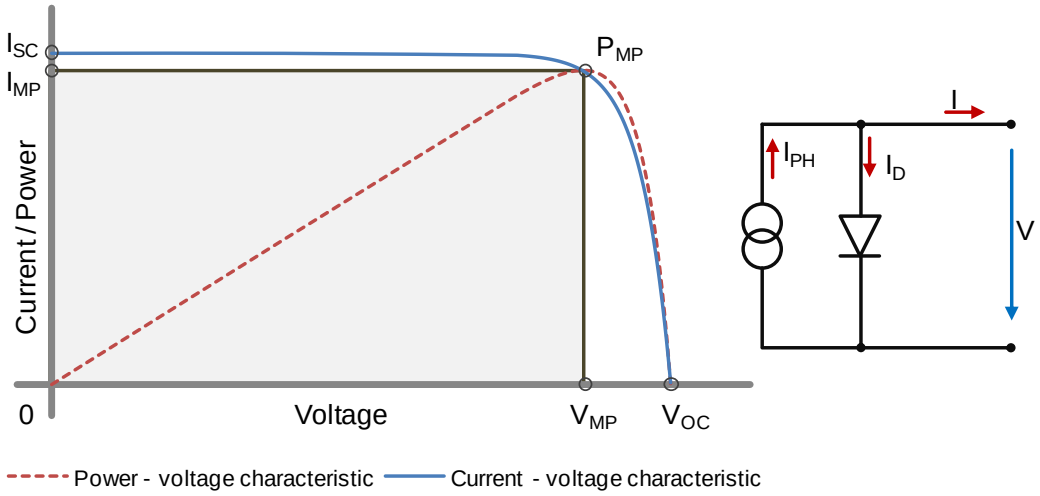

Figure 2.1: A typical I-V characteristic (left) with the main performance indicator points and the equivalent circuit diagram of an ideal solar cell (right)

A schematic I-V characteristic of a solar cell is shown together with the equivalent circuit diagram in Figure 2.1. The figure also indicates the characteristic points used to evaluate the performance of a solar cell. Those are further described in the following:

Short circuit current (I_{SC}) is the current at 0V voltage. In the typical case of a linear solar cell short circuit current is directly proportional to the sunlight intensity.

Open circuit voltage (V_{OC}) is the voltage potential at which no current is flowing. V_{OC} behaves logarithmically to changes in I_{SC} as described in the following equation (2.2), derived from the ideal solar cell equation.

$$V_{OC} = \frac{nkT}{q} \ln\left(\frac{I_{PH}}{I_0} + 1\right) \tag{2.2}$$

Maximum power point (P_{MP}) is a specific voltage and current condition at which the power output of the solar cell has reached its maximum. Maximum power is the point where the first derivative of the product of the voltage and the current equals zero, these values are then called maximum power point voltage (V_{MP}) and maximum power point current (I_{MP}).

As described in equation (2.3), the ratio between P_{MP} and the product of I_{SC} and V_{OC} is called the fill factor (FF). A factor close to unity (1) indicates a high quality photovoltaic device.

$$FF = \frac{I_{MP} \cdot V_{MP}}{I_{SC} \cdot V_{OC}} = \frac{P_{MP}}{I_{SC} \cdot V_{OC}} \tag{2.3}$$

Probably the most important performance indicator of a solar cell is the efficiency η. This is the ratio of output to input power, or, in other words, the ratio of the electrical energy coming out of the device to the light energy incident on the device. Solar cell efficiency is generally reported at maximum power condition and calculated as in (2.4), where G is the incident light power density in [W/m^2] and A the cell area in [m^2].

$$\eta = \frac{P_{MP}}{G \cdot A} \tag{2.4}$$

Solar cell behaviour with parasitic resistances:

Solar cells are not ideal and have additional series (R_S) and shunt resistance (R_{SH}). A modified equivalent circuit diagram is illustrated in Figure 2.2. Equation (2.5) is the modified ideal solar cell equation with incorporated series and shunt resistance.

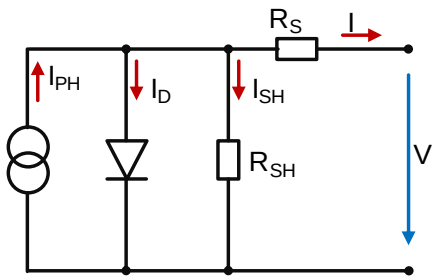

Figure 2.2: Non-ideal equivalent circuit diagram of a solar cell with series and shunt resistance

$$I = I_{Ph} - I_0\left\{\exp\left[\frac{q(V+IR_S)}{nkT}\right]-1\right\} - \frac{V+IR_S}{R_{SH}} \qquad (2.5)$$

High series and low shunt resistance both reduce the fill factor of the device. Contributing to the series resistance in a solar cell are the resistance of the metallic contacts, interconnections and the bulk resistance of the semiconductor. A photovoltaic module also has additional series resistance through cable connects and cell interlinks. Shunt resistance is due to imperfections in the solar cell and is thus a useful quality indicator. In a high quality solar cell R_S is very low and R_{SH} is as high as possible. Figure 2.3 illustrates the effects of R_S and R_{SH}.

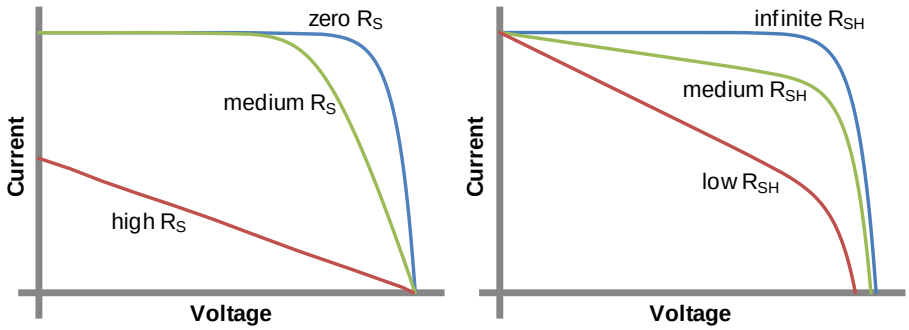

Figure 2.3: Effects of parasitic resistances: series resistance (left) and shunt resistance (right)

Behaviour of an amorphous silicon solar cell:

The I-V curve behaviour of amorphous silicon (a-Si) solar cells is slightly different to the non-ideal solar cell model with parasitic resistances as given in equation (2.5). Amorphous silicon solar cells have an additional intrinsic layer between the p and n junction. This p-i-n junction instead of the usual p-

n junction means that they show a voltage dependent photocurrent. The current output of a-Si solar cells decreases with increasing voltage due to an increase in recombination of electron-hole pairs that is driven by a reduction in the electrical field. Figure 2.6 illustrates the modified equivalent circuit diagram.

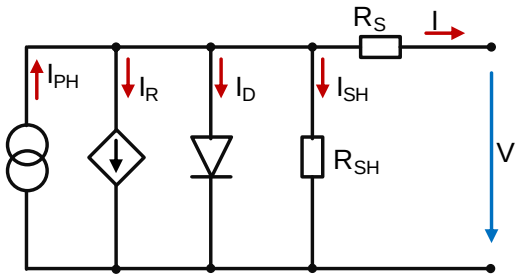

Figure 2.4: Equivalent circuit for amorphous silicon solar cells that accounts for the additional recombination of electron-hole pairs dependent on the voltage of the device; I_R is the recombination current

To accurately describe the I-V curve of an amorphous silicon solar cell equation (2.5) requires an additional loss term to account for the recombination. Merten et al. [3] developed the equation given in (2.6) to model the behaviour of an a-Si solar cell. Where d_i is the thickness of the intrinsic layer, μ is free carrier mobility, τ carrier live time and V_{bi} is the built-in voltage of the amorphous silicon solar cell. The $[(\mu\tau)_{eff} \bullet (V_{bi}-V+IR_S)]$ product is the effective drift length of a generated electron at a given internal voltage in the solar cell.

$$I = I_{Ph} - I_{Ph}\left\{\frac{d_i^{\,2}}{(\mu\tau)_{eff}\left[V_{bi}-(V+IR_s)\right]}\right\} - I_0\left\{\exp\left[\frac{q(V+IR_S)}{nkT}\right]-1\right\} - \frac{V+IR_S}{R_{SH}} \qquad (2.6)$$

Figure 2.5 compares the modelled I-V curve of an amorphous silicon device with the non-ideal solar cell. Clearly visible is that the recombination losses in the photocurrent are dependent on the thickness of the intrinsic layer, indicating a stronger voltage dependence of the photocurrent with increasing thickness of the devices.

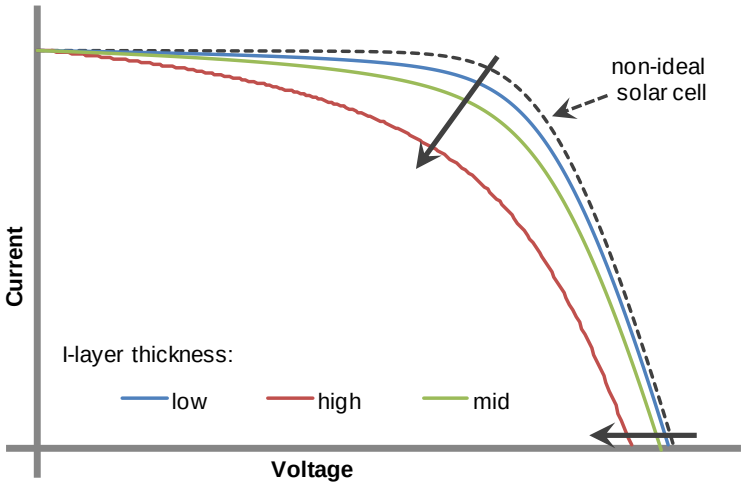

Figure 2.5: Simulated I-V curves of an amorphous silicon solar cell at different I-layer thickness compared to a modelled non-ideal solar cell with the same common input parameters

2.1.2 Solar cell mismatch

A photovoltaic module is made from a number of solar cells connected in series and in parallel, which gives a higher voltage and current output respectively. Ideally, all cells in a module should be identical, but in reality this can be very different due to manufacturing defects, degradation or also simply due to environmental influences as such as partial shading (e.g. trees, buildings or dirt on the device). In a photovoltaic module the output is limited by the cell with the lowest output. The difference between the ideal and the actual performance is called a mismatch loss. Mismatch is possible in both series and parallel connection of solar cells, but is most problematic with series connected solar cells and can result in drastic performance losses from even a single under-performing cell.

If electrical elements are connected in series, the current through each of the elements is by Kirchhoff's current law constrained to be the same. In the case of a series connection of an un-shaded and shaded cell, the shaded cell produces a lower current output than the other and can be pushed into reverse bias, consuming power. This will heat up the cell and can lead to its destruction. Figure 2.6 illustrates the effect of current mismatch in a series connection of two cells of which one is shaded.

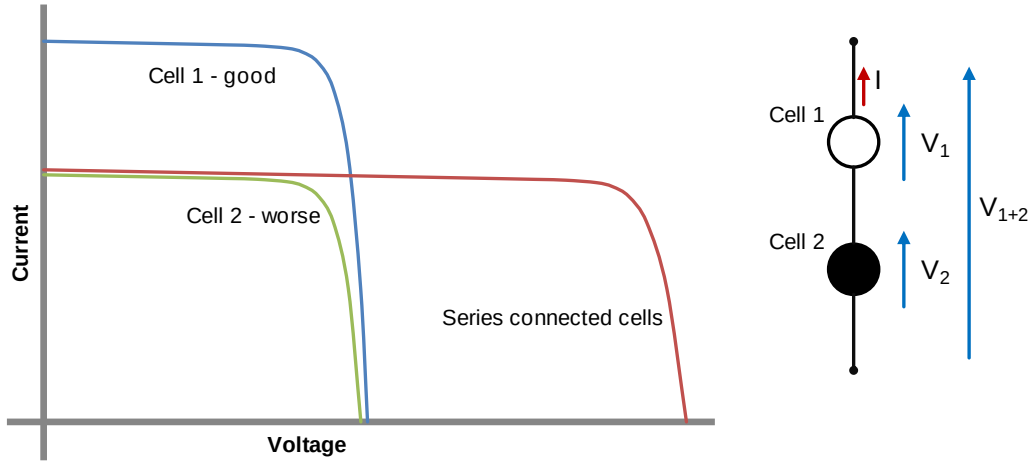

Figure 2.6: Mismatch of solar cells in a series connection

Similarly, the voltage in a parallel connection of cells is forced to be the same (Kirchhoff's voltage law). A mismatch can push the cell with lower voltage beyond its open-circuit voltage and into dissipating power (Figure 2.7).

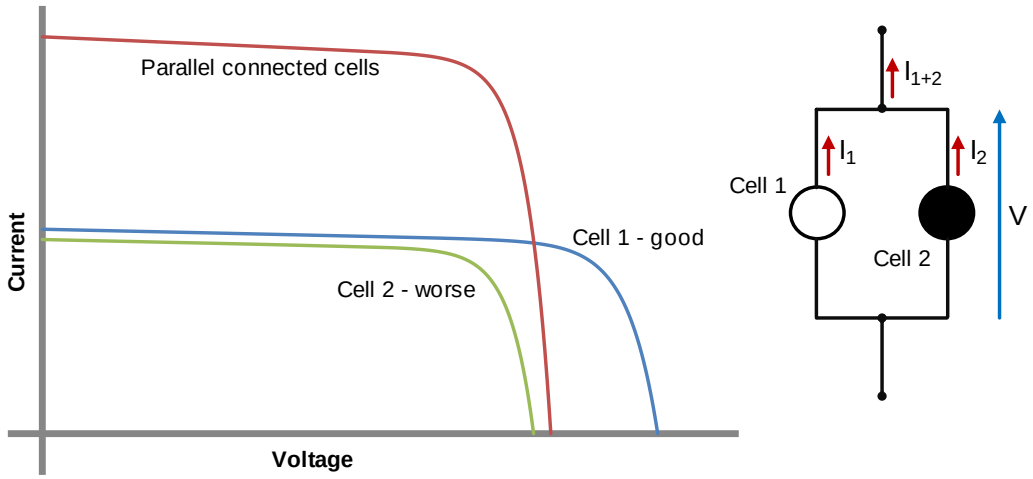

Figure 2.7: Mismatch in parallel connection of solar cells

To prevent reverse current flow into a mismatched solar cell, bypass diodes are fitted on most crystalline silicon modules. More details on this can be found in chapter 5 of [4].

2.1.3 Spectral response

Solar cells respond to changes in the incident light colour, or spectral distribution of irradiance. The main reason for this is the limitation due to the

band gap of a solar cell, which is the difference between energy levels of valence and conduction bands. Only photons with energy higher than the band gap can be converted to electricity, photons of a lower energy are either transmitted through the device or lost as heat. This means that only a fraction of the photons from different energy levels (wavelengths) is absorbed and converted into electricity. Losses as such as electron-hole pair recombination, reflection and incomplete absorption take place that reduce the amount of light that is converted into electricity.

The ability of a solar cell or module to convert photons of different wavelengths into electricity is described by the spectral response (SR) or external quantum efficiency (EQE) curves. The SR describes the amount of current that is produced by a solar cell at a particular wavelength for a given input power in the form of light [A/W]. The efficiency of this conversion is described with the EQE curve. Equation (2.7) can be used to calculate the SR of a device at a given wavelength. P_{IN} is the input power at wavelength λ, S is the absolute spectral response. Since SR and EQE are directly related, they can be converted easily. This is done in the 2nd part of the equation (2.7), where h is the Plank constant and c is the speed of light.

$$S(\lambda) = \frac{I_{SC}(\lambda)}{P_{IN}(\lambda)} = \frac{q\lambda}{hc} EQE \qquad (2.7)$$

Typical examples of spectral response curves are given in Figure 2.8. With the spectral response curve and the spectrum incident on the solar cell, the generated I_{SC} can be calculated with equation (2.8), where E stands for the absolute spectral irradiance.

$$I_{SC} = A\int S(\lambda)\cdot E(\lambda)d\lambda \qquad (2.8)$$

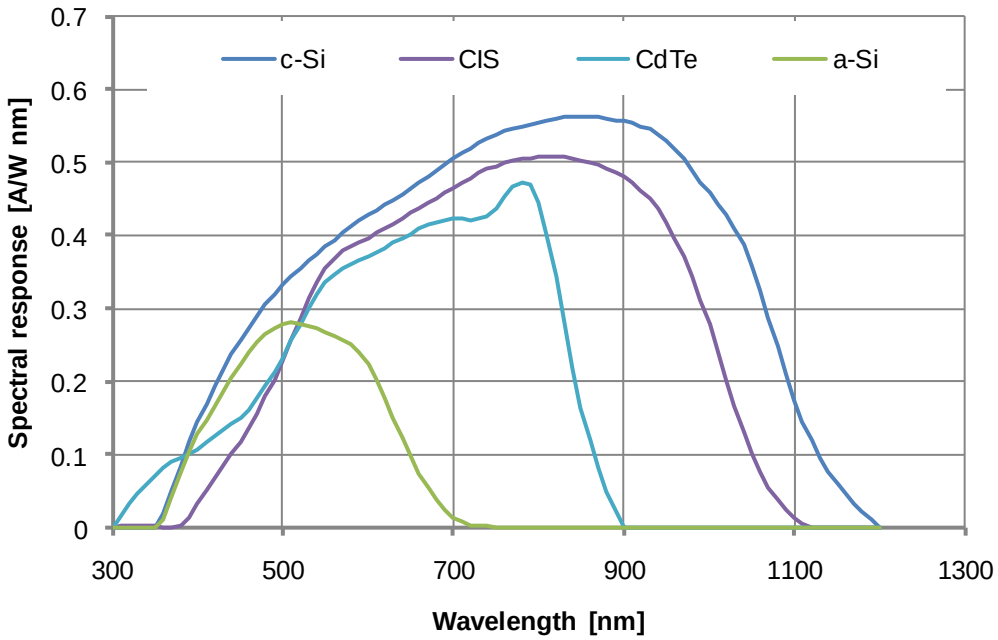

Figure 2.8: Spectral response curves of various solar cell materials: a-Si – amorphous silicon, c-Si – crystalline silicon, CIS - copper indium selenide, CdTe – cadmium telluride

2.1.4 Multi-junction solar cells

As mentioned in the previous section, the spectral response of a solar cell is limited by its band gap. This also limits the efficiency of solar cells with a single band gap to about 30%, assuming un-concentrated 6000K black body radiation of the sun and 300K cell temperature [5]. This limitation on single-junction (SJ) solar cells has been overcome by stacking multiple solar cells and thus achieving a multi band gap “multi-junction” (MJ) solar cell. This way, light over a much longer wavelength range is absorbed. In principle this means for a double junction solar cell that blue light is absorbed in the top junction with larger band gap energy while red light passes through this junction and is then absorbed in the bottom junction which has a smaller band gap. The theoretical efficiency limit is in this way pushed to 68% under the same conditions with an infinite number of junctions [6].

Multi-junction devices are categorised into several types: mechanically stacked, monolithic and so-called hybrid multi-junction solar cells [7]. Mechanically stacked solar cells are physically placed one on top of the other. Those usually have terminal connections for each of the junctions,

meaning that they can be accessed separately and interconnected in any which way. A monolithic multi-junction solar cell has the junctions built in internally and has only two connection points. The most common form is the two-terminal series connected structure. Hybrid multi-junction solar cells are a mix of both, for example a double-junction monolithic solar cell stacked onto a separate single junction cell. An illustration of the working principle of a two- and four-terminal multi-junction solar cell can be found in Figure 2.9.

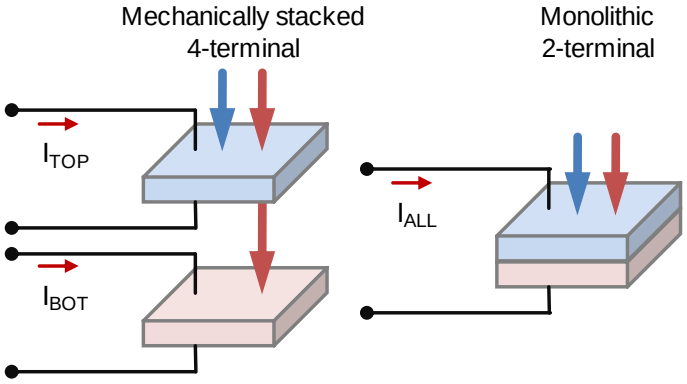

Figure 2.9: Working principle of 4-terminal and 2-terminal double-junction solar cells

The effect of mismatch as discussed in the previous section is a big challenge for multi-junction solar cells. The biggest challenge is posed by two-terminal MJ solar cells, as the junctions are inaccessibly connected in series. Since each junction in a MJ solar cell has a different band gap and spectral response, it is possible that one junction receives less light in its spectral response range and generates less current than the others. In this case the cell producing less current is limiting the current output of the complete device much like in a series connection cell mismatch [8]. To overcome this problem the current generation of all junctions needs to be matched to keep power loss as low as possible. However, the natural sunlight spectrum is constantly changing, as described in the following sections.

2.2 Environmental factors influencing solar photovoltaic performance

The performance of a solar cell depends not only on its material properties and structure, but also on the operating environment. The 4 main environmental factors influencing performance are light intensity, irradiance spectrum, operating temperature and angle of incidence of the light. Each is described in the following subsections. Additionally details on solar cell performance degradation and variation are given.

2.2.1 Effects due to light intensity

The main environmental factor influencing the device power output is the intensity of the irradiance incident on the photovoltaic device. An increase in light intensity generates a proportional increase in the device photocurrent and thus I_{SC} (equation (2.1)). The increase in photocurrent has a proportional logarithmic effect on V_{OC} (equation (2.2)). The effects of changes in light intensity are illustrated in Figure 2.10.

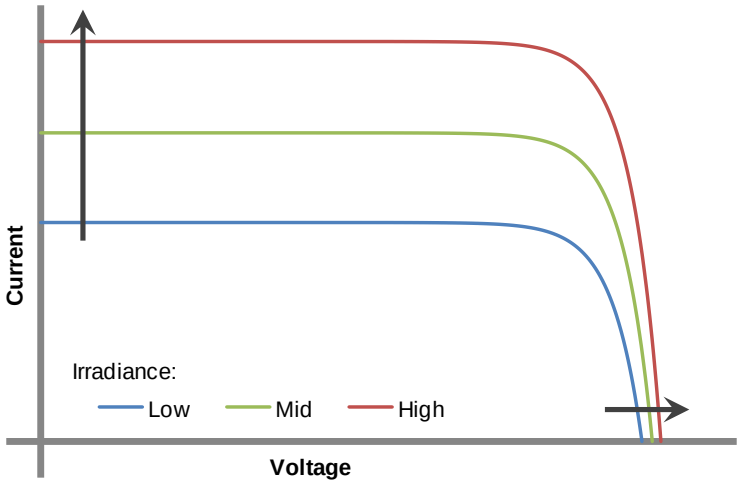

Figure 2.10: Irradiance effects on the I-V characteristic of a solar cell

The increase in maximum output power of solar cells is only approximately proportional to the increase in light irradiance. This is because of the logarithmic changes in V_{OC} and thus non-linear changes in V_{MP} whereas the

I_{MP} very much follows the increase in I_{SC}. In principle, an increase in irradiance leads to a very steep increase in efficiency at low irradiance conditions. At high irradiance conditions this changes to a shallow increase. The effect of increase in efficiency has further use in concentrator solar cells, where a high concentration of light can lead to a significant increase in efficiency and thus power output [9]. However, if the PV device has a large series resistance, such as for amorphous silicon (a-Si) solar cells, the efficiency curve reaches a maximum and then falls again at the point where the effect of series resistance becomes significant [10].

Irradiance can also have an effect on the spectral response of the solar cell or module. This is observed as a slightly non-linear behaviour in I_{SC}. This is most pronounced with thin-film silicon solar cells as such as a-Si [11]. A-Si devices also exhibit strong initial light-induced degradation that affects device performance and spectral response (further explained in section 2.2.4).

2.2.2 Temperature effects

In the first instance the operating temperature of a PV module depends on air temperature. Another main influencing factor is the incident energy that heats up the module with increasing irradiance levels. Additionally, operation temperature is also dependent on module characteristics and wind speed.

The major effect of increasing temperature on a PV device is a reduction in V_{OC} and consequently P_{MP}. This stems from a small reduction in the band gap energy and an increase in recombination. Looking at the ideal solar cell equation (2.1), this can be explained with an increase in the diode saturation current I_0. This can be calculated with equation (2.9), where B is a temperature independent constant and γ includes the remaining temperature dependencies of the material parameters. E_{g0} is the band gap of the solar cell semiconductor linearly extrapolated to zero Kelvin [12].

$$I_0 = BT^{\gamma} \exp\left(-\frac{E_{g0}}{kT}\right) \tag{2.9}$$

The reduction in the band gap energy of the device also has an effect on the spectral response. It means that a smaller energy is needed to generate an

electron-hole pair and directly results in a small increase in photocurrent [4]. The effect of temperature on I_{SC} is in most cases linear, depending on where the energy equivalent to the band gap sits in the incident spectrum. Other temperature coefficients (e.g. P_{MP}, FF, V_{OC}) are nonlinear over irradiance and reduce with increasing V_{OC} of the device [4]. Figure 2.11 demonstrates the effects of temperature on the I-V characteristic of a solar cell.

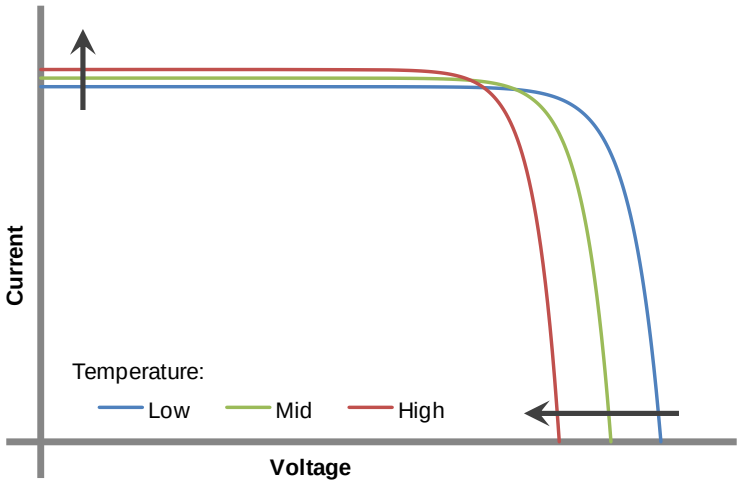

Figure 2.11: Operating temperature influences on the device I-V characteristic

The extent of temperature influences very much depends on the material and structure of the photovoltaic device. Crystalline silicon solar cells have temperature coefficients of P_{MP} ranging from -0.3 to -0.5%/°C while amorphous silicon solar cells have a much lower temperature coefficient with only up to -0.2%/°C [13]. The temperature behaviour of solar cell performance parameters over temperature itself is most cases linear, but not necessarily, as reported in [14] for amorphous silicon-based thin-film solar cells. As further described in section 2.2.4, high operation temperature is also known to cause thermal annealing in a-Si devices.

2.2.3 Spectral and angle of incidence effects

The sunlight spectrum incident on a PV device is constantly changing and is influenced by a large number of factors. The main contributing factors are air

mass (AM), sky clearness (clearness index k_t) and angle of incidence (AoI) with regards to the position of PV device.

Air mass is correlated to the angle of incidence (solar elevation) of the sun into the atmosphere. This angle changes over the day as the sun position changes from sunrise to sunset and also over the course of the year with seasonal elevation changes of the sun. AM describes the ratio of the thickness of the atmosphere to the actual path length of the solar radiation through the earth's atmosphere. Air mass 0 spectrum (AM 0) is the spectrum from the sun as observed just outside the atmosphere. AM 1 refers to the spectrum on the earth's surface from the sun in position directly overhead at the zenith and AM 2 refers to a solar elevation of 60° to zenith. The relationship between solar elevation of the sunlight into the atmosphere and air mass is illustrated in Figure 2.12.

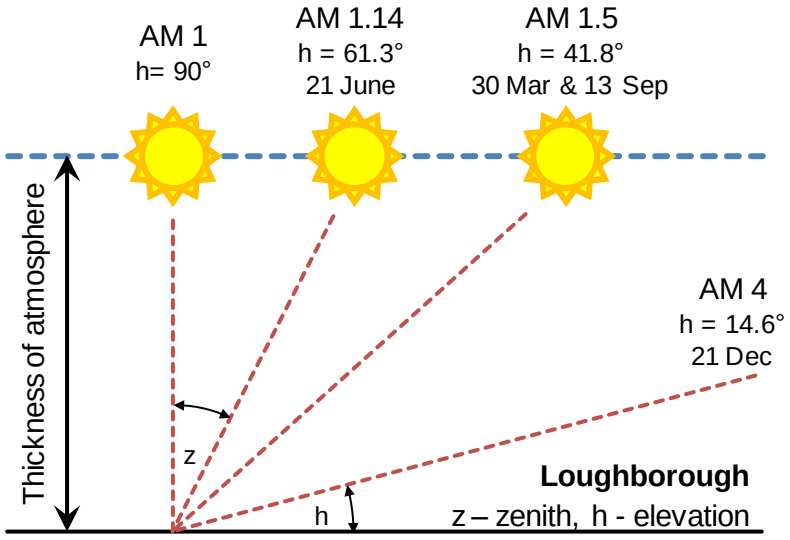

Figure 2.12: Relationship between air mass (AM) and solar elevation, the values shown are for noon at Loughborough throughout the year

The AM 0 spectrum entering the atmosphere has an annual mean irradiance of approximately 1367W/m^2 ±7W/m^2 [15] and is similar to the black body spectrum at 5762K [16]. As light passes through the atmosphere molecules scatter, absorb and reflect different wavelengths of the light and thus change its spectral distribution. Furthermore, a diffuse component of incident irradiance is added from the scattered light. On a clear sky day with AM 1,

about 70% of the light reaches the earth's surface directly, with an additional diffuse component of 7% [17]. Figure 2.13 shows the different terrestrial AM spectra on clear sky days.

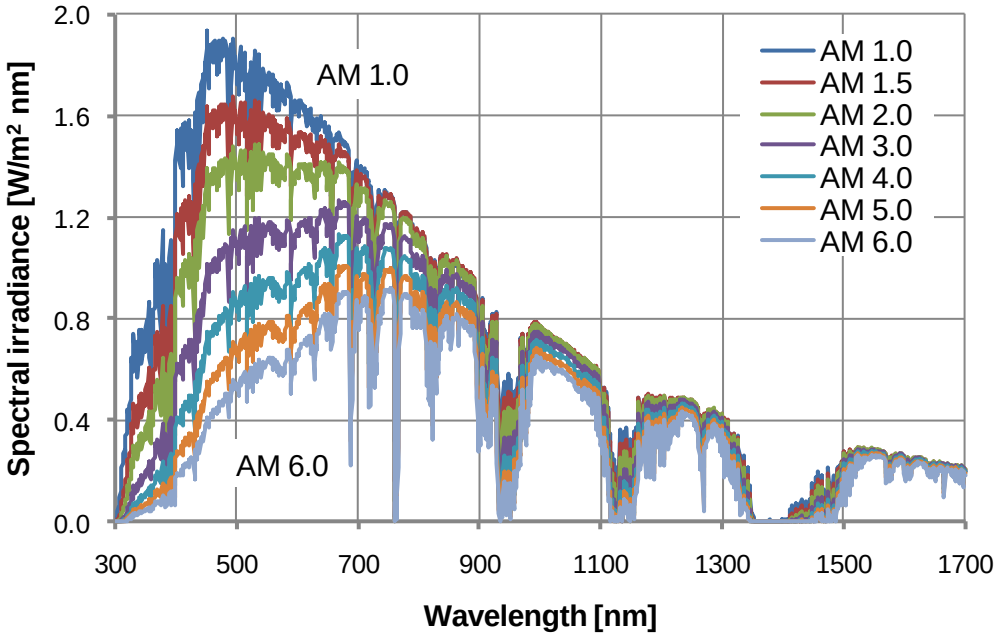

Figure 2.13: Modelled clear sky air mass spectra in the range from AM 1 to AM 6; low air mass spectra are blue-rich, whereas high air mass spectra are referred to as red-rich

Clearness is another factor that has an impact on the sunlight spectrum and thus influences the performance of a PV device. This factor is a combination of cloud cover, humidity and pollution. Most solar energy is delivered under sunny and clear conditions. However, a location as such as Loughborough has a significant amount of cloudy days over the year and thus a large part of the energy is generated in cloudy conditions, i.e. it is of low intensity and blue rich. A low clearness also indicates that the ratio of diffuse to direct beam irradiance is high, i.e. the contribution of direct light is low. Figure 2.14 illustrates the changes in spectrum due to clearness.

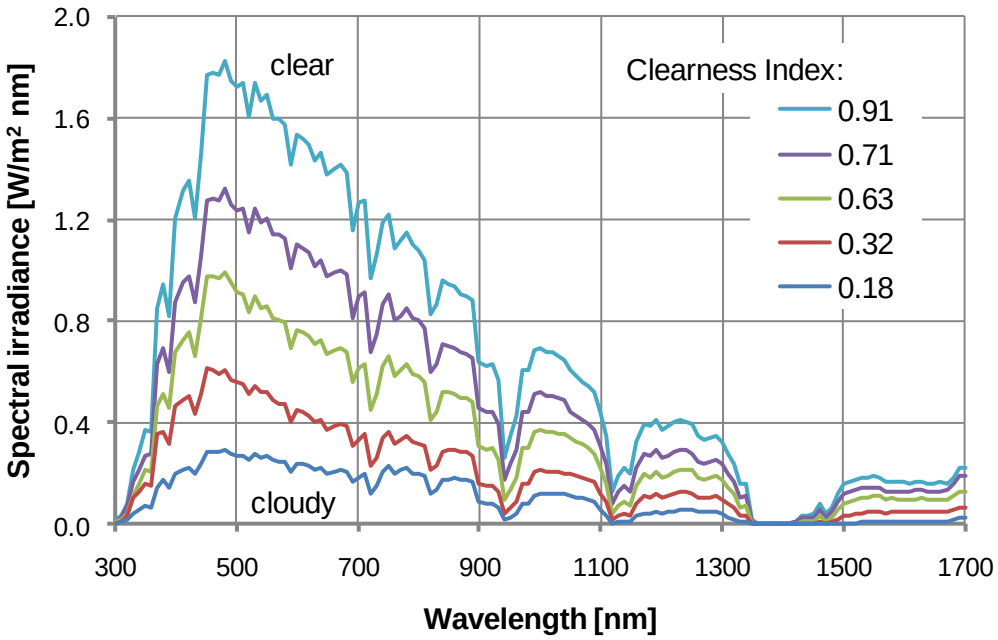

Figure 2.14: Measured changes of the sun light spectrum due to clearness (Loughborough midday in summer ~AM 1.15)

The last main factor influencing the incident sunlight spectrum is the mounting of the PV device in a solar power plant or on a roof. PV devices are either mounted in a fixed position in an angle facing a certain direction dependent on the location (outdoor measurement system in Loughborough: tilt angle 45° facing south) or on a tracker that is moving with the sun. For a device in a fixed position the angle between the beam component and the receiver is constantly changing due to the movement of the sun. This means that the ratio between direct and diffuse light and the amount of light that is received by the PV device changes. This has an impact on the overall spectrum received. On a tracking system the device is repositioned to face into the direction of the sun, which in clear sky conditions can significantly increase the energy harvested. The solar spectrum is, however, still changing with air mass and changes in the diffuse component of the light are dependent on the surroundings of the location of the tracker.

Since solar cells have spectral response in a well defined wavelength region, the constantly changing sunlight spectrum also means that the operating efficiency of the PV device is changing. For multi-junction devices this affects the current balance of the junctions as well. This leads to additional changes

in the device performance with varying spectra because of variable junction mismatch. Multi-junction solar cells [8, 18] and some single-junction devices such as amorphous silicon also show non-linear spectral behaviour on the fill factor [19, 20].

2.2.4 Performance degradation and meta-stability

The performance of all types and materials of PV devices slightly deteriorates over its operation lifetime, which is a process also referred to as degradation. Module performance degradation over its lifetime and the eventual failure is caused by a range of factors such as [4, 21, 22]:

- Cell degradation with increases in series and decreases shunt resistance
- Optical degradation of modules through yellowing or delamination of encapsulating materials
- Short circuiting due to module or cell interconnection or corroded or damaged cell semiconductors
- Open circuiting or high series resistance due to cracked cells or failed module interconnects

How much the performance deteriorates is difficult to determine as it is dependent on the operating conditions and manufacturing quality.

A strong degradation is experienced with a-Si devices for roughly the first 6 months until they stabilise and degrade at a normal rate [23, 24]. The final efficiency is dependent on the operation conditions the device experienced and the device structure. Multi-junction a-Si devices show less of an effect than single-junction devices.

In addition to normal degradation, a-Si devices also show a strong meta-stability influenced by light intensity and device operating temperature as the main driving factors. High incident light intensity causes in a-Si devices a light-induced degradation mechanism. High operation temperatures result in thermal annealing, which is a performance recovery effect from light induced degradation. This phenomenon has first been observed by Staebler and

Wronski [25] and is also referred to as Staebler-Wronski effect. Both factors affect spectral response, the fill factor and efficiency of the device. They are known to cause strong seasonal variations in the performance of a-Si devices dependent on the location and the actual operation conditions the device experiences. The exact minimum activation temperatures of thermal annealing are to-date not well defined as they may vary between different a-Si material compositions. Temperatures as low as 40°C to as high as 80°C have been reported [26-28] However, some papers [27, 29] show that the major contribution of seasonal variations its due to spectral effects of amorphous devices, supporting high activation temperatures. This indicates that the operation temperatures for strong thermal annealing are not reached under normal operation conditions especially in colder environments.

2.3 Photovoltaic device characterisation

2.3.1 Power rating

As indicated in the introduction of this thesis, characterisation of photovoltaic devices is currently based mainly on power rating measurements at standard test conditions (STC). STC defines a specific set of measurement conditions as defined in [30] and given in Table 2.1 below.

Environmental condition	Value
Spectrum	AM 1.5G
Irradiance	1000 W/m^2
Device temperature	25 °C
Angle of incidence	Normal to device

Table 2.1: Definition of standard test conditions (STC) [30]

The air mass 1.5 global (AM 1.5G) spectrum is the standard terrestrial spectrum defined in the IEC 60904-3 [1] and shown in Figure 2.15. This spectrum corresponds to a clear sky day with a 48.2° solar zenith angle and a south facing module tilted at 37°. The spectrum includes direct and diffuse component [31-33].

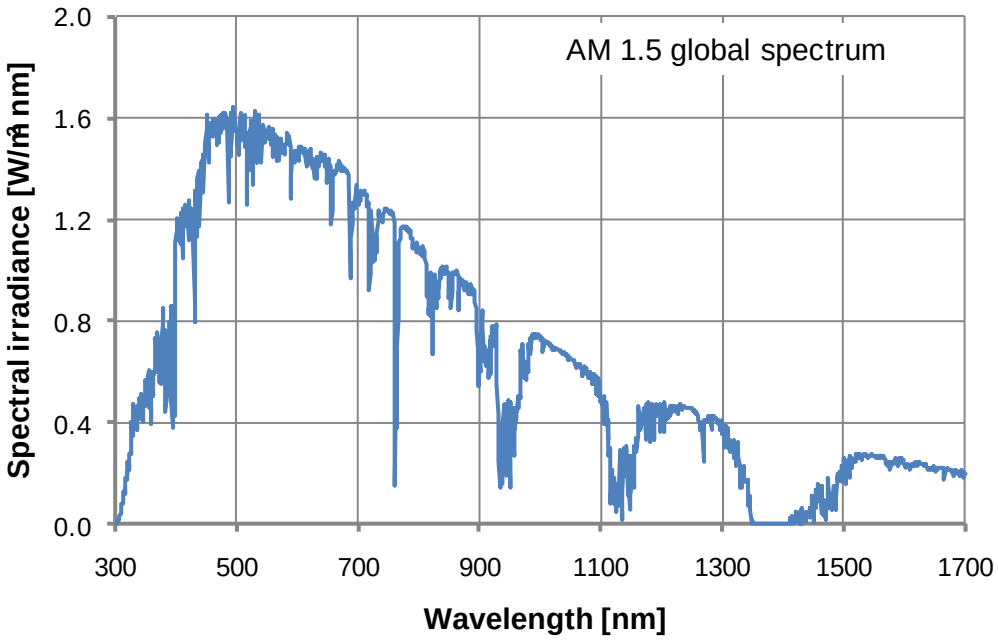

Figure 2.15: Irradiance distribution of the air mass 1.5 global (AM 1.5G) spectrum used in standard test conditions

STC measurements can be carried out outdoors or indoors in solar simulators. Since measurement conditions are standardised, it is a very convenient way of comparing the power output of different module types and technologies. The module pricing is predominantly based on the efficiency and power output in Wp (Watt peak) measured at STC. However, as explained in section 2.2, under realistic conditions environmental factors are changing constantly and very rarely do STC conditions apply (0.3% of all outdoor measurements in Loughborough in 2003, excluding angle of incidence [2]). This leads to operating efficiencies of PV devices outdoors being usually lower than those at STC. Different technologies respond differently to changes in the environmental conditions. Thus it is difficult to predict the outdoor performance of a PV device by means of STC measurement results alone.

2.3.2 Energy rating, energy yield prediction

Unlike power rating, energy yield prediction takes into account the variability of operating conditions outdoors. This makes it a much better comparator between different device technologies. It also means that the best performing

device at a given location can be easily selected and financial return of an installation can be maximised.

Energy yield prediction is a complex process that requires measured PV device characteristics at varying operating conditions as well as meteorological data from the site to be investigated. Both meteorological data and device characteristics are fed into a procedure that predicts the energy yield in a kWh unit. A basic flowchart diagram of this procedure is illustrated in Figure 2.16. The main difference between energy rating and energy yield prediction is that energy rating is based on standardised meteorological datasets instead of data from a local met station. The exact datasets are not yet finalised and the IEC 61853 energy rating standard is still in draft version [34].

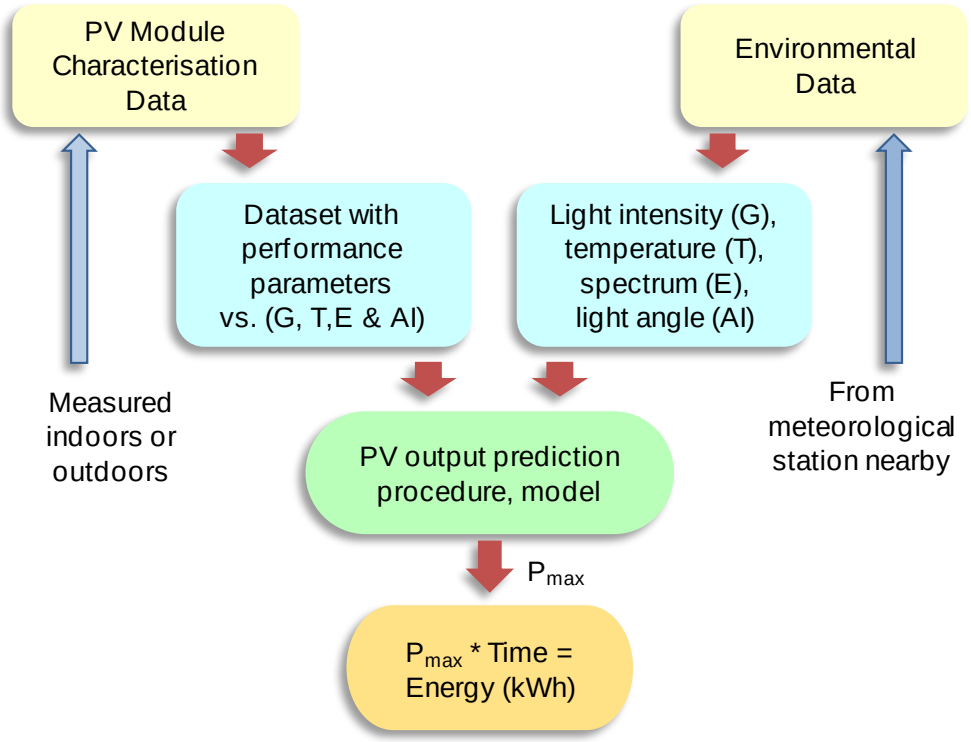

Figure 2.16: Basic schematic flow chart of energy yield prediction

The work in this thesis, particularly chapter 6, focuses on the measurement of PV device performance characteristic data for energy rating and energy yield prediction. PV device characterisation data can be acquired from measurements made indoors or outdoors. Currently, PV device characterisation datasets consist of measurements at different irradiance,

operating temperature and angles of incidence. The effect of spectrum on the device performance is modelled or simply neglected [34-37]. However, as previously stated, some materials such as amorphous silicon and multi-junction devices show a further effect on the fill factor that is difficult to model without further measurements and the simplified spectral effect modelling can lead to additional uncertainties. Hence, to create a reliable and accurate way of comparing technologies under realistic conditions it is better to measure the effect of spectrum directly. This has been done in this work and is described in detail in chapter 6.

2.4 PV device measurement technologies

A major part of this thesis concentrates on the development of a new indoor measurement system for calibrating and assessing the performance of photovoltaic devices. This section gives an introduction into the current state-of-the-art measurement technology that is used indoors and outdoors to carry out research on the performance and behaviour of PV devices.

2.4.1 Outdoor measurements

Outdoor measurement systems are either used to calibrate the STC performance of a device under natural sunlight or they can be used to monitor the performance of a PV device over short or long periods of time. A typical outdoor measurement facility is the CREST outdoor measurement system (COMS) in Loughborough, which is currently in its 3rd version (COMS 3). A basic schematic layout of COMS can be found in Figure 2.17. The system measures the I-V characteristics of up to 64 PV devices with an active 4-quadrant power supply in 5 minute intervals. Sunlight spectra are measured at the same time interval and meteorological data is recorded from a number of sensors every 5 seconds. Detailed information about the system can be found in [38, 39].

The advantage of an outdoor measurement system is that PV devices are monitored under most realistic conditions. This enables comparison of device behaviour and energy yield of different device technologies. As indicated in

the last section, outdoor measurements are also used for prediction of the energy yield. This aspect is further discussed and reviewed in chapter 6.

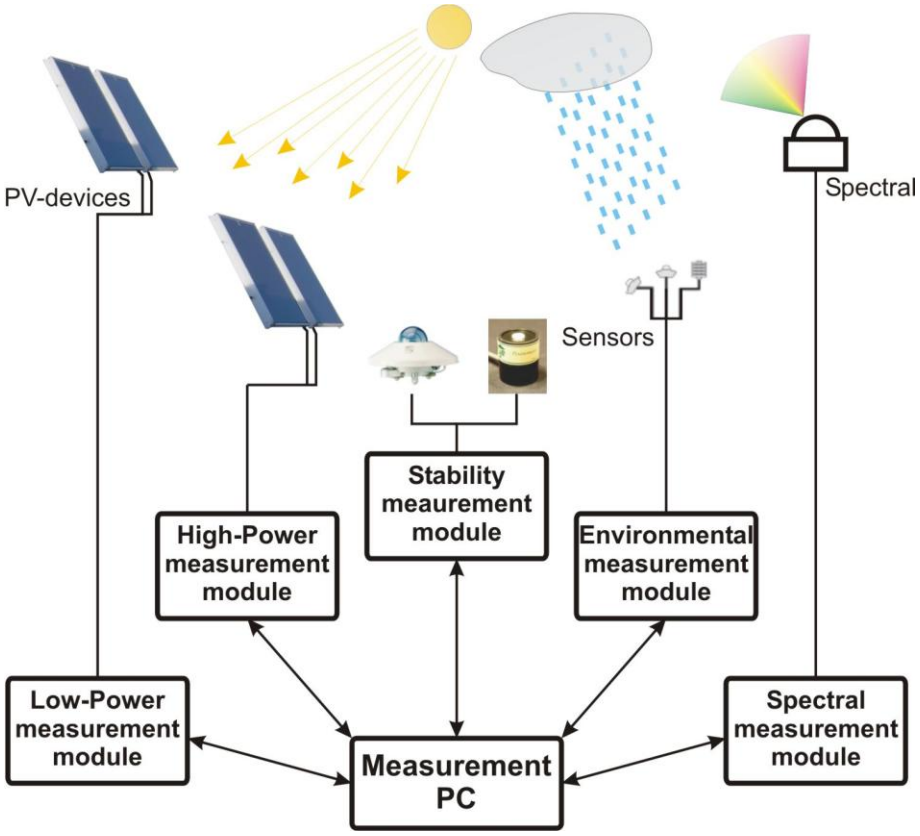

Figure 2.17: Schematic layout of the CREST outdoor measurement system (COMS 3)

2.4.2 Indoor measurements

Indoors, the performance of a PV device is mainly measured with two different types of equipment: solar simulators and QE measurement systems.

Solar simulators are used to measure I-V characteristics of PV devices under artificial light conditions in a controlled environment. This is of advantage, as the user can simulate measurement conditions without having to wait for the weather outdoors. The main use of solar simulators is power rating of PV modules under standardised conditions as described in section 2.3.1. However, the reproduction of the outdoor environment indoors is to date mostly limited to light intensity and operating temperature adjustments. This poses problems for energy yield predictions in solar simulators as they do not provide the variability in operating conditions as seen outdoors to make an

accurate assessment of the predicted energy. This thesis demonstrates and evaluates the concept of a new type of solar simulator based on LEDs that can simulate not only varying light intensity and device temperature but also spectrum. This has potential to enable a more accurate energy rating as the effect of spectrum due to changes in sunlight conditions can be directly measured. A review on indoor measurement systems and a detailed description of the solar simulator developed in this work can be found in chapter 3. Its application to energy rating and energy yield prediction is further discussed and tested in chapter 6.

Spectral response measurement systems are used to evaluate the conversion performance of photons to electrons in PV devices. The SR of the solar cell is required to correct for spectral mismatch between the simulated light in the simulator and the standard spectrum or respectively for differences between the reference device and test device. SR is measured in purpose build systems that illuminate the device with monochromic light and measure the changes in short circuit current (further reviewed in section 5.1.3).

As mentioned earlier in this chapter, monolithically interconnected two terminal multi-junction solar cells provide no direct access to the individual junctions. This poses a challenge for both spectral response measurement systems and solar simulators. Spectral response measurements require correct light and voltage bias to measure the SR of each of the junctions separately. For I-V curve measurements, the solar simulator additionally needs to be spectrally adjustable to be able to adjust the current balance in the junctions to exactly the same as it would be under the reference sunlight spectrum (generally AM 1.5G). To be able to adjust the spectrum correctly, the SR of each junction in the device is required. In factory environments, the SR cannot be measured in relevant timescales with today's conventional monochromator and filter-based systems, as a single measurement takes around 30 minutes. Furthermore, SR measurement systems for full sized modules are virtually nonexistent. With the technology of the newly developed solar simulator it is possible to overcome this problem and a new approach on the characterisation of MJ solar cells has been developed. This

method can work fully automatically on single and multi-junction devices and the solar simulator itself acts as an SR measurement system delivering the SR of each junction and I-V performance measurements, which has potential for a number of advantages. The details of this method and a review of standard characterisation methods of SJ and MJ solar cells can be found chapter 5.

2.5 Conclusions

The aim of this chapter was to provide information on solar cell performance indicators and how these are influenced in the outdoor environment. Furthermore, introductory details of device performance characterisation and measurement technologies have been given.

The areas on which this thesis is concentrating have been identified. A more detailed review of these areas can be found in the introduction to the following chapters. Indoor measurement technologies are further explained in chapter 3 and a novel measurement system is presented. Solar simulator classification and measurement uncertainty are briefly reviewed in chapter 4 before details of the performance assessment of the new measurement system are explained. More information on the measurement methods for acquiring I-V characteristics and spectral response curves can be found at the start of chapter 5 prior to the presentation of a new approach for power rating of single- and multi-junction solar cells. Chapter 6 reviews methods used to acquire PV device characteristic data for energy yield prediction and demonstrates a new method that includes spectral variations into device performance measurements.

3 LED-based solar simulator development and description

One of the main goals in this work was to demonstrate the feasibility of a solar simulator based on LEDs, capable of reproducing outdoor conditions realistically indoors with adjustable output spectrum, light intensity and device temperature. Such a system would have potential to outperform today's solar simulators in providing power rating of single- and multi-junction devices as well as a more realistic energy rating that incorporates most major environmental factors (irradiance, temperature, spectrum). The last remaining environmental factor one would implement for energy rating is the angle-of-incidence, which has not been set as an initial goal of this work, to reduce complexity.

In order to achieve the main goal, a simulator prototype has been developed. A detailed hardware and software description is given in this chapter in sections 3.3 and 3.4. Prior to this, in section 3.1, a detailed analysis of the state-of-the-art in solar simulators and their light sources is presented to highlight the need for the new system as well as identify advantages and disadvantages of conventional systems. Section 3.2 reviews the characteristics of LEDs, stating the reasons why LEDs have been chosen as the light sources for a solar simulator. Furthermore, the current progress in this technology and its implications on the design of the LED-based solar simulator is described.

3.1 Review on current state-of-the art solar simulators

In general, a solar simulator for measuring I-V characteristics of PV devices consists of a light source for illuminating the test device. The spectral output is often manipulated by optics and filters to achieve a good match to the AM 1.5G standard spectrum, which is required for high quality power rating

measurements. Equipment to monitor the light intensity is also required, usually done with a reference PV cell. The temperature may have to be controlled if longer measurements (lasting several 100ms) are to be taken or devices have to warm up. Otherwise it is sufficient to use the air temperature to thermally condition the device. Finally, measurement electronics to obtain an I-V characteristic are required.

Solar simulators can be characterised as two main groups: steady state and flash solar simulators. Steady state simulators employ continuous light while flash simulators utilise pulsed light sources, similar to a flash in photography. The state-of-the-art on both simulator types and their light sources is reviewed in the following subsections. Additionally, details of I-V characteristic measurements and temperature control are given.

3.1.1 Solar simulator light sources

Solar simulators either utilise a single lamp set-up such as the Spire SPI-SUN 240A in CREST and the Wacom WXS standard series [40] or can consist of several lamps illuminating the PV test device as for example the Pasan Sun Simulator IIIb in CREST [41] and the TÜV Rheinland large area steady state solar simulator [42]. In some cases, solar simulators also use different types of light sources and filters simultaneously to achieve some degree of spectral variation. These types of solar simulators have been reported from different labs around the world [18, 43-46] and are mainly used for characterising multi-junction solar cells. With regards to energy rating at varying spectrum, this is not sufficient because only large bands in the spectrum can be varied and some spectral changes, especially in the ultraviolet (UV) and blue range, cannot be reproduced.

Many different types of light bulbs are in use, they can be categorised into filament lamps and arc lamps. Filament lamps can only be used in steady state solar simulators as the filament needs some time to heat up and stabilise. The most useful in this category are tungsten halogen light sources, preferably with selective dichroic back reflectors to reduce the excess infrared (IR) light. Arc lamps are utilised in steady state and flash solar simulators. Most commonly used are Xenon high pressure arc lamps,

Hydrargyrum medium-arc iodide (HMI) and Hydrargyrum quartz iodide (HQI) lamps. A more detailed review on the light sources used in conventional solar simulators can be found in a paper from Matson [47] and Emery [48]. Spectral distributions of different light sources are reviewed in Figure 3.1.

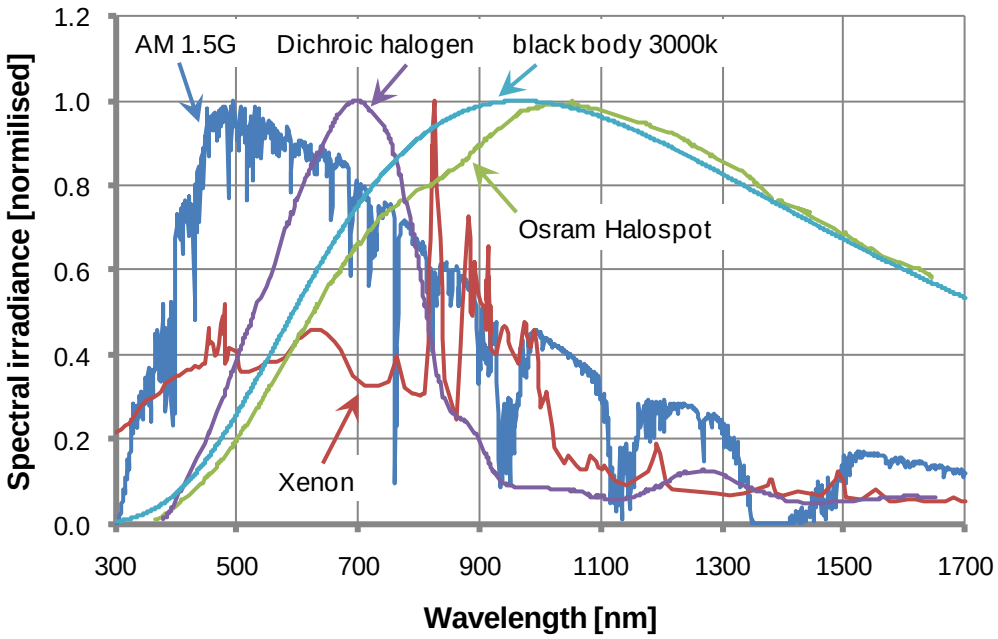

Figure 3.1: Spectral output of different light sources used in solar simulators; Xenon light sources are most commonly used as they achieve the best spectral match to the standard spectrum AM 1.5G

The reference sunlight spectrum can be represented to a very good accuracy with for example a filtered Xenon arc lamp. Nevertheless, none of the conventional light sources fulfil the criteria for a highly flexible and adjustable spectrum. This is mainly because they are broad band emitting light sources that cover the complete spectral range from UV to IR and partly because the lamps output spectrum is changing with adjustments of the intensity. Using these light sources for a solar simulator with good spectral variability requires a large number of filters, each with suitable lamp for the required wavelength, to limit the spectrum to sufficiently small bands for an accurate reproduction of the spectral changes in sunlight.

3.1.2 Steady State solar simulators

A typical steady state simulator for measuring solar cells and mini modules is the WXS series from Wacom Electronics Co. Ltd. [40]. Figure 3.2 shows the basic structure of this simulator. The light beam from the xenon lamp passes through a number of mirrors that redirect light or focus the light into beam homogeniser optics that improve light homogeneity before it hits the PV device. Noticeable is that this simulator uses a Xenon lamp with additional AM 1.5 filter to achieve a better spectral match to the standard spectrum.

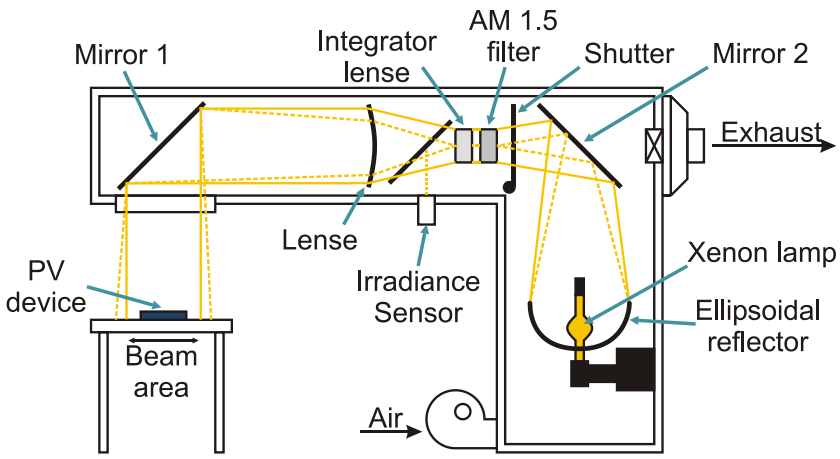

Figure 3.2: Basic structure of a Wacom WXS series standard solar simulator with path of the light beam

For measurements of large PV modules, steady state solar simulators can reach the size of building-integration as for example in TÜV Rheinland [42]. This steady state simulator measures modules of up to 2x2m size and uses 15 4kW HMI lamps to provide the required 1kW/m^2 irradiance under STC. The system utilises an air blow table as the temperature control system to keep the PV device at the desired temperature. The simulator operates without additional filters and a wire mesh net in between the lamps and the PV test device is used to improve the light output uniformity over the illumination area. During calibration, the light intensity can be altered in the required areas by cutting wires from, or adding additional wire to, the mesh at the correct position, although this is a very time consuming process.

The advantage of steady state simulators is that they can measure I-V characteristics without any influence of capacitive effects (further explained

below), because of stable light conditions and long measurement times in the range of seconds. Problematic is that the PV device can heat-up during a voltage sweep if the temperature of the device is not stabilised or no temperature control for the test specimen is used. In this case the I-V measurement is distorted as V_{OC} and I_{SC} (as well as all other parameters) change during the measurement [49]. Steady state simulators have in general very high operational costs, because of high energy consumption of the light sources and limited lamp lifetime of 500 to around 2000h, dependent on the type of lamp. Down-time due to maintenance or homogeneity adjustments significantly increases costs as the re-calibration is a slow and elaborate procedure. It is also required to check specifications from time to time, because the properties of the light bulbs are changing with age in both intensity and spectral distribution [47, 48].

Steady state systems are most useful for power rating at STC, but not necessarily suitable for device characteristic measurements for energy rating, as the adjustment of the light irradiance is very limited. Mesh filters or optical filters are used in this case to adjust the light intensity over a larger range.

3.1.3 Flash solar simulators

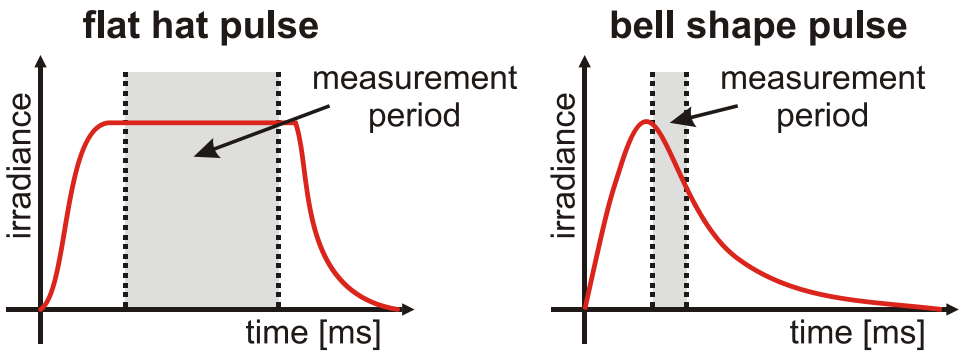

Figure 3.3: Two main groups of flash solar simulator types

Flash simulators can be separated into two groups: flat hat pulse and bell shape pulse systems. The major difference between them is that the I-V characteristic is measured in a flat hat pulse system at regulated light conditions while in a bell shape pulse simulator the light intensity is unregulated. In a bell shape pulse simulator the measurement starts at or

after the highest irradiance point and continues during the pulse falling tail as illustrated in Figure 3.3.

According to Shimotomai [50] flash simulators can be further classified into 5 categories (type A to E as given in Table 3.1) by their measurement method dependent on the pulse length, number of I-V points measured per pulse and light pulses required to measure a full I-V curve. Type A is in this definition a typical multi-flash bell shape pulse system and type D and E is a typical single-flash flat hat pulse solar simulator.

Type	Number of pulses	Pulse width [ms]	Measurements per Flash
A	>80	1(at the foot of pulse)	1 point
B	>80	3-10	1 point
C	3 or 4	3-10	Half or All
D	1	5-10	All
E	1	<100	All

Table 3.1: Classification of flash simulators by measurement method

A typical, but in today's technology, slightly outdated vertical bell shape pulse multi-flash simulator is the Spire SPI-SUN 240A used at CREST. The type A system uses an xenon arc lamp. The PV device characteristic is measured on a point by point basis over 256 flashes with a pulse length of 1.2ms. The total measurement time is about 21s at a flash rate of 12.5Hz [51]. Problematic on such bell shape pulse systems is that each point measured has to be corrected for irradiance fluctuations between pulses. This can be corrected with the procedures described in the IEC 60891 standard [52] and according to a paper by Müllejans [53].

Today's flat hat pulse simulators with large test areas for PV devices like the Wacom WPSS or the Pasan IIIb solar simulator in operation at CREST (see Figure 3.4) are usually structured horizontally for an increased distance between lamp and test device area for better illumination uniformity. The downside is that in thermally uncontrolled rooms, modules can have a temperature distribution from the bottom to the top of up to 2-3K.

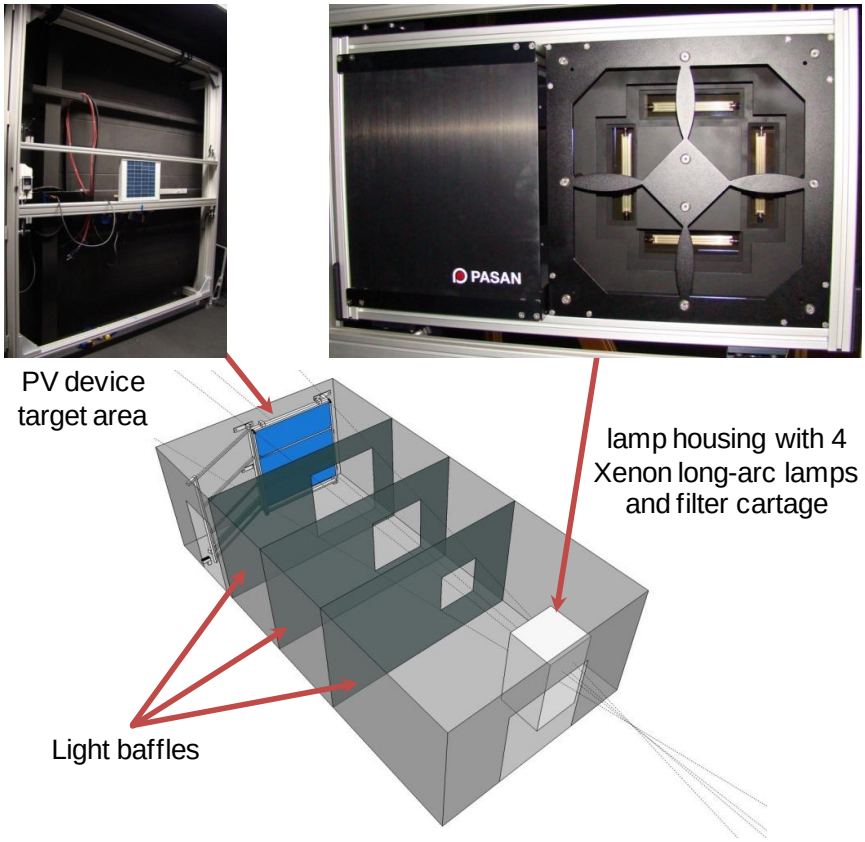

Figure 3.4: Pasan Sun Simulator IIIb in operation at CREST; shown is the room layout with pointers to the main parts

One advantage of flash simulators is that the heat-up of the test device is negligible, due to the short flash time. Furthermore, the operation and maintenance costs of this type of simulator are far lower than those of steady state simulators with the same measurement area, because light bulbs have around 10,000 flashes lifetime (varying between different lamps) and the energy needed during operation is far lower.

Problematic in flash solar simulators (or Xenon flash lamps in general) is that the output spectrum changes with the operating voltage (i.e. when adjusting the light intensity) and that the spectrum changes over the lifetime of a single pulse, which can have an impact on the measurement result, especially when testing multi-junction solar cells, as the junction current balance changes during a measurement [54, 55].

Other disadvantages are the high voltage sweep rates and the rapidly changing light output. This can cause capacitive effects on slow responding PV devices and skew the I-V curve effecting P_{MP}, FF and V_{OC} significantly.

This occurs if the measurement speed is too fast or if the measurement is triggered too early [56-59]. The effect is due to the total capacitance of a PV device consisting of two parts: The junction capacitance and the free carrier capacitance. Free carrier capacitance is voltage dependent and increases exponentially with increasing voltage [59]. Sweeping too fast in forward direction from short circuit to open circuit voltage increases capacitance rapidly with voltage, resulting in a charge-up of the device and in a reduction of the actual measured current at the load. While sweeping too fast in the other direction has the reverse effect: the PV device capacitance is high and reducing the voltage decreases free carrier capacitance and releases the stored energy. Thus a higher current is measured at the load. Any effects due to capacitance can be determined by tracing the I-V curve in both directions and checking for hysteresis. Figure 3.5 shows a diagram of capacitance effects in I-V measurements taken with too fast voltage sweeps in reverse and forward direction [57]. Materials known with slow optical and electrical responses are dye sensitised devices and high efficiency crystalline devices.

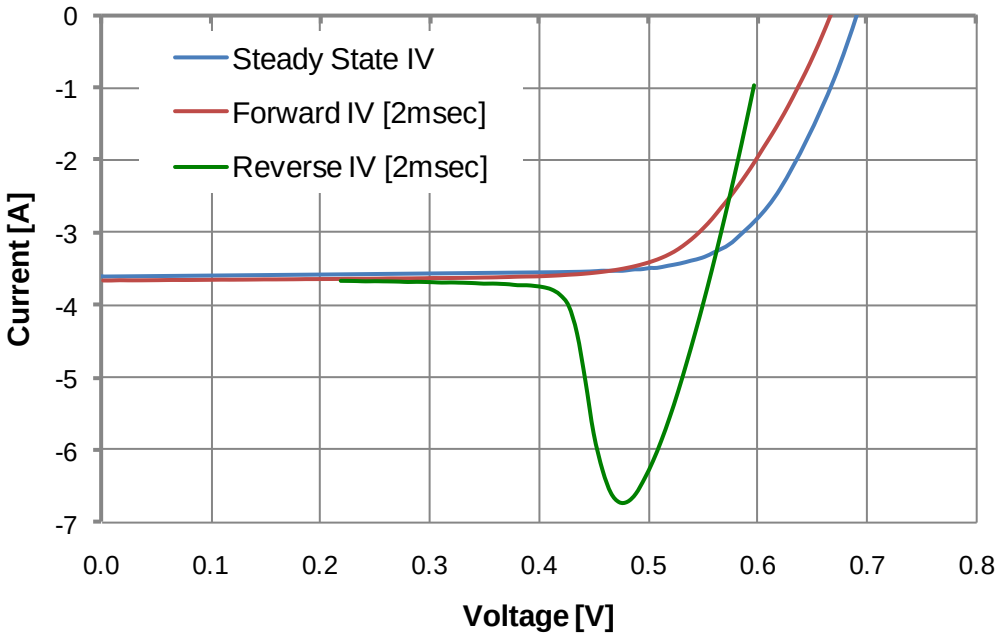

Figure 3.5: Capacitance effects during too fast I-V sweeps

Flash solar simulators are, as steady state simulators, mostly used for power rating at STC. Their application in energy rating is also limited to adjustments

in irradiance via optical filters and lamp voltage and temperature, if a temperature control system is available.

3.1.4 Temperature control and measurement

In most solar simulators, the reference cell for measuring irradiance is temperature controlled to a junction temperature at STC conditions of 25°C for compensating temperature coefficients of the cell and thus allowing more accurate measurements [60]. The cell is mounted on a temperature-controlled plate and can be cooled or heated with conditioned air or gas ventilation, by water circulation or, most reliably, by thermoelectric element. The regulation feedback is enabled by measuring the temperature with a thermistor, thermocouple or via resistive temperature dependent (RTD) platinum resistor.

Because of the large size of the test cell or PV module it is ineffective to control the temperature by thermoelectric element. For this are three different methods in use:

- using a water circulation plate under the test device, which is most suitable for flat test cells
- via blown air table, as used in the TÜV Rheinland steady state simulator described in section 3.1.2, which is also suitable for large modules that are not completely flat
- employing an environmental chamber with conditioned air flow, which provides the best temperature control, because of the isolation to the environment, but has the disadvantage of possible spectral adulteration of the simulator light which has to pass through the chamber glass

3.1.5 Current - Voltage measurements

The most common way of assessing the performance of a solar cell is the measurement of its current – voltage (I-V) characteristic. In principle this is done by setting the device operating point in steps from short circuit to open

circuit (or in the opposite direction) with an I-V tracing load and recording at each step the device current and voltage. The main techniques in use to set the device operating points are:

- Static, via switching through a number of resistors as used by TÜV Rheinland [42]
- Passive, with a variable transistor-controlled load resistance (such as explained in [61]) or with a variable DC-DC converter [62]
- Active, via a 4-quadrant power supply as used on the outdoor measurement system in CREST

The control range of all three techniques is illustrated in Figure 3.6. The method of most interest in this work is the active I-V tracing. The advantage of this technique is that a 4-quadrant power supply can both source and sink power. In this way the I-V curve can be traced into the adjacent quadrants over the open circuit and short circuit points. Furthermore, dark I-V curves can be recorded. More details regarding I-V tracing hardware can be found in the review by Duran et al. [63].

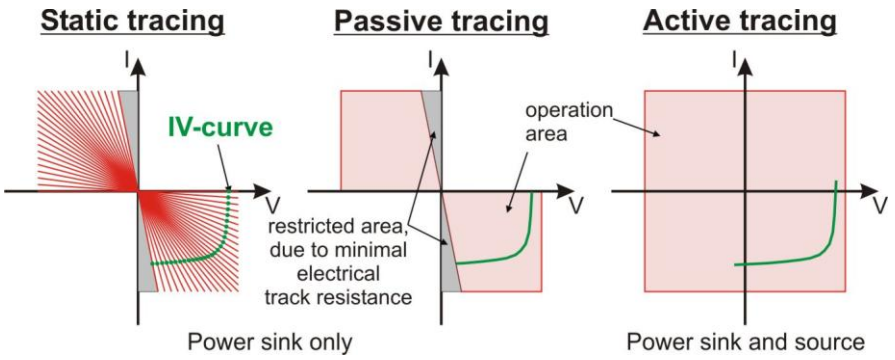

Figure 3.6: I-V tracing measurement techniques

If an I-V curve is measured in 2-wire configuration, the FF and P_{MP} of the device under test are underestimated depending on the device I_{MP} and the contact resistances. To overcome this problem I-V characteristics are in most cases measured in 4-wire setup to ensure that the correct voltage on the test device is measured at any given current flow. Figure 3.7 illustrates the problems arising from 2-wire measurements.

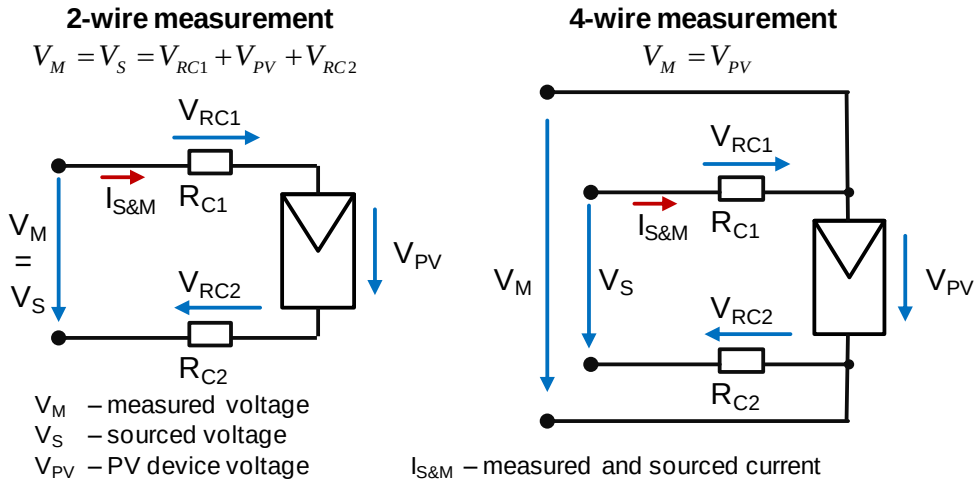

Figure 3.7: Comparison of 2-wire and 4-wrie I-V measurement; using 4-wire connection to the test device reduces uncertainties in determination of the maximum power and fill factor

3.2 LEDs as solar simulator light sources

3.2.1 Characteristics of LEDs

A light-emitting diode (LED) is a semiconductor diode that emits a narrow-spectrum light when electrically biased in the forward direction of the p-n junction. This effect is called electroluminescence.

Due to their unique characteristics, LEDs have many advantages over conventional light sources used in today's solar simulators. They also have characteristics which can lead to problems and uncertainties when left unattended and used in a solar simulator. However, these are engineering issues and can be overcome with by using good design and appropriate electronics.

Advantages:

First of all LEDs react and can be regulated accurately in matters of microseconds (see Figure 3.8 for the measured light control step response in the LED-based solar simulator). LEDs also can be kept stable at a given light output intensity continuously for very long times as long as appropriate control and regulation electronics are employed. Thus, a flash solar simulator can be combined with a steady state solar simulator with additional functions

as such as variable pulse length and shape. Hence, capacitive effects as seen with the use of flash simulators can be prevented, minimising thermal changes of the device compared to the steady state simulator. It also opens possibilities to measure and investigate these effects. A further application would be to investigate preconditioning and sweep rate effects on solar cells as such as CIS [64]. The high stability of LEDs would also overcome instabilities in conventional lamps, such as arc-jumping of xenon arc lamps [47] and are thus a very attractive solution for increasing measurement accuracy.

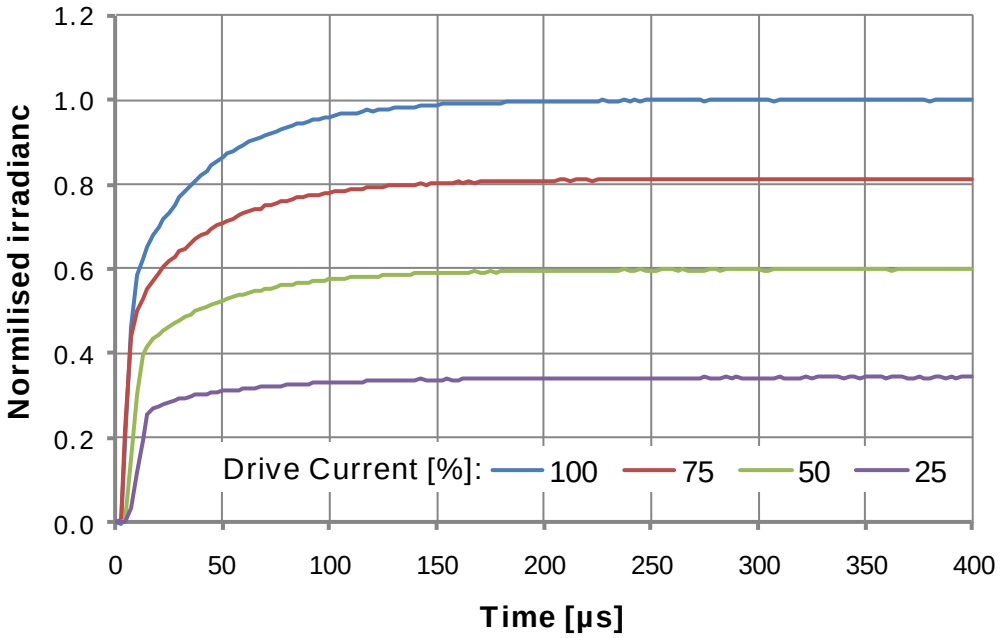

Figure 3.8: Control speed of LEDs in LED-based solar simulator at various current regulation step responses

The second advantage is that LEDs have a relatively narrow, almost monochromatic, output spectrum (except for white LEDs) and are available in a wide variety of colours and wavelengths from ultraviolet to infrared, although anything outside the visible range is seen as a specialist item and thus is very costly. An individual LED cannot meet the spectral standard for solar simulation, but combining a number of different colours opens the possibility of creating a closely-matched AM 1.5G spectrum. Such a combination also provides the ideal base for high variability of the simulator output spectrum, due to the ability to dim LEDs by regulating the current flow.

By adjusting the intensity of each colour, PV devices can be measured under red-rich spectra as during sun set or under blue-rich cloudy conditions rather than only at AM 1.5G. In other words, it allows the possibility of measuring device characteristics for energy yield prediction with varying spectra under more realistic light conditions. Also, a variable spectrum enables at the same time accurate characterisation of multi-junction photovoltaic devices. The incident spectrum could be changed easily so that all junctions operate under the same current balance as it would have under reference sunlight. With a large number of separately controllable narrow wavelength band LED colours it is also possible to measure spectral response of solar cells as presented in references [65, 66]. Additional information on measurements of multi-junction devices and spectral response is provided in chapter 5.

Thirdly, recent developments in new high power LEDs have improved the light intensity, efficiency and power output of LEDs immensely. Bundled in arrays, they have the potential for reaching intensity levels of more than 1000W/m^2, as required for STC power rating. The very long lifetime of LEDs is a further advantage to other light sources on the market. At up to 100.000h [67] (dependent on type and production quality) it surpasses multiple replacements of flash or steady state sources, which not only compensates the initial higher cost per light intensity but also means less maintenance, recalibration and reclassification costs and downtime.

Drawbacks:

A minor drawback is the slight nonlinearity of the LEDs light intensity versus its drive current. LEDs are more efficient at low drive currents than at high ones, which means that the relative intensity increase is lower at high current than at low drive current. This is a minor problem that either can be calibrated out or can be overcome by a direct intensity regulation. Figure 4.6 in the following chapter 4 illustrates the nonlinear response over drive current.

One drawback of LED characteristics is that despite being very efficient light sources, they tend to get very hot and need rapid and efficient cooling. Due to the negative voltage temperature coefficient, the LEDs light output energy and efficiency drops with rising operating temperature of the dye. This can

lead directly to temporal light instability during I-V measurements when the LED is current regulated. Figure 3.9 illustrates this effect on cyan LEDs. The voltage temperature coefficient generally increases with wavelength, which means that red and infrared LEDs are more affected than blue ones (as also shown in the datasheets of LUXEON LEDs [67]). The output efficiency and intensity drop can be overcome with a direct irradiance regulation, which simply increases power input to overcome the light energy output change.

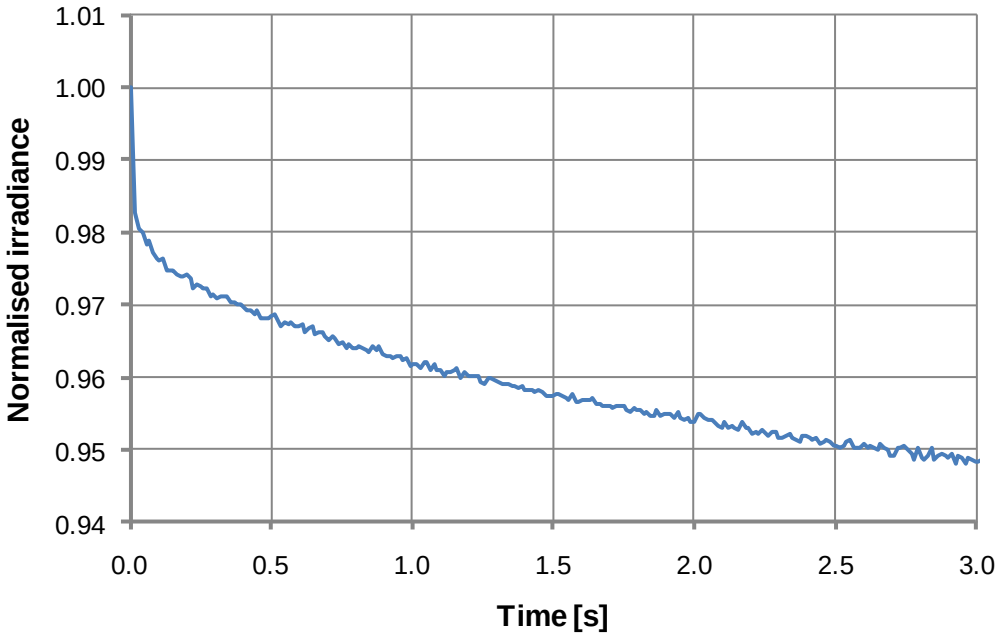

Figure 3.9: Initial drop in intensity due to increasing operation temperature of current regulated cyan LEDs; measured in the LED-based solar simulator

The dominant output wavelength or peak wavelength is also affected by temperature. An increase in temperature means that the spectral output of the LED shifts slightly into higher wavelengths. Although the wavelength shift with temperature is negligibly small (see Figure 3.10 for cyan LEDs), good cooling of LEDs is essential and at the same time reduces intensity drop and increases lifetime.

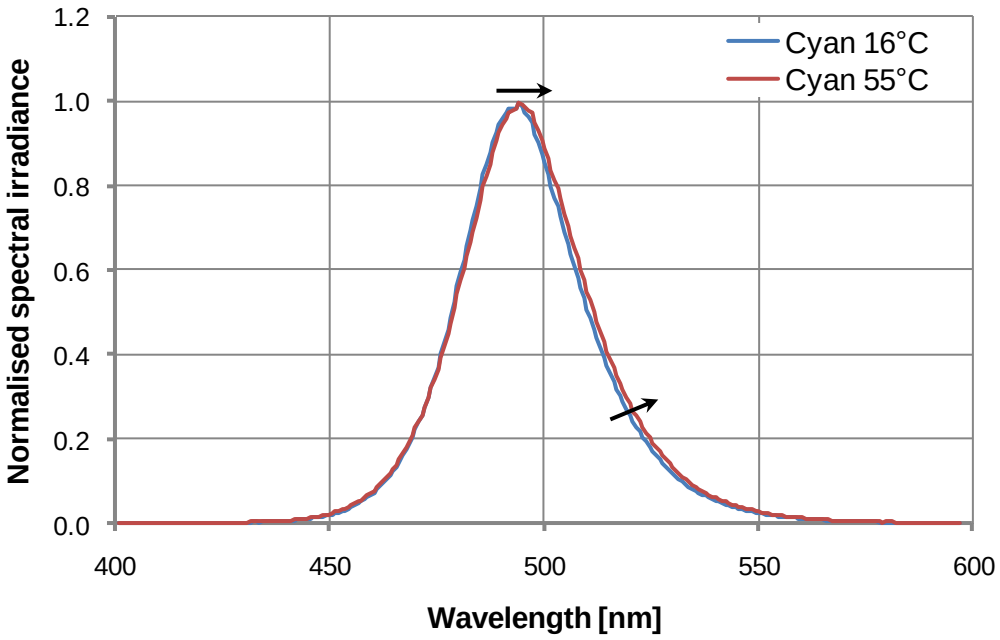

Figure 3.10: Spectral output of cyan LEDs at different dye operation temperatures; the dominant wavelength shifts by about 1nm and the spectral emission curve slightly widens

As with all light sources, LEDs also show some dependence of the relative spectral output on drive current. As illustrated in Figure 3.11, it has been observed that the spectrum slightly shifts into the lower wavelength region for cyan LEDs. However, this effect also depends on the material and peak wavelength of the LED. Red LEDs shift slightly into higher wavelength region (section 4.3.3 of [68]). Compared to spectral changes seen from other light sources as such as halogen, the effect is very small and LEDs are in general seen as being virtually unaffected from spectral change due to dimming. Nevertheless, the highest accuracy during characterisation of photovoltaic devices can be achieved by monitoring not only the irradiance but also the output spectrum of the simulator.

An unavoidable disadvantage is the degradation of LEDs throughout their lifetime. Degradation-rate depends very largely on the operating temperature of the LED and the effect can be largely reduced by appropriate cooling and by operating the LED at lower currents than rated [69]. Since the degradation effect can only be reduced, the main solution is a system designed to initially supply higher irradiances than required under STC and for energy rating, so required conditions can still be applied when the LEDs have degraded to a

large percentage. While the effect of degradation is clearly not desirable, degradation is also seen with conventional light sources.

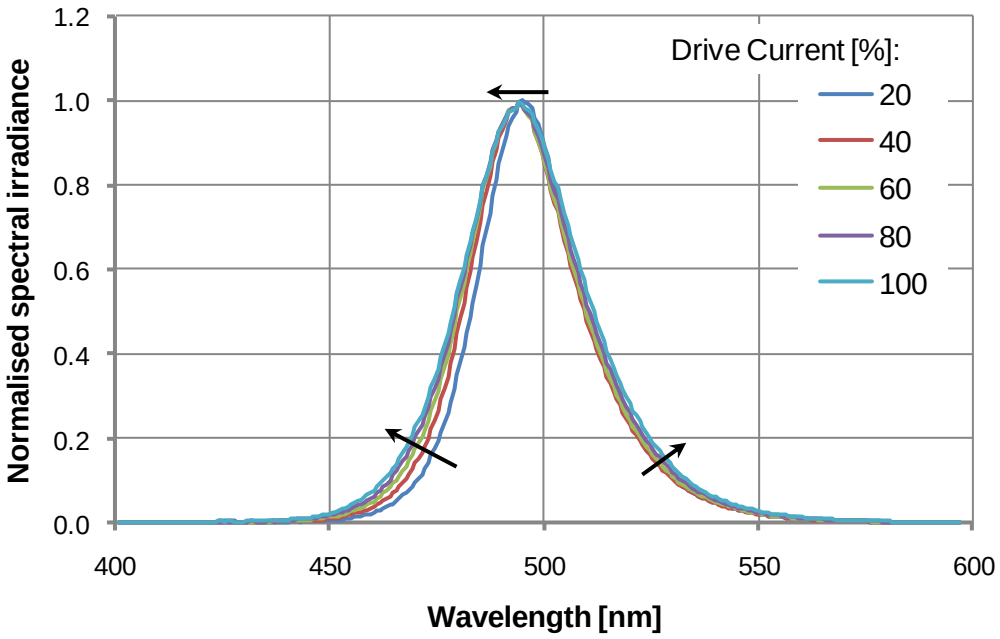

Figure 3.11: Normalised spectral output of cyan LEDs at different intensities; spectral output slightly widens in direction to the blue region of the spectrum, dominant wavelength shifts about 5nm lower

Conclusion on LED characteristics:

LEDs are a good candidate for an advanced solar simulator that is capable of measuring characteristics of all PV device types and materials. Furthermore, the light control opens the possibility to fully characterise a PV device indoors much faster than is possible today using outdoor measurements.

3.2.2 Existing LED solar simulators

Two LED simulators have been developed in the years prior to the completion of the major work on the LED-based solar simulator presented here (1st results published December 2007 at the 17th International Photovoltaic Science and Engineering Conference in Fukuoka, Japan). Strictly speaking, these systems are not solar simulators, as they do not meet the requirements set out on the properties of the spectral output allowable for

a solar simulator [70]. Nevertheless, these are the first steps taken in the direction of a new technology with high potential and much has been learned from the publications of the early versions of such systems.

One LED simulator was developed at the Tokyo University of Agriculture and Technology [71] and a second one in Germany at Institut für Solarenergieforschung Hameln/Emmerthal [72] in conjunction with Halm Electronics. The basic schematic of an LED simulator (Figure 3.12) is not fundamentally different from conventional simulators. The main difference is that many LEDs in different colours are used instead of one or more conventional light sources. The different colours mix on the test area that holds the solar cell and give in the ideal case a uniform irradiance and spectral distribution. A noticeable difference is the much smaller distance between the LED array and the test cell on the early systems (84mm for the simulator at Tokyo University), because otherwise these would not achieve any useful levels of irradiance.

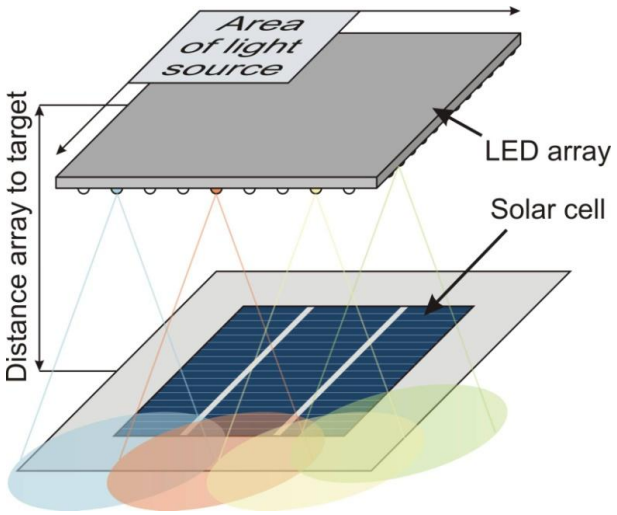

Figure 3.12: Basic schematic diagram of an LED simulator

The discrete-wavelength LED simulator at Tokyo University operates 784 low current LEDs on an area of 205x205mm^2 with a maximum irradiance of approximately 100W/m^2 (one tenth of a sun). It uses four LED colours: blue, red, infrared and white. Early measurements results published did show that I-V curves extrapolated to 1-sun (1000W/m^2) where underestimating the I-V characteristic compared to measurements of a conventional solar simulator.

This initial problem was later corrected by applying better methods for irradiance correction [73].

A three colour (Blue, Red and Infrared) LED flasher array (LFA) was developed in Germany. The paper by Grischke [72] stated that simulation results showed an expected error below that of today's standard flash light sources with the potential to outperform conventional flash simulators, in spite of the discrete and very different spectrum to other light sources. A six colour version of the LFA was planned and expected to reach class A certification. Class A spectral match is possible by using one colour for each of the wavelength bins of the spectral match classification table, but the LEDs bandwidth is not wide enough to cover 400-1100nm with 6 colours in a continuous spectrum [72]. More information on spectral match can be found in section 4.1.1 and in Table 4.2. The publication by Grischke was the only one found of this working group.

A drawback of both systems is that the irradiance achieved is low compared to other simulators. Additionally, the intensity uniformity and spectral uniformity on the test cell is strongly dependent on the array size and distance between LEDs of the same colour. Since the distance to the target is small, this problem is much worse. Another main drawback of these early LED simulators is the fact that they do not use a sufficient number of colours to produce a continuous-wavelength light output, which is the largest source of uncertainty for I-V measurements and spectral mismatch correction.

3.2.3 Implementation of the new LED-based solar simulator prototype

Analysing the LED characteristics, predecessor LED simulator systems and the current state-of-the-art in conventional solar simulators has lead to a range of ideas and improvements that have been implemented into the LED-based simulator prototype system.

The main improvement to existing LED systems was to change the discrete-wavelength spectral output to a quasi-continuous-wavelength design that has the potential to closely match the total AM 1.5G sunlight spectrum and meet

the IEC requirements in spectral match. This also meant an implementation of electronic control for functions such as variability of spectrum, intensity, flash speed and shape as described earlier in this chapter.

Existing versions of LED solar simulators have used low current LEDs, but even replacing them with high current ones would require a large number of LEDs, because intensity levels also need to increase by a factor of 10 to meet STC. The problem identified at this point was that it can cause non-uniformity over the test area (spectral as well as intensity), which is the largest factor reducing measurement quality and increasing uncertainty of any calibration. Two solutions have been found for avoiding this: Improved optics, which first of all mix all the different colours and secondly spread the light homogenously over the illumination area, or manually adjustable electronic circuitry, which provides an intensity adjustment of every single LED. As further explained in this chapter, the 2nd option was chosen in the presented prototype version for reasons of cost, development time and the need for a first proof of concept with maximal control.

To meet the last STC requirement of 25°C test device temperature and to be able to measure at temperatures different from that, a temperature control and regulation system was also required for the new LED solar simulator.

To reduce complexity of the new solar simulator an angle of incidence (AOI) control system for energy rating characteristic measurements at varying angles was excluded at an early stage. Requirement for this is a rotating PV device target stage and a high uniformity not only in 2 dimensions over the flat illumination target but over the volume in which the PV device is tilted. Further information on AOI measurements can also be found in chapter 6.

Implementing all possible features and making the most out of the LEDs' potential can open the possibility for a wide range of research tasks with measurements of:

- Power rating at STC and other conditions
- Device performance measurements at varying irradiance, temperature and spectrum for energy yield prediction and energy rating (plus angle of incidence)

- Irradiance, temperature and spectral influences
- Quantum efficiency, spectral response
- Capacitive, preconditioning and degradation effects
- Light soaking, thermal annealing

Such a system could be used for measurements of single and multi-junction devices of all kinds of materials and structures. Not only would it enable one to do research in various different areas, but the system could also work automatically and combine the functionality of several different types of costly equipment which would have been needed in the laboratory to be able to carry out the same tasks.

3.3 Hardware description of the LED-based solar simulator

In this section, the hardware of the LED-based solar simulator prototype is described in detail. Additional information on circuit diagrams, PCB designs and wiring connections is given in Appendix A to Appendix K.

3.3.1 System overview

A solar simulator with variable spectrum, temperature, irradiance, flash speed and shape is a complex measurement system. To break down the complexity as a whole unit, the system has been separated into the following seven smaller parts:

- Simulator housing, with the light sources and the test PV device
- Light source power supplies and regulation system
- I-V tracing device and measurement
- PV device temperature control
- Water and air cooling system
- Power distribution system

- Control PC, the processing centre with additional DAQ cards.

The PC controls and monitors all parts of the simulator. The sub-systems are all linked together, take over different parts of the work in the complete system and guarantee full function of the solar simulator. Figure 3.13 shows a schematic hardware overview of the solar simulator with all sub-systems and how the different parts are linked together.

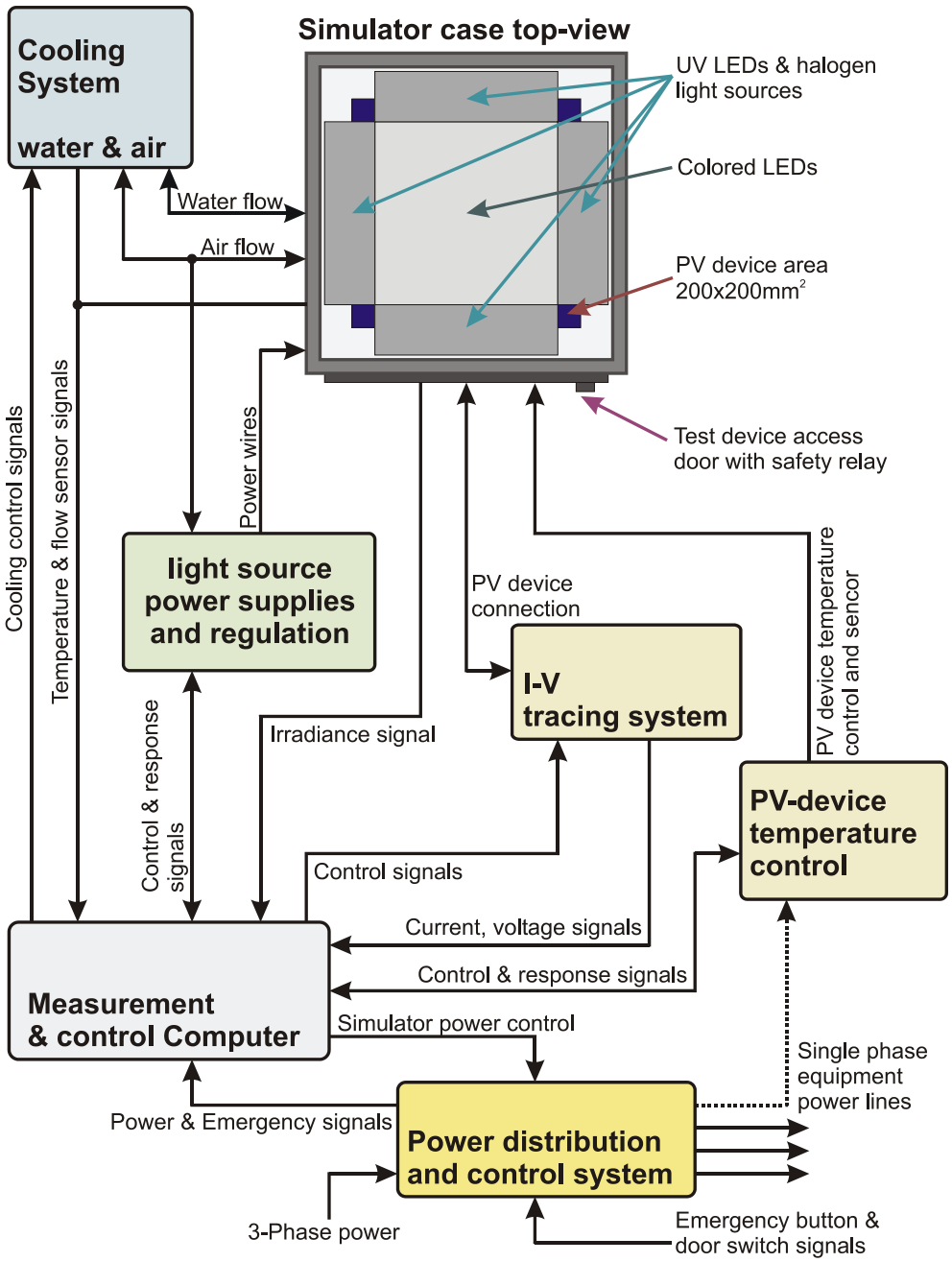

Figure 3.13: Schematic overview of the LED-based solar simulator with links between the sub-systems

Figure 3.14 illustrates a photograph of the solar simulator with pointers to the positions of each of the main parts.

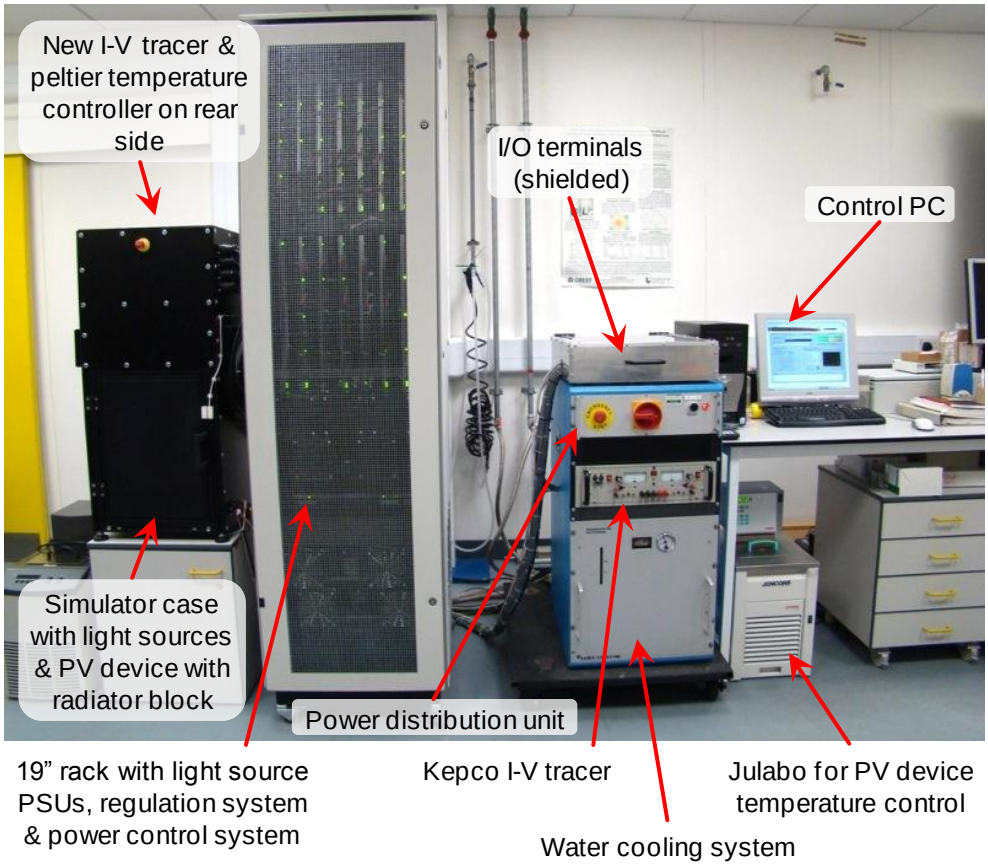

Figure 3.14: LED-based solar simulator prototype with parts description

3.3.2 Simulator housing with light sources

Light sources are the most important parts of a solar simulator. If the types and colours are not carefully chosen, measurement data quality can be very poor due to a large deviation of the output spectrum to the standard AM 1.5G spectrum. For this reason, different types of LEDs had been tested and their spectral outputs were measured. This data was used to simulate how many LEDs of which colours would be needed for a good fit to the target spectrum with its intensity.

One reason why earlier versions of LED simulators did not reach high intensity is because they used low power LEDs (<0.1W). This was changed here and only LEDs with at least 3W output power have been chosen.

Additionally, to reduce spectral variations between LEDs of the same colour, specially binned LEDs with the same dominant wavelength within (±5nm) have been used. Halogen light sources were chosen to represent the deep red and infrared part (IR) of the output spectrum. This was done to simplify the construction of the prototype and most critically, to reduce costs, as high power IR LEDs were then priced at over £200 per piece (20 to 40 times higher than the visible LEDs used). However, halogen lights can be replaced with LEDs in future versions of the simulator.

The final choice of LEDs consisted of 7 different narrowband colours and warm white to cover the light spectrum from ultraviolet (UV) at 375nm to red at about 680nm. Osram Ministar halogen lights have been chosen because of their small size. Halogen covers the spectrum above 680nm. Table 3.2 summarises which colours and manufacturers have been used with additional information on quantity, dominant wavelength / colour temperature and power output. Detailed information on the spectral output and irradiance achieved are included in chapter 4.

LED type	Colour	Dominant Wavelength	Power consumption	Quantity
Norlux	Ultraviolet	375nm	8W	24
Norlux	Ultraviolet	395nm	8W	24
Luxeon K2	Royal Blue	440nm	4W	21
Luxeon III	Royal Blue	460nm	4W	21
Luxeon III	Cyan	490nm	4W	21
Luxeon K2	Green	520nm	4W	24
Luxeon III	Green	545nm	4W	21
Upec	Warm White	2800 – 3200K	3W	214
Osram Ministar	Halogen	3000K	50W	24

Table 3.2: Final choice of LED colours and halogen lights; data in Kelvin defines colour temperature based on black body radiation.

The light engine in the simulator consists of two main parts: a main centre LED array and additional arrays on each side around the main array. All 322 LEDs in the visible colour range are mounted on the centre array over an

area of 280x280mm^2 on a printed circuit board (PCB). Mounting the LEDs evenly spread and equidistant to each other ensured an even light distribution with as little spectral change as possible over the target field without having to adjust the intensity of each LED. LEDs on the centre area have 6° optics fitted to concentrate light onto the PV device target area. Detailed drawings of the centre LED array PCB with colour distribution can be found in Appendix A and Appendix B.

The four side arrays are mounted on an adjustable angle to improve light intensity uniformity and spectral uniformity. Each side holds 12 UV LEDs (6 of each type) with additional 12° optics and 6 halogen lights. The total area of light sources is 380x380mm^2. A detailed drawing of the side arrays is given in Appendix C.

The complete array is mounted at around three-quarter height in the simulator housing at a distance of 650mm to the target area. The target area has been designed to fit test devices of up to 200x200mm^2 size. Figure 3.15 illustrates the mounting structure of the light sources and a picture of the array in the simulator is presented in Figure 3.16.

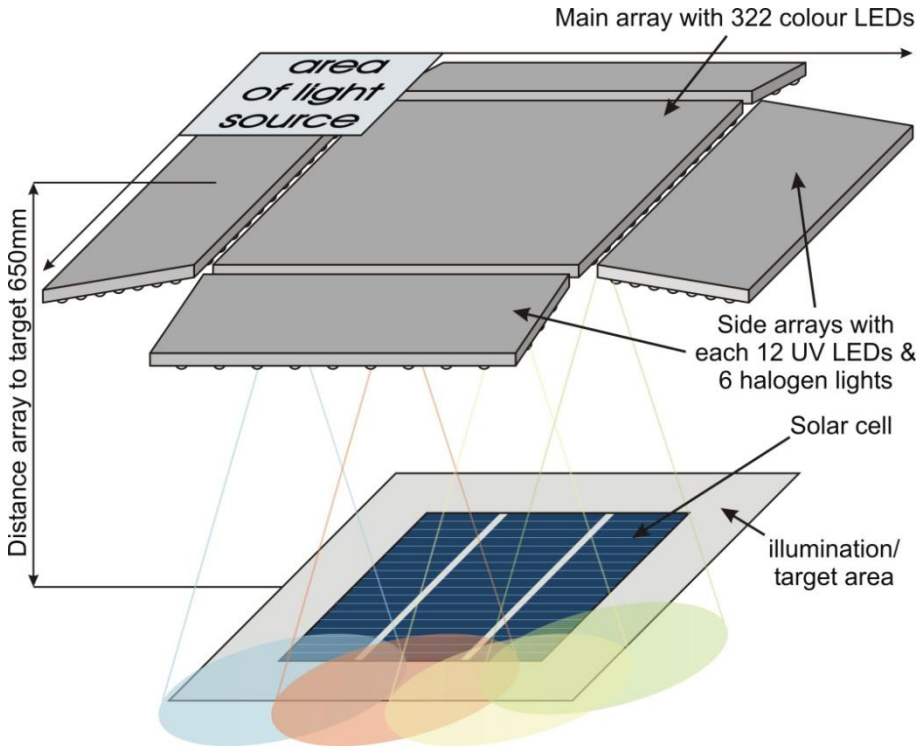

Figure 3.15: Light source mounting structure in the LED-based solar simulator

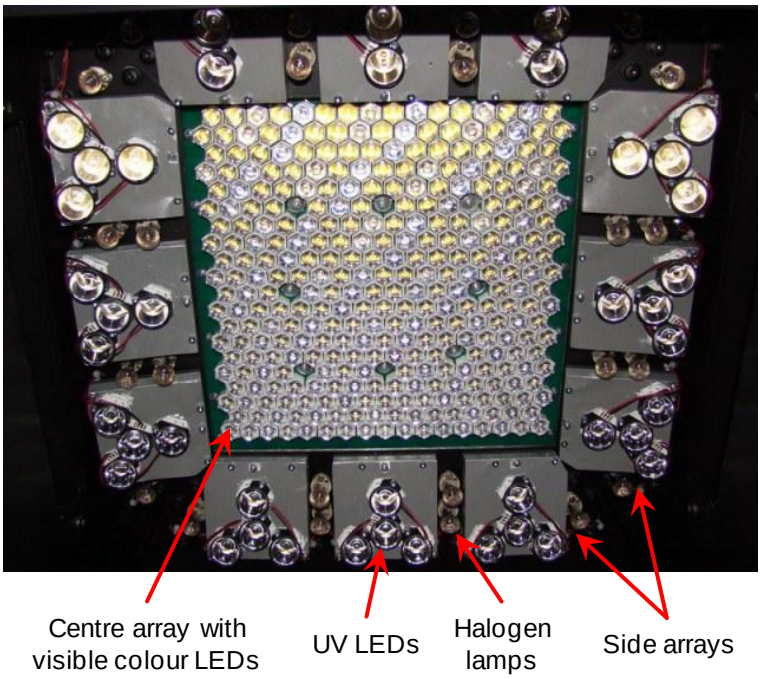

Figure 3.16: Picture of the LED array in the simulator

3.3.3 Light source control and regulation system

The light source control realises an independent control and adjustment of the intensities of all light source types and colours. Thus, it is the essential part that enables the spectral variability of the output spectrum.

As illustrated in Figure 3.17 the control system for the light sources consists of four individual parts:

- Power supplies for light sources (12V or 24V), amplifiers (±15V) and signal relays (12V).
- DC power cut-off boards for protection of the LEDs in case of a failure in the supply of the signal conditioning and current regulating amplifiers.
- Main control board for control mode switching and light source current regulation reference signal conditioning.
- Current regulation boards for regulating the output current of each LED and halogen light source.

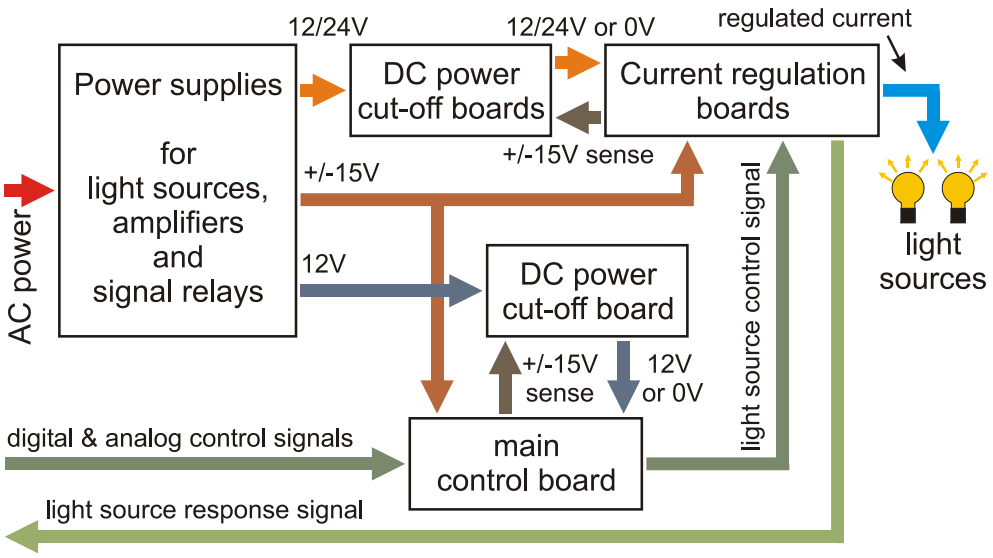

Figure 3.17: Light source control and regulation system overview with signal and power flow

Circuit diagrams of the DC power cut-off boards, main control board and current regulation board can be found in Appendix D to Appendix F.

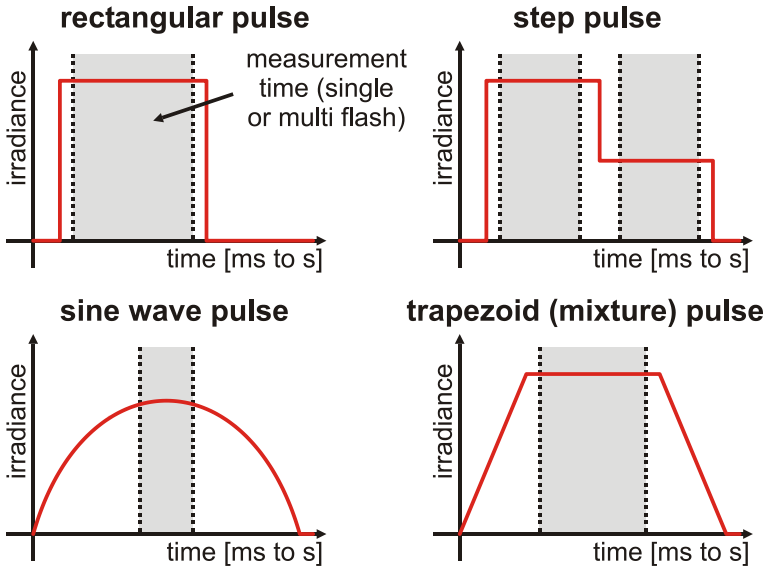

Figure 3.18: Light pulse shapes possible in the solar simulator

The light source control allows LED pulse frequencies of up to 1kHz in theoretically all imaginable pulse shapes (see Figure 3.18). Although the most useful and so far only implemented pulse shape in the system is the normal rectangular pulse. In this pulse form the I-V curve is measured in a single, light pulse of constant intensity. The length of the light pulse can be varied to reduce effects such as capacitance and module heat-up. However,

multiple flashes and other pulse shapes are easily implemented and rely purely on software programming.

To ensure maximum flexibility in spectral output control, each colour can be separately configured for static or dynamic control mode. In static control, the light source type is held in an adjustable intensity stably over the whole measurement time. In dynamic mode, the light source is controlled during the measurement by an analogue intensity control signal. This signal is the same for all light sources set into dynamic mode, but each light source type can have a different amplification to its signal, which allows setting of a certain spectral distributions during a dynamic flash measurement. In a normal I-V measurement, halogen lights are driven in static mode, to give them a longer start-up time and LEDs are driven in rectangular pulse in dynamic mode.

All light sources are individually current regulated. The relative intensity of each light source can also be adjusted manually on the current regulation circuit boards, so that the homogeneity of light intensity over the illumination area can be maximized.

3.3.4 Current-voltage tracing and measurement

The original layout used a 4-quadrant Kepco BOP 50-8M power supply for I-V tracing. This system was capable of tracing the I-V curve within a range of ±50V and ±8A. The Kepco unit was at a later stage replaced by a new in-house built 4-quadrant I-V tracer. The new system was designed and constructed as part of this work during the optimisation process of the measurement system and has been implemented for several reasons:

- To solve stability issues of the previously used power supply unit (PSU) when using solar cells with high capacity.
- To fully control the output of the I-V tracer in 4-wire set-up, as in the previous system the I-V curve could only be measured in 4-wire but was traced in 2-wire because of a voltage transient dependent leakage current into the sense terminals of the Kepco power supply that effected measurement accuracy.

- To improve measurement and I-V tracing accuracy, because the Kepco had a high output noise and ripple and too large tracing ranges for the size of PV devices measurable in the simulator.

Problems in the above areas were either eliminated or much reduced with the new I-V tracing system and control and measurement could be done accurately in all 4-quadrants in a 4-wire arrangement. This eliminated the risk of damaging the device due to high reverse voltage control when changing the light intensity without adjusting the tracing range. The unit (see photo in Figure 3.19) is capable of tracing I-V curves within a range of ±10V and ±1.8A. To protect the solar cell, the system has individually adjustable compliance limits for positive and negative voltage and current, which are controlled via USB connection. The output voltage is directly controlled by analogue signal. A simplified circuit diagram of the I-V tracer can be found in Appendix G.

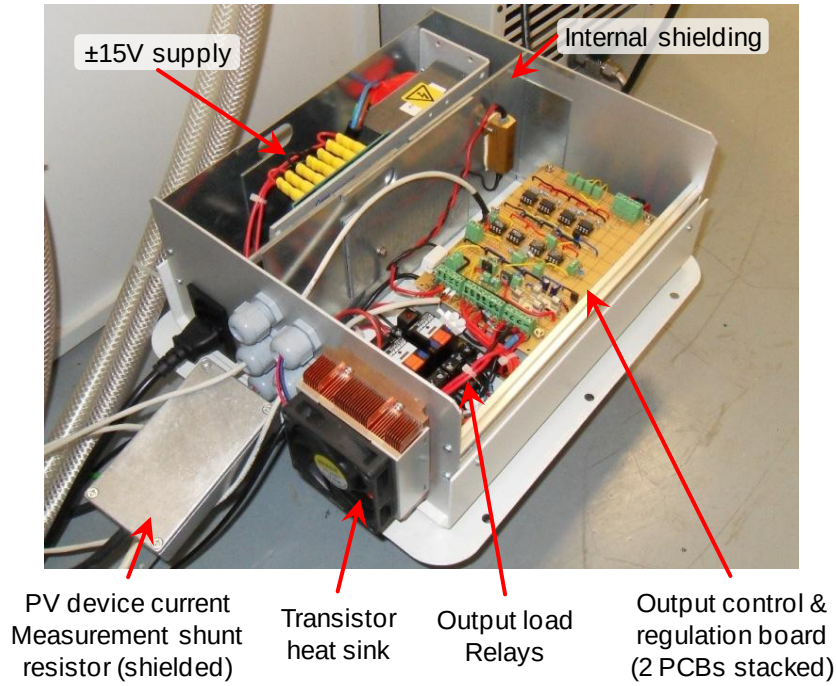

Figure 3.19: 4-quadrant power supply for I-V tracing (lid taken off)

Current and voltage measurements are taken with a PCI-6120 S-series multifunction DAQ card. This is a 4-channel simultaneous measurement card from national instruments (NI). The card measures up to 800k samples per second (once every 1.25µs) at a resolution of 16bits [74]. The signals are

preconditioned with differential amplifiers. For voltage measurements, a unity gain amplifier is used. PV device current is measured over a 1Ω shunt resistor. The signal is then amplified by a factor of 3.3 before it goes to the DAQ card. Irradiance and light stability can be measured with two independent sensors or reference cells. Currently a Kipp & Zonen SPlite sensor is used to measure light stability. The measurement range can be controlled on the DAQ card itself in six steps from ±0.2V to ±10V.

3.3.5 Temperature control and measurement

The PV device temperature in the simulator is controlled by two different systems that are used dependent on the size of the solar cell or mini module. A water circulator with radiator block is used for devices larger than 90x90mm^2 and a peltier stage control system for smaller devices.

Figure 3.20: Left: aluminium radiator block (before painted black), Right: Julabo cooler and heater

The control system for larger devices consists of a remotely controllable Julabo F32 cooling and heating water circulator and a custom made water radiator aluminium block, on which the test device is positioned. The water circulates from the Julabo unit through the radiator block at the bottom of the simulator case and back. Figure 3.20 shows the aluminium radiator block and the Julabo unit. With a heating and cooling power of 2kW and 450W respectively, the Julabo can operate at temperatures in the range of -20°C to 240°C [75]. However, the usable range is restricted by the liquids freezing

and boiling point and the thermal properties of the external components. The range is currently limited to 15°C and 95°C because water is used as circulating liquid and higher temperatures might result in water boiling and lower temperatures would result in condensation on the PV device.

The majority of the work anticipated is carried out on smaller devices. This allowed the introduction of a peltier stage to overcome the slow response of the Julabo unit's temperature control. The system developed and constructed throughout this work consists of two main parts: a peltier stage heater/cooler and a controller. The heater/cooler consists of four peltier elements connected in series which are loosely sandwiched between two aluminium plates to allow for thermal expansion and contraction. The controller (shown in Figure 3.21) is capable of controlling the PV device temperature accurately within a range of 0°C to 80°C in 0.1°C steps, albeit only temperatures above 15°C are used. The unit is fully controlled via USB and utilises a digital P-I (proportional-integrator) controller on a microcontroller to regulate the power input to the peltier devices (see Appendix H for a simplified circuit diagram). A K-type thermocouple placed under the PV device is used to read out the temperature.

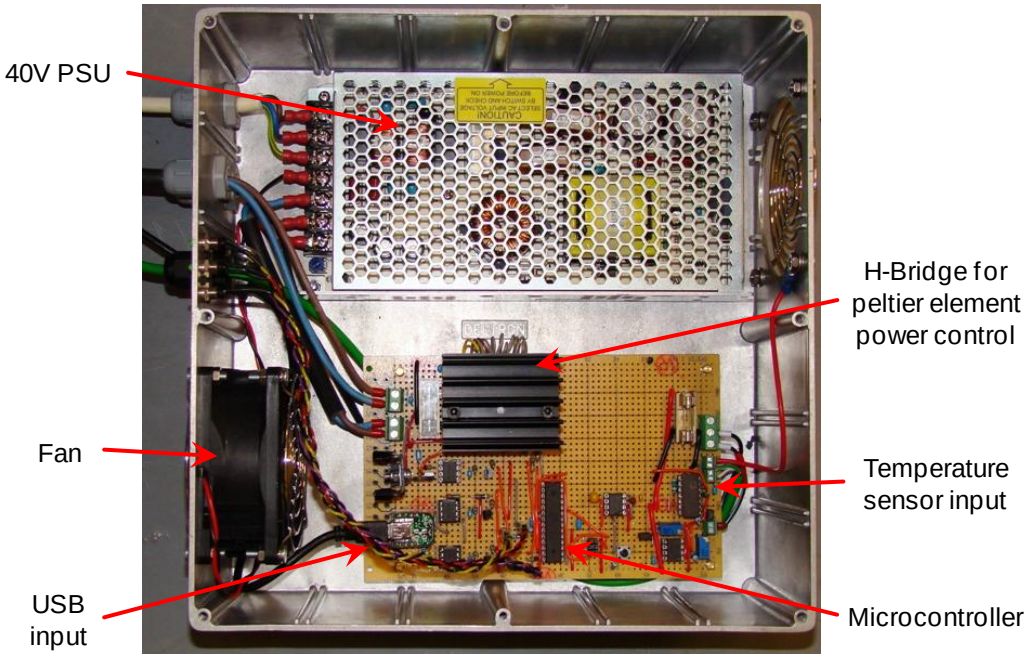

Figure 3.21: Peltier stage temperature control unit (lid taken off)

The remaining air gaps between the device under test and the peltier radiator are filled with thermal gap filling sheets. This reduces the thermal resistance from the peltier stage to the device and ensures that the temperature distribution on the device is even. Additional stability is achieved due to the fact that the peltier stage is positioned on top of the aluminium radiator block that is kept at a constant temperature by the Julabo unit.

3.3.6 Water and Air cooling system

Light sources, current regulation boards and other equipment in the simulator could not be operated continuously without cooling and some of the electronic parts would overheat after a short operation time. The simulator cooling system consists of two main parts: the water cooling system and the simulator case and equipment rack air cooling.

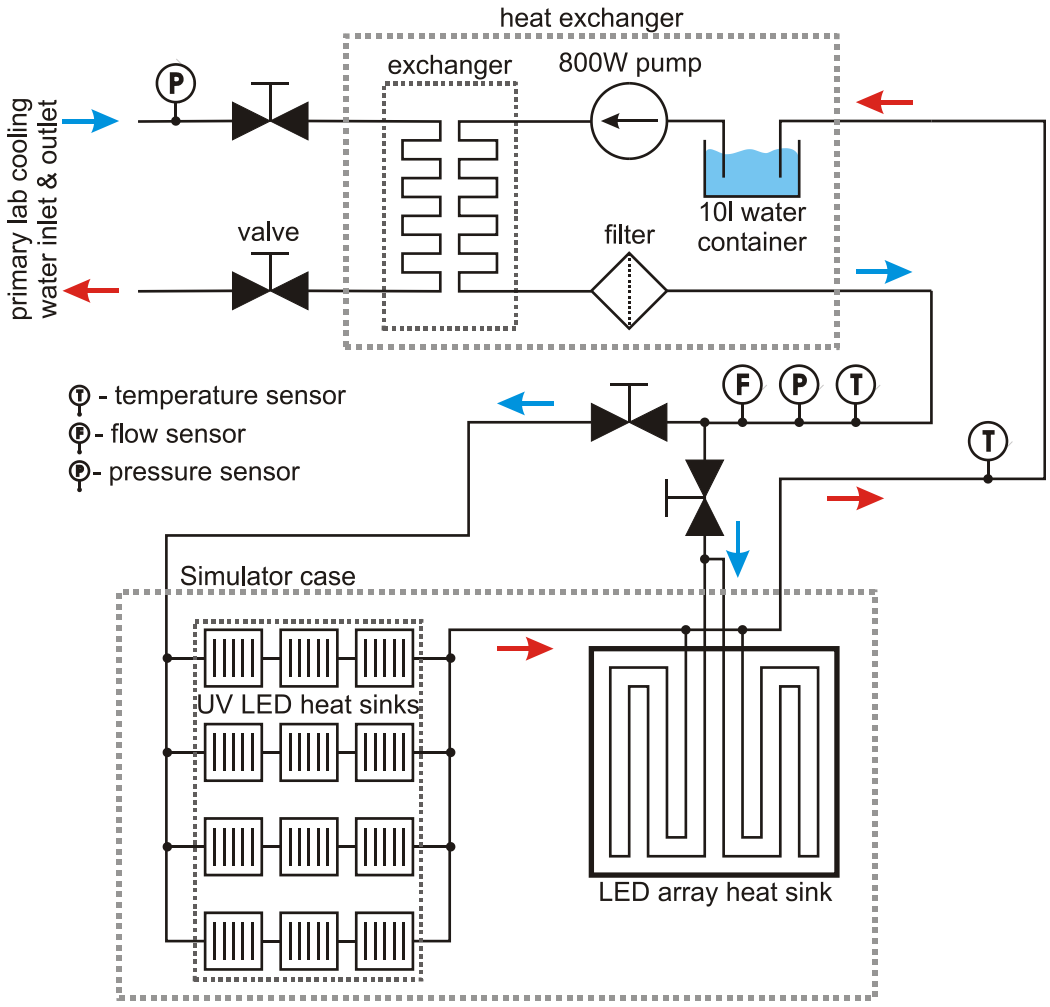

Figure 3.22: Water cooling system flow chart

The 370 LEDs in the system use approximately 1.6kW of electricity when running at full power. To ensure that the solar simulator can run in steady state for a long time, a water cooling system was installed. This system does not run directly off a chiller unit, instead a heat exchanger transfers waste heat from the secondary LED cooling circuit to the primary water cooling supply of the lab. To ensure optimum cooling performance, the centre LED array has all LEDs mounted on a PCB with a 5mm hole under each LED. The water cooling block fits through these holes, so that the LED sits directly on the aluminium surface with just an insulation sheet and thermal paste in-between. Additionally, UV LEDs are mounted on three smaller heat sinks on each of the four sides. The water temperature is monitored with a K-type thermocouple at the secondary water inlet and outlet. The complete cooling circuit is presented in Figure 3.22.

Since the solar simulator also houses approximately 1.2kW of halogen light sources, the simulator case is also convectively cooled to keep the surrounding parts from overheating. This is done via four 240V AC fans on top of the simulator. Ventilation holes are installed on three of the four sides of the simulator case. Those are fitted with blinds to let air in but not any light out or in. A significant amount of waste heat is also generated by the regulation electronics and power supplies. To keep components as cool as possible the 19” rack system houses 27 cooling fans. The air temperature in the simulator case and equipment rack is monitored by three PT100 temperature sensors.

3.3.7 Power distribution and control system

The prototype version of the solar simulator is unfortunately not the most power efficient system. The estimated energy requirement is 13kW when running at full power. This amount of energy is difficult to deliver by 13A sockets. Instead, a 32A 3-phase power output socket is used to supply most of the equipment. This required a designated power distribution system that consists of two main parts: a power distribution unit and a power control unit.

The power distribution unit has been built into the upper section of the 19” rack with the heat exchanger. This unit distributes the power from the 3-

phase power input in a star connection (240V phase to neutral) to most of the system components and in a delta set-up (415V phase to phase) to the pump of the heat exchanger. The layout of the power distribution unit is given in Figure 3.23. A circuit diagram can be found in Appendix I. The only parts not supplied by the distribution unit are the measurement PC, the Julabo unit, the peltier temperature controller and the I-V tracer. The latter two were added at a later time, for which the distribution unit was not altered.

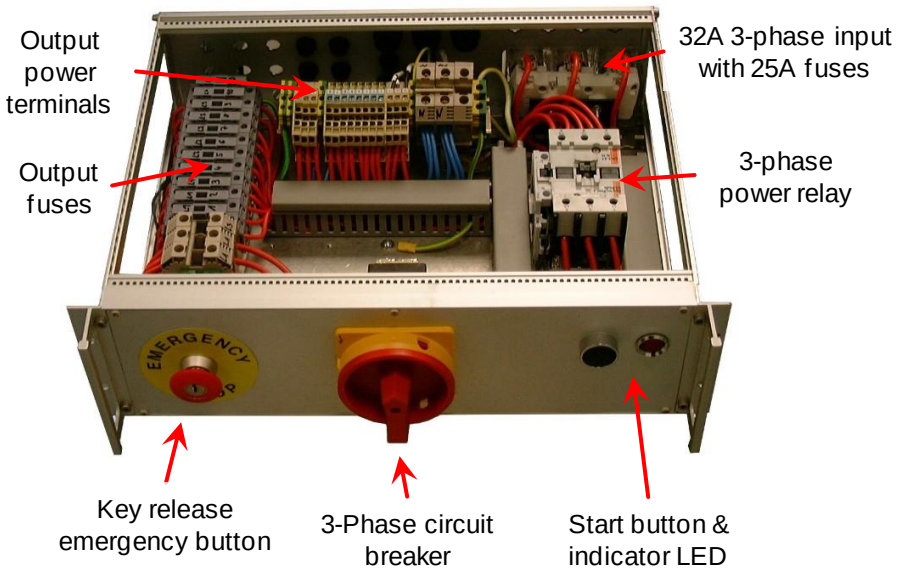

Figure 3.23: Layout of the power distribution unit

The power control system has four main tasks: controlling equipment power, setting power control interlocks, emergency button and door release actions and reporting to the measurement PC the simulator power status. The heart of the system is the power control board with a microcontroller that is controlled via direct serial input from the computer and responds with digital flags back to the PC. Figure 3.24 illustrates the structure and the operation principle of this system. A detailed circuit diagram and a picture of the power control board are attached in Appendix J.

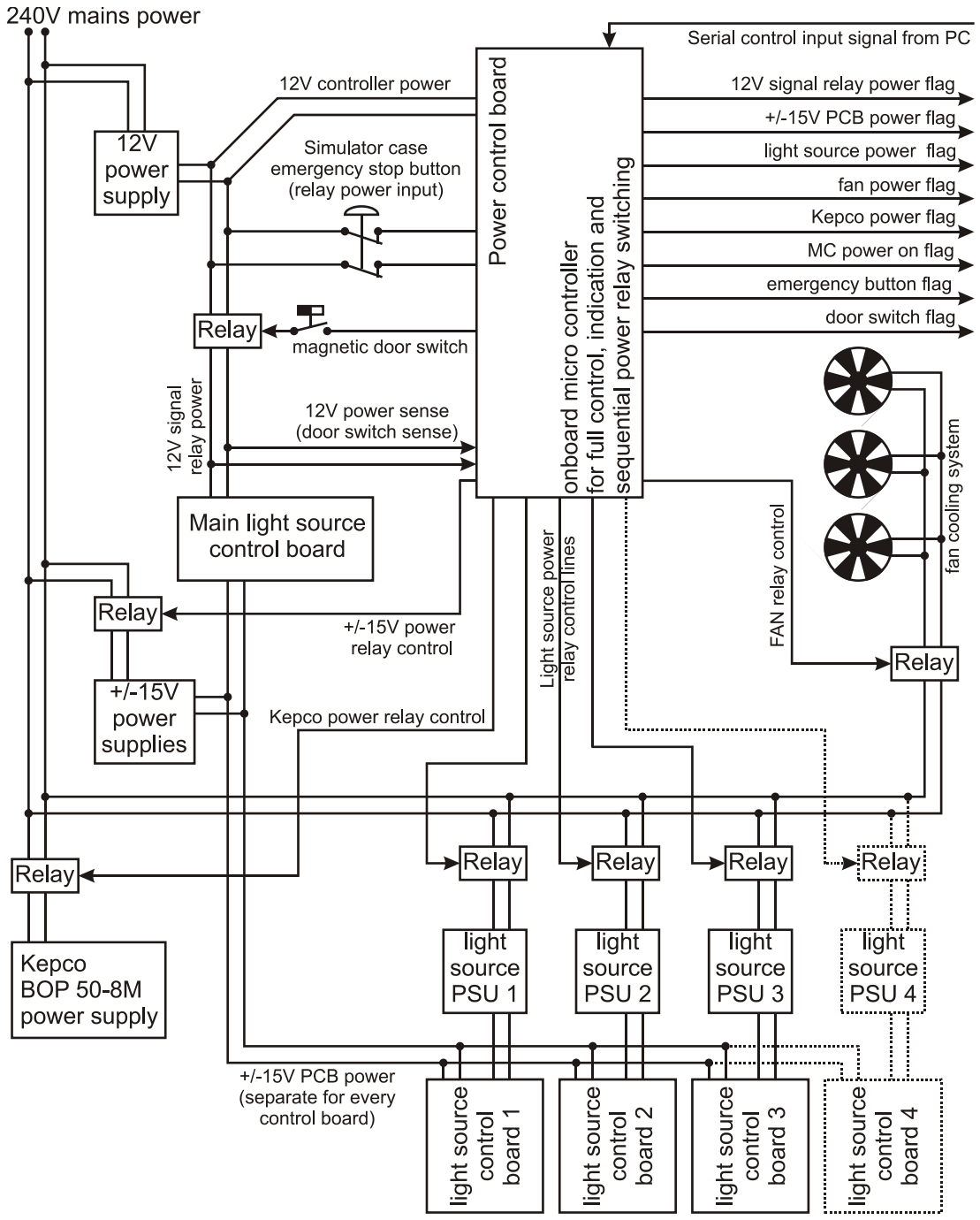

Figure 3.24: Schematic overview of the power control system

3.3.8 Measurement computer

Two measurement DAQ cards from NI built into the computer are the link between the hardware and the software part of the solar simulator. The first card is, as previously mentioned in section 3.3.4, a NI 6120 S-Series simultaneous multifunction DAQ card used for controlling the I-V tracing system and taking current, voltage and irradiance readings. The second is a

NI 6229 M-Series multifunction card with 32 analogue inputs and 48 digital input/output (DIO) channels. This card has several functions, such as communicating with the power control unit, setting of static light source control and amplification signals and simulator status monitoring.

Simulator status monitoring includes checking of power status, equipment temperatures, water cooling system flow rate and light source current flow. This is needed to make sure that all parts in the system work within their specifications and ensures that the system can be shut down automatically in case of a fault. With this functionality, the user can leave the system running unattended, which is especially useful during long measurements that take several hours.

Figure 3.25 shows a picture of the input/output (I/O) terminals from the DAQ cards of the simulator. A full list of the terminal connections can be found in Appendix K.

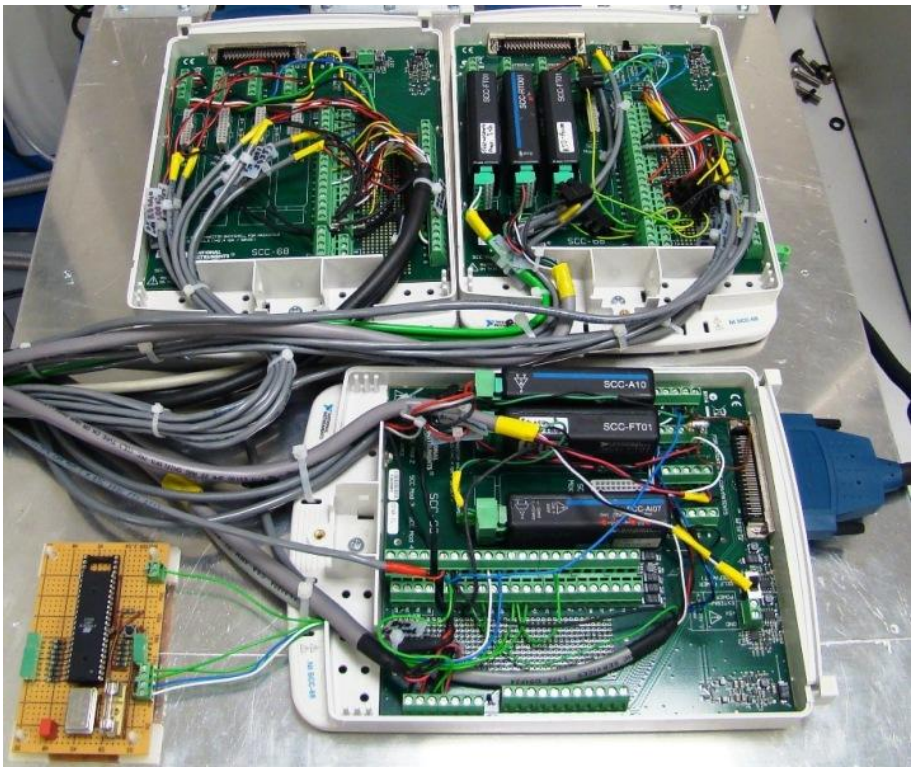

Figure 3.25: Simulator DAQ card input / output terminals (lids taken of)

3.4 Software description of LED-based solar simulator

Programming of the simulator software was done in LabVIEW. Updating and expanding the software has been a continuing task throughout this work to improve the functionality of the simulator and to include new measurement functions.

In the following subsections, it is briefly described how the software is structured and operating and details of the user interface are given.

3.4.1 Internal structure and operation principles

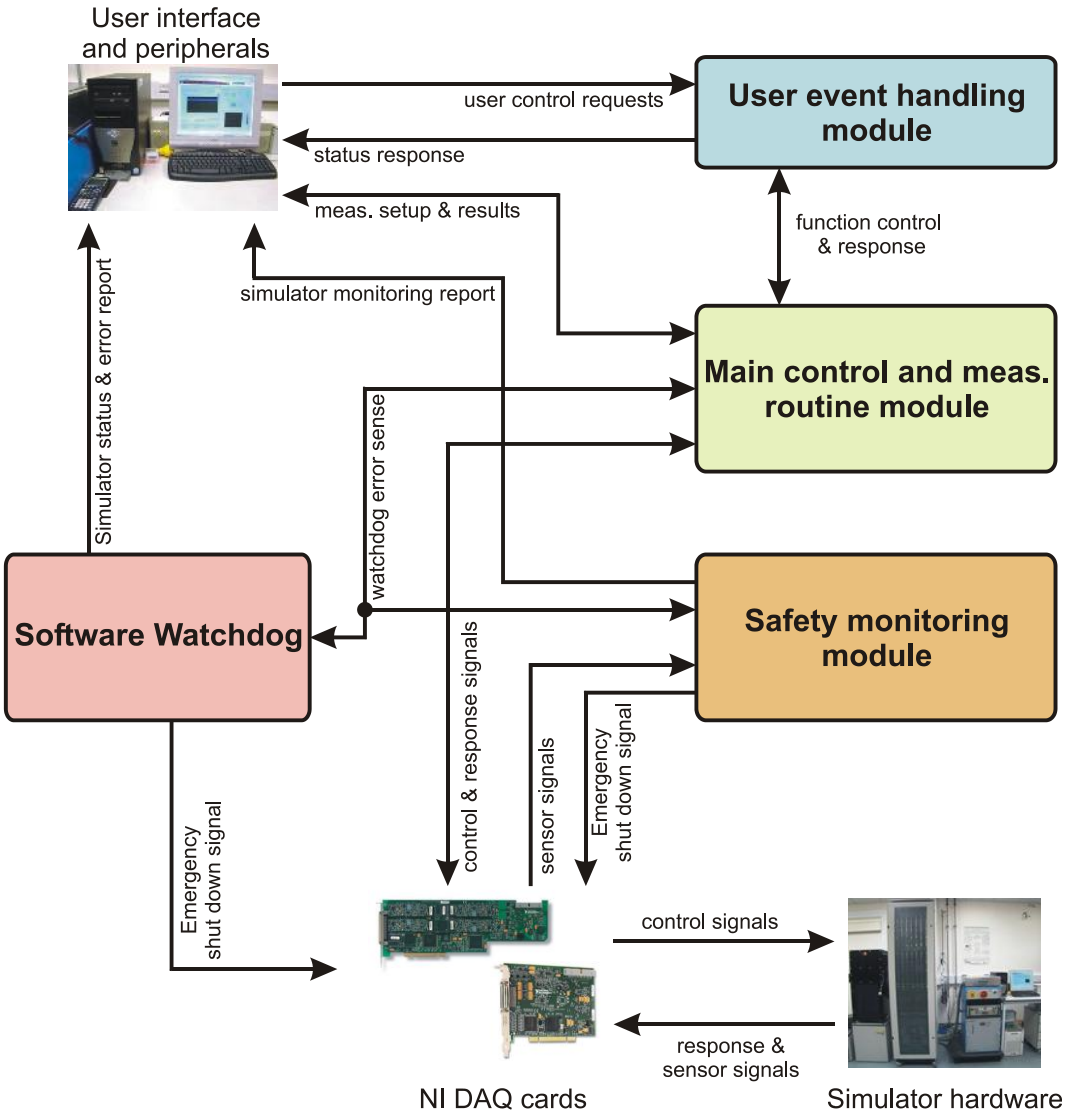

Figure 3.26: Module structure of the solar simulator software

The software has been programmed in a modular structure in which several parts run in a multi-tasking environment largely independent of each other. Communication between these running tasks/modules is established via global variables. Programming a modular structure has the advantage that the software can be expanded easily without having to reprogram existing parts of the system. As illustrated in Figure 3.26, the software consists of the following 4 modules: user event handling, control and measurement routine executer, safety monitoring and watchdog.

The user event handling module is the direct interlink from the user interface to the internal routines. If the user, for example, requests a function in the menu, the event handler is processing the request and initializes or executes the function.

The control and measurement function module is completely controlled by the event handler and executes functions such as hardware initialisation, normal system power up/down and taking I-V measurements with analysing, saving and displaying the data.

The safety module monitors continuously the status of the simulator and reacts in case of unusually high or low temperatures, too little water flow in the water cooling system or instability of light sources. The module works in the background and checks every 250ms if the system is running normally. This relatively low frequency of 4Hz was chosen, because the errors monitored will not cause any catastrophic events in this interval.

The last module is the watchdog. This small part of the software checks that the safety monitoring and measurement control module are functioning. This module acts in case of any critical internal errors like a malfunction in measuring system temperature, switching of the light sources or when the safety module is not responding within a certain time interval. In such an event the module automatically powers down the complete simulator to prevent any hazards. Errors arising such as those mentioned are displayed and also always immediately stored in a log file on the hard drive, so that the user can check what happened at a later stage.

3.4.2 User interface

A system such as the LED-based solar simulator can provide a vast range of functionality and thus requires good background knowledge for correct operation. However, a good user interface is vital for clarity of options and functions, ease of use and good overview. The user interface of the solar simulator has been divided into three main parts that can be accessed via a tabbed menu: general control and measurement set-up, measurement results and health monitor.

The main tab page in the simulator software, illustrated in Figure 3.27, is the “general control and measurement set-up” tab. This view first of all provides the user an overview of the simulator status and error reports. Secondly, it provides all controls for configuring and starting or stopping a measurement.

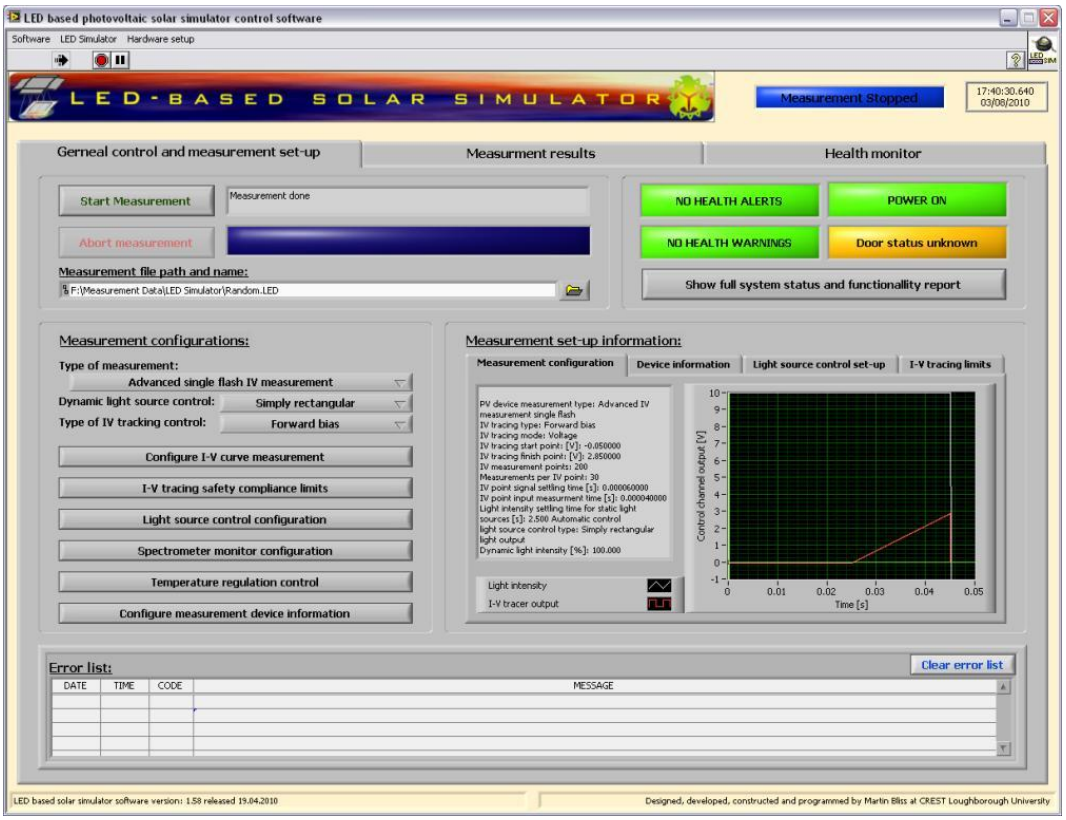

Figure 3.27: General control and measurement set-up tab in the LED-based solar simulator software

The second tab page is important for reviewing the measurement results. This can be done after a single measurement or during the measurement if multiple I-V curves are measured. The information given ranges from device

temperature to extracted I-V characteristic points, I-V curve data, light intensity measurement data and estimated measurement spectrum (more information on this is given in section 4.2). Figure 3.28 shows a screen print of this tab.

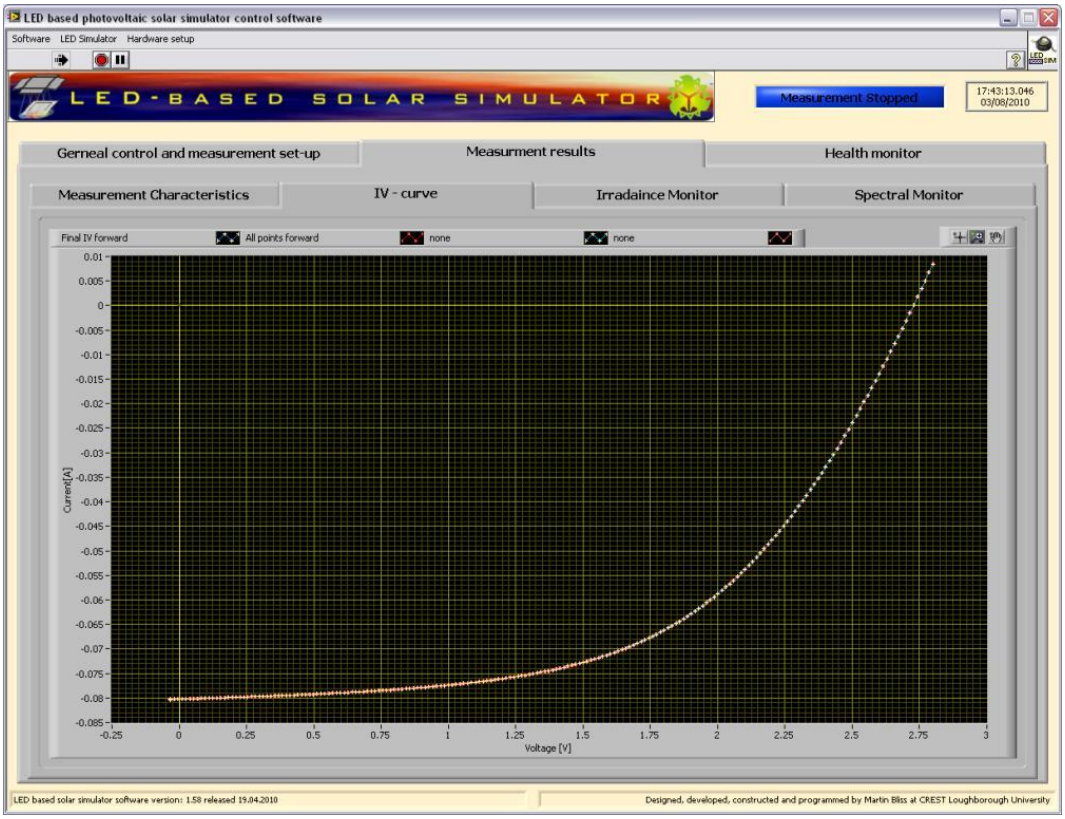

Figure 3.28: Measurement results tab showing an I-V measurement

The last tab page is labelled “Health monitor” (Figure 3.29). It has two functions. The main function is to provide the user with status information of the simulator’s various equipment temperatures, water flow rates and LED cooling conditions. In case of any active warnings, or alerts because of unusually high or low readings, the background of the monitoring value display changes colour similar to a traffic light (OK = green, warning = yellow, alert = red). The second function of the heath monitor is the so-called super-user manual control. Although this part is password protected to prevent unauthorised access, it provides manual control of light sources and I-V tracer for testing purposes. Other functions given in this tab are an overview of the PV device temperatures and status of the Peltier stage temperature

control system as well as a graph showing the current measurement feedback of the light sources and a function for offset zeroing of the I-V input channels.

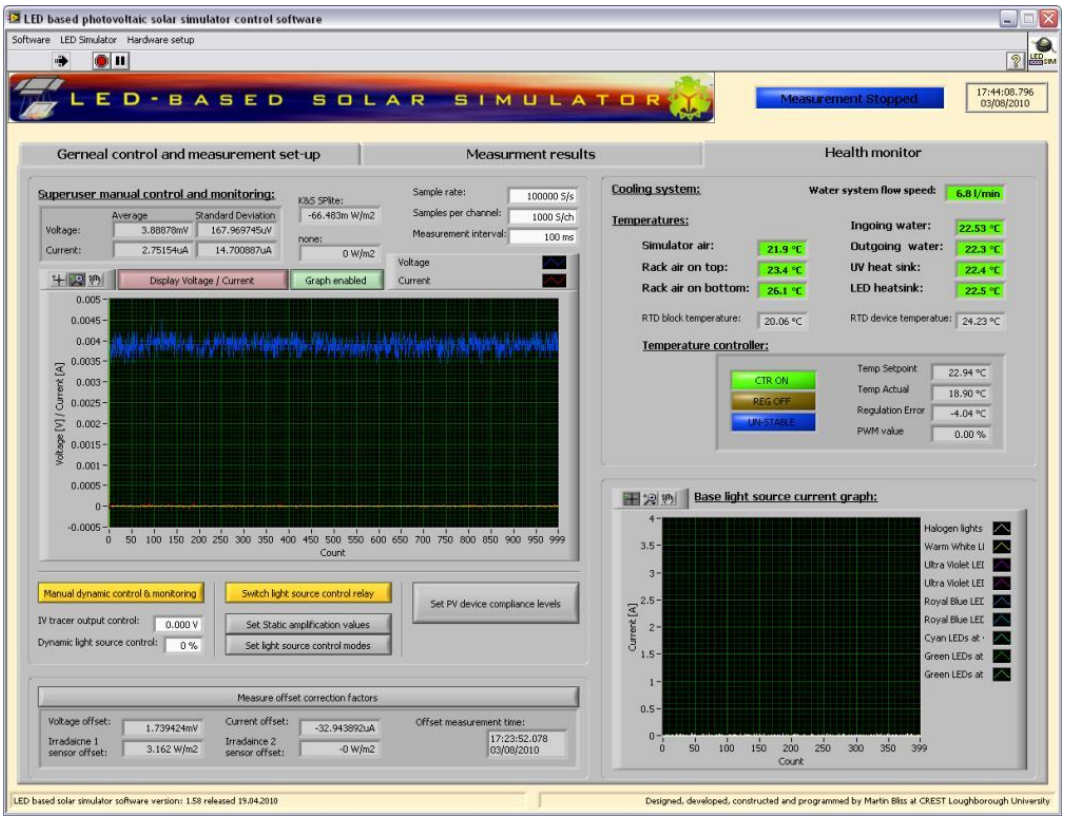

Figure 3.29: Print screen of the health monitor tab in the software

The software also utilises a menu bar that accommodates additional functions as such as power control and simulator software and hardware set-up. Again, these are partly password protected to prevent users from accidentally making undesirable changes (e.g. in I/O terminal configuration).

3.5 Conclusions

This chapter has identified the advantages and drawbacks of today's state-of-the-art solar simulators. An analysis of the characteristics of LEDs and a review of early solar simulators based on LEDs clearly demonstrates that these light sources are excellent candidates for light sources in solar simulators. LEDs do have characteristics that are inconvenient such as temperature coefficients and ageing, but most of them can be dealt with

using appropriate electronics and design and don't differ too much from other light sources.

A major element of this work was to design and develop a new advanced version of an LED simulator that provides continuous spectrum and spectral, temperature and irradiance variability for power rating and energy rating I-V characteristic measurements. The LED-based solar simulator was described in detail within this chapter.

To identify the strengths and weaknesses of the simulator, rigorous testing has been carried out of which the results can be found in the following chapter 4. Nevertheless, it will also be shown that the simulator "proof of concept" version is the world's first fully qualified LED-based solar simulator.

4 LED-based solar simulator classification and uncertainty

For any new measurement system, its true performance can only be determined by a detailed test and analysis of the system after commissioning. Furthermore, the acquired data can be used to improve the new technology, so that the system works as reliably and accurately as intended. The aim of this chapter is to give details of the performance analysis that has been carried out on the newly developed LED-based solar simulator. The strengths and weaknesses of the system are presented and potential improvements upon the prototype are identified.

The performance of the solar simulator has been analysed in three main steps: solar simulator classification, measurement test and a measurement uncertainty analysis. Findings in each of the steps can be found in sections 4.2 to 4.4. A short overview of the state of the art of solar simulator classification and in uncertainty analysis is given in section 4.1.

Testing of the solar simulator prototype has revealed room for improvements to be implemented into future incarnations of the system to realise its full potential and to really outperform current solar simulator technology. These are described in section 4.5 before concluding the chapter.

4.1 Overview of solar simulator classification and measurement uncertainty

Uncertainty describes the dispersion of the values attributed to a measurement. It has a probabilistic basis and reflects the incomplete knowledge of a result. When a measurement is taken, the outcome depends on the measurement system, the applied procedure, the skill of the operator and the environment. A low uncertainty reflects a high confidence that the measurement result is close to the true value.

The ability of a solar simulator to simulate sunlight has a direct influence on the measurement uncertainty of the I-V characteristic. The classification describes the quality of a solar simulator and to some extent the uncertainties that are associated with the measurements. This section first reviews simulator classification definitions and thereafter explains the general terms in uncertainty further with respect to solar simulators and PV device characteristic measurements.

4.1.1 Classification of solar simulators

According to the IEC 60904-9 [70], the quality of a solar simulation system is split into three main classification groups: Spatial or irradiance non-uniformity, temporal instability and spectral match. Table 4.1 illustrates the classification specifications of each characteristic.

Class	Spectral match	Non-uniformity of irradiance	Temporal instability	
			STI	LTI
A	0.75 – 1.25	2%	0.5%	2%
B	0.6 – 1.4	5%	2%	5%
C	0.4 – 2.0	10%	10%	10%

Table 4.1: Class definitions of solar simulators [70]; STI – Short term instability; LTI – Long term instability

Temporal instability of irradiance is further subdivided into two categories: Short term instability (STI) and long term instability (LTI). The STI defines how much the incident light intensity on the test device changes during the data sampling period of one measurement point with irradiance, voltage and current. This is important since analogue input channels in a data acquisition (DAQ) card are mostly multiplexed (converted one after the other in one analogue-to-digital converter (ADC) unit) and signals can change very quickly, especially in bell shaped-pulse multi-flash solar simulators. To keep the sampling data correlated to each other, it is of advantage to measure all input channels simultaneously without delays in multiplexing. This requires multiple ADC units and results in most cases automatically in a class A STI. The STI can be worst than class A even with simultaneous DAQ if the light

intensity is changing too much during the time of taking multiple measurements for averaging to one point of the I-V curve, as the complete acquisition time for all data to one point is counted. The LTI defines the changes in incident light intensity over the whole I-V measurement time. In case of a multi-flash simulator this is the irradiance change between the actual measurements of each point. If the change in irradiance over the I-V measurement is too large, a point to point irradiance correction can be carried out to reduce uncertainties to some extent in device current.

Spatial uniformity of irradiance over the PV device area is crucial for measurement accuracy. The effect of non-uniformity is to induce cell-to-cell mismatch and is most pronounced for modules in which all cells are connected in series [76]. If one cell in a series connection is illuminated with less light, it will limit the total current flow and directly affect the I_{SC} of the test device to the same extend as the non-uniformity. A further problem arises when the reference device is positioned in a particularly bright or dark spot. Then the determination of the light intensity is affected, influencing the I_{SC} and also P_{MP} and FF.

The classification of spectral match describes the quality of the simulated spectrum with regards to the AM 1.5G standard spectrum as defined in [1]. To define spectral match, the measured output spectrum is divided into separate bins in the range of 400nm to 1100nm and the proportion of the total irradiance in each bin is calculated. The spectral match classification is then determined using the deviations of irradiance share in each bin between the simulated and standard spectrum. The worst class of all bins defines the total result. The bin ranges and irradiance percentage share values are set in the standard and are given in Table 4.2.

If the output spectrum of the simulator does not match well to the AM 1.5G spectrum, the I-V measurement of the test device can be distorted and the apparent efficiency will have a higher uncertainty. This can usually be compensated by a spectral mismatch correction [77, 78], but it is virtually impossible with multi-junction devices due to the different spectral responses of the series-connected stacked junctions as previously explained. Furthermore, and as indicated in chapter 2, some technologies, such as a-Si

and multijunction devices, show a spectral dependence of the fill factor, which introduces further uncertainties of largely unknown value.

Wavelength bin [nm]	Proportion of total irradiance
400 – 500	18.4%
500 – 600	19.9%
600 – 700	18.4%
700 – 800	14.9%
800 – 900	12.5%
900 – 1100	15.9%

Table 4.2: Irradiance fraction in each of the wavelength bins of the AM1.5G spectrum [70]

4.1.2 Measurement uncertainty

The measurement error describes the difference between the measured quantity and the real quantity. Two types of errors relate to measurement uncertainty: systematic and random errors. A systematic error is an offset or bias of a measured value. This type of error should be corrected or calibrated out as far as possible. An example would be the spectral match between reference sunlight and simulator output spectrum, which to a large extent can be corrected out, as mentioned above. Random errors are associated with the observed fact that when measuring a quantity multiple times, a different measurement value is generated each time, subject to the measurement resolution of the system. The value in a random error, such as noise in a voltage measurement, cannot be predicted. If it were predictable, the effect could be explained and accounted for as a systematic error. Nevertheless, the random error can be reduced by increasing the number of observations (i.e. averaging a number of measurements) [79].

Uncertainties are split into two categories: Type A uncertainties are obtained by statistical analysis from a series of repeated measurements and type B uncertainties are obtained by other means. They can be based on experience, scientific judgement or other information [80]. Both types can be

characterised with the standard deviation evaluated from a probability density function (e.g. Gaussian, rectangular).

The *standard measurement uncertainty* is expressed as a standard deviation, whereas the *combined measurement uncertainty* is obtained using individual standard measurement uncertainties that are associated with the measurement system. An example of combined uncertainty could be the uncertainty related to current measurements, which includes the uncertainty of the analogue to digital conversion, the calibration of the shunt resistor and its temperature dependence. Combined uncertainty U_C is in simplified terms the square root of all related standard uncertainties $U(x_i)$ and is calculated as in equation (2.7).

$$U_C = \sqrt{\sum_{i=1}^{n} U(x_i)^2} = \sqrt{U(x_1)^2 + U(x_2)^2 + ... + U(x_i)^2} \qquad (4.1)$$

The *expanded measurement uncertainty* is the combined standard uncertainty with an additional coverage factor (symbolised as k) applied. The coverage factor defines the level of confidence p (e.g. for k=1 p=68.27% or for k=2 p=95.45%) [79]. The level of confidence states the probability of which the measurement result is within the measurement uncertainty margins. In solar photovoltaic research, a coverage factor of 2 is normally used [81, 82].

The uncertainty in a PV performance measurement depends on a range of factors associated with the measurement system that not only includes the solar simulator classification with irradiance non-uniformity and temporal instability of light but also, for example, uncertainties in reference cell calibration, spectral mismatch calculation, temperature measurements, I-V tracing and DAQ [82, 83]. Uncertainties are also associated with human factors and the method applied. Examples for this are the determination of the test cell area, irradiance correction or inappropriate measurement configurations [84]. Uncertainties are also specific to the test device and device technology and are in general higher for thin film solar cells than for crystalline silicon devices [58, 85].

In PV device characterisation, uncertainties are typically evaluated separately for irradiance, current U(I), voltage U(V) and fill factor U(FF). The uncertainty in determination of maximum power U(P_{MP}) is calculated as a combined uncertainty of the last three factors according to equation (4.2).

$$U(P_{MP}) = \sqrt{U(I)^2 + U(V)^2 + U(FF)^2} \tag{4.2}$$

Many variations in influencing factors are not directly related to uncertainty in the measurement value (i.e. irradiance, current, voltage and fill factor) as in, for example, the case with uncertainty in irradiance determination and measured I_{SC}. In most cases these are related through a functional relationship. For example, the uncertainties in voltage (or V_{OC}) due to uncertainties in the temperature measurement are dependent on the voltage temperature coefficient α. In this case, the standard uncertainty in voltage U(V) is calculated according to equation (4.3) as following:

$$U(V) = \frac{U(T)}{k_{U(T)}} \cdot \alpha \tag{4.3}$$

U(T) is the uncertainty in temperature measurements and $k_{U(T)}$ is its coverage factor. The uncertainty in the influencing factor needs to be reduced by the coverage factor, so that the resulting uncertainty is within a probability of p=68.27% as one standard deviation.

More discussion of measurement uncertainties are provided with the uncertainty analysis in the following sections of this chapter.

4.2 Solar simulator classification and light source calibration

The target of the LED-based simulator development was to achieve a class AAA solar simulator rating according to the IEC 60904-9 [70] standard with class A spectral match, irradiance non-uniformity and temporal stability. As apparent throughout the following sections, the first prototype has been assessed as class BAA (class B spectral match, others class A), which is largely due to shortcomings of the halogen illumination rather than the LED

sources. The following subsections describe how this assessment was carried out and how the solar simulator spectral output has been calibrated.

4.2.1 Light intensity temporal stability

The short-term light intensity instability is classified as class A due to the use of simultaneous measurements for current, voltage and irradiance, as previously described in section 4.1.1.

The long-term instability of the different light sources in the simulator was measured with an SP-Lite silicon photodiode pyranometer from Kipp & Zonen [86]. This has a time constant similar to that of solar cells and thus can detect changes of relevance to solar cell calibration.

The light intensity stability has been measured in different pulse length configurations of the LEDs and halogen lights, while the sensor was positioned in the centre of the illuminated area. Additionally, a 24h steady state measurement test was carried out. The measurement results are illustrated in Table 4.3.

Light sources	Start / Warm-up time	Time / pulse length	LTI	Class
LEDs	250µs	10ms	1.14%	A
LEDs	250µs	100ms	2.02%	B
LEDs	250µs	1s	4.03%	B
LEDs	25ms	20ms	0.26%	A
Halogen	2.5s	2.5s	0.28%	A
Halogen	2.5s	25s	1.49%	A
All light sources	25s	24h	4.72%	B
All light sources	15min	24h	0.84%	A

Table 4.3: Measured long-term temporal instability (LTI) and classification at different measurement conditions; light sources intensity stability was measured at full power output

Irradiance changes during pulsed measurements with only the LEDs are mainly due to their negative voltage temperature coefficient as explained in section 3.2.1 of the previous chapter. The intensity of the LEDs decreases

until the operating temperature stabilizes, which takes approximately one minute. This effect is due to the current regulation of the LEDs and can be removed with a more sophisticated light intensity feedback regulation (more details can be found in section 4.5.2).

Light intensity variations of the halogen light sources are mostly due to warm-up of electrical components in the regulation circuits (mainly the current sense shunt resistor). The secondary effect after the initial start-up period is a change of the filament temperature. This problem can also be resolved with an intensity feedback control. The complete warm-up and stabilization process of the halogen light sources takes around 15 minutes.

As seen in Table 4.3, after a 15minute warm-up period of light sources and electronics, the light intensity varied by less than ±1% over a test duration of 24 hours in steady state condition at full light intensity. Variations over the remaining time are mainly due to changes in the temperature of the water cooling system (3°C increase observed) and the room temperature (air conditioned). The light intensity changes measured during the 24h steady state test are presented in Figure 4.1.

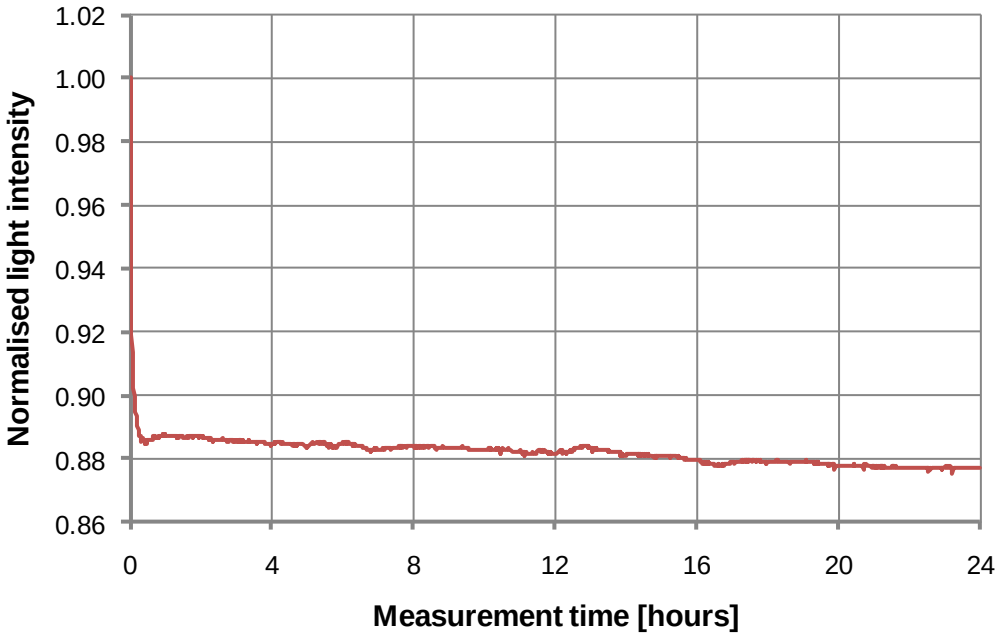

Figure 4.1: Normalised light intensity during 24h steady state test; measured with Kipp & Zonen SP-Lite sensor; the sensor was

temperature stabilised by the PV device temperature control system

Depending on the application, it is virtually always possible to maintain a class A temporal instability, with significantly less than two percent intensity changes. In most of the measurements made during this work, a warm-up time of 25ms has been chosen for the LEDs and a stabilisation time of 2.5s has been chosen for the halogen light sources when they are driven at full intensity. The overall temporal stability was in this configuration better than ±0.3% over an I-V curve measurement time of up to 20ms.

4.2.2 Light intensity uniformity

A Hamamatsu S2387-66R silicon photodiode was used to measure the light intensity uniformity over an area of 205x205mm^2 at a resolution of 5x5mm^2 (detector size was 5.8x5.8mm^2). The Si detector was mounted on a motorised X-Y-stage. Unfortunately, the uniformity measurement could not be carried out at the same height as the target plane because of the height of the X-Y-stage. Instead, the top of the silicon diode was approximately 6.5cm above the PV device measurement plane. One can expect better uniformity on the actual measurement plane because uniformity of light intensity improves with greater distance due to light divergence. A warm-up period of 15 to 30 minutes was included in ever test to stabilise the intensity. The measurement time of the homogeneity field at the stated resolution was approximately 22 minutes.

Figure 4.2 illustrates the measured normalised light intensity field in the solar simulator with the output spectrum adjusted to best fit AM 1.5G. The non-uniformity over the full area was, at 21.7%, well outside the boundary of standard classification and thus class F (failed). Reducing the test area to the centre 125x125mm^2 area reduces non-uniformity to 9.3% and attains Class C. On an area of 85x85mm^2 in the centre class B has been achieved with 4.9%. Class A classification with 1.9% non-uniformity has been achieved in the centre 45x45mm^2 area.

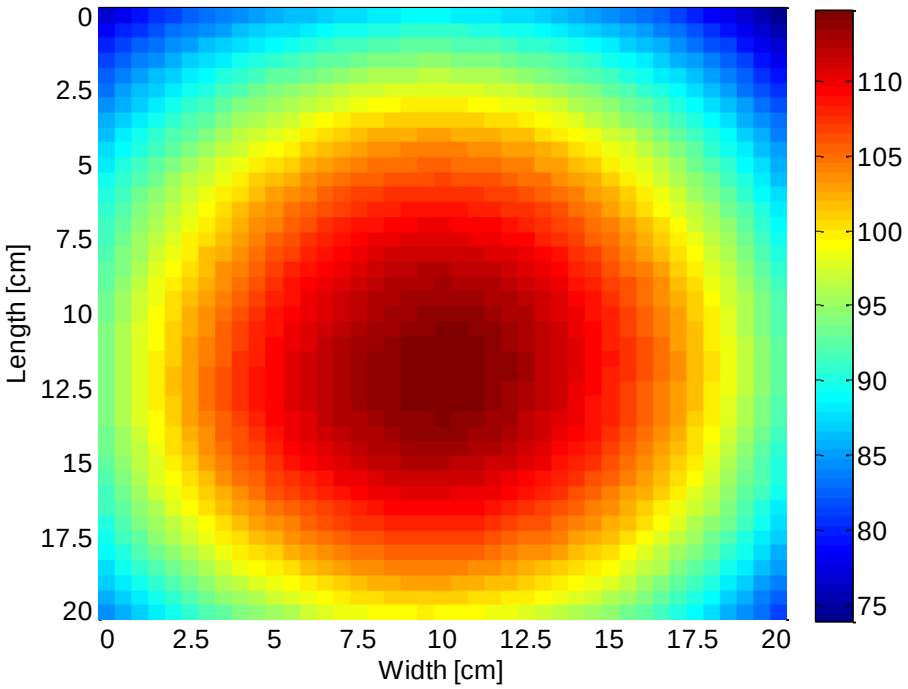

Figure 4.2: Relative light intensity field in the LED-based solar simulator with output spectrum adjusted to best AM 1.5G fit; the colour bar scale is given in percentage of average intensity

Further separate light intensity uniformity measurements of each individual LED colour and halogen lights showed that the intensity pattern between them changes slightly (see Figure 4.3). This means that the spectral output is also slightly changing over the illuminated area. This can be especially problematic when measuring larger mini modules or multi-junction devices. Due to the electronic system used in the simulator, it is possible to adjust the intensity of each light source separately, which would improve the situation significantly. Another option for improving homogeneity might be to include mirrors at the side of the module to reflect stray-light back into the measurement plane and thus increasing illumination at the sides of the illumination field. However, this work has not been carried out on the prototype unit, as future versions could use specially designed optics to deliver a better intensity uniformity and spectral homogeneity without further adjustment of the output intensity of every LED (see section 4.5.1).

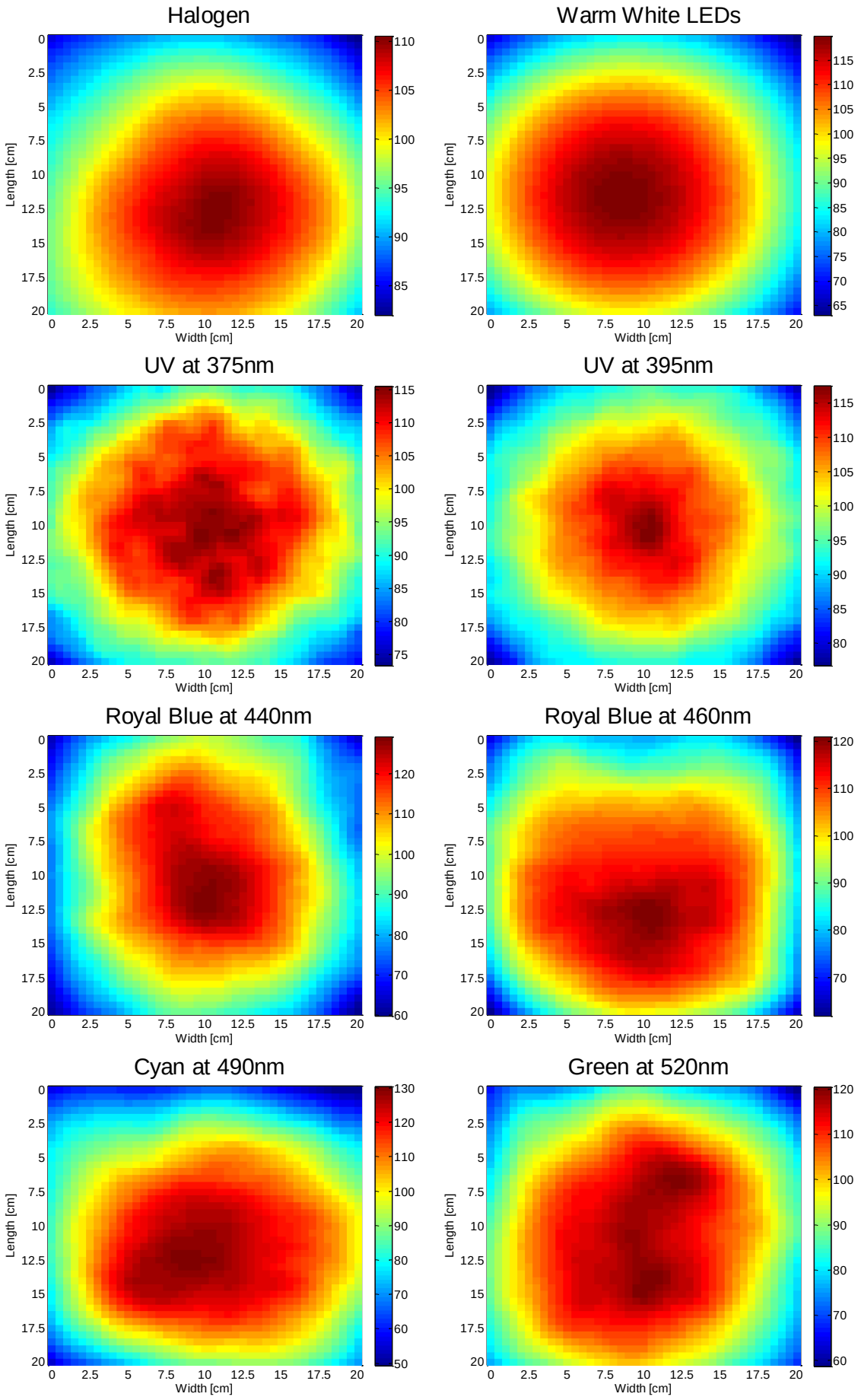
Halogen
Warm White LEDs
UV at 375nm
UV at 395nm
Royal Blue at 440nm
Royal Blue at 460nm
Cyan at 490nm
Green at 520nm
Length [cm]
Width [cm]

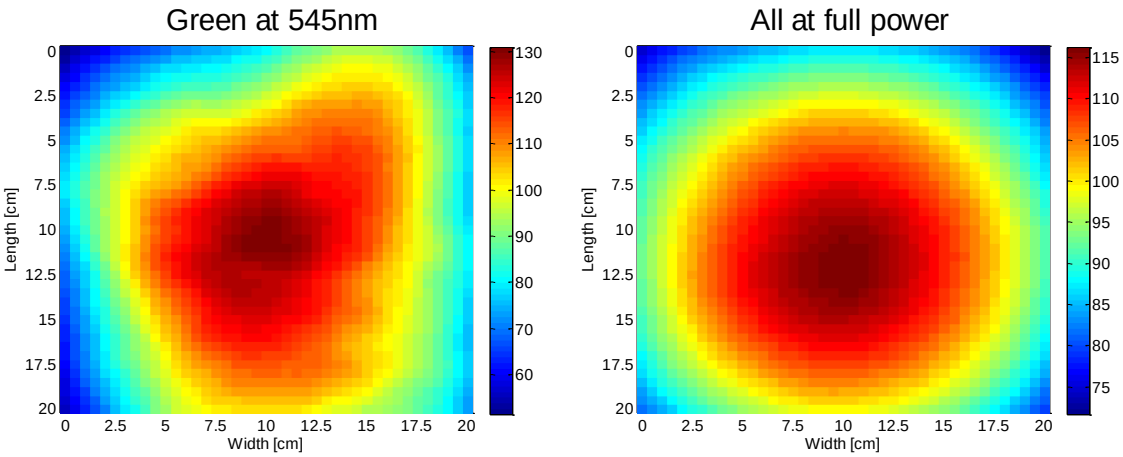

Figure 4.3: Comparison of relative light intensity patterns of each light source colour in the LED based solar simulator; colour scale given in percentage of average intensity.

4.2.3 Spectral match and light source calibration

The simulator light output needs to be calibrated prior to assessing the classification in spectral match. This has been done in two steps: relative calibration of the spectrum with help of a spectroradiometer and absolute calibration of the light source intensity using a calibrated reference cell.

Relative calibration of light sources:

The first of the two steps of the light source calibration has been carried out with a StellarNet EPP2000 spectroradiometer with total spectral range of 260nm to 1080nm [87]. However, due to the fibre optics, diffuser input, detector signal response and measurement noise, the useful range of the spectroradiometer was limited to 340nm to 800nm. This obviously posed a problem for the measurement of the halogen light sources, as their output extends far beyond 800nm. Since there was no alternative spectroradiometer available during this work, the spectral response of the halogen light sources has been extended from 800nm with the theoretical output of a black body with 3000k radiation temperature. The radiation temperature of the halogen lamps was given in the datasheet of the supplier [88]. Comparing the example output spectra of halogen and black body radiation in Figure 3.1 of the previous chapter it is apparent that this is a reasonable estimation;

nevertheless it is an additional source of uncertainty in the relative spectral output.

The spectroradiometer was calibrated using a secondary reference calibrated 1000W quartz tungsten halogen lamp to achieve best possible measurement accuracy. The simulator's spectral output has been measured at full light intensity in pulsed mode with a start-up time of 25ms for the LEDs and 2.5s for the halogen light sources. The spectroradiometer integration time was set to 12ms for measuring the LEDs and 50ms for the halogen light sources. Choosing the exact timings as used during most I-V measurements meant that the spectrum is best represented without having to measure it during an actual I-V scan. The spectral output was averaged over 50 measurements to further improve measurement quality.

Absolute calibration of light source spectrum:

Despite the spectroradiometer having been calibrated and used to the best possible knowledge, the results of a crosscheck between the calibrated light spectrum and generated I_{SC} in a c-Si reference cell (secondary calibrated by JRC-ESTI[1]) revealed a significant deviation between the measured I_{SC} and that of the theoretical I_{SC}. The latter was calculated with equation (2.8) in chapter 2 using the reference cell spectral response from the calibration report and light source output spectrum as measured by the spectroradiometer. Table 4.4 illustrates the differences between the currents. The large deviations are thought to be due mainly to the nonlinearity of the charge-coupled device (CCD) detector in the spectroradiometer. Testing as part of a separate work on a similar but improved spectroradiometer from a different supplier revealed a non-linearity of ±6% over a detector signal input range of 70% (lower end), which is a scale similar to the majority of the observed deviations. Furthermore, due to the difference between spectroradiometer input and solar cell, a deviation in angular response is to be expected.

[1] European Solar Test Installation of the Joint Research Centre of the European Commission, which is one of the few primary calibration laboratories world wide

Light source	Calculated [mA]	Measured [mA]	Deviation [%]
Halogen lights	50.13	52.05	-3.70
Warm White LEDs	34.62	32.26	7.31
Ultra Violet at 375nm	1.73	1.59	9.13
Ultra Violet at 395nm	5.96	5.50	8.40
Royal Blue at 440nm	10.21	9.35	9.17
Royal Blue at 460nm	10.58	9.55	10.77
Cyan at 490nm	9.67	8.69	11.21
Green at 520nm	5.57	5.05	10.28
Green at 545nm	5.59	5.09	9.84
All light sources	134.06	129.14	3.81

Table 4.4: Results of the spectroradiometer light source calibration crosscheck

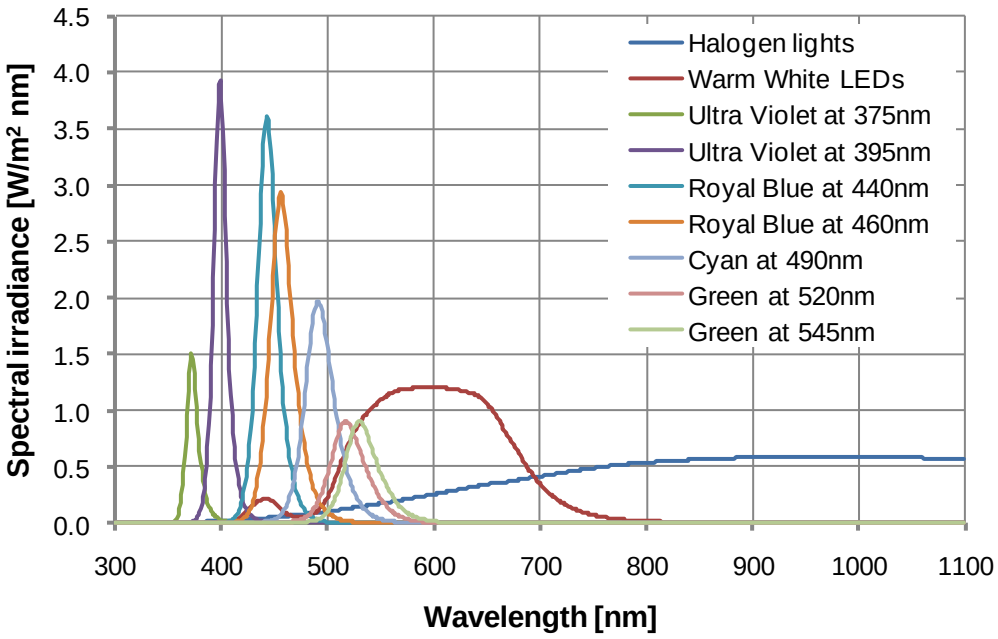

Figure 4.4: Absolute output spectra of the light sources in the LED-based solar simulator

The SR calibration as well as the linearity of the reference cell can be trusted to a higher degree than the spectroradiometer. Therefore, the light source spectral output intensity was rescaled to match the current output of the reference cell. To achieve best possible accuracy, measurements have been carried out using the same timings as the first calibration step. Additionally,

the light source intensities (reference cell I_{SC}) were also measured using background illumination of the unused LEDs to reduce possible uncertainties arising from increasing nonlinearities at low light levels. Figure 4.4 shows the final absolute spectral output calibration of all light sources.

Classification of the spectral match:

One advantage of the solar simulator is its ability to vary the spectral output. To demonstrate this, the spectral match has been calculated for two configurations: one at full intensity of all light sources without any further adjustments and one with the light source intensities set to best match the AM 1.5G spectrum. The intensity factors for the best match have been acquired by fitting and manual adjustment, to achieve high intensity and a good fit to the standard spectrum. Both spectral output curves are presented in Figure 4.5.

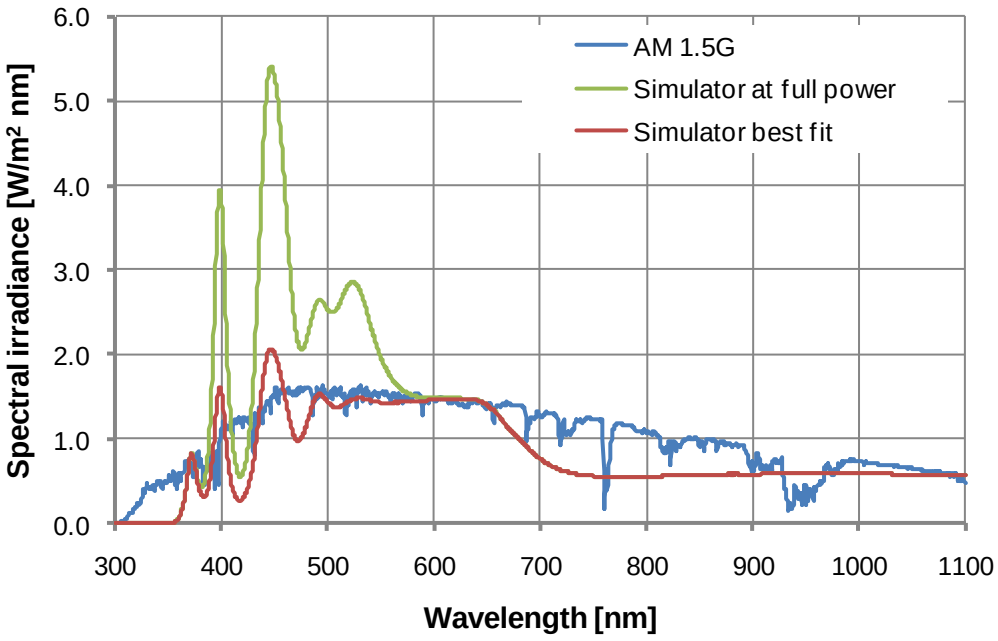

Figure 4.5: LED simulator spectral output in two conditions; with all light sources at full intensity and at best fit to AM 1.5G

Note that both spectra given in Figure 4.5 are not directly measured, because the spectroradiometer available showed large measurement problems, which meant that it was more accurate to calculate the total output spectrum by adding all light source spectra together. This is a very good assumption, as

LEDs do not significantly change their spectrum with intensity and the halogen light sources are in both spectra at full intensity and are thus best represented.

The spectral match classification results are summarised in Table 4.5. In the full intensity case, the spectral output is still within class C spectral match. Adjusting the intensity of the different light sources to match the standard spectrum as closely as possible achieved a class B spectrum.

Wavelength interval	Simulator output at full power		Simulator output adjusted to fit AM 1.5G	
	Spectral match	Class	Spectral match	Class
400 – 500	1.75	C	1.03	A
500 – 600	1.25	A	1.16	A
600 – 700	0.83	A	1.11	A
700 – 800	0.47	C	0.64	B
800 – 900	0.55	C	0.74	B
900 – 1100	0.87	A	1.18	A
Worst case:	**1.75**	**C**	**0.64**	**B**

Table 4.5: Spectral match classification with regards to the output spectrum at full power and at best fit to AM 1.5G

The target of class A spectral match has not been achieved in the current arrangement. Looking at Figure 4.5 and Table 4.5, it is apparent that this is entirely due to the choice of halogen lights (‘warm halogen lights’) and does not affect the possibility of an LED-only simulator achieving class A. In the current setup, the spectrum could be improved by either adding another set of LEDs in the 700nm to 800nm range or exchanging the halogen lights to dichroic ones (which currently are not available in this particular range) or ones with a higher colour temperature. The latter was not possible due to the axial reflector halogen light sources used and the Ministar not being offered in dichroic designs. Future versions of the LED-based solar simulator should use significantly more LED colours and no halogen lights, so that the target spectrum can be better represented.

4.2.4 Total irradiance and light intensity control

An irradiance of approximately 1350W/m^2 at full power output of all light sources has been measured in the centre of the illumination area with a Kipp & Zonen CMP11 thermopile pyranometer [89] that responds over a range of 310nm to 2800nm. Adjusting the simulator spectrum to match AM1.5G reduced the maximum irradiance to ~1100W/m^2. When using only the LEDs, an irradiance of up to 605W/m^2 can be reached at full power. Continued improvements in high power LEDs have made it easier to reach the target 1000W/m^2 and future versions can take advantage of these emerging LEDs.

When calculating the irradiance in the range of 300nm to 1100nm it is noticed that the irradiance in the solar simulator at best fit AM 1.5G output spectrum is 648W/m^2. This is lower than the 802W/m^2 irradiance of the standard AM 1.5G spectrum over the same range. The significantly lower irradiance in the solar simulator in this range is mainly the result of a lack in output intensity in the 700nm to 900nm region. The CMP11 measured a higher irradiance because of the halogen lights that have a spectral output far into the infrared region. As apparent from Table 4.6, the lower irradiance in the 300nm to 1100nm region directly results in a lower equivalent irradiance in the solar simulator when measuring PV devices. Thus, when calibrating devices under STC an irradiance correction will need to be carried out.

PV device material	Current density (300-1100nm) [A/m^2]		Equivalent irradiance
	at AM 1.5G	in solar simulator	
c-Si	301.1	233.7	776.0
a-Si	87.8	81.8	931.6
CIS	259.8	205.0	789.2
CdTe	198.4	155.7	784.7

Table 4.6: Calculated equivalent irradiance in the LED-based solar simulator for various PV device materials; the effective irradiance is based on the AM 1.5G spectrum at 1000W/m^2, the spectral response curves of different technologies are illustrated in Figure 2.8 of chapter 2.

As mentioned previously, the light sources in the simulator are current regulated. However, during some measurements, such as of I-V characteristic measurements used for energy yield prediction, it is required to measure at the same spectrum in different intensities. To accurately change the intensity in the solar simulator, without affecting the spectrum, the LED-based solar simulator utilises a calibration curve of the intensity versus drive current (G vs. I_D) of each light source type. This is used to calculate the I_D required to achieve a new intensity setting at which the relative intensities of the light sources are changed equally and the actual spectrum is unchanged. It reduces control errors arising from the slightly non-linear G versus I_D behaviour of the LEDs. With regards to the halogen light sources this calibration ensured that the current generated by the light is as linearly changing as possible. Despite this, the spectrum shifts to the infrared with lower intensities (e.g. for a setting of 5% halogen light intensity, the drive current of the halogens is controlled at 55%).

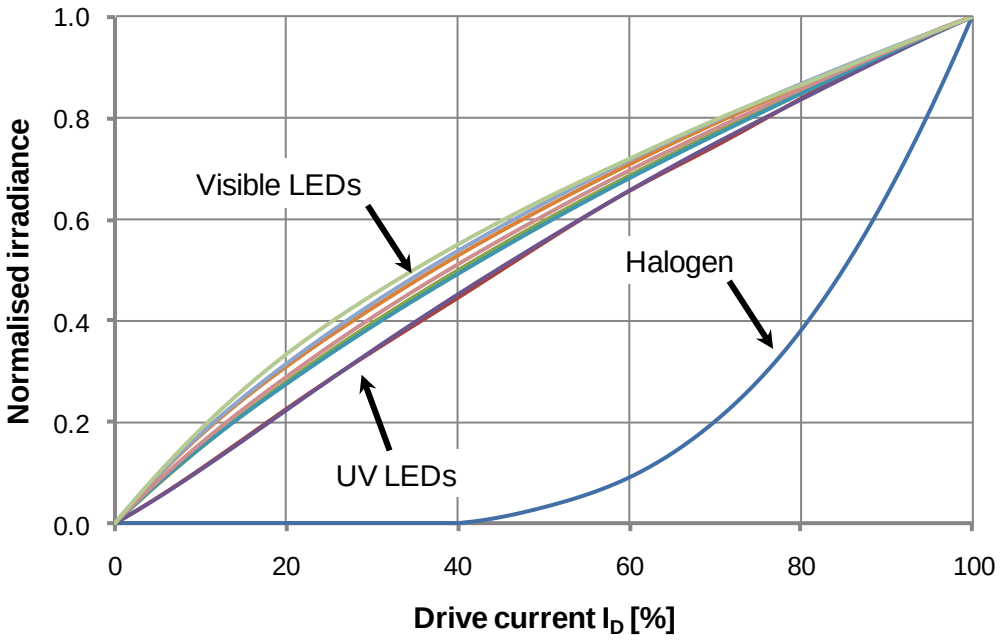

Figure 4.6: Light source intensity control calibration results; LED light intensity changes are slightly nonlinear with drive current; halogen light intensity is behaving exponentially with increasing current

The G vs. I_D calibration was carried out with the calibrated c-Si reference cell using background illumination from other LEDs and the same 25ms warm-up time for the LEDs as given previously. Since the halogen lamp filament takes considerably longer to heat up at lower input currents, stabilisation time for halogen lights was varied from 2.5s at 100% drive current to 15s at 55% I_D. The calibration results are illustrated in Figure 4.6.

4.3 Initial solar cell characterisation test

Having classified a solar simulator by itself does not ensure good measurement quality when carrying out real tests. This depends not only on light conditions and spectrum, but also on the accuracy of temperature, current, voltage and irradiance measurements as well as the measurement set-up. Preventing mistakes in the set-up is only possible by following a procedure, checking carefully that details such as the PV connections and the measurement timing are correct. Direct measurement errors are more predictable and can be determined with an error analysis of the measurement equipment.

To analyse how well the LED-based simulator prototype is actually measuring, the c-Si reference cell calibrated by JRC-ESTI has been tested. The following sections describe how the measurement was carried out, what measurement results have been acquired and how they have been corrected according to standards. This section is concluded with a short discussion.

4.3.1 Measurement method and configuration

The c-Si reference cell has been measured in a single pulse configuration with a start-up time of 3s for the halogen lights and 25ms for all LEDs for stabilisation prior to the actual measurement time of 10ms. The simulator light output spectrum was set to AM 1.5G as described in section 4.2.3 and the temperature of the test device was regulated to 25°C.

Before the actual measurement, I-V tracing tests have been carried out in direction from short circuit to open circuit and in reverse, to make sure that no capacitive effects are distorting the measurements (i.e. no measurement

hysteresis is detected). The measurement itself was carried out from short circuit to open circuit voltage in 100 points. For each point a voltage settling time of 50µs and measurement time of 50µs was allowed. During the 50µs measurement time current, voltage and irradiance were measured 30 times and averaged for signal noise reduction.

Since the reference cell was actually the test device, the SP-Lite silicon pyranometer was used for irradiance stability measurements. It is important to clarify that the SP-Lite sensor was not used for measurement irradiance determination but only for stability measurements. This was done because the SP-Lite was not recently calibrated, its spectral response is unknown and because of the increased spectral and light intensity non-uniformity outside the 45x45mm^2 class A illumination area. The sensor could only be positioned in the outer area because the test device was already positioned in the centre. For determination of irradiance, it was assumed that the simulator correctly sets the best fit AM 1.5G spectrum as shown previously in Figure 4.5.

4.3.2 Uncorrected measurement results

The c-Si reference cell was measured 3 times with approximately 1½ minutes time in between the measurements for ensuring equilibrium of light source and device temperatures. Figure 4.7 shows the uncorrected measurement results in comparison to the “true” I-V curve extracted from the calibration certificate. It is clearly visible that all 3 measurements hardly differ from each other.

Irradiance stability measurements (shown in Figure 4.8) show a temporal instability of approximately ±0.04% with a slight drop in intensity over the measurement time.

The device temperature, manually measured with a K-type thermocouple, was constant at 24.7°C during all measurements. The IEC 60904-1 [90] indicates that a temperature correction at this point was not necessary, since the temperature difference to STC was much less than ±2°C.

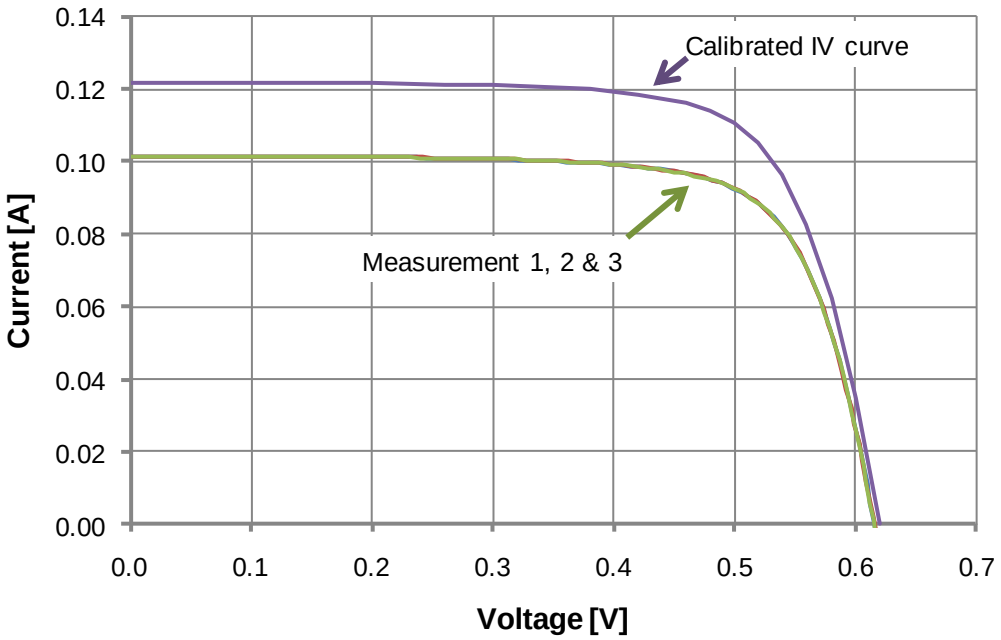

Figure 4.7: Uncorrected I-V measurement results in comparison to the calibrated I-V; min to max deviation between the three measured IV-curves is 0.08% in P_{MP} and 0.05% in I_{SC}.

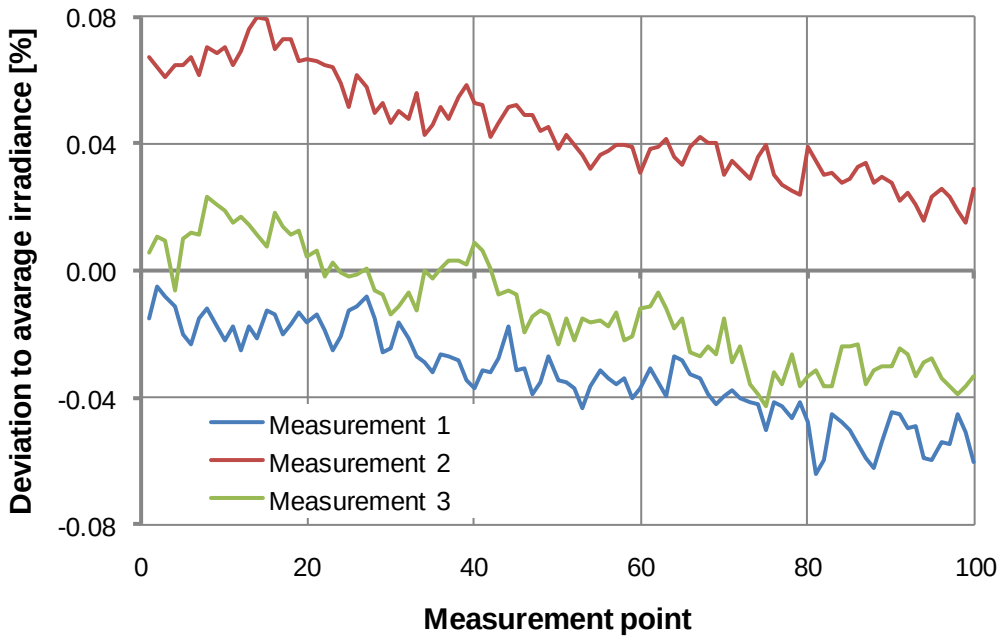

Figure 4.8: Irradiance stability during measurements; the irradiance between the measurements was within is ±0.08%.

4.3.3 Spectral mismatch and irradiance correction

The spectral mismatch factor MMF corrects for the differences in spectral response of the test device and reference cell. According to the IEC 60904-7 standard [77] spectral mismatch is calculated using the AM 1.5G standard spectrum [1], the simulator output spectrum and the SR data of test device and reference cell. Since in this measurement case the test device is the reference cell, there is no difference in spectral response and thus no mismatch due to spectrum (MMF=1). Hence, the differences in the I_{SC} that has been measured and the I_{SC} from the calibration certificate are entirely due to measurement irradiance.

Since no reference cell was used for determination of the light intensity and the reference cell itself was measured, it is not possible to calculate the irradiance correction exactly as given in the correction procedure of the IEC 60891 [52] using the measured I_{SC} of the reference cell and its calibrated I_{SC} under STC conditions. As previously mentioned, it was assumed that the simulator correctly sets the best fit AM 1.5G spectrum with its intensity. This meant that the irradiance correction was carried out using the theoretical I_{SC} calculated with help of the SR curve of the reference cell and the output spectrum of the simulator instead of the directly measured I_{SC} of the reference cell.

An I_{SC} at STC of 121.8mA was given in the calibration certificate. Under simulator spectral output an I_{SC} of 101.2mA was calculated. This resulted in an irradiance difference of -16.9% to STC conditions or in other words, the I-V curve was measured at an effective irradiance of 830W/m^2 instead of 1000W/m^2. An R_S of 0.23Ω has been determined with help of 6 I-V curves measured at different light intensities using correction procedure 1 for internal series resistance determination given in the IEC 60891 standard [52]. The current and voltage of the I-V curve was then corrected using procedure 1 of the IEC standard, of which the final results can be found in Figure 4.9.

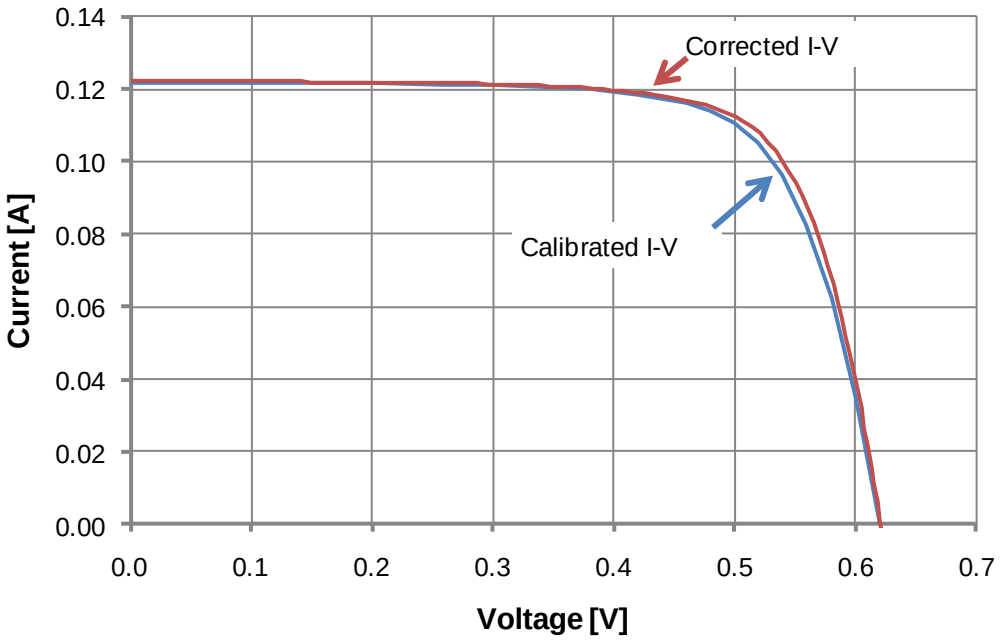

Figure 4.9: Comparison of corrected I-V measurement and calibration I-V curve; a visibly larger fill factor has been measured

As visible in the graph, both I-V curves, the irradiance-corrected measurement and that of the calibration certificate by JRC-ESTI, differ slightly from each other. Table 4.7 shows a comparison between corrected values from the measurement and values from the calibration certificate. The main difference appears to be a different resistance in the circuit as the corrected FF is slightly higher and the difference is largely in the V_{MP}.

Value	Measured and corrected	Calibration	Deviation
V_{OC} [mV]	621.1	620.0	0.18%
I_{SC} [mA]	122.1	121.8	0.21%
V_{MP} [mV]	506.9	500.4	1.29%
I_{MP} [mA]	111.1	110.8	0.24%
P_{MP} [mW]	56.30	55.44	1.55%
FF [%]	74.3	73.4	1.17%

Table 4.7: Comparison of I-V characteristic parameters

4.3.4 Measurement discussion

Despite the fact that no reference cell could be used during the measurement and the spectrum and intensity were estimated to be as calibrated, the deviation between the corrected I_{SC} to the calibrated one is smaller than expected, bearing in mind that calibration accuracy has a great impact on the total error. At this point it should also be noted that the calculated I_{SC} at AM 1.5G spectrum of the tested c-Si reference cell did not match the certificate I_{SC} value; it showed a deviation of +2.4%. This is just outside of the stated uncertainty of 2.3% given in the calibration certificate, but still overlaps with the uncertainties being presented for the LED based simulator. The deviation indicates an absolute error in the calibrated SR of the reference cell. This absolute error also influenced the irradiance corrections carried out with calculated I_{SC} at simulator spectrum. A correction without this error would have led to a lower I_{SC} in the range of the 2.4% deviation. When characterising solar cells in the simulator it is therefore useful to measure the irradiance in the simulator with a reference cell before and after measuring the test cell. Doing so would reduce the uncertainty to the actual repeatability of the measurement conditions and light intensity setting.

Another important factor is that temperature control and measurement accuracy also play significant roles, especially for devices with large temperature coefficients. For this device, the deviation of -0.3°C to 25°C at STC should have had an impact of approximately -0.1% on V_{OC}. In other words this means that if the measurement temperature would have been exactly 25°C then the deviation at V_{OC} would have been in the range of 0.08%.

The main reason for the difference in FF is that the reference cell has only a 3-wire main terminal connector to the reference cells bus bars. During calibration, JRC-ESTI did use a second 3 wire cable connected to the main connector because it was a part of the Spire solar simulator in CREST. This cable was not used during measurements made during this work, which means that the 4-wire probe was connected with a lower series resistance to the main connector. Thus the measured fill factor and device efficiency was

larger. The uncertainty in determination of R_S during irradiance correction is not thought to be a major contributing factor.

4.4 Measurement repeatability and uncertainty analysis

In addition to the findings of the solar simulator classification and device characterisation tests, the repeatability and variability of measurement conditions also need to be accounted for in the uncertainty analysis. The findings here show the extent of variations that are to be expected in all measurements made with the simulator prototype and can also be used for optimisation of the measurement process to reduce uncertainties. This is presented in the first two subsections, where section 4.4.1 concentrates on the light control accuracy and section 4.4.2 on I-V curve measurement repeatability. Finally in section 4.4.3 a detailed overall measurement uncertainty analysis is carried out to determine the robustness of the measurement system and the confidence with which measurements can be trusted when characterising PV devices.

4.4.1 Light intensity control repeatability

The repeatability of light intensity control has been measured for different measurement periods for the LEDs and halogen light sources with the SP-Lite sensor. The sensor was positioned in the centre of the illumination area and the normal light pulse timing as defined in section 4.2.3 was used.

During a repeatability test of the light intensity control of each LED colour, using a measurement interval of 1s, it was found that the light intensity drops during the first measurements and then stabilises. The rate and amount of irradiance decrease was dependent on the LED colour with green and warm white LEDs being the worst affected. The effect is mainly due to the heat up of the LED die and is dependent on the thermal resistance between LEDs and heat sink and its temperature coefficient. The water cooling process of the LEDs is much slower than the heat-up due to thermal resistance in the system. Furthermore, the short measurement period does not allow for

complete cooling to the initial state as the cooling time-constant is too slow. To be able to determine at which measurement interval the intensity drop becomes insignificant, a second test with varying measurement intervals was carried out for worst case of warm white LEDs the results of which are depicted in Figure 4.10. The best repeatability and measurement speed trade-off is a measurement interval of 8s when the only light sources being used are LEDs. This results in light intensity not varying by more than ±0.1%. This does not consider other external influences such as e.g. cooling water temperature changes, which can lead to larger deviations.

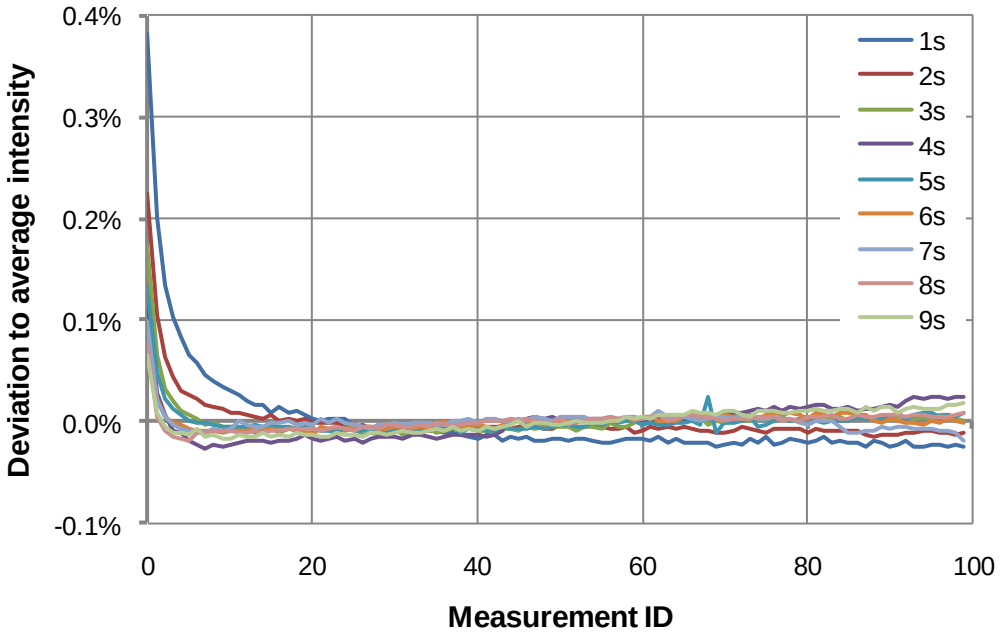

Figure 4.10: Light intensity of white LEDs at varying measurement periods from 1s to 9s; changes towards the end part are influenced by water cooling and air temperature changes and are more pronounced for long measurement periods

In the case of the halogen light sources, a much larger drop in light intensity has been observed (Figure 4.11). This is because of the regulation electronics. The current flow through the light source is regulated with a shunt resistor that provides voltage feedback. The resistor heats up when operated at full intensity as 4A current flow through it. Thus, resistance increases which causes a similar change in the voltage feedback signal resulting in the current flow through the light source being reduced by the

regulation circuit. A minimum measurement time interval of 45s seconds is necessary to keep the intensity changes below 1% over all measurements.

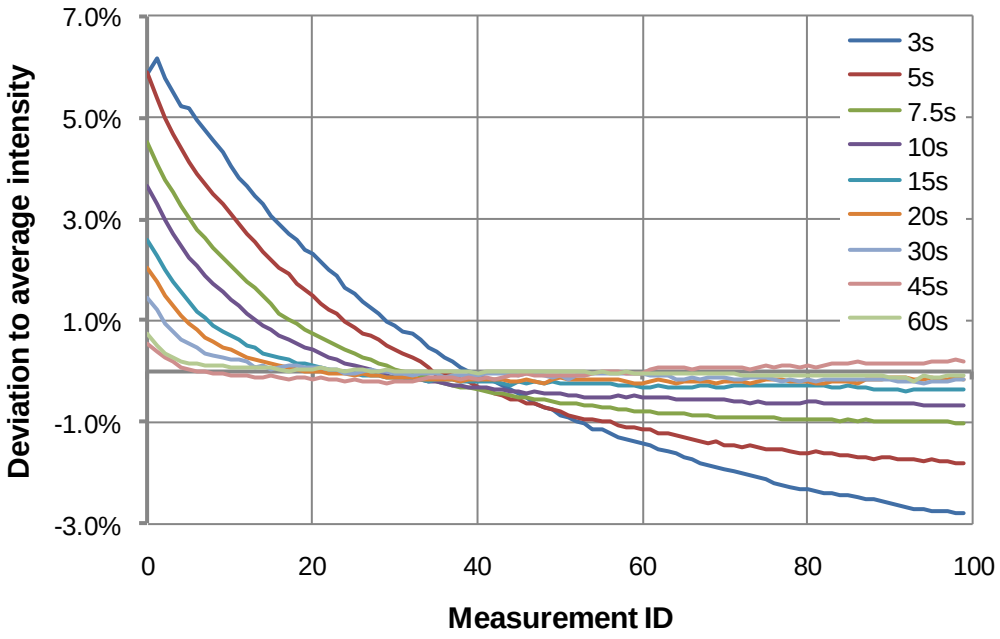

Figure 4.11: Light intensity changes of halogen light sources at varying measurement intervals

4.4.2 Measurement repeatability

As apparent from the previous section, considering cooling periods for the light sources increases the repeatability of the light source intensity settings. This has a direct effect on the repeatability of the actual I-V curve measurement, as the current generation in the cell is strongly correlated with it. Repeatability measurements of the I-V curve have been carried out with different measurement intervals using an un-encapsulated 30x30mm^2 c-Si solar cell. In Figure 4.12 and Figure 4.13 results at a measurement interval of 90 seconds are presented. Those gave the best measurement speed and repeatability trade off. Still, the initial drop of intensity, mainly in the halogen light sources, is visible in I_{SC} and P_{MP}.

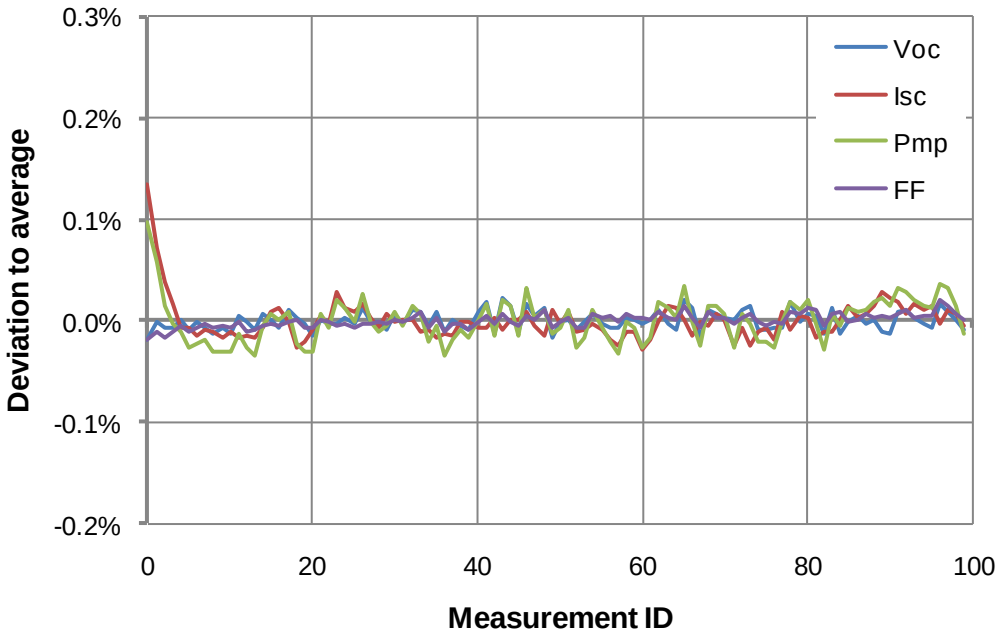

Figure 4.12: Deviation of key I-V points from average value acquired at a measurement interval of 90 seconds; variations in device I_{SC} are mostly related to light intensity changes

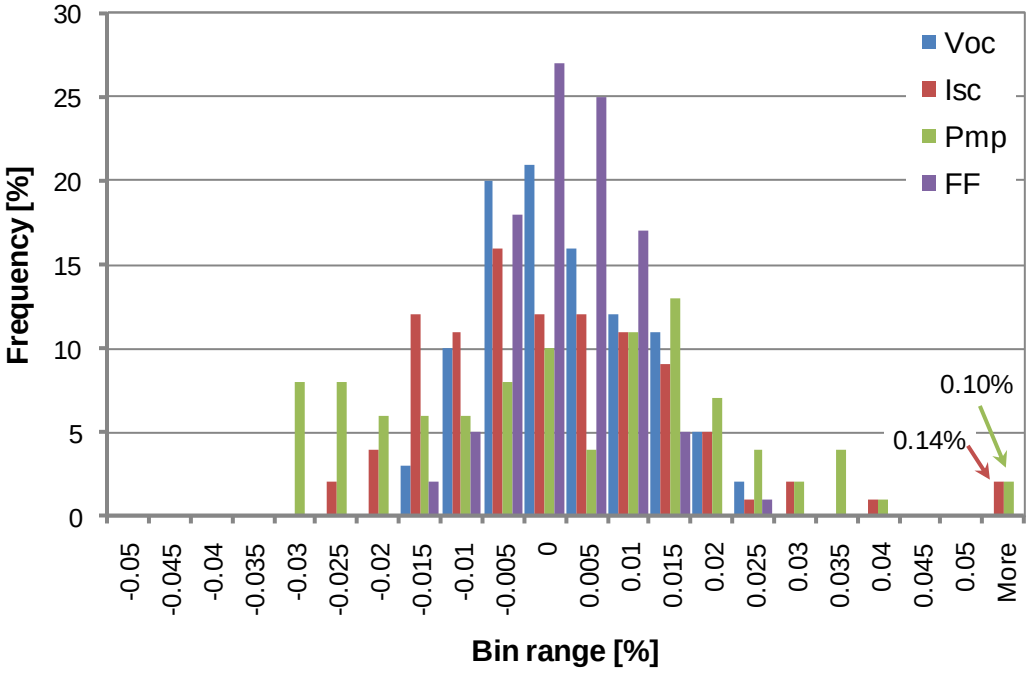

Figure 4.13: Histogram in the deviation of key I-V curve points to the average measured value at 90 seconds interval

Parameter	Max	Average	Min	max deviation	STD
V_{OC} [mV]	589.63	589.49	589.39	0.041%	0.009%
I_{SC} [mA]	245.02	245.09	245.41	-0.162%	0.020%
V_{MP} [mV]	493.39	493.25	493.09	0.061%	0.013%
I_{MP} [mA]	228.40	228.48	228.76	-0.157%	0.020%
P_{MP} [mW]	112.66	112.70	112.81	-0.132%	0.022%
FF [%]	78.02	78.00	77.99	0.039%	0.007%

Table 4.8: Measurement variations of key points in the I-V curve

In total it can be said that variations from minimum to maximum (Table 4.8) in key parameters are below ±0.2%. The highest variations can be seen in I_{SC}, which is due to changes in light intensity. The standard deviation stays below 0.03% which indicates a very good repeatability of measurements.

4.4.3 Measurement uncertainty analysis

To determine the robustness of the measurement system, an uncertainty calculation was carried out according to ISO/IEC Guide 98-3 [79] using the approach of Müllejans et al. [82].

The influencing factors on measurement uncertainty can be grouped into four main sections:

- Electrical data acquisition and calibration
- Device temperature measurement and conditioning
- Irradiance setting and spectral measurements
- Device mounting and connections

The measurement uncertainty analysis given in Table 4.9 has been carried out with regards to the calibration of devices similar to the c-Si reference cell that has been measured in section 4.3 but with a size of up to 45x45mm^2 (area for class A light intensity uniformity).

Influencing factor	Standard Uncertainty in parameter (k=1) [%]				
	Irradiance	**Voltage**	**Current**	**FF**	**P_{MP}**
Electrical data acquisition and calibration:					
	± 0.10	± 0.09	± 0.17	± 0.02	± 0.19
Device temperature measurement and conditioning:					
	± 0.00	± 0.08	± 0.01	± 0.03	± 0.09
Irradiance setting and spectral measurements:					
	± 1.59	± 0.08	± 1.95	± 0.00	± 1.83
Device mounting alignment and connections:					
	± 1.48	± 0.08	± 1.48	± 0.45	± 1.55
Combined uncertainty at high intensity:					
k=1	**± 2.18**	**± 0.16**	**± 2.45**	**± 0.45**	**± 2.50**
k=2	**± 4.36**	**± 0.32**	**± 4.90**	**± 0.90**	**± 5.00**

Table 4.9: Absolute uncertainty in I-V curve measurements when characterising similar devices to the c-Si reference cell

Electrical data acquisition and calibration:

Uncertainties in this group are mainly influenced by four factors: measurement card accuracy, calibration, measurement noise and temperature influences. The contribution to the absolute measurement accuracy is the largest in P_{MP} with 0.16% (k=1). The second largest contribution is due to the calibration of the shunt resistors and amplifiers. This was done with a Keithley 2440 power supply unit to an accuracy of 0.02% (k=1) in voltage and 0.11% in current. The contribution of measurement noise and the variation due to changes in operating temperature of the shunt resistor (±5°C used) is minor.

Device temperature measurement and conditioning:

This incorporates uncertainties due to the measurement and control of the device temperature. As indicated in the previous chapter, the temperature of the test device in the solar simulator is measured with a K-type thermocouple. The signal of the sensor is read directly by temperature controller hardware with a digital resolution in steps of ~0.1°C. The K-type thermocouple together with the controller ADU have been comparison

calibrated at multiple temperatures using a Fluke 7340 thermal bath and a secondary calibrated resistive temperature device (RTD). This has a total calibration uncertainty of better than ±0.05°C. On this basis, a temperature measurement uncertainty of ±0.25°C has been estimated. This includes fluctuations due to room temperature influences on electronics and other similar effects. A non-uniformity of ±0.1°C over the test device was estimated using an InfraTec VarioCAM PO thermal imager. The temperature increase during measurements due to the incident light is mainly caused by the halogen light sources. This heating effect was estimated at 0.3°C.

Irradiance setting and spectral measurements:

Uncertainties in irradiance and spectrum have major contributions in the measured I_{SC} and P_{MP} of the test device. A significant part of this comes from the calibration of the reference cell that has an uncertainty of 2.3% (k=2). The spatial non-uniformity over the illumination area of the LED-based solar simulator was measured at 1.9% over an area of 45x45mm^2. This result was used in the uncertainty calculation estimating a rectangular distribution with a reduction factor of 1.73. A temporal stability in the light intensity of 0.1% has been included in the calculations, as measurement tests in the previous sections have shown that this is achieved when using appropriate measurement timing.

Uncertainties in the determination of the spectral match are due to uncertainties in the relative SR measurement of the reference cell (estimated 5%) and the relative spectral output calibration of the light sources (estimated 10%). It has been shown in [91] and confirmed by [82] that the contribution of these factors to the spectral mismatch is 10 times lower. Thus, the uncertainty arising due to spectral mismatch is 1.1% (k=1).

Since the reference cell cannot be measured at the same time as the test device, both devices have to be measured separately one after the other, this means that an additional uncertainty in the range of measurement irradiance repeatability has to be accounted for. During repeatability measurements (presented in the previous section) a maximal deviation of ~0.20% was measured, which has been included here.

Device mounting and connections:

The main uncertainty contribution in the group of device mounting and connections is from the angular distribution of the light. The angle of incoming light is up to about 17° in the solar simulator because of a very large area of light sources with respect to the test device. For angles of incidence within this range a cosine response is a good approximation of the PV device performance at varying angles of incoming light as also shown by Balenzategui et al. [92]. Assuming a rectangular distribution of the incoming light this has an uncertainty impact of 1.48% (k=1) on irradiance and current respectively. The influence of cell alignment (estimated at ±1°) is negligible in comparison. The uncertainty in the fill factor due to the 4-wire connection of the test device was estimated to be the same as in [82] (0.45%).

4.5 Recommendations for future versions of the solar simulator

The analysis of the performance has given clear indicators that the LED-based solar simulator prototype has some shortcomings. Nevertheless, with its functionality and the ability to deliver a variable quasi-continuous wavelength output, it also proves that the main concept works and only needs some minor refinements. The evaluation of the prototype identified improvements to be implemented in future designs. In the following subsections those improvements are discussed.

4.5.1 Simulator light sources and optical set-up

The first and main improvement needed is in the output spectrum. With 8 different LED colours a good spectral match was achieved up to a wavelength of 680nm. This should be enhanced by using many more different LED colours (20 to 30) in the full spectral range of 350nm to 1100nm and thus replacing the remaining halogen light sources. An initial simulation, illustrated in Figure 4.14, shows that it is possible to achieve a near perfect match to the standard spectrum. Using more colours will also have positive effect on automated measurements and spectral response fitting (more

information in chapter 5) and G-T-E measurements for energy rating (see section 6). Additionally, by using purpose-designed LEDs, the light intensity output density can be increased and the LED array size reduced at the same time.

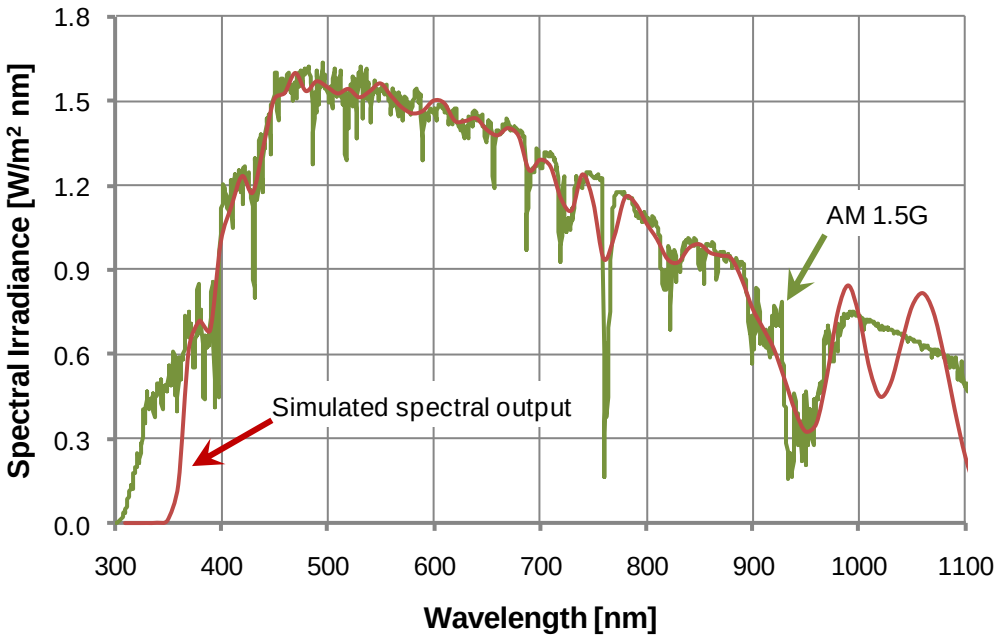

Figure 4.14: Initial simulation of achievable spectral output of an LED-based solar simulator

The prototype version achieved class A homogeneity over an area of 45x45mm^2. This needs to be extended to a larger area to be able to measure full wafer solar cells and eventually PV modules. This can be done with the help of specially designed optics that first of all mix the incoming light from all different LED colours and then collimate it onto a square target area. This should not only improve irradiance uniformity but also largely eliminate spectral variations over the illumination area. It would also increase the efficiency of light collection, since a large part of light energy in the prototype actually does not hit the test area and is wasted. Additionally, with a larger uniformly illuminated target area it would be easy to position a reference cell next to the PV devices for measurement intensity feedback which would eliminate light intensity repeatability uncertainty [0.2% (k=1)] on PV device calibrations. Initial simulations on a 300x300mm^2 target area, as shown in

Figure 4.15, demonstrate that a non-uniformity of approximately ±0.5% over the full test area is theoretically possible.

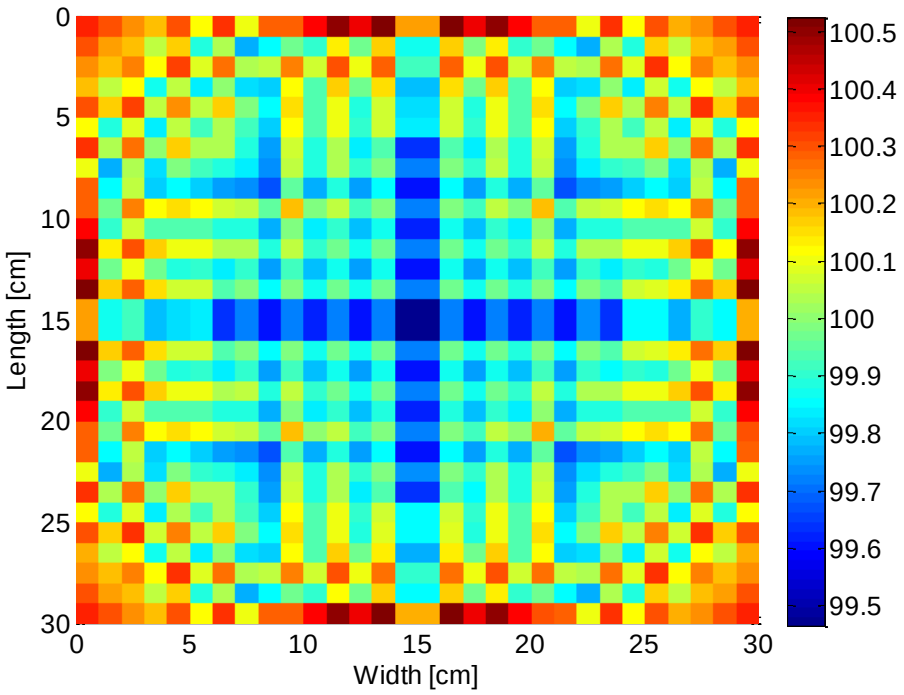

Figure 4.15: Simulated relative intensity field [%] achievable in future designs of the solar simulator; a non-uniformity of light intensity within ±0.5% is possible

To reduce the angle of incidence of the incoming light onto the PV device the distance of the LED array to the PV device needs to be increased. Additionally, the simulator case should be equipped with horizontal blinds, to reduce possible reflections from the side walls. Reducing the angle of incidence from 17° down to 5° would reduce the uncertainty impact from angle of incidence on irradiance and current from 1.48% down to 0.13% (k=1).

4.5.2 Light source control electronics

With careful measurement set-up on the prototype version it was always possible to keep the light intensity variations during measurements at class A levels (well below ±2%). Even so, this can be further improved, since no direct light intensity feedback has been used. By implementing such

feedback, many obstacles in the prototype version can be overcome, which include:

- The light intensity drop over measurement time
- Spectral variations due to different light source temperature coefficients
- Light intensity and spectral variation between measurements
- Room and water cooling temperature influences on light intensity
- Relatively long measurement and cool down periods

This new light source control would be an intensity-current cascade regulation circuit, separate for each colour with an outer regulation circuit for controlling the intensity and an inner regulation circuit, controlled by the outer circuit, driving the current of the LED. This kind of control increases the drive current of the LED as it heats up and the voltage drops down. Thus, this would deliver a highly stable and repeatable light output with the additional benefit of a better spectral control, since intensity rather than LED drive current is the main controlling factor. This type of regulation has been used successfully in other types of solar simulators, stabilising intensity variations from power fluctuations.

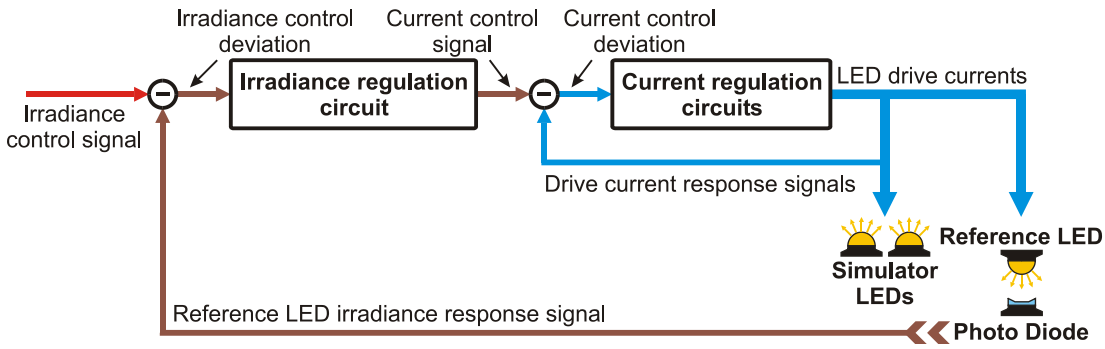

Figure 4.16: Basic cascaded intensity / current regulation circuit for LEDs: The inner current regulation circuit drives the LEDs using the current feedback signals. The current control signal is provided from the outer irradiance regulation circuit, which is driven by the irradiance control signal and receives intensity feedback from the photodiode of the reference LED.

The prototype version used one regulation circuit per light source to be able to adjust intensities. When implementing optics, this would no longer be necessary and light sources of the same type could be largely driven in series connection. This would reduce complexity and costs and energy consumption from dumped heat of the regulation electronics.

4.5.3 Other improvements

Very important for future designs would be the implementation of an additional measurement range selection for current, voltage and irradiance. This could halve measurement uncertainties in the electrical data acquisition and calibration group and would also keep them from increasing rapidly when measuring at very low intensities as such as for energy rating device characterisation (see chapter 6 for more information).

While a better light source engine and driver electronics have the potential to greatly enhance the system quality and measurement repeatability it is also possible to implement a spectroradiometer for monitoring the light output spectrum. If not using a spectroradiometer, a reference diode can be used for each LED colour as needed for direct irradiance control of the LEDs. The reference diode would monitor the actual intensity of the colour from which the complete spectrum can be calculated using previously measured spectral output data of each colour. Spectral output feedback has potential to largely reduce uncertainty in spectral output control and spectral mismatch calculations.

A more stable water cooling system that does not rely on the lab primary cooling for heat exchange is also desirable for future systems. This should use a water chiller that regulates the water temperature actively, which would improve stability and lifetime of the LEDs.

To enhance I-V characteristic measurements for energy rating and energy yield predictions, an automatic rotating stage could be implemented into a future LED-based solar simulator, as it would enable measurements at varying angle of incidence.

On the prototype version the temperature control system could only be regulated down to about 15°C due to condensation appearing on the test device at lower temperatures. To counteract this, one idea is to embed a double glazed chamber into future designs in which the air around the PV device is dehumidified and temperature regulated. This would also vastly improve the accuracy of regulating the temperature of PV devices that have a junction box or a frame and thus are not flat on the rear side.

By implementing the suggested improvements into future systems, the uncertainty in calibrating devices similar to the reference cell used in the initial measurements of this chapter can be reduced down to an estimated 2.9% (k=2) in P_{MP}. The estimated value includes an uncertainty in spectral mismatch of 1.4% (k=2) and is thus valid across all spectra. An uncertainty of 2.3% (k=2) of the secondary calibrated reference cell is also included. If a primary reference with an uncertainty of 0.5% (k=2) is used the estimated final uncertainty is reduced by more than one third to 1.8%.

4.6 Conclusions

The analysis of a prototype LED simulator has shown that it has the potential to deliver good quality PV device measurements. Measuring solar cells within an area of 45x45mm^2, the simulator has achieved a class BAA (spectral match class B, irradiance non-uniformity and temporal stability class A). An initial characterisation of a c-Si reference cell has been carried out. Uncertainty analysis shows that similar devices can be characterised to an accuracy within approximately 5% (k=2) in P_{MP}, which compares to 3% in most calibration houses [93] with standard equipment and irradiance sensors which are better calibrated.

The concept of a high quality solar simulator using LEDs as main light sources and thus providing exceptional variability in measurement conditions has been proven with the prototype version. Even so the measurement system has its shortcomings, improvements mentioned show that achieving the required intensities and qualities of a class AAA solar simulator is possible, but not trivial. Furthermore, the rapid improvement of LED

technology will make the overall energy delivery, spectral matching and control even better.

Research and development in LED-based solar simulators was advancing rapidly over the last years, supporting the strength of the argument. Currently two research groups have reported new LED-based solar simulator systems, one group at Myong Ji University in Korea [94] and another at the National Laboratory for Sustainable Energy at the Technical University of Denmark [95]. Strama MPS offers a large area LED solar simulator using white LEDs for modules up to a size of 2.2x2.6m^2 and achieving an intensity of more than 1000W/m^2 [96]. Additionally, a class AAA version produced by Strama MPS using four colours has been reported [97]. ZAE Bayern in Germany is one research group that is reportedly currently developing an LED-based system [98]. Spire Corporation recently received a grant to develop an LED-based solar simulator as well [99].

It should be highlighted that the system developed here is the first solar simulator of its kind that could be classified to the IEC standards as a solar simulator, i.e. meeting the minimum standards in terms of spectral match and intensity.

5 Method for Automatic Characterisation of Single- and Multi-Junction Solar Cells

Multi-junction solar cells have led to record efficiencies in solar energy conversion but are difficult to calibrate, especially at production relevant speeds. Due to the increased device complexity, measurements with commonly used single-lamp solar simulators are associated with large uncertainties as the accuracy of the calibration depends to a large extent on the agreement of the test spectrum with that prescribed by the standard. This defines the matching of the junctions within a multi-junction device and changes in the simulator light can lead to significant non-linear differences in current production and fill factor of the device (see illustration in Figure 5.1).

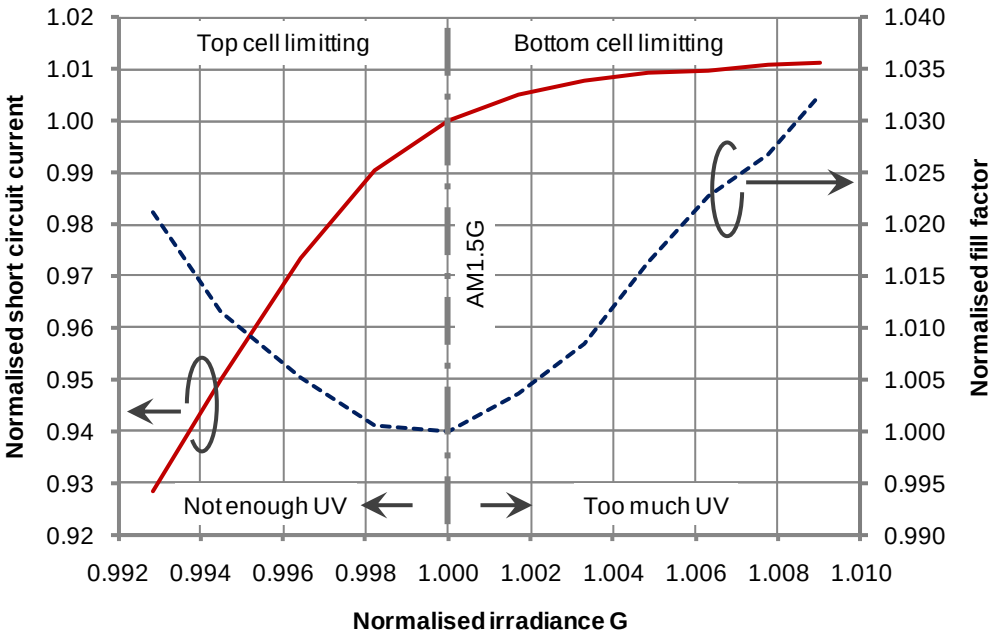

Figure 5.1: Nonlinearities in I_{SC} and FF caused by changes in the ultraviolet (UV) part of the solar simulator output spectrum on a double junction amorphous silicon (a-Si) solar cell; measured in the LED-based solar simulator

The non-linearity is caused by the current mismatch effect of stacked (series connected) cells as previously explained in section 2.1.4: if one of the stacked junctions receives less light than the other(s), it will limit the device current output. This can occur due to changes in the incident spectrum which, in combination with the spectral response of each junction, then determines the output of each sub-cell. At this point the surplus electrons in the junction with excess current are reabsorbed and the junction operates closer to its open-circuit voltage, which in most cases increases the squareness of the I-V characteristic and thus improves the fill factor [8].

As indicated in the previous chapters, one needs to operate a multi-source or spectrally adjustable solar simulator (e.g. with filters) to properly characterise multi-junction solar cells. By adjusting the spectral distribution of the simulator light output, stacked cells can be current balanced to a particular reference spectrum.

All measurement methods available require knowledge of the spectral response (SR) of each junction or at least the use of closely matched reference cells, which is costly since they must be fabricated specially. In production, most companies use reference modules that are calibrated in a test laboratory. The solar simulators in manufacturing plants are calibrated with the reference device to match the characteristics measured by the test house (e.g. I_{SC}, P_{MP} and V_{OC}) [100]. However, this method assumes that all devices tested in the production line have the same spectral response characteristics. In the case of thin film silicon devices, normal variation during production makes this assumption questionable. Especially in the case of amorphous silicon (a-Si), which is a meta-stable material, any change in its electronic state will result in a change of the SR of the device (see section 2.2.4 for more detail). In order to eliminate this additional uncertainty, one would need to measure the SR of each junction in each module. This is time consuming and currently not possible in production relevant times with today's monchromators and filter-based systems. The only system capable of measuring SR in these timescales is a real time EQE measurement system developed by the U.S. National Renewable Energy Laboratory (NREL) (see section 5.1.3 for further information). SR measurements are also normally not

carried out on full size modules because of additional difficulties. Thus there is an identifiable need for a fast and automated method for device characterisation without the need of previously obtained SR data or closely matched reference cells. This can reduce uncertainty in the determination of the power value, which has been identified as a key risk in PV system building.

The situation is similar for single-junction a-Si devices and other materials whose performance changes during operation. Without knowledge of the SR, no closely matched reference can be chosen. Thus, a method applicable for multi- and single-junction devices is needed. Further problems are experienced in characterising previously unknown or new technologies, which need to be calibrated in an institute. In some cases there is no detailed device information available and then a characterisation method that can detect the device type (i.e. number of junctions) additionally would be useful.

The LED-based solar simulator prototype, developed and constructed during this PhD work, provides a good variability of the output spectrum with 8 different LED colours and halogen light. This can be used to calibrate multi-junction solar cells. Since the system can work in a fully programmable automated mode, this opens the possibility for the development of a novel measurement method that can fully characterise PV devices automatically. The key to this method is a new SR measurement and fitting step approach, which acquires the SR data needed for accurately calibrating I-V curves taken in the solar simulator. It does not require additional SR measurements or closely matched reference cells. Furthermore, the method proposed here detects the device type (SJ or MJ) and can be used not only for power rating but could also be extended for PV device performance measurements for energy rating and energy yield prediction.

In the following sections, existing device characterisation methods for single- and multi-junction solar cells are first briefly reviewed. In section 5.2 the developed measurement procedure is explained in detail. Its theoretical capability and functionality are presented with results of two simulated measurements in section 5.3. Initial live measurements on the LED-based solar simulator are presented in section 5.4. In the penultimate section,

measurement results are discussed and implications for measurement accuracy are given followed by the conclusions of the chapter.

5.1 Review of device characterisation methods

Before one is able to discuss an automated measurement process for solar cells it is important to review the existing main characterisation methodologies and requirements in power rating of both single- and multi-junction devices. Those are described in this section with additional information on spectral response measurements.

5.1.1 Single-junction

Typically, single-junction solar cells are measured with a reference cell that has a SR closely matched to the test specimen. Reference cells are typically calibrated at STC conditions with regards to the IEC 60904-4 standard [81]. In this case the calibration value CV at STC conditions can be used to determine the intensity in the solar simulator. In the most basic power rating measurement at STC conditions the intensity of the simulator is adjusted until the I_{SC} of the reference cell is equal to the CV value of the calibration certificate and the I-V curve of the device under test is measured.

If the CV value at STC is unknown, or does not relate to the desired reference spectrum (i.e. any other than AM 1.5G), the theoretical short circuit current $I_{SC,R}$ or calibrated value CV_{REF} of the reference cell under any reference spectrum can also be calculated from the spectral response by means of equation (2.8):

$$I_{SC,R} = CV_{REF} = A_R \int S_R(\lambda) E_{REF}(\lambda) d\lambda \qquad (5.1)$$

Where S_R is the absolute spectral response of the reference cell, E_{REF} is the absolute reference spectrum, A_R is the reference cell area and λ is the wavelength. The measurement of the absolute SR can be associated with large uncertainties [84], which will furthermore affect the setting of the simulator light and thus the final uncertainty in the I-V curve measurement.

In most cases measuring with the basic method as described above is not possible as the SR of the test cell is normally different to that of the reference cell. Since the simulator light output does often not exactly match the reference sunlight spectrum this difference can lead to additional uncertainties. This error can be reduced by applying a spectral mismatch correction according to the IEC 60904-7 standard [77]. This methodology was first reported by Emery et al. [78]. The spectral mismatch factor MMF is calculated as given in equation (5.2), where E_S is the spectral irradiance of the simulator output and S_T is the SR of the test device. The CV of the reference cell under the reference spectrum is divided through MMF to obtain a new I_{SC} that corrects for the spectrum and spectral response differences. The simulator light intensity is adjusted to the corrected I_{SC} and the I-V characteristic of the device under test is more accurately obtained.

$$MMF = \frac{\int S_R(\lambda)E_{REF}(\lambda)d\lambda}{\int S_T(\lambda)E_{REF}(\lambda)d\lambda} \frac{\int S_T(\lambda)E_S(\lambda)d\lambda}{\int S_R(\lambda)E_S(\lambda)d\lambda} \tag{5.2}$$

The calculation of MMF requires knowledge of only relative spectral irradiance distributions and spectral responses. Since relative values are associated with smaller uncertainties, as previously mentioned in section 4.4.3, any uncertainties introduced are usually significantly smaller than the uncertainty of spectrally uncorrected measurements.

If the simulator light cannot be adjusted to the desired intensity, an additional irradiance correction according to IEC 60891 [52] must be carried out. This requires that the test specimen is linear over the range of interest (IEC 60904-10 [101]). For voltage corrections, the series resistance of the device under test is required. This can be obtained from additional I-V measurements at different intensities.

If no reference cell is available and the absolute SR of the test cell is known, one can also calculate the theoretical I_{SC} of the test cell at reference spectrum with equation (2.8) and adjust the simulator light until the calculated value is measured on the test cell [7]. Irradiance correction is in this case possible as well, substituting the reference cell I_{SC} and the theoretical I_{SC} with the ones from the test cell. In this method, however, it should be noted that

the significantly increased uncertainty in the absolute SR can lead to a large error in calculating the theoretical I_{SC} and setting the correct light intensity. Thus, there is a larger uncertainty in the actual calibration [84].

5.1.2 Multi-junction

The methods for measuring two-terminal MJ devices are in principle similar to the ones for SJ devices, with the exception that the simulator light is set differently to achieve the correct junction current balance in the device to test [7]. To do so, a range of approaches have been developed over time. They can be categorised into three main methods as reviewed in a paper by Heidler, K et al. [102] of which the differences between them lie in the initial requirements:

- the solar simulator method
- the absolute spectral response method
- the reference cell method

The solar simulator method relies on the solar simulator output being virtually identical to the standard spectrum AM 1.5G. If this is the case, there is no need to adjust the solar simulator spectrum for power rating, as the junction current balance is correct and only intensity is to be adjusted prior to I-V characteristic measurement. Since I_{SC} and FF especially in a MJ PV device are very sensitive to the incident spectrum, the only way to reduce uncertainties is to expend large technical effort to match the simulator spectral output to the AM 1.5G spectrum. This is possible with multi-source, multi-filter solar simulators. The advantage of this approach lies in its measurement simplicity, because no SR or spectrally matched reference cells are required. It has been used on simulators reported by Bennett [44] and Sopori [46].

As the name suggests, the absolute spectral response method uses mainly the absolute SR of each of the junctions in the MJ solar cell. The reference cell method uses reference cells for adjustments of the solar simulator. Both categories are further subdivided and differ in their additional requirements.

Emery et al. have reported two methods, one in each of the category, that require only a single source solar simulator [103]. In the reported absolute SR method the simulator light intensity is adjusted to match the I_{SC} of the limiting sub-cell in the MJ device under test. The uncertainty in the absolute SR approach arises from the difficulty of obtaining the correct I_{SC}, especially when testing devices with low shunt resistance. The I_{SC} of the MJ device can be higher than that of the limiting sub-cell, due to the limiting sub-cell being driven into reverse bias at I_{SC} condition (see Figure 2.6 of chapter 2). An improvement is the approach that uses a reference cell and a MMF correction to the limiting sub-cell to set the light intensity. Here, the absolute error in the setting of the light intensity is corrected and the actual measured I_{SC} of the MJ device under test is of lower uncertainty. Both approaches have a larger uncertainty in the FF however, as it depends also on the current of the non-limiting cell(s). Despite this, the reference cell approach is widely used as single source solar simulators are cost efficient and the method is simple.

Methods that involve multi-source solar simulators can achieve higher accuracy as they may be used to set the correct currents of all junctions in the device. The most simple and cost efficient reference cell method involving a multi-source simulator has been reported by R. Shimokawa et al. [104]. This method, named by the authors “supplementary-light method”, uses spectrally matched reference cells with a filter for each junction of the device under test to adjust the solar simulator spectrum and light intensity. As the method does not require the SR of the junctions in the device, it is relatively cost efficient and can be used in factory relevant time cycles. Although this method can achieve higher accuracy than using single-source solar simulators, it heavily depends on the spectral match of the reference cells to the test device and choosing a closely-matched reference cell without SR data is difficult.

Approaches that yield highest measurement accuracy use one or more reference cells and the SR of the sub-cells in the device under test to account for the differences between reference and test device. However, the methods are very time consuming, as they require prior SR measurements of

the junctions in the test device. The first method of this kind was developed by T. Glatfelter and J. Burdick [105]. The light intensity and spectrum of the solar simulator are set with help of calibrated reference cells with junction-SRs closely matched to that of the test sample. It utilizes the MMF correction approach on the CV of the reference cells for each junction and consequently uses only relative quantities of the reference cell and test device junction SRs, and relative simulator output spectral irradiance as measured by a spectroradiometer. Thus, the uncertainty in setting the accurate junction current balance in the test device is reduced to the relative measurement error. Further information on this approach can be found in [105]. A very similar method using an automated iteration process to adjust the spectrum was later reported by Heidler et al. in [106].

The approach of most interest in this work is this reference cell method further developed by Fraunhofer Institute for Solar Energy Systems (FhG-ISE) [107]. The iterative process to adjust the spectral output of the solar simulator is very much simplified in this method and its principle requirement is a multi-source solar simulator with separately controllable light sources that allow intensity adjustments without changing spectral distribution. The LED-based solar simulator meets this requirement (with the exception of the halogen lights) and thus the method has been adapted here to set the simulator intensity and spectrum. This approach is further explained below, based on details given in [107]:

In the case of a dual junction solar cell and two available adjustable light sources, each mainly influencing one junction, the simulator light can be adjusted with this method by first solving the two dimensional linear equation system in (5.3). The two unknowns B_1 and B_2 represent the intensity factors of the light sources. The relative spectral outputs of the two light sources are e_1 and e_2 and the relative SR of the top- and bottom-cell are s_{Top} and s_{Bot}.

$$\begin{aligned} B_1 \int s_{Top} e_1 d\lambda + B_2 \int s_{Top} e_2 d\lambda &= \int s_{Top} E_{REF} d\lambda \\ B_1 \int s_{Bot} e_1 d\lambda + B_2 \int s_{Bot} e_2 d\lambda &= \int s_{Bot} E_{REF} d\lambda \end{aligned} \tag{5.3}$$

With knowledge of the intensity factors it is now possible to calculate the theoretical short-circuit current density of the reference cell from each light source J_{RC}^{E1} and J_{RC}^{E2} (5.4), where S_{RC} is the absolute spectral response of the reference cell.

$$J_{RC}^{E_1} = B_1 \int S_{RC} e_1 d\lambda$$
$$J_{RC}^{E_2} = B_2 \int S_{RC} e_2 d\lambda \qquad (5.4)$$

In the presented case of using only one reference cell, it is important that the cell responds over the complete range of all sub-cells. Higher accuracies can be achieved with one reference cell per junction having closely matched spectral responses.

The simulator light sources need to be adjusted separately until the correct I_{SC} at the reference cell is measured. Afterwards the I-V characteristic can be acquired as normal. Irradiance correction is possible as long as the same junction current balance is set and the device is linear in the range of the correction.

5.1.3 Spectral response measurements

Spectral response is mostly measured with a grating or a filter wheel monochromator. The grating monochromator has advantages in terms of measurement resolution, as it is not limited to a given number of filters and has a much narrower wavelength band light output. The SR is measured in a tiny spot area of the cell (under-illumination), which means that measurements might not represent the actual average response over the complete cell. This can lead to higher uncertainties if the SR is measured in a particular good or bad spot [108, 109]. This problem normally does not exist with filter wheel EQE systems, since those usually illuminate the complete cell area (over-illumination).

It is also possible to measure SR of full sized modules. However, during measurements of wafer based silicon modules usually only one entire cell in the device is illuminated and not the complete module [110]. With thin film modules the situation is more difficult since a single cell is continuing over the

complete length or width of the module. On those devices the module is illuminated with a single monochromatic point and the current measurement is taken directly from the back side of the module [111], as otherwise the generated current signal is not measurable. A relatively new method uses a solar simulator with interchangeable narrow band interference filters. This way the complete PV module is illuminated and the average spectral response over the whole device is measured. The method has been developed by JRC-ESTI and is further described in a paper from Pasan SA [112], a company which is now offering a complete range of optical filters for its solar simulators. However, SR measurements using a solar simulator with interference filters as reported by Pasan SA have so far only been tested on single junction solar cells.

Similar to I-V measurements, spectral response measurements are much simpler with single- than with multi-junction solar cells. The SR of a SJ device can be measured relatively easily according to the IEC 60904-8 standard [113] by applying appropriate bias light onto the device under test and measuring the current response to a monochromatic incident light. Bias light is required because the photon collection efficiency is especially in low light conditions (below 300W/m^2) dependent on the light that is being absorbed by the PV device during the measurement [114, 115]. Ideally, the SR should be measured under AM 1.5G bias light at 1000W/m^2 intensity and 25°C cell temperature, as device temperature can also effect SR [11].

When measuring the SR of multi-junction devices, the application of white bias light is not suitable because the current response measured could be from any junction. By current limiting the junction to be measured, the correct current response without influence of the other junctions in the device is measured by taking advantage of the current mismatch effect. For a dual junction a-Si solar cell this means blue-rich bias light is needed to limit the bottom cell and red-rich bias light for the top cell [8] (see also Figure 5.1). In addition to the bias light, a bias voltage is also required because the limited sub-cell of a MJ device operates in reverse when the device is kept at overall I_{SC} which would lead to an overestimation of the SR. To make sure the limited sub-cell to measure is operating at I_{SC}, a forward voltage bias needs

to be applied to the MJ solar cell (i.e. for a-Si tandem cells a bias voltage of about ½ V_{OC} is required). Furthermore, the limiting junction should be generating about half of the current of the other junctions. This ensures that the other non-limiting sub-cells operate near V_{OC} so that the chopped monochromatic light does not significantly change the operating voltages of the sub-cells [8, 107, 116].

CREST operates an in-house developed filter based SR measurement system that is capable of measuring devices of up to ~100x100mm^2. Details of the system have been reported by C.J. Hibberd et al. [117]. The lamp and optical set-up have since been optimised and a four colour (Blue, Amber, Red, and IR) LED bias light system has been fitted which allows for accurate junction limiting and thus measurement of MJ devices. A single SR measurement on this system takes about half an hour. Considering that a reference cell measurement is needed for comparison calibration and several measurements might be averaged to reduce random errors, measurement of a SJ device alone can take several hours. On this timescale, SR measurements in the production line are impossible.

However, a new real time EQE measurement system technology has been developed at the NREL that is capable of measuring SR in production relevant speeds. The system, reported by D. Young et al. [66], uses monochromatic light from LEDs to illuminate a spot area of a solar cell. It is capable of measuring SR in less than one second over 10 points by applying alternating LED light in several frequencies at the same time. The SR data is extracted via fast Fourier transform (FFT).

Work on SR measurements with a LED solar simulator has been done previously at Tokyo University of Agriculture and Technology (TUAT). The idea was first proposed in a paper by S. Kohraku et al. [65]. The method developed used modulated light over a bias component from the LEDs to measure the discrete current response. A non-linear least square fitting method with a theoretical photocurrent formula was then applied to the measured points to acquire the complete SR curve. Further development with a complete description of the applied method and photocurrent formula was later published by Y. Tsuno et al. [118]. The current of a c-Si solar cell

was measured at three points (blue, red and near IR), while the peak wavelength of the LED defined the corresponding wavelength. The complete SR curve was fitted directly to the measured points using a 16 parameter photocurrent formula for c-Si devices of which two were actually fitted. The demonstrated result was a near perfect fit between measured and calculated SR from just three input points. It is not known how well the fit works with different devices or devices from a different production process.

A further method has been developed as part of this work. As further explained in section 5.2.2 it uses a novel method of fitting the short circuit currents measured with help of additional spectral output data. It allows using broad band spectral output light sources for fitting of the SR, which could not be done with the method at TUAT, hence the data from the white LEDs in TUAT's LED solar simulator (previously details given in section 3.2.2) was not used in the fitting.

The method developed during this work also allows for a cost effective measurement of the SR of entire modules in a solar simulator with stronger illumination of light and fewer artefacts from slow responding test devices. Additionally, voltage-dependent SR measurements, as reported in [119, 120], should be possible within one measurement set, because the complete I-V curve is recorded and not only a current value at a single applied voltage bias.

5.2 Automated measurement approach

The aim of this approach is that no information about the device under test is required, which means that the measurement system itself acquires all data in one automated routine, which includes:

- Detection of the device type (SJ or MJ) with number of junctions
- Spectral response determination of all junctions
- I-V measurements to any given reference spectrum (i.e. AM 1.5G, AM 3, AM 10, etc.)

The use of this method is not limited to the LED-based solar simulator. The main requirement for this methodology to work is a multi-source solar simulator that uses several light sources that have their spectral output spread over the spectral response of the test cell. Ideally, but not necessarily, light sources should not change their spectral output when changing intensity. If this is the case, then a monitoring sensor for each of the light sources is sufficient to calculate the total spectral output in the solar simulator during I-V curve measurements. If not, then the spectral output of simulator should be monitored using a spectroradiometer.

The final requirement is a reference cell of known absolute spectral response without zero response over any part of the test cell SR band.

As shown in a simplified flow chart in Figure 5.2, the complete measurement routine can be separated into several tasks. In the following sections each part is described in more detail.

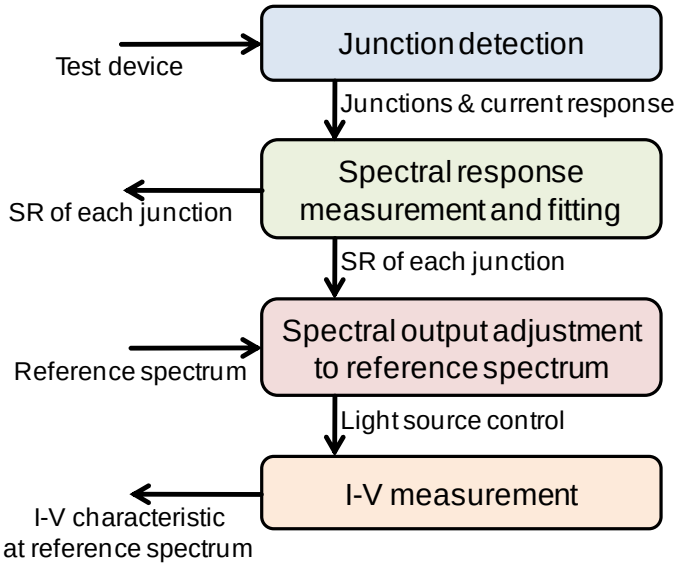

Figure 5.2: Simplified flow chart of the automated characterisation approach for single- and multi-junction devices

5.2.1 Junction detection

Since the SR measurement for SJ and MJ devices differs largely from each other, it is vital to first detect how many junctions are in the test device. Also, in the case of a MJ test device one needs to know roughly how much

influence each of the light sources has on the junction currents in order to properly limit the junctions during SR measurements. This data is acquired in the first step of the method: the junction detection. As apparent from Figure 5.3 this step can be separated into several smaller parts. The basic principle of the junction detection is to take advantage of the current limitation effects that cause non-linearity in MJ devices.

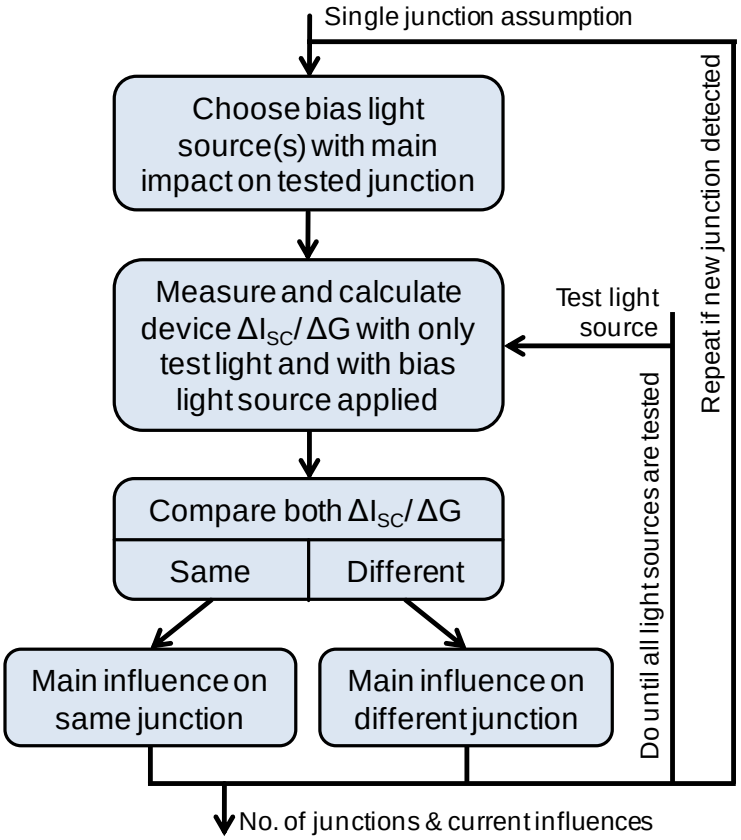

Figure 5.3: Flow chart diagram for detecting the junctions and for measuring the current generation on each junction from the light sources of the device under test

At first, a light source needs to be chosen as bias light which definitely has greatest influence on one junction (e.g. UV light for the top junction). In the following step, the I_{SC} of the device is measured at two different light intensities (high and low) in two configurations: without bias light and with the bias light held at one intensity level. During these four measurements the intensity G is recorded using a reference cell, spectroradiometer or by means of intensity sensors on each light source. With the acquired data the ΔI_{SC}

over ΔG (ΔI_{Ln}) behaviour can now be calculated for the two conditions without and with bias light according with the following equation (5.5):

$$\Delta I_{Ln} = \frac{\Delta I_{SC}}{\Delta G} = \frac{I_{SC1} - I_{SC2}}{G_1 - G_2} \tag{5.5}$$

Where I_{SC1} and I_{SC2} are the short circuit currents of the device under test measured at high and low intensity. G_1 and G_2 are the respective measurement irradiances.

Both results are then compared. If they are the same within a measurement error margin (5% used here) then the tested light source influences the same junction as the bias light source. If this is not the case then the light source tested has its main influence on a different junction, as with the application of the bias light a different junction was current limiting compared to without bias light. A relatively large error margin of 5% has been used here because measurements are carried out at low light conditions that are associated with larger measurement uncertainties. Furthermore, some nonlinearity can be expected even from single junction devices.

The measurement procedure is repeated until all available light sources are tested. If only influence on the same junction has been detected, then the device under measurement is a SJ device and all the ΔI_{Ln} factors calculated correspond to one junction. If one or more light sources influenced a different junction (a second junction has been detected) then the procedure will need to be repeated by choosing a new bias light source, which has most influence on the other junction. By doing so, the current limitation effect is used to determine the current influence ΔI_{Ln} of all light sources on the junctions. The ΔI_{Ln} value calculated is valid for the limiting junction at the time of measurement.

The output of this step and input for the SR measurement and fitting part is the number of junctions and the approximate light source current influence on each junction. The result here cannot be seen directly as SR measurements as the device was not properly irradiated (and in the case of a MJ device voltage) biased, but high accuracy is not needed at this point.

The procedure has been successfully tested for double junction devices. If for example three junctions need to be detected, the procedure can be extended by using not only one but two bias light sources, each having a main effect on a different junction.

5.2.2 Spectral response measurement and fitting

The second and main part of the measurement method is, as illustrated in Figure 5.4, separated into three smaller tasks. The SR is not measured as in the conventional approach at each point directly (see review in section 5.1.3). Instead, the SR is obtained based on fitting algorithm with an optical model from a number of measured currents of the limiting cell under different incident spectra.

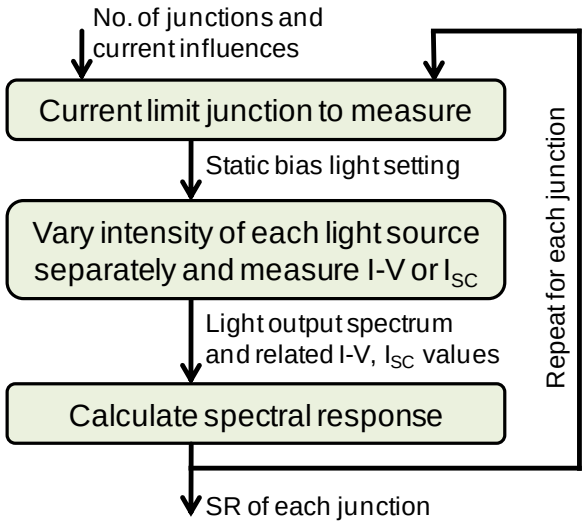

Figure 5.4: Basic schematic flow diagram for acquiring the spectral response of each junction

The first task, to limit current of the junction to measure, differs slightly depending on the PV device type detected in the previous step (SJ or MJ). In the case of a SJ device, this step is simplified and only the appropriate bias light intensity (i.e. 1000W/m^2 at roughly AM 1.5G) is calculated from the ΔI_{Ln} factors acquired previously. For MJ devices, the junction current balancing is additionally very important to obtain valid SR results. Since the ΔI_{Ln} data of each junction is available, it is possible to calculate a bias light setting at which the junction to measure in the test device only generates about half of

the current as the other junctions available, thus strongly limiting the cell to measure.

After current limiting the cell to measure, the intensity of each light source is independently increased and decreased on top of the applied bias lighting. After every adjustment, a new current (I_{SC}) is measured with either a bias voltage applied as necessary or as a complete I-V curve. At the same time the spectral output (E) of the simulator is recorded, which is ideally done with a spectroradiometer or using a reference detector for each of the available light sources, from which the spectrum can be calculated if the spectral output is not significantly changing with light intensity.

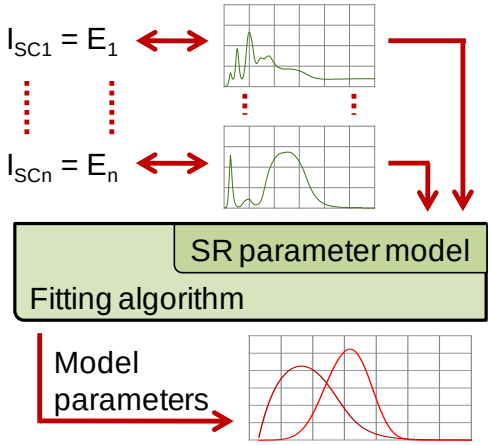

Figure 5.5: Spectral response fitting method; measured I_{SCn} and spectral output (E_n) pairs are fed into a fitting algorithm that fits the parameters of the SR parameter model by comparing calculated currents with the measured ones, if the resulting fitting error is low enough, the SR of the device should be accurately described

Acquiring the SR curve for each junction is the most critical part. For this, the measured I_{SCn} and spectral output (E_n) pairs are fed into a parameter fitting algorithm. This algorithm calculates new theoretical device short circuit currents with an embedded parameter model of the SR and the measured spectral outputs. These are then compared with the measured I_{SCn} values and, depending on the result, the model parameters are adjusted. This iteration step is repeated until the error between the calculated and measured I_{SCn} values is below a pre-set minimum. The obtained result is a

set of model parameters that describe the SR curve (see illustration in Figure 5.5).

The Levenberg–Marquardt fitting algorithm is used here, because of its capability to fit parameters of highly nonlinear models. Further details can be found in [121, 122]). However, the optimal choice of fitting algorithm may be dependent on the type of SR parameter model used and essentially any fitting algorithm could be implemented.

Fitting with a SR model based on device physics can achieve better results than, for example, using a general polynomial function. The limitation in this approach is that the SR model used for fitting must be suitable for the SR of the device under test otherwise the obtained result may be nonsensical. In the case of an unknown device, it can be useful to test different SR models and select from the best result, i.e. the one with the lowest residual error.

The minimum number of measurements at different spectra required is dependent on the model used. In other words, a model that uses 12 parameters cannot be fitted from 11 I_{SCn} and E_n data pairs, being underdetermined. Generally, the more data points are available, the higher the chances of a successful fitting of the SR. The solar simulator does not necessarily have to have as many different lamps as parameters in the model, as long as the sources present can generate a sufficient number of different spectra. Nevertheless, a larger number of different sources spread over the entire wavelength response of the test device will have a positive impact on fitting results. Light sources do not have to have a narrow band wavelength output, i.e. do not need to be LEDs. A sufficient number of different broad band light sources should result in a good fit as well.

In the case that the device type is known and a similar reference device is available, the SR measurement and fitting can also be carried out without the junction detection using the reference cell for bias light setting, which shortens the measurement time. In the case of a MJ test device this means that similarly responding reference devices for each junction are required to give feedback of the actual junction current balance.

5.2.3 Spectral output adjustment

Since the SR of the junctions in the device under test is now known, the spectral output can be adjusted to achieve the same balance of junction currents within the PV device as it would have under the given reference spectrum. This is possible with different methods for SJ and MJ devices as described in section 5.1. Within this work, the reference cell method developed from ISE was applied. A schematic diagram of the required tasks is illustrated in Figure 5.6.

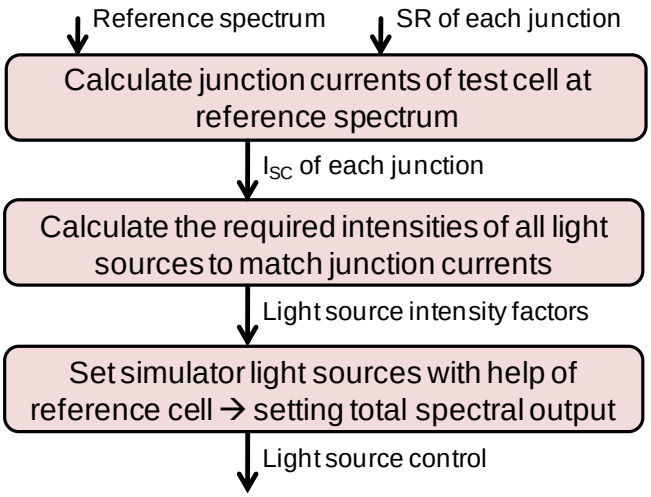

Figure 5.6: Schematic for adjusting the spectral output to achieve the same junction currents as experienced under reference spectrum

Simulators with more adjustable light sources than junctions require an identification of the light sources influencing each junction the most. An intensity factor can then be used for each junction including the light sources that have most influence on this junction to optimise the balance. Every junction in the device requires a minimum of one light source predominantly influenced by it. This ensures that the system of linear equations in (5.3) can be solved and no negative values are solutions as light source intensity factors [107].

5.2.4 Current-voltage characteristic measurement

Finally, once the light intensity and spectrum is adjusted and set, the actual measurement of the I-V curve can be carried out. The result is an I-V curve measured at conditions of the reference spectrum and the correct I_{SC}, V_{OC}, FF and P_{MP} will have been acquired.

5.3 Simulation of a full measurement

To underline the functionality of the proposed method, and to demonstrate the concept, a simulation has been carried out. It presents the ideal case without any measurement uncertainties. Two devices have been simulated: a single junction and a double junction a-Si solar cell. In the following sub-sections, it is explained under which conditions the simulated measurements were done and simulation results are presented and analysed.

5.3.1 Simulation conditions

The measurement approach has been fully programmed in LabVIEW and embedded into the LED-based solar simulator software. For testing and optimisation purposes, the software includes an additional function for simulating an I-V curve instead of a direct measurement. The simulation uses the same light source spectral outputs and range of intensity variations as seen and calibrated on the real system (see section 4.2.3 for details of the calibration of the simulator light sources).

The I-V curve of the both devices was simulated using the analytical model for a-Si solar cells developed by J. Merten et al. [3] as described section 2.1.1. In the case of the double junction device, both junctions have been simulated separately first and then the voltages were added to form the complete I-V curve with both junctions being connected in series.

Each junction in the test device was given a realistic SR curve that was measured previously using CRESTs filter based SR measurement system on similar devices. To simulate the I-V curve, the I_{SC} of each junction was first calculated using the SR and the estimated spectral output. From this point

the photocurrent of each junction was determined. The full I-V curve was then calculated with help of a Newton-Raphson fitting algorithm for a range of input voltages.

Two SR parameter models have been implemented for SR fitting. The first model is an optical model specifically developed for a-Si devices. This model by H. Schade and Z. E. Smith [123] uses the following equation (5.6):

$$\begin{aligned} EQE(\lambda) &= \left[1 - A_{TCO}(\lambda)\right] \cdot \left[1 - A_P(\lambda)\right] \cdot \left[A_I(\lambda)\right] \\ A(\lambda) &= 1 - \exp\left[-\alpha(\lambda) d\right] \\ \alpha(\lambda) &= p_1 + p_2 \exp\left(\frac{\lambda - p_3}{p_4}\right) \end{aligned} \tag{5.6}$$

Where p_n are the model parameters (12 in total) and EQE is the external quantum efficiency. The layer thickness d was fixed to a value of 1 to reduce the number of unknowns, as the parameters p_1 and p_2 describe d as well. The EQE was converted into SR for current calculations.

The second SR model implemented is a very much simplified exponential (EXP) model that only explains the shape of the SR without the underlying physical detail. It can be used for a wider range of devices and, as apparent from equation (5.7), uses only seven parameters. In principle, the first part of the equation with the parameters p_1 to p_3 describes the absorption and reflection losses of the encapsulation and front glass surface. The second part describes the absorption curve of the active layer in the device.

$$EQE(\lambda) = \frac{1}{p_1 + EXP\left(\frac{\lambda - p_2}{p_3}\right)} \cdot \left\{ \frac{1}{1 + EXP\left(\frac{\lambda - p_4}{p_5}\right)} - \frac{1}{1 + EXP\left(\frac{\lambda - p_6}{p_7}\right)} \right\} \tag{5.7}$$

The EXP model has been developed as part of this work. Its development was inspired by the absorption function of glass stated in [118]. This function was corrected to transmission in equation (5.8), where λ_0 is the centre wavelength of the UV transmitting cut-off and a is the change rate.

$$f(\lambda) = \frac{1}{1 + EXP\left(\frac{\lambda - \lambda_0}{a}\right)} \tag{5.8}$$

Since the solar simulator, as previously indicated in section 4.2.4, is not capable of measuring PV devices at AM 1.5G spectrum at 1000W/m^2 the reference target spectrum used here is the AM 1.5G spectrum scaled down to 700W/m^2. This has been done to avoid the use of irradiance corrections procedures.

5.3.2 Single junction simulation results

The result of the junction detection step in the automated measurement method is presented in the left graph of Figure 5.7. For this graph, the acquired ΔI_{Ln} values were converted to current densities (i.e. divided by device area) and plotted versus the peak wavelength of each light source type to be able to compare the result with the SR used for I-V simulations. As apparent from the figure, the points in the range of 350nm to 550nm from the coloured LEDs match the actual SR curve quite well. This is due to their narrow band output and is not seen with light sources that have a wide band output such as the warm white LEDs and halogen lights. Here the average response over the range is more obvious.

The complete simulation has been carried out using both SR parameter models. As apparent from the SR fitting results illustrated on the right side of Figure 5.7, both parameter models were able to describe the SR of the simulated device with good agreement. The a-Si model achieved a better match in the red to infrared range of the spectral response. The larger deviation in this area on the EXP model can be explained by a lack of corresponding light sources. Since only the broad band halogen light supplies significant output over this wavelength, the fitting resulted in a more averaged SR. The deviation is not due to the EXP model itself as during development of this function the SR was also fitted directly as part of the validation and the resulting fit was near perfect.

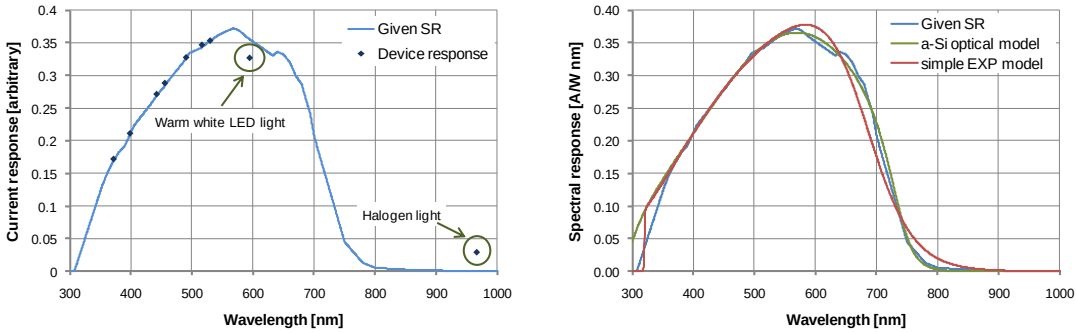

Figure 5.7: Simulated results of the measurement approach using a single junction a-Si solar cell: junction detection (left), spectral response fit (right)

A deviation in the SR used for I-V simulations is also seen on both fitting results in the UVB area. This was caused by a lack of data to fit in this range, as no UVB spectral output is available from any of the light sources.

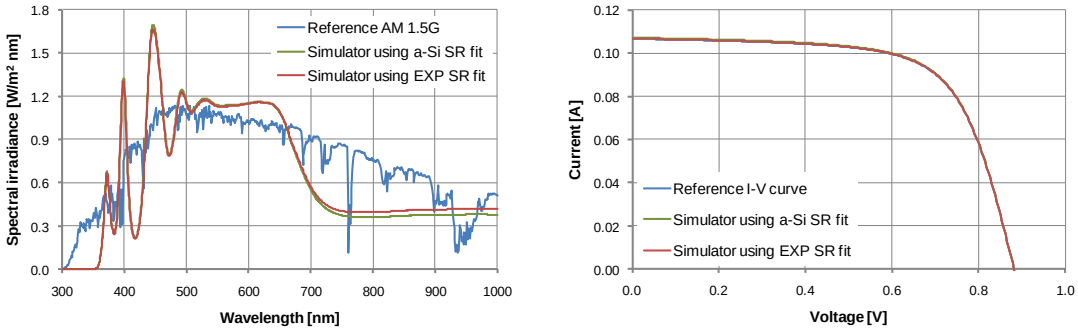

Figure 5.8: Simulated results of the measurement approach using a single junction a-Si solar cell: calculated output spectra (left) and final I-V curve (right)

For spectral output adjustments the standard spectrum scaled to 700W/m^2 was used as reference. The resulting spectral output of the simulator is illustrated in on the left side of Figure 5.8 for both SR fitting results. The settings are slightly different for the two methods but would give the same currents for the corresponding SRs.

The final results in the simulated I-V curve measurements show that the I-V curve acquired in the simulator as result of the different SR fitting models are near identical to the I-V curve at AM 1.5G reference spectrum (right side of Figure 5.8). Table 5.1 details the deviations of the key parameters between

the I-V curves. Contrary to expectations based on the SR fitting, the simple exponential SR fitting gave a better I-V curve end result.

Parameter	Reference I-V curve	Deviation with EXP SR fit	Deviation with a-Si SR fit
V_{OC} [V]	0.88	0.00%	0.00%
I_{SC} [mA]	106.58	0.08%	0.49%
V_{MP} [V]	0.69	0.00%	-0.04%
I_{MP} [mA]	92.31	0.07%	0.47%
P_{MP} [mW]	63.36	0.07%	0.44%
FF [%]	67.43	-0.01%	-0.06%

Table 5.1: Deviation between the simulated end result I-V curves to the reference I-V at AM 1.5G spectrum; the end result using the EXP model yielded a better match

5.3.3 Double junction simulation results

The 2nd junction in the double junction a-Si device simulated was successfully detected in the first step of the measurement approach. Again, the resulting current influence from the light sources on each of the junctions in the device matched the SR curve quite well for narrow wavelength spectral emissions, as apparent from the illustration on the left side of Figure 5.9.

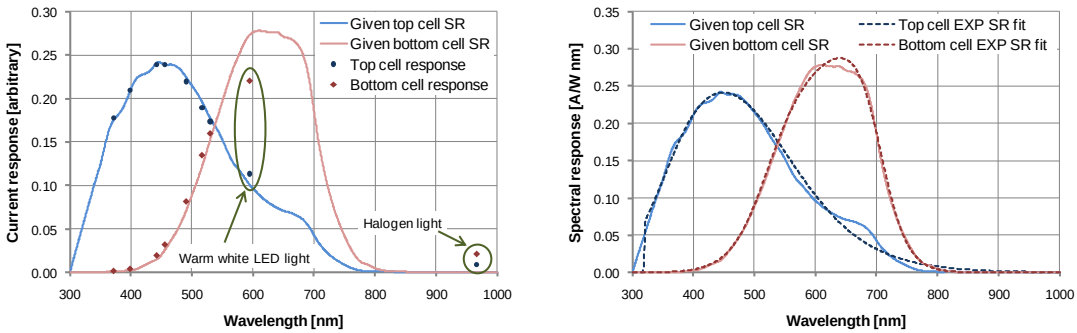

Figure 5.9: Simulated results of the measurement approach using a double junction a-Si solar cell: junction detection (left), spectral response fit (right)

In the SR measurement and fitting step of the method a voltage bias of 0.8V has been used on the I-V curves simulated under bias light to extract the current values for the fit. This is approximately equal to ½ V_{OC} [8]. As

previously indicated, this has been done to get a better approximation of the I_{SC} of the limiting junction. As apparent from the right side of Figure 5.9, the fitting result using exponential SR parameter model matches well to the real SR curve used for I-V simulations. The hump in the 650nm to 700nm region of the given top junction SR curve could not be represented by either model. The fitted SR is instead averaged around this area. The a-Si optical model fitting (not shown) resulted in a very similar fit but a strongly negative SR in the UVB region due to the lack of spectral output from light sources in this region.

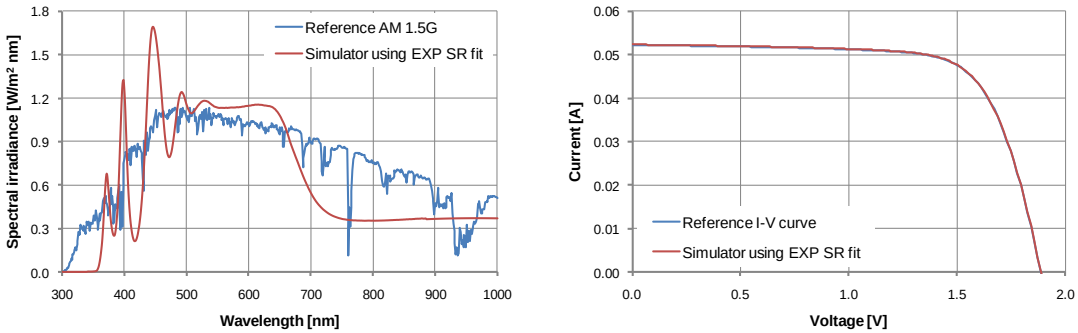

Figure 5.10: Simulated results of the measurement approach using a double junction a-Si solar cell: calculated output spectra (left) and final I-V curve (right)

A spectral output similar to the AM 1.5G reference spectrum has been calculated in the adjustment step (see left side of Figure 5.10). The spectrum was calculated to generate the same junction currents and current balance as under the reference spectrum based on the SR fitting result. The starting parameter set for the adjustment was a configuration of the light sources at best AM 1.5G fitting which means that the algorithm calculated the required absolute intensity change and adjusted the balance as needed.

The final I-V curve result in the simulated measurement, presented on the right side of Figure 5.10, shows that the acquired I-V curves would have been near identical to the reference I-V curve at AM 1.5G spectrum. Table 5.2 details the deviations in the I-V critical values between both. Results shown here are based on the SR fitting results using the EXP model. Using the a-Si model for fitting (not shown) led to a very similar result but with underestimated I_{SC}.

Parameter	Reference I-V curve	Simulator I-V curve	Deviation
V_{OC} [V]	1.89	1.89	0.00%
I_{SC} [mA]	52.21	52.31	0.19%
V_{MP} [V]	1.51	1.51	-0.02%
I_{MP} [mA]	47.26	47.33	0.14%
P_{MP} [mW]	71.36	71.44	0.12%
FF [%]	72.41	72.35	-0.07%

Table 5.2: Deviation between the end result I-V curve to the reference I-V at AM1.5G spectrum of the simulated double junction a-Si solar cell; details shown here are with regards to the SR fit using the simple EXP model

5.4 Initial measurement results on the LED-based solar simulator

From the results of the simulated measurements in the previous section it is apparent that the demonstrated approach has the potential to deliver high measurement accuracy without the need of additional spectral response measurements. To test the potential of the measurement routine under real conditions, initial measurements have been carried out with the LED-based solar simulator. Those are analysed in the following part of this chapter. Limitations due to non-ideal measurement conditions in the presented case are explained.

5.4.1 Measurement conditions

Initial tests of the automated measurement approach using real PV devices in the LED-based solar simulator have been carried out on two different a-Si mini modules: The first device is a 50x47mm^2 single junction mini module with 3 cells connected in series and the second device is a double junction a-Si/a-Si device with 5 cells connected in series and an area of 62x46mm^2.

The AM 1.5G reference spectrum for I-V measurements was scaled to 700W/m^2 to avoid additional irradiance corrections. The simple exponential

model has been used for SR fitting, as it gave slightly better results in the simulations.

Both devices have been calibrated beforehand to provide a base for comparison between the results of the automated measurement approach and the actual device performance. The SR curves have been calibrated against the JRC-ESTI-calibrated c-Si reference cell using the filter based SR measurement system in CREST (details in section 5.1.3). The I-V curve of each device was measured in the Pasan solar simulator at CREST using the same reference cell with spectral mismatch correction applied. Since the Pasan solar simulator does not have the ability to change the spectrum, the mismatch correction for the double junction device was applied to the limiting junction. This was the top junction under the solar simulator spectrum and reference spectrum.

It was mentioned previously (section 5.2) that the measurement approach requires a reference cell and a spectroradiometer to monitor the intensity and irradiance spectrum of the solar simulator light. As stated in chapter 4, this was not possible due to the increased spatial non-uniformity in the corner areas and the low measurement quality of the available spectroradiometer. The determination of light intensity and spectrum was instead estimated to be as previously calibrated. The calibration was based on the I_D vs. G curve and spectral output measurement of each of the light sources (see section 4.2.3). Due to this limitation, the following measurement results should not be seen as the full potential of the abilities of the automated measurement method, but more as initial measurements with large potential for improvements.

5.4.2 Single junction measurement

In the first step, the solar simulator successfully detected only one junction. Comparing the measured current response of the mini module from the light sources against its previously measured SR (left of Figure 5.11) shows that the response of the narrow band output LED sources matches quite well to the SR as previously shown in the simulated measurement (see left of Figure 5.7 for comparison).

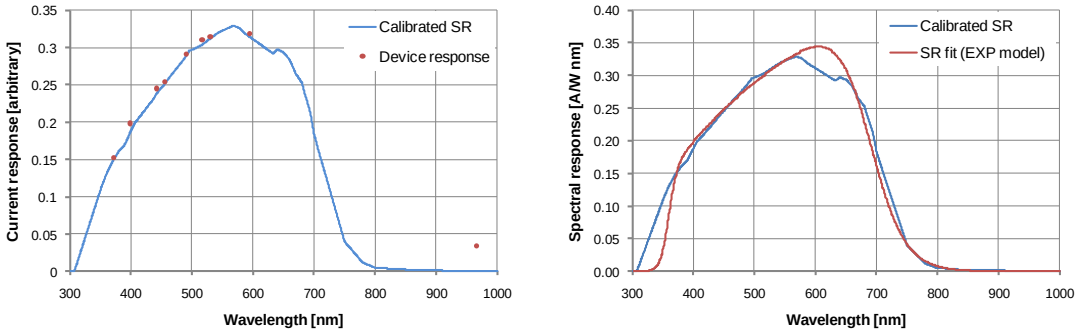

Figure 5.11: Initial results on a single junction a-Si mini module: junction detection (left), spectral response fit (right); fitted and calibrated SR match to an acceptable degree.

The result of the SR measurement and fitting part (right side of Figure 5.11) shows a relatively good match with an overestimation of the device spectral response in the 600nm region. The differences in the UV region are due to a lack of spectral output from the light sources as previously explained in section 5.3.2.

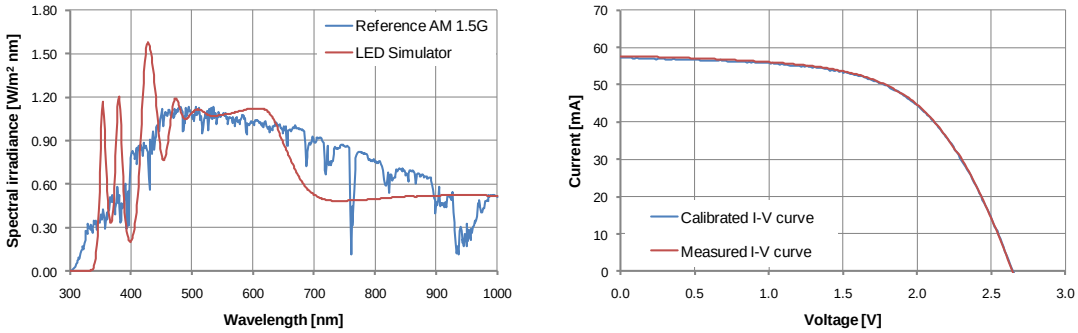

Figure 5.12: Initial results on a single junction a-Si mini module: calculated output spectra (left) and final I-V curve measurement result (right);

The small error in the SR measurement and fitting step carries through to the final parts of the method and affects the setting of the spectrum. The output spectrum itself is set to a good match of the reference spectrum, as visible on the left of Figure 5.12. However, the theoretical device I_{SC} calculated from the fitted spectrum slightly overestimates the current output and thus leads to the final I-V curve being measured at a higher intensity than required (right of Figure 5.12).

The deviations in the I-V curve characteristic parameters are given in Table 5.3. In principle, the deviations between the calibrated and measured I-V curve are within the standard uncertainty range (k=1) given in section 4.4.3 of the previous chapter. Even so, the I_{SC} was overestimated by 0.6% and the V_{OC} is underestimated by -0.1%. The main reason for this is an increased uncertainty in temperature control and measurement as during calibration in the Pasan solar simulator only the air around the mini module was controlled at 25°C and the device temperature itself could not be measured. Interestingly, the deviation in P_{MP} is lower than that in I_{SC}. This is due to the lower V_{OC} and FF measured in the LED-based solar simulator.

Parameter	Measured I-V curve	Calibrated I-V curve	Deviation
V_{OC} [V]	2.65	2.65	-0.11%
I_{SC} [mA]	57.65	57.29	0.64%
V_{MP} [V]	1.90	1.87	1.54%
I_{MP} [mA]	47.63	48.23	-1.24%
P_{MP} [mW]	90.33	90.08	0.28%
FF [%]	59.23	59.38	-0.24%

Table 5.3: Deviation between measured and calibrated I-V curve; the error in the SR measurement and fitting step has resulted in an overestimation of the device I_{SC}.

5.4.3 Double junction measurement

As illustrated in the top left site of Figure 5.13, the current response of the double junction a-Si mini module from the narrow-band output LEDs does not accurately match the SR curve of the top junction as one would expect from simulations. This can be seen as an early indication of an incorrectly estimated light intensity of the light sources.

The current data for the SR fitting was extracted from the measured I-V curves at a voltage bias of 4.3V (~½ V_{OC}). The SR fitting resulted largely in an underestimation of the spectral response of the top and bottom junctions (top right side of Figure 5.13).

Due to the large deviation between the calibrated SR and the SR acquired through the measurement and fitting step, the spectral output of the solar simulator was set incorrectly (see bottom left of Figure 5.13). This also means that the junction current balance is set incorrectly.

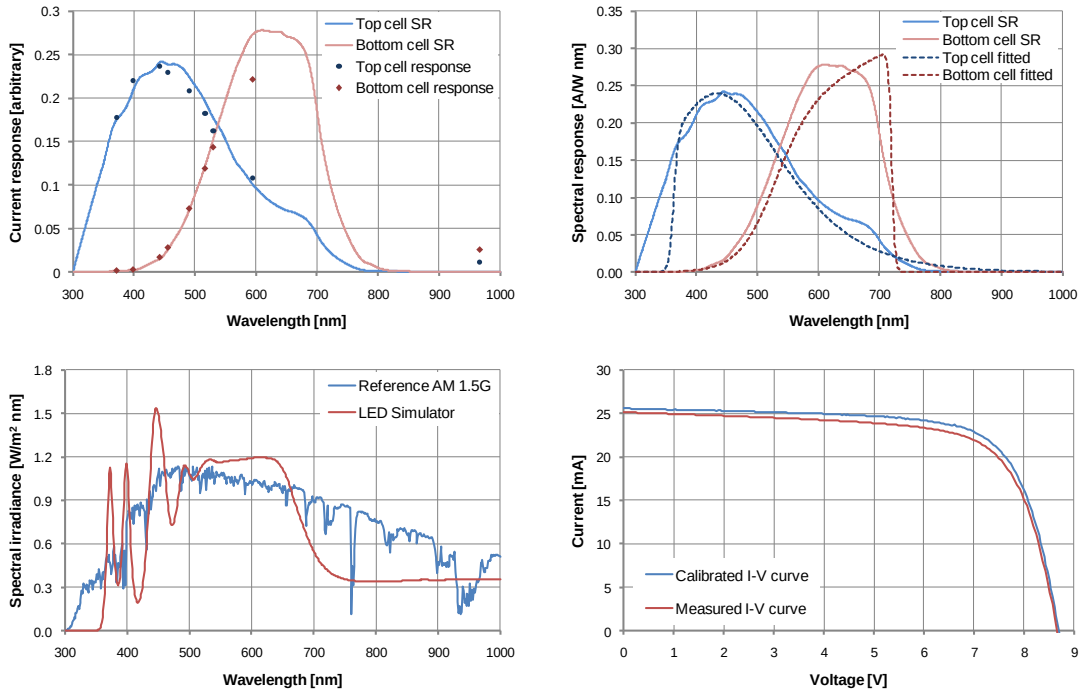

Figure 5.13: Initial results of the double junction a-Si mini module: junction detection (top left), spectral response fit (top right), calculated output spectra (bottom left) and final I-V curve measurement result (bottom right);

The final I-V measurement resulted in an underestimation of the device I_{SC} of -1.8% as given in Table 5.4, which is mainly due to the lack of feedback in measurement spectrum and light intensity (a worst case scenario) rather than a problem in the measurement method. The FF is underestimated by -2.3% leading to a significant error in P_{MP}. This is a clear indicator of a deviation in junction current balance and points out that the junction balance during the measurement was nearer to junction current match rather than more top junction limiting as it would be under AM 1.5 reference spectrum (see also Figure 5.1).

Parameter	Measured I-V curve	Calibrated I-V curve	Deviation
V_{OC} [V]	8.66	8.70	-0.40%
I_{SC} [mA]	25.13	25.59	-1.80%
V_{MP} [V]	7.09	7.12	-0.35%
I_{MP} [mA]	21.66	22.58	-4.07%
P_{MP} [mW]	153.57	160.66	-4.41%
FF [%]	70.54	72.18	-2.27%

Table 5.4: Deviation between measured and calibrated I-V curve; P_{MP} shows a larger deviation than I_{SC} which is mainly due to the difference in the FF as result of an incorrectly set junction current balance.

5.5 Measurement discussions

The simulated measurement results of a SJ and a double junction solar cell show that the developed measurement approach can achieve high measurement accuracy in the theoretical case. However, initial real measurements using the LED-based solar simulator have shown that a wrongly estimated SR has a direct influence on I-V measurements and quite drastically increases the measurement uncertainty. In turn, this is exactly the same case as when measuring the SR with dedicated equipment.

To achieve a good SR fitting the parameter model used needs to be able to correctly represent the actual SR of the device under test. Since the device can be completely unknown, it is useful to implement several parametric models, of which the best fit model can be chosen based on the residual difference between the fitted currents and the actual measured values. A suitable parametric model does not necessarily have to represent the complete device physics. Although SR is a product of device physics, the model only needs to describe the shape of the SR curve. A simplified model can lead to more reliable fitting results, as the number of unknowns may be lower and the fitting method has a lower probability of becoming stuck in a local minimum and stopping prematurely. The initial parameters of the model

for the fitting algorithm are best acquired by first fitting directly a generic SR curve and using the acquired parameters as the starting point.

For the parameter model to work reliably, a relatively large number of light sources with different spectral outputs are required. Although the fitting works with broad-band light sources, simulated measurements suggest that most light sources should be of relatively narrow spectral range. This reduces the chance of a fit that fails to represent the upper and lower boundaries of the SR curve correctly. Furthermore, spectral fitting works only within the limits of the spectral output of all light sources, i.e. model fitting will most likely fail to estimate the SR in an area where no light source or only one broad band emitting light has a spectral output. Nevertheless, fitting might work outside these boundaries if the physics of the device are accurately represented in the model as shown in [118].

The initial measurements show that accurate monitoring of spectral irradiance and light intensity conditions is vital. A deviation in the estimation of the spectral output and light intensity resulted in the acquired SR of the double junction a-Si mini module in particular being rather different from the actual SR. This inaccurate estimation was the main source of error between the final measured I-V curve and the calibrated one. A spectroradiometer is not necessarily needed in the case that the simulator uses only LEDs. Then, a separate monitoring sensor for each LED colour should already achieve high measurement accuracy. However, if one of the light sources changes its spectrum with intensity such as halogen lamps, the spectral output should be measured directly. It is important that the spectroradiometer is either calibrated absolutely or has a relative calibration and a reference cell of known absolute SR is used to monitor intensity.

Methods exist for SJ and MJ devices, that make use of spectral mismatch factor correction and reference cells to set the simulator output spectrum and intensity (as explained in section 5.1). Those do not require the absolute SR of each junction in the device under test, which means that the absolute error that has occurred during the SR fitting in the presented approach would have been corrected in the I-V curve measurements with help of the calibration value of the reference cell or its absolute spectral response. Since no

reference cell was used in the presented measurements, it was not possible to make use of this technique, which could have reduced the error significantly.

5.6 Conclusions

A new method for automated characterisation of single- and multi-junction photovoltaic devices has been presented. The method needs virtually no information on the device under test. The key element is a fitting method for calculating the SR of the junctions in the device under test. Consequently, it eliminates the need for dedicated SR measurement equipment and closely matched reference cells for each junction.

The method requires a multi-source solar simulator with a sufficient number of light sources with different spectral outputs, such as the LED-based solar simulator developed here. The presented approach automatically detects up to two junctions in the device under test (extendable), delivers spectral response, adjusts the solar simulator spectrum and light intensity, and delivers I-V curve measurements with junction conditions set as experienced at any given reference spectrum.

This method has time- and cost-saving potential. Since the method works automatically, it could be adapted in a slightly modified way in factory settings (without the junction detection step), with potential improvements in measurement accuracy by measuring the SR of the modules in production at least once per batch without having to remove the PV device directly from the process line. In the laboratory, this method might prove useful for faster I-V characterisation with SR measurements of complete modules with possible cost reduction. Additionally, slow responding devices can be measured easier, as the SR is not acquired using alternating light pulses of monochromatic light.

Results of a simulation of the complete measurement routine have shown that the method works in its theoretical case on the LED-based solar simulator and can deliver high accuracy. Initial direct measurements of the single-junction a-Si mini module have shown agreement to the calibrated SR

and I-V curve that is within the measurement uncertainty margins. However, measurement tests of the double-junction mini module have shown large deviations between the measured and the calibrated SR and I-V curve. It should be noted that this did not disprove the feasibility of the measurement approach itself, as measurements had been carried out under worst case conditions without a reference cell and without spectral output feedback, relying purely on the calibration of the system.

The proposed method can be extended to acquire SR at multiple voltages within one measurement cycle, which could prove useful for spectral match corrections at multiple points in the I-V curve. Furthermore, spectrometric characterisation, a systematic method to measure the influences of the junction current balance on multi-junction devices can be carried out. The method can also be extended to not only measure the I-V characteristic at one condition (usually STC) but also at multiple conditions such as measurements required for energy rating and energy yield prediction. This could be done systematically under varying irradiance (E), device temperature (T) and spectra (E) delivering a complete device characterisation in one measurement run. The feasibility of such G-T-E performance matrix measurements is studied in the following chapter 6.

6 Performance measurements for energy yield prediction

Energy yield prediction takes into account realistic variations of environmental conditions. Its outcome is the number of kWh generated at certain sites, which is useful for the system user (to identify faults) and the final investor (to make an estimate of revenue). In a rapidly maturing industry, it is gaining in importance. However, as explained in section 2.3.1, energy yield prediction is a complex process that requires measured PV device performance characteristics at varying conditions as well as meteorological data from the site to be investigated. This chapter reports on a novel measurement strategy for obtaining the former set of data, which utilises an additional dimension (spectrum) compared to standard approaches.

Typically, a PV device performance matrix consists of a number of I-V measurements at different irradiances (G) and device temperatures (T). While a performance matrix derived from outdoor measurements can include spectrum (E), indoors the effect of spectrum needs to be accounted for separately, typically with a sub-model. This additional step can lead to uncertainties in the energy prediction. Multi-junction and wide band gap solar cells in particular are non-linear with spectrum. Thus the accuracy of energy yield prediction depends on how much a device is affected by these spectral variations. Some materials, such as amorphous silicon [19, 20, 124] not only show spectral effects on generated current, but show also a further effect on the fill factor. One should thus expect additional uncertainties in the yield prediction. The spectral mismatch correction [77] is therefore only of limited applicability and it appears advisable to measure the effects of varying spectrum directly.

Spectral effects on yearly energy yield prediction do not necessarily average out to the standard AM 1.5G spectrum as assumed in some papers such as [37] or [125]. More often and in many locations a bluer spectrum is observed on average ([126, 127]). However, the energy weighted average spectrum is

very much dependent on the latitude of the location and the weather conditions experienced. The spectrum is bluer at lower latitudes. Even in Loughborough, with relatively high latitude of 52°75N, a slightly blue-rich spectrum is observed as illustrated in Figure 6.1. This is partly due to high cloud cover and a higher energy production at low air mass in summer. Minemoto et al. have reported in [127] a significantly blue-shifted average spectrum at a lower latitude of 34°58N in Shiga, Japan, with the minority of measured spectra at or above AM 1.5. The magnitude of this effect is still not fully understood as it correlates to other environmental effects and cannot be separated easily from outdoor performance measurements. This illustrates the need of measuring this in controlled, laboratory conditions.

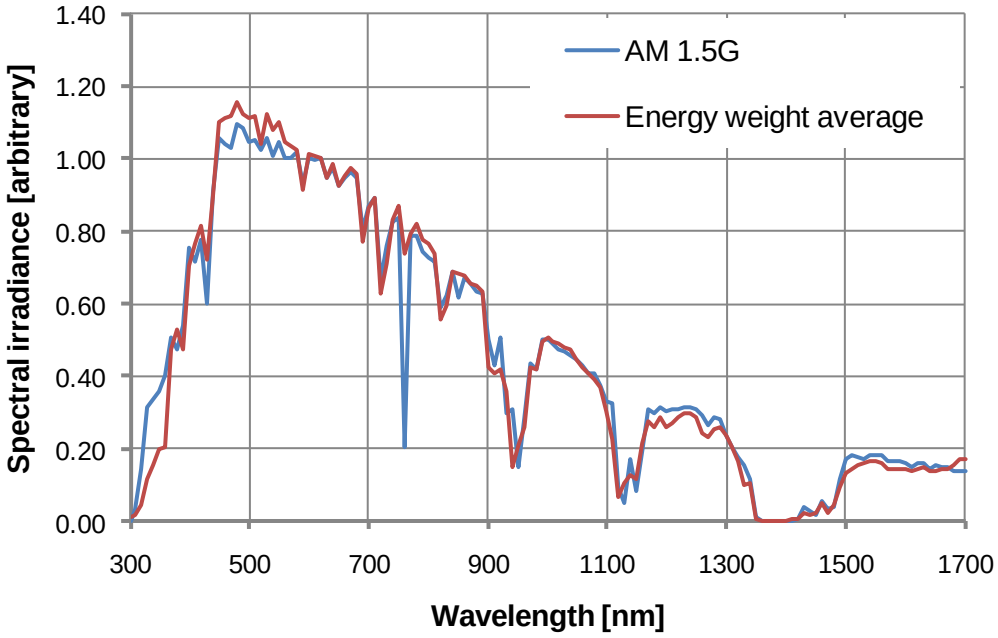

Figure 6.1: Energy weighted annual average spectrum in Loughborough, UK from Sep. 2003 to Sep. 2004; the spectrum is close to AM 1.5G with a slight blue-shift

A realistic set of PV device performance measurements would contain a matrix of measurements taken at all realistic conditions for G, T and E, as they would be seen at the given site to be investigated. This has not been possible to date because solar simulators did not provide the variability of spectral conditions required. However, the LED-based solar simulator developed and tested throughout this work can closely reproduce operating

conditions seen outdoors, i.e. varying spectrum (E), irradiance (G) and device temperature (T). The work presented in this chapter demonstrates the concept of measuring a G-T-E PV device performance matrix that can be used for energy rating and energy yield prediction. Furthermore, it demonstrates a clear separation of spectral effects from other environmental effects, which to date has not been possible. The first performance matrixes under varying G-T-E measured indoors on single junction a-Si and c-Si devices are presented. The variation in clear sky air-mass is demonstrated here, albeit there is no problem to include any measured spectral dataset. The G-T-E performance matrix measured is the device characteristic required for including non-linear spectral effects in an energy yield prediction. Including this will certainly improve the accuracy of short time energy predictions over a month timescale rather than a full year. These timescales and shorter are essential for PV system health monitoring and yet have been reported in several papers with significantly higher error compared to year-long periods ([125, 128, 129]).

Outdoor and indoor PV device performance matrix measurements are reviewed in the following section 6.1. The section thereafter explains the measurement approach developed during this work. The G-T-E measurement range of measurements on a c-Si and an a-Si device is explained in section 6.3 and measurement results are analysed and compared in section 6.4. To evaluate the robustness of the measurements taken, an analysis of measurement uncertainties is presented in section 6.5.

6.1 Overview of device performance measurements for energy yield prediction

This section reviews the differences in performance measurements for energy rating and energy yield predictions performed using outdoor and indoor methodologies. Difficulties and advantages in both approaches are highlighted.

6.1.1 Outdoors

The module under test is usually mounted on a fixed plane rack when performance measurements are carried out. However, the device can also be positioned on a tracker that follows the path of the sun. Both approaches have been investigated at the outdoor measurement facility at CREST and for example at the Institute for Applied Sustainability to the Build Environment (ISAAC) in Switzerland. Positioning the PV device on a tracker is useful because data collected is independent of changes in the angle of incidence (AOI). Furthermore, the effect of AOI can be measured directly, without the influences of changes in air mass and irradiance of the sunlight over the course of the day. This simplifies the separation of AOI effects from other influences, such as spectrum, irradiance and temperature.

Measurements are collected either by recording the complete I-V curve of the device or by just measuring P_{MP} (including I_{MP} and V_{MP}) with an electronic maximum power point tracking device [130]. However, P_{MP} is not sufficient when correcting for spectral effects and AOI effects because I_{SC} is needed for this. When just measuring P_{MP} one should expect larger uncertainties in energy yield prediction.

It has been shown by Kenny et al. [131] and Friesen et al. [125] that energy yield predictions derived from outdoor measurements can be very accurate. As reported on a c-Si device in [35], the length of data collection can be as short as one day and still an accurate answer (less than 1% error) of energy yield can be given. This is the case when a reference cell is used as irradiance sensor instead of a pyranometer, marginalising influences of spectral effects and AOI. However, even then, the day for measurements would have to be chosen carefully as results depend on the weather conditions on the day and the time of the year. Since environmental conditions cannot be controlled outdoors, it is questionable whether the approach of collecting data for such short periods is reliable. In general, one should expect more reliability and accuracy in energy yield prediction over longer periods of data collection. Even when data is collected over a complete month the deviation between yearly energy yield predicted and

measured depends on the time of the year in which the performance data is collected [35, 125]. The effect is most pronounced when predicting yields from devices with large spectral influences, such as a-Si or multi-junction PV modules. Hence, one would need to measure over at least several months to collect a sufficient amount of data at conditions the device is experiencing over the year to reliably predict energy yield for all device types and materials.

However, even when measuring over several months to enable a reliable energy prediction for all device types, the effects of G, T, E and AOI in the performance data still need to be separated to enable a site–to-site translation. This is a difficult task that can leave remaining dependencies due to errors associated with the specific outdoor measurement system [128, 132]. Furthermore, data collected at a given site cannot always be transferred to another as the full range of conditions at the investigated site might not have been seen at the location of data collection. In other words, an additional uncertainty should be expected when collecting data in Loughborough and predicting energy yield e.g. for the Sahara desert because Loughborough experiences different environmental conditions (lower maximum device temperatures and higher minimum air mass).

6.1.2 Indoors

As indicated in the chapter introduction, performance measurements can be carried out indoors in a shorter time period as there is no need to wait for the correct environmental conditions. An advantage of indoor measurements is the higher repeatability of measurement conditions and I-V measurements, which makes energy yield predictions more consistent. Furthermore, measurements are site independent as conditions seen in, for example, Loughborough or the Sahara desert can be reproduced as long as the necessary laboratory equipment is in place. Different factors influencing performance, such as temperature and irradiance, can be controlled and measured independently of each other. This makes a separation of these influences easier and more accurate than in the case of untangling outdoor data.

To date, indoor PV device performance characteristics are typically measured over a series of different irradiances and temperatures. The JRC-ESTI method [37, 129, 131] for example is to fit a performance surface to the matrix of G-T device performance points. The fitted surface is then used as an input for energy yield predictions. It has been shown for c-Si devices that the performance surface approach can lead to high accuracy, even though AOI and spectral effects are not considered in the in the algorithm [37]. Using an in-plane pyranometer as reference in the meteorological dataset achieved deviations of less than 1% to the actual measured yield over a period of one year. Accuracies of better than 0.5% have been achieved when using reference data of a matched reference cell. It should be noted that the uncertainty in power measurements was stated at 2% in [37], meaning that the uncertainty in energy prediction cannot be lower than this value.

Irradiance data measured with a PV reference device is rarely available as part of a meteorologically derived environmental data set. Typically, only global irradiance (not in-plane) measured with pyranometers or satellite data is widely available. An in-plane pyranometer as reference sees exactly the same light intensity as the module but does not correct reflection and spectral effects. A matched reference device as irradiance sensor yields better accuracies as it performs almost exactly as the actual module under test. It has the same spectral influence and angular response as the device under test.

High accuracy in indoor energy yield prediction as stated above has been achieved with crystalline silicon modules, a very stable device material. Additional uncertainties are expected with multi-junction devices or thin film materials such as a-Si, as they show larger sensitivity to spectral variation. If the effects are not corrected for and the site investigated has a particularly blue-rich or red-rich average spectrum or a high latitude, this uncertainty can be significant.

The proposed energy rating standard IEC 61853 [34], currently in a draft version, requires the measurement of a G-T performance matrix and additional measurements at varying AOI. The latter can be measured by tilting the device under test in the solar simulator. Furthermore, the proposed

energy rating standard requires measurement of the spectral response. The SR data is necessary when correcting for the effects of spectrum, which can give a better approximation of the energy yield. Nevertheless, since only measurements in a G-T matrix are required, the standard is currently not applicable to multi-junction devices because the junction current balance is not correctly set. Furthermore, single-junction devices with large spectral effects on FF such as a-Si PV modules may be problematic.

An indoor measurement method for energy rating and energy yield predictions that is applicable to all PV device types and structures would need to measure a G-T-E performance matrix. However to date, spectral variation could not be reproduced accurately enough to be included into the performance matrix. Multi-source solar simulators with abilities of changing the spectral output such as presented in [133] and [18] are primarily used to calibrate the performance of multi-junction solar cells. They change the balance of sections of the spectrum, e.g. the bands 300nm to 800nm in one single adjustment, but they are not able to reproduce the intricacies of variable air mass. They may be used for spectrometric characterisation as well as optimisation of device structures [134]. The prototype LED-based solar simulator improves on this as the system provides a wider variability of spectral conditions with a better control of the shape of the sunlight spectrum. The following sections demonstrate the concept of measuring a G-T-E performance matrix indoors on two different SJ device technologies, showing that spectral influences should not be discounted.

6.2 Performance matrix measurement approach

The measurement method used in this work consists of three main steps. As illustrated in Figure 6.2, the first is to define the measurement ranges and points in the G-T-E matrix. The last two steps are repeated for all selected reference spectra and include the adjustment of the simulator output spectrum and the measurement of the GT-matrix under that spectrum. In the following subsections each of the steps is explained in detail.

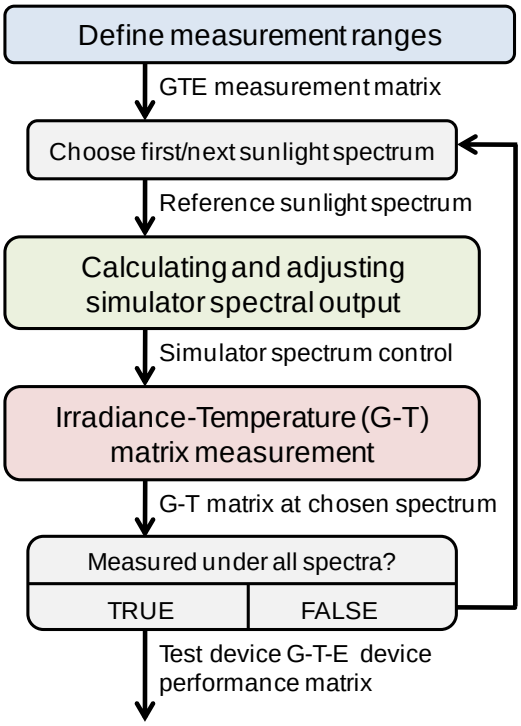

Figure 6.2: Basic approach for measuring a G-T-E device performance matrix

6.2.1 Defining measurement ranges

When defining the measurement ranges, the measurement points in the G-T-E matrix should be relevant to realistic conditions, i.e. points pertinent to what is seen outdoors should be chosen. This is important because the chosen points can have a large impact on the final accuracy of the energy yield calculation. Also the number of measurements can easily become very large. This is dependent on how many different spectra, intensities and temperatures are chosen.

The input spectra can either be simulated (e.g. with SMARTS [135]) or defined by measurements or arbitrarily set. They would have to be classified by additional factors such as air mass, clearness index or cloud cover, but this detailed classification is part of a different project. The work demonstrated here is intended as a proof of the overall measurement concept.

6.2.2 Calculating and adjusting spectral output

Prior to the measurement of a light intensity and temperature (G-T) matrix, the solar simulator output spectrum must be adjusted to the chosen reference spectrum. This is done by first calculating the required irradiances of each available light source and reproducing them in the simulator.

The intensity configuration of each light source colour can be acquired either manually or else with a fitting algorithm that minimises the deviation between the required sunlight spectrum and the spectrum in the solar simulator. Input parameters for the fitting algorithm are the spectral outputs of the light sources in the solar simulator. The parameter to minimise would be the standard deviation over wavelength between reference and combined simulator spectra. Adjustable parameters are the intensity factors of the light sources. In the presented case, the intensity of the halogen light sources was fixed at 100% during the adjustments of the output spectrum. This reduced uncertainties from spectral changes of the halogen light sources during adjustments. The spectrum of the halogen lights has been calibrated at this intensity and was thus best represented.

If the test device is a multi-junction device, it is important to ensure that the junction current balance is the same as it would be under the reference spectrum. This means that the intensities of the light sources slightly need to be re-adjusted for the correct balance. This can be done with various methods as given in section 5.1.2.

In the case of single-junction devices the simulator output spectrum can be adjusted with the help of the reference cell SR curve, once the intensity factors of the light sources are known. The device under test can also be used for adjusting the output spectrum, which has been done during this work as is eliminates uncertainties due to spectral mismatch between the test and reference device. The intensity of each of the light sources in the solar simulator is adjusted separately until the measured I_{SC} matches the calculated ones. The theoretical value is calculated using the relative spectral output of the light source, its intensity factor and the SR of the test device. At

the end of the light adjustment, the same I_{SC} as generated for the reference spectrum should be measured on the test device.

It is also possible to use a spectroradiometer to check the spectrum and set the light source intensities. In the presented case this was not possible and the achieved spectra were assumed based on previous spectroradiometer measurements. The difference between the actual spectrum and the estimated spectrum should be insignificant as demonstrated by the earlier repeatability tests (see section 4.2 and 4.4 for details). The main uncertainties are due to SR measurements of the test device and the relative spectral output calibrations of the light sources at full intensity.

6.2.3 Irradiance-Temperature matrix measurement

Once the solar simulator's light spectrum has been adjusted, a G-T matrix at this spectrum can be measured. High measurement accuracy is achieved by ensuring spectral stability of the light sources used in the simulator (i.e. minimal spectral variations of light sources when changing intensity). The intensity in the simulator can then be changed by adjusting the intensity of all light sources to the same degree with regard to their nominal intensity, leaving the actual output spectrum unchanged. If light sources change spectrum significantly with intensity, such as with halogen light sources, a re-adjustment of the solar simulator spectrum or a mismatch correction is required for each intensity step.

The test device I-V curves are then measured. The reference cell I_{SC} can be used to determine the light intensity in the measurement. During the measurements presented here, the test device has been used as a self reference, i.e. the I_{SC} and the SR of the device have been calibrated prior to the measurements and a linear response is assumed. This was done to correct for the effects of spectral shift of the halogen light sources. They shift towards the infrared when reducing the intensity because of lower operating temperature of the filament. Nevertheless, self referencing introduces additional uncertainties, as it relies on the linearity of the test device and its SR measurement. Self reference was used only at a device temperature of 25°C in order not to eliminate the effects of device temperature changes in

the G-T matrix measurement. For all other temperatures in the G-T matrix, the same irradiance was assumed for the same light source setting. This should not contribute significantly to uncertainty, as the simulator has a good repeatability of light conditions as demonstrated in section 4.4.

In order not to eliminate the influences of spectrum in the G-T-E matrix, self referencing was carried out with respect to the reference sunlight spectrum used in the G-T matrix measurement. The conversion from measured I_{SC} to measurement irradiance was recalculated for each spectrum used. This was done by first calculating the theoretical short circuit current $I_{SC,R}$ of the test device under reference sunlight spectrum E_R with equation (6.1). The final measurement irradiance G_M is then calculated as per equation (6.2).

$$I_{SC,R} = A\int S_T(\lambda)E_R(\lambda)d\lambda \tag{6.1}$$

$$G_M = G_R \frac{I_{SC,M}}{I_{SC,R}} \tag{6.2}$$

A is the test device area, S_T is the spectral response of the device under test, $I_{SC,M}$ is the measured short circuit current and G_R is the irradiance of the reference spectrum E_R.

To accurately change the intensity, without changing the spectrum, the LED-based solar simulator utilises a calibration curve for each light source. This corrects non-linearity in the light source intensity with drive current (G vs. I_D). It is used to calculate the correct drive current to achieve a new setting at which the relative intensities of the light sources are changed equally. With regards to the halogen light sources this calibration ensured that at least the current generated by the light is as much as possible changing linearly with the control even though the spectrum is shifting. Further details have been given in previously in section 4.2.

6.3 Configuration of first demonstrated G-T-E performance measurements

To demonstrate the concept of measuring a G-T-E performance matrix for energy rating and energy yield predictions, the first measurement results of a single-junction c-Si and a-Si device are presented. Prior to the actual performance comparison of the two device technologies, it is important to define the measurement ranges and to detail the configuration of the I-V measurement, on which information can be found in this section.

6.3.1 G-T-E measurement range

The performance measurements have been carried out on a non-encapsulated 30x30mm^2 mono-crystalline silicon solar cell fabricated at CREST and on a commercially available 50x47mm^2 a-Si mini-module with three cells connected in series. To enable a good comparison between the PV device materials, the measurement ranges in the G-T-E performance matrix are the same for both devices and have been defined as follows:

- 8 different spectra (as detailed in Table 6.1)
- 4 different device temperatures between 15°C and 45°C, where the maximum was chosen to not cause any annealing in the a-Si device
- 13 intensities ranging from 5% to 100% of the highest irradiance possible at each specified spectrum

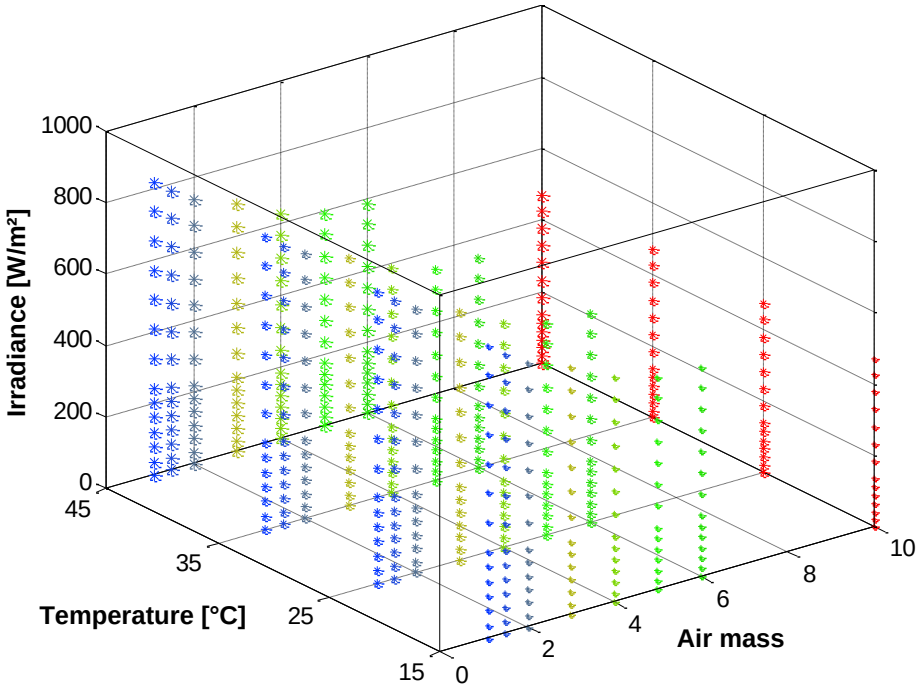

Figure 6.3: 3D graph of the measurement points in the GTE-matrix; the irradiance scale given is from the c-Si device tested

Figure 6.3 shows the measurement points at which the device I-V characteristics have been measured. The measurement points have been selected to cover a wide range and within the scope of this work are for demonstration purposes only. Further work is required to analyse realistic environments and minimise the number of measurements required to adequately characterise a given PV device. Some of the conditions are not immediately intuitive in real conditions, e.g. the lower temperatures at higher irradiances. However, considering rapidly changing cloud cover would make them possible, especially when considering cloud enhancement [136]. The selection also includes extreme points such as AM 1.1 at 800W/m^2 and 15°C or AM 4 at 50W/m^2 and 45°C. It would have been useful to measure conditions such as AM 1.1 at 1100W/m^2, but the prototype simulator is not capable of reproducing the sunlight spectra below AM 4 at full intensity for the c-Si device and AM 2 for the a-Si device. Instead the simulator light was adjusted to the maximum possible intensity at the given spectrum. Table 6.1 shows a comparison between the normal sunlight irradiance and the effective maximum irradiance on the test device reached in the simulator.

Solar spectrum	Irradiance [W/m^2]		
	Sunlight (280-4000nm)	a-Si simulator effective	c-Si simulator effective
AM 1.1	1090	1049	818
AM 1.5	1030	1000	778
AM 2.0	950	951	739
AM 3.0	813	907	692
AM 4.0	704	804	628
AM 5.0	617	754	592
AM 6.0	547	776	586
AM 10.0	291	522	470

Table 6.1: Irradiance comparison between the reference sunlight spectra used and the effective maximum achieved in the solar simulator with regard to the measured c-Si solar cell and a-Si mini-module

The reference spectra chosen have all been simulated with SMARTS for a device that is mounted on a tracking plane under various air mass conditions as stated. All other input parameters have been set as given in the IEC60904-3 [1]. The simulator output spectrum was set to match the reference spectrum as closely as possible (see Figure 6.4 for AM 1.5, AM 3 and AM 6). The largest deviations between reference and output spectra were found in the 700nm to 800nm region with up to 39% lower intensity at AM 1.1 (worst case) using the same wavelength binning as defined by the IEC 60904-9 [70]. The large deviation is due to low adjustability in the area from red to infrared, as only the halogen lights produce light in this region. All spectra are classified as a class B spectral match. As mentioned in the previous section 6.2.2, the spectra here are assumed to be as simulated in the fitting algorithm.

As previously explained in section 3.3.5, the Peltier stage temperature control in the LED-based solar simulator can reach temperatures up to 80°C. Such high temperatures have not been chosen in G-T-E measurements of this work to avoid possible thermal annealing effects on the a-Si device (see section 2.2.4).

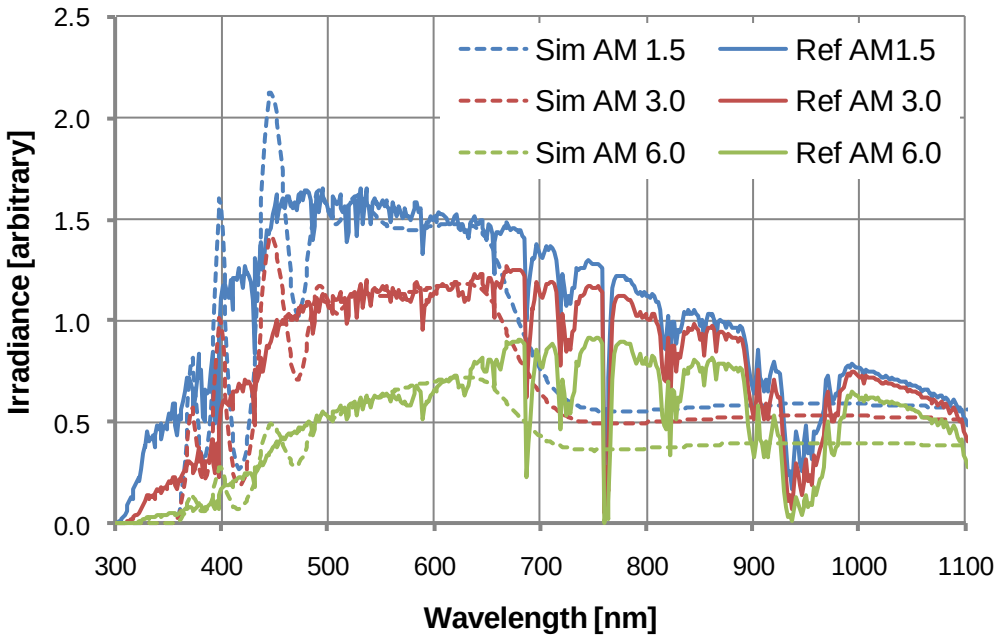

Figure 6.4: Reference and simulator spectra; all output spectra used are within class B, with the largest deviations in the 700nm to 800nm region; simulator output spectra have been scaled to the reference sunlight spectra to illustrate the spectral match

6.3.2 Current-Voltage measurement set-up

Each I-V curve was measured from short circuit condition to open circuit voltage with a resolution of 200 points. The halogen light sources were given a slow warm-up time varying from 2.5s at 100% intensity to 15s at 5% of their full intensity. After the warm-up of the halogen light sources all LEDs were driven in a long rectangular pulse over 45ms, allowing a 25ms warm-up and a period of 20ms for the actual I-V measurement (0.1ms per point). I-V measurements were taken every 90 seconds. This allowed the light sources and electronics to cool down and the solar cell temperature to re-stabilize and thus thermal influences were minimised. The solar cell operating temperature was changed from one point on the matrix to the next over a time of about 3 minutes, allowing for temperature regulation and settling. A complete G-T matrix measurement at one spectrum took about 90min measurement time.

The SR curves of the test devices were measured in the filter-based SR measurement system at CREST (detailed in section 5.1.3). The devices were

measured at approximately 0.1 suns background illumination and compared against the SR curve of a reference cell with traceability to JRC-ESTI. An absolute calibration of the SR was done in a Pasan solar simulator against the calibrated I_{SC} of the same reference cell with mismatch correction applied for both devices.

As stated earlier, self-reference was used for measuring irradiance during the test sequences. To quantify the measurement errors introduced, both devices have been tested for linearity in I_{SC} utilising the two lamp method given in the IEC 60904-10 standard [101] and further explained in [137]. The results, illustrated in Figure 6.5, show a good linearity of both devices over the complete range, in that the non-linearity is less than the ±2% threshold given in the IEC standard. This means that the additional uncertainties introduced with self-referencing can be considered insignificant compared to other uncertainties.

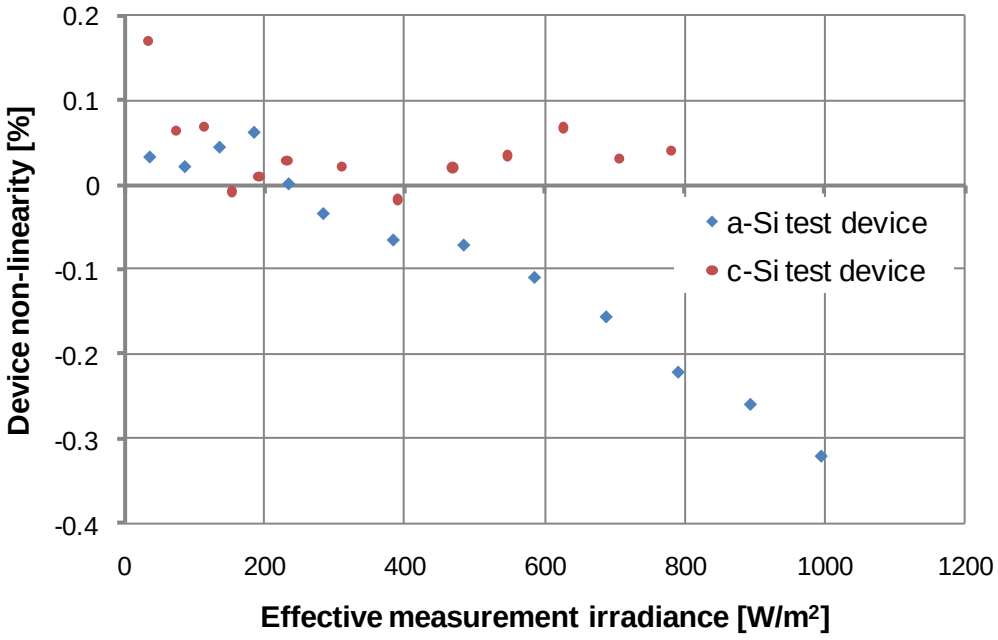

Figure 6.5: Measured I_{SC} linearity of both test devices; the a-Si shows a higher non-linearity at high intensity, while the c-Si device is less linear at low very low irradiance

6.4 Analysis and comparison of G-T-E device performance of two different technologies

In this section the measurement results of both devices are presented and compared. The c-Si solar cell has been chosen as the material is well known to be largely unaffected by changes in spectrum. Measurements of an a-Si mini-module have been included because this device material is known to be the complete opposite, showing a large spectral effect even so being a single junction structure. This dependence on spectrum, also noticed in the FF of the device, has previously been very difficult to analyse as varying spectra could not be reproduced indoors and effects are difficult to separate from outdoor measurements.

6.4.1 Influences of Irradiance Spectrum

PV device performance influences due to changes in spectrum are today largely neglected in energy yield predictions. The following figures demonstrate that neglecting spectral influences on single-junction amorphous devices is a potentially significant source of uncertainties in the final energy yield prediction.

Short circuit current and efficiency:

Figure 6.6 compares the short circuit current over irradiance (I_{SC}/G) behaviour versus air mass of both devices. It is apparent from the figure that the a-Si device is significantly more affected than the c-Si device. Increasing air mass results in a large drop in I_{SC}/G of the a-Si device, while only small changes are observed on the c-Si device. The large spectral effect on the amorphous silicon device is due to its SR being in the ultraviolet to red (~300-750nm) region where the sunlight spectra (and simulator light spectra) decreases the most with air mass. Similar behaviour of devices made of the same material has also been observed in outdoor measurements and reported in [26, 29, 138, 139]. The exact relationship of the gain or loss of I_{SC}/G with red-shifting of the spectrum depends on the SR of the specific device under test.

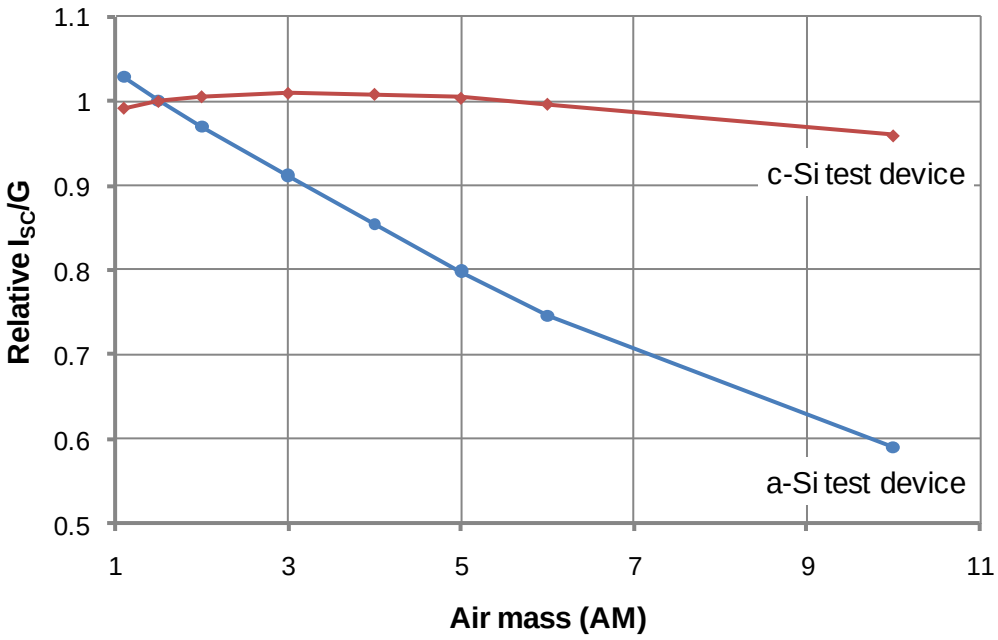

Figure 6.6: Relative I_{SC}/G versus air mass (AM) normalized to the measurement at AM1.5 spectrum; the a-Si mini module shows a significantly larger spectral influence in I_{SC}.

Changes in I_{SC}/G also affect the device efficiency as shown in Figure 6.7. Similar to the spectral influences in I_{SC}/G, the c-Si solar cell experienced a much smaller change in efficiency with increasing air mass than the a-Si mini module.

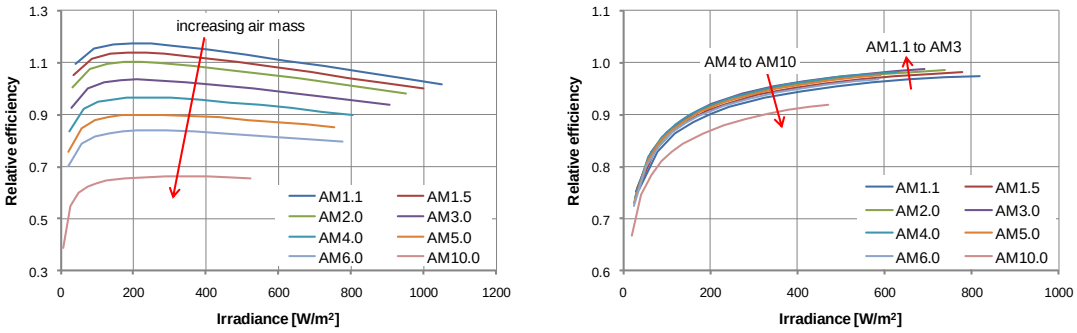

Figure 6.7: Efficiency versus G with increasing air mass at 25°C temperature; the a-Si device (left) significantly drops in efficiency with increasing air mass, while the c-Si device (right) shows much smaller influences due to spectrum. Efficiency is shown relative to the value measured at STC.

Open circuit voltage:

The behaviour of V_{OC} versus G at varying spectra of both devices is illustrated in Figure 6.8. Clearly visible on the a-Si device is the drop in V_{OC} with increasing air mass. This is due to the significantly lower relative I_{SC}/G at high air mass as previously shown in Figure 6.6. Changes in V_{OC} versus G due to spectrum can also be observed on the c-Si device, but on a much smaller scale.

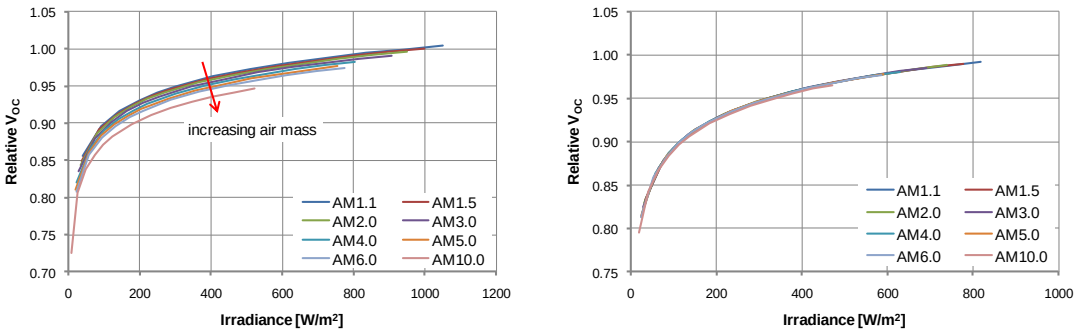

Figure 6.8: V_{OC} versus G at varying spectra; the V_{OC} of the a-Si mini module (left) drops visibly with increasing air mass, some small effects are visible on the c-Si device (right). V_{OC} is shown relative to the value measured at STC.

Plotting the V_{OC} versus I_{SC} curves reveals a very different behaviour (Figure 6.9): V_{OC} is strongly correlated to I_{SC}. The c-Si device shows no visual spectral influence on the V_{OC} versus I_{SC} curve. However, the a-Si device tested shows a very small effect of spectrum on V_{OC}. This could be an artificial effect due to temperature instability, but no change is visible on the tested c-Si device. Since both devices were measured at the same spectra, with the same control set-up and method, and the temperature dependence on voltage is larger for the c-Si device, an artificial effect can be ruled out. Although to the author's knowledge this behaviour has not been measured previously (as no accurate enough measurement system was in existence), a detailed optical and electrical model for a-Si devices developed by C. Monokroussos et al. [140] has predicted a small reduction in V_{OC} versus I_{SC} with increasing redness of the spectrum (i.e. increasing air mass). This is consistent with what has been observed here and underlines the accuracy of the developed model and as well as the measurements.

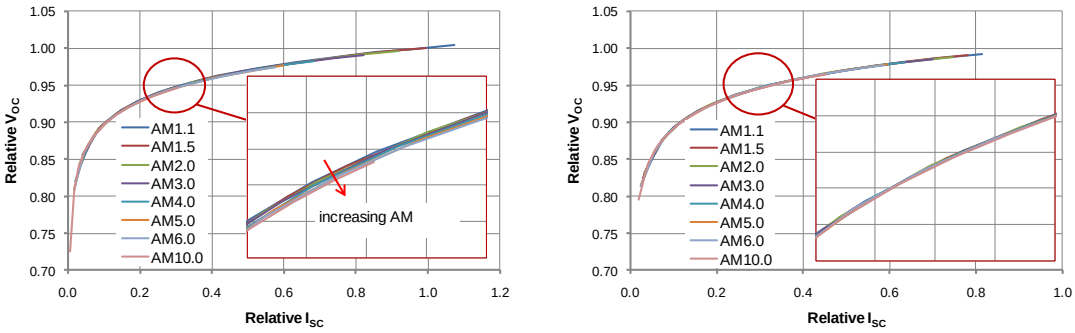

Figure 6.9: V_{OC} versus relative I_{SC} normalised to the calibrated value at STC; the c-Si device (right) shows no visible dependence on spectrum while the a-Si (left) shows a small effect.

Fill factor:

The a-Si mini module shows a large spectral effect on the FF versus irradiance, as illustrated in Figure 6.10. At high air mass, the fill factor peaks at light intensities of around 100W/m^2. The peak FF reduces and shifts into the higher light intensity region with increasing air mass (~130W/m^2 at AM 10). At irradiances above the peak fill factor the FF is benefiting from red rich high AM spectra and at intensities below it benefits from blue rich spectra.

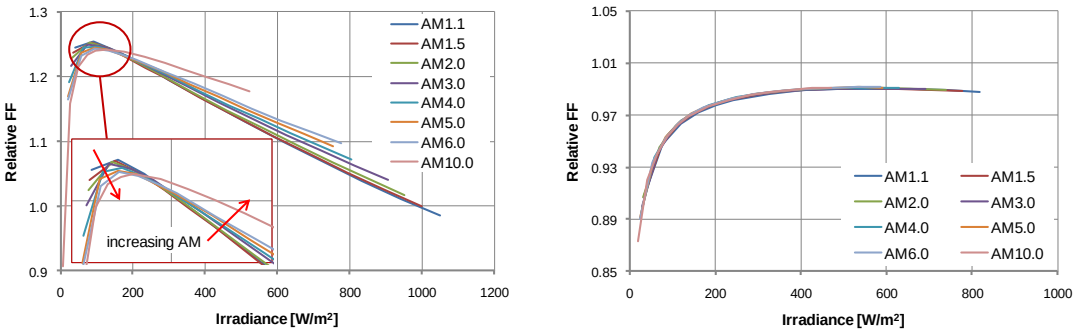

Figure 6.10: FF versus G at varying spectra of the a-Si (left) and c-Si device (right); plotting FF versus irradiance reveals a very different pattern compared to plotted versus I_{SC}.

Plotting FF against the I_{SC} of the device (see Figure 6.11) reveals a very different behaviour of the a-Si mini module. The FF is significantly increased over the complete I_{SC} range at lower air mass spectra. The drastic change in the shape of FF of the a-Si devices between curves versus G and I_{SC} again can be explained with the large reduction in relative I_{SC}/G with increasing air mass as shown previously in Figure 6.6. The diagram shown in Figure 6.11

illustrates the more generally reported behaviour of amorphous silicon solar cells: device fill factor is benefitting from blue-rich, low air mass spectra. This has been reported by R. Rüther et al. [19] and has also been observed in measurements from the CREST outdoor system.

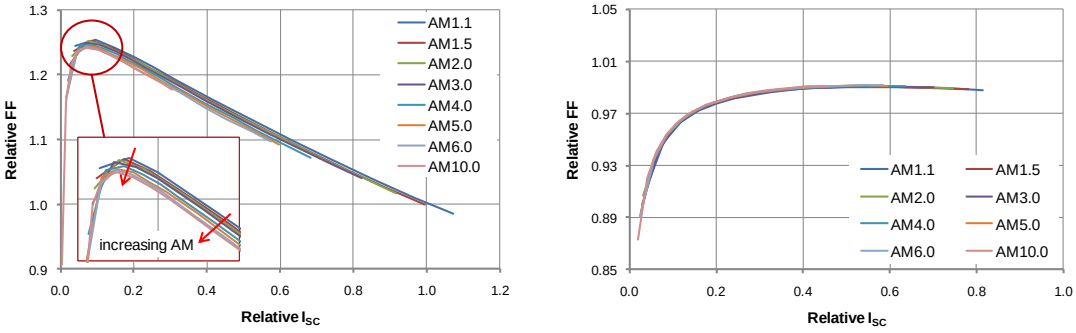

Figure 6.11: FF versus relative I_{SC}; the a-Si device tested (left) shows a large spectral influence on the FF, while the c-Si device (right) shows no visible dependence on spectrum.

The spectral effect on the FF of the a-Si device can be explained by the voltage dependent SR of a-Si devices as reported by J. Bruns et al. [120] and also measured by C.J. Hibberd et al. [119]. The a-Si device tested is of a P-I-N junction structure. Due to the physics of the device, an increase in voltage results in a shift of the relative spectral response into the shorter wavelength region (more responsive to blue light). This blue shift in SR leads to a reduction in collected photocurrent at increasing voltages, i.e. the photocurrent at I_{SC} (0V) is larger than at FF (V_{MP}). This blue shift in SR also means than the amount of photons that can be collected at V_{MP} is reducing with increasing air mass faster than the photons collected at 0V, which can be seen as a reduction in FF with air mass. This effect has also been predicted by the detailed optical and electrical model for a-Si devices developed by C. Monokroussos and is reported and further explained in [140]. The same blue shift in SR with voltage is responsible for the slight reduction in V_{OC} of the a-Si device as shown in Figure 6.9.

Maximum power point voltage and current:

To highlight which of the factors (I_{MP} or V_{MP}) has the largest influence on FF of the a-Si device, the V_{MP}/V_{OC} and I_{MP}/I_{SC} versus I_{SC} (relative to STC) curves

are illustrated in Figure 6.12 and Figure 6.13. As apparent from the left-hand graph of both figures, the major contribution to the change in FF of the a-Si device is a reduction in I_{MP} with increasing air mass. V_{MP} has only a small contribution to changes in FF. This supports the previous explanation with the voltage dependent SR of a-Si devices.

The c-Si device shows no spectral effect in either figure, which agrees with published literature as no spectral effects on V_{MP}/V_{OC} or I_{MP}/I_{SC} (neither FF) have been reported for c-Si solar cells.

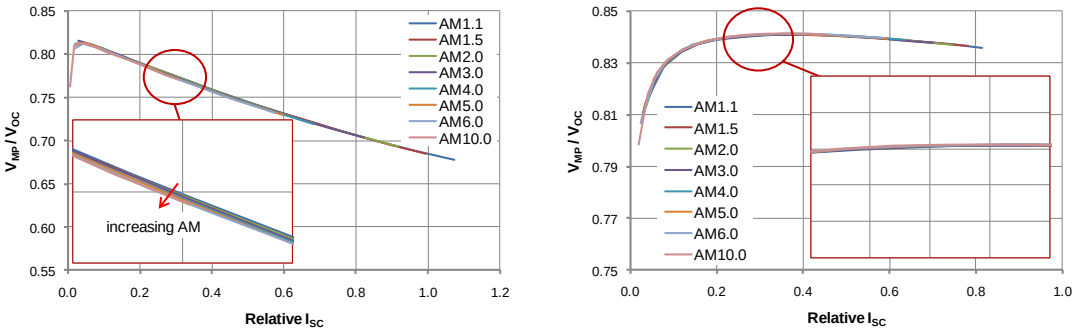

Figure 6.12: V_{MP} / V_{OC} versus relative I_{SC} at STC at varying air mass of the a-Si (left) and c-Si device (right).

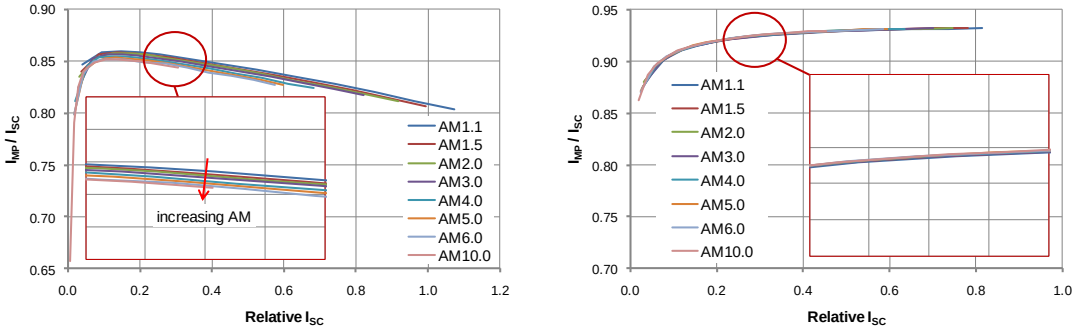

Figure 6.13: I_{MP} / I_{SC} versus relative I_{SC} at STC at varying air mass of the a-Si (left) and c-Si device (right).

Current-Voltage characteristic:

Figure 6.14 compares the spectral influences on the actual I-V curves of both devices. For this comparison the I-V curves of different spectra have been translated to the same I_{SC} via linear interpolation from the nearest measured I-V curves at 25°C. No change in fill factor is visible on the c-Si device, while on the a-Si device the reduction in FF with increasing air mass is apparent.

The FF of the a-Si device changed by -1.8% between AM 1.1 and AM 10 at 25°C, which led to the same reduction in power output. This seems a relatively small change over a relatively large spectral range. However, only clear sky reference spectra are reproduced in this G-T-E performance matrix. At this point it is not clearly known how the FF of a-Si devices is affected by very blue rich cloudy skies. Furthermore, the device tested is in its non-degraded, as-purchased state. It has been predicted in [140] that degraded a-Si devices show a significantly larger spectral effect on FF and thus P_{MP}. It is also not known how other devices react and in particular full modules.

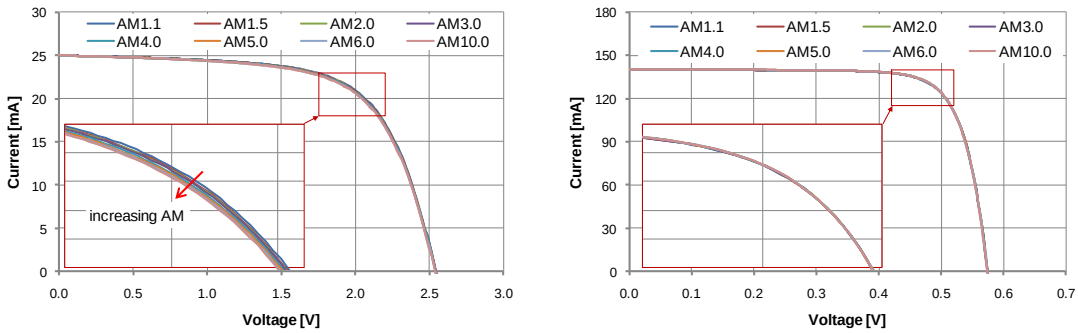

Figure 6.14: Comparison of the spectral influences between the I-V curves of the a-Si (left) and c-Si (right) device;

6.4.2 Temperature and light intensity influences

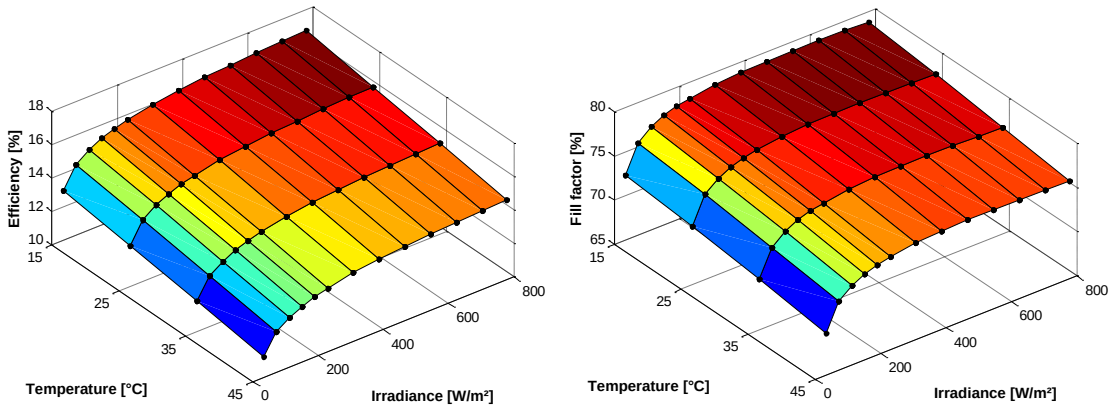

Figure 6.15: 3D diagram of c-Si device efficiency (left) and FF (right) versus G-T at AM 1.5 spectrum

Figure 6.15 presents the influences of temperature and light intensity on the efficiency and fill factor of the c-Si solar cell. As reported in the literature, e.g. [141] or [142], efficiency increases sharply with irradiance in the lower

intensity region and flattens out at higher intensities. This pattern is largely followed by the fill factor of the c-Si device. The observed difference is that the FF reaches a maximum at 450W/m^2 and slightly decreases at higher intensities (see right of Figure 6.15), indicating that the resistive losses in this device are becoming significant.

Comparing the performance data of the c-Si device in Figure 6.15 with that of the a-Si mini module in Figure 6.16 immediately highlights that the a-Si device has much larger resistive losses. The voltage dependent SR of the device also effects FF and efficiency. Both efficiency and FF peak at low light intensity.

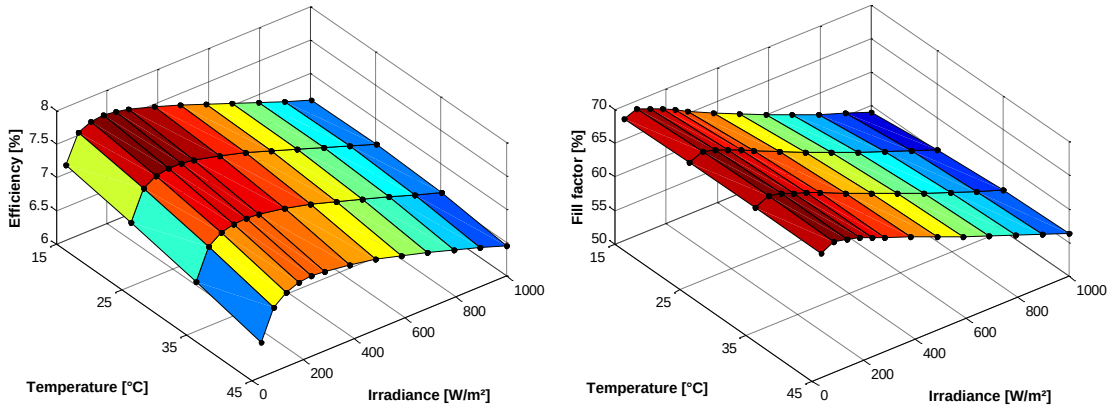

Figure 6.16: 3D diagram of a-Si device efficiency (left) and FF (right) versus G-T at AM 1.5 spectrum

The temperature coefficients of the I-V parameters extracted from the G-T-E performance matrix are illustrated for the c-Si and a-Si devices in Figure 6.17. The extracted coefficients are within the ranges reported in a review by K. Emery et al. [13] and similar to what is seen in the CREST outdoor monitoring system data.

By comparing the coefficients of both devices over irradiance in Figure 6.17 one can observe that the thermal effect on P_{MP} of the a-Si device is around 4 times larger at low intensities than at high intensities, while the temperature coefficient of P_{MP} of the c-Si device increased only by about 20%. The changes in P_{MP}, especially on the a-Si device, may be significant in the context of the generally assumed global temperature coefficient for energy modelling. Interestingly, the variation of FF of the a-Si device with increasing temperature is positive. This increase in FF with temperature is also visible in

the surface diagram of Figure 6.16. Furthermore the effect of temperature increases with light intensity. A reduction in the coefficient of V_{MP} (below that of V_{OC}) and an increase in positive I_{MP} coefficient contribute to the increase in FF and to the large reduction in P_{MP} temperature coefficient. In contrast, the temperature coefficient of FF for the c-Si device is negative and stable over the complete intensity range.

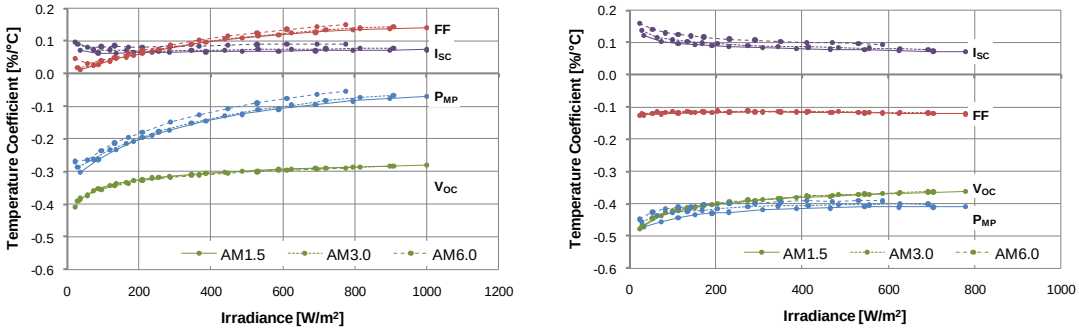

Figure 6.17: Temperature coefficients of the a-Si (left) and c-Si (right) device parameters over light intensity at different air mass; extracted from G-T-E performance measurements over the range 15°C to 45°C and relative to the performance at 25°C

Since measurements have been taken at different spectra, coefficients have also been extracted from measurements under spectra other than AM 1.5. Clearly visible for both devices are the increasing temperature influences in I_{SC} and a reduction in P_{MP} temperature coefficient with higher air mass. The temperature coefficient of V_{OC} is not affected by spectrum for either device. Changing temperature coefficients with spectrum have not yet been reported from outdoor measurements to the author's knowledge. The reason for this may be the difficulty to extract such influences from outdoor data. Nevertheless, the observed increase in I_{SC} temperature coefficient with air mass can be explained with the change in SR due to a change in the band gap energy with temperature as previously indicated in section 2.2.2. As reported by H. Müllejans et al. in [11, 143] the c-Si and a-Si device both gain in SR in the red and IR region. Since the proportion of red/IR light increases with air mass, the temperature coefficient increases as well because a larger proportion of light is in the wavelength range of red to IR. Increases in I_{SC} temperature coefficient also have an effect on I_{MP}, which is the main

contributor to the reduction in temperature effects on P_{MP} with increasing air mass.

Interestingly, the a-Si device's thermal coefficient of FF benefits from high air mass spectra (right side of Figure 6.17). This is due to the same gain in SR in the red region as for I_{SC}, with a slightly larger net gain on I_{MP} than on I_{SC} due to the additionally voltage dependent SR. V_{OC} and V_{MP} temperature coefficients are not affected by spectrum, thus I_{MP} is the only contributing factor in the change in FF, which further affects the temperature response of P_{MP}.

6.4.3 Temperature effects versus temperature

By closely observing the previously presented Figure 6.16 it is notable that the temperature influence on efficiency and FF is not constant with temperature. To further examine this phenomenon, a further set of measurements was carried out at full light intensity at AM 1.5 spectrum settings over the same range of temperatures from 15°C to 45°C but in 5°C steps. Device temperature was ramped up and down to detect any hysteresis that could indicate further secondary effects such as thermal annealing of the a-Si device. The time between each measurement is approximately 5 minutes. This includes regulation of the device to the new operating temperature and ~3.5 minutes settling time for stabilisation. Measurements were repeated 3 times. All results measured on both devices are illustrated in Figure 6.18.

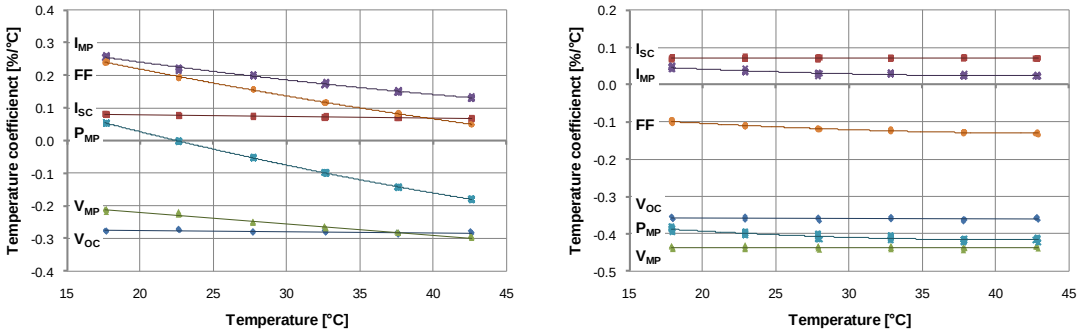

Figure 6.18: Changes in temperature coefficients of parameters versus device temperature of the a-Si device (left) and c-Si device (right); all 3 measurement sets (ramp up and down) are plotted

here and resulted in the same parameters and behaviour without hysteresis.

Clearly visible in Figure 6.18 is that the temperature coefficients of the c-Si device (right side of figure) are much more stable than those of the tested a-Si device (left side of figure). It is noticeable that the coefficient of I_{MP} is slightly decreasing with increasing temperature in the case of the c-Si device. This results in a change of temperature coefficients of FF and P_{MP}.

However, on the a-Si device nearly all temperature coefficients are changing to a much greater extent, except for I_{SC} and V_{OC} which are constant over temperature. The drop in I_{MP} temperature coefficient and the increase in V_{MP} coefficient versus temperature lead to an overall reduction in temperature effects on the FF. Consequently, the temperature coefficient in P_{MP} becomes increasingly negative with rising temperatures. The temperature coefficient recorded for P_{MP} is positive at temperatures below ~22.5°C. This means that the amorphous silicon device tested has an optimum operation temperature at this point with maximum in power and efficiency, rather than performing better at low temperatures.

At this point is not known how much the observed temperature behaviour is a trend seen generally. Significant changes in temperature coefficients of a-Si devices have been reported by K. Sriprapha et al. [14]. However, the paper does not report measurements below 25°C and the sign change in P_{MP} temperature coefficient is not shown. Nevertheless, positive temperature coefficients in P_{MP} have been reported for an amorphous silicon carbide (a-SiC) solar cell even up to a temperature of 60°C [144], indicating that a positive temperature response of P_{MP} is not impossible. If the data presents a more general behaviour, which in the first instance can be expected from at least the same material type and composition, then energy yield calculations may need to incorporate non-linear temperature effects for a-Si devices. The change in P_{MP} temperature coefficient is significant and assuming a global temperature coefficient may lead to unexpected uncertainties especially in particularly hot or cold climates.

6.5 Measurement uncertainty

In order to determine to what extent the G-T-E performance measurements on the LED-simulator can be trusted on an absolute scale, a measurement uncertainty analysis was carried out. This has been done similarly to the uncertainty calculations given previously in section 4.4.3. Since the G-T-E device characteristics data was acquired with a new measurement method, additional introduced sources of uncertainty have been included in the irradiance and spectrum measurement and control group. These are explained further in this section. Uncertainties have also been calculated for measurements at the lowest light intensity to highlight trustworthiness at the worst case point. Table 6.2 and Table 6.3 summarise the measurement uncertainty for the c-Si and a-Si device, respectively.

One new uncertainty contribution comes from the calibration of the test device for self referencing in the Pasan solar simulator. For this, the main influencing factors have been included: reference cell uncertainty of 2.3% (k=2), 0.5% non-uniformity of light (rectangular distribution) and an estimated 1% (k=2) in spectral mismatch. The uncertainty in non-linearity of both test devices has also been included as it was measured without reduction factor (see previous Figure 6.5 in section 6.3.2).

Another uncertainty in the group of irradiance and spectrum that needs to be accounted for is the relative change of spectrum due to the halogen light sources when changing the intensity. As previously mentioned, the G vs. I_D control of the light sources for calculating the new measurement irradiance was measured with a c-Si reference cell. This meant that the induced current on the test cell from the halogen light sources was correct in relative terms for the c-Si device even though the spectrum of the halogen lights shifted to the infrared with lower measurement intensity. Thus, the balance in the current generation of each the light source on the c-Si device was relatively accurate. Furthermore, it should be noted that self-referencing largely eliminated the spectral mismatch errors on both the c-Si and a-Si device. A full analysis of the remaining uncertainty due to relative spectral changes has not yet been done for the LED-based solar simulator. It is known that this

uncertainty increases with reduction in light intensity, as the light sources are calibrated at maximum intensity. An estimated remaining uncertainty due to the spectral change of the halogen lights of 2% (k=1) on irradiance and current at low measurement irradiance has been included for both devices. Additionally, since the FF of the a-Si device is also influenced, an estimated uncertainty of 0.25% in fill factor was included at low intensity.

Influence & intensity	**c-Si standard uncertainty (k=1) [%]**				
	Irradiance	**Voltage**	**Current**	**Fill Factor**	**P_{MP}**
Electrical data acquisition and calibration:					
High	± 0.10	± 0.09	± 0.14	± 0.01	± 0.17
Low	± 0.98	± 0.12	± 1.95	± 0.08	± 1.96
Device temperature measurement and conditioning:					
High	± 0.00	± 0.08	± 0.02	± 0.03	± 0.10
Low	± 0.00	± 0.11	± 0.04	± 0.03	± 0.11
Irradiance setting and spectral measurements:					
High	± 1.74	± 0.08	± 2.07	± 0.00	± 2.07
Low	± 2.11	± 0.12	± 2.39	± 0.00	± 2.39
Device mounting alignment and connections:					
High	± 1.48	± 0.06	± 1.48	± 0.45	± 1.55
Low	± 1.48	± 0.09	± 1.48	± 0.45	± 1.55
Combined uncertainty at high intensity (778W/m^2):					
k=1	**± 2.29**	**± 0.16**	**± 2.55**	**± 0.45**	**± 2.59**
k=2	**± 4.57**	**± 0.32**	**± 5.09**	**± 0.90**	**± 5.18**
Combined uncertainty at low intensity (34W/m^2):					
k=1	**± 2.76**	**± 0.22**	**± 3.42**	**± 0.46**	**± 3.46**
k=2	**± 5.52**	**± 0.44**	**± 6.84**	**± 0.92**	**± 6.92**

Table 6.2: Uncertainty in I-V curve measurements of the c-Si solar cell G-T-E performance matrix at high (778W/m^2) and low (34W/m^2) light intensity at AM 1.5 spectral setting

With regards to the spectral sensitivity of the FF on the a-Si device an estimated uncertainty of 0.25% has been included to account for the uncertainty in setting of the spectrum and for the imperfections of the simulator spectrum to the reference spectrum. The value is estimated as a full analysis of the impact on FF has not been carried out on the simulator

prototype. This would require a more detailed understanding of spectral effects and voltage dependent spectral response of a-Si devices, which could not be carried out in the timeframe of this work. However, a much better accuracy and reproduction of the sunlight is predicted for future versions of LED-based solar simulators.

Influence & intensity	**a-Si standard uncertainty (k=1) [%]**				
	Irradiance	**Voltage**	**Current**	**Fill Factor**	**P_{MP}**
Electrical data acquisition and calibration:					
high	± 0.09	± 0.05	± 0.19	± 0.01	± 0.19
low	± 0.90	± 0.08	± 4.02	± 0.23	± 4.02
Device temperature measurement and conditioning:					
high	± 0.00	± 0.07	± 0.02	± 0.03	± 0.02
low	± 0.00	± 0.09	± 0.02	± 0.00	± 0.07
Irradiance setting and spectral measurements:					
high	± 1.77	± 0.07	± 2.09	± 0.28	± 2.11
low	± 2.10	± 0.11	± 2.38	± 0.35	± 2.41
Device mounting alignment and connections:					
high	± 1.48	± 0.06	± 1.48	± 0.45	± 1.55
low	± 1.48	± 0.07	± 1.48	± 0.45	± 1.55
Combined uncertainty at high intensity (1000W/m^2):					
k=1	**± 2.31**	**± 0.13**	**± 2.57**	**± 0.53**	**± 2.63**
k=2	**± 4.62**	**± 0.25**	**± 5.14**	**± 1.06**	**± 5.26**
Combined uncertainty at low intensity (36W/m^2):					
k=1	**± 2.73**	**± 0.17**	**± 4.90**	**± 0.62**	**± 4.94**
k=2	**± 5.45**	**± 0.35**	**± 9.80**	**± 1.24**	**± 9.88**

Table 6.3: I-V curve measurement uncertainty of the a-Si mini module tested at high and low light intensity at AM 1.5 spectral setting

6.6 Discussion

G-T-E performance matrix measurement results of the c-Si solar cell show an agreement to reported behaviour of PV modules of the same material outdoors. This is a good indication that the measurement method presented in this chapter is working well and allows indoor based measurements of

spectral effects of pertinence to outdoor operation. The performance measurements of the a-Si mini module made it possible for the first time to analyse and quantify the reported spectral influences from outdoor measurements directly, under a controlled environment in a solar simulator. The controlled environment allowed a dissection of influences which gives an unprecedented agreement with theoretically predicted behaviour. The findings on the tested a-Si mini module show a clear trend and are in no case of random nature, which is a further indication that the concept of a G-T-E measurement works. This is further confirmed by the uncertainty analysis, although low light measurements require further improvements. Nevertheless, this is in agreement with recent round robin intercomparisons of test laboratories where the deviation between the participants was significantly worse at low measurement intensity than at high irradiance [85]. The problem is somewhat more convoluted if the spectrum is also changing (deliberately) and further work needs to be done in this area.

Using the test device as a self-reference for irradiance determination and solar simulator spectrum adjustment reduced uncertainties in the I-V measurement as the simulator prototype at the time did not allow the positioning of a reference cell next to the test device without introducing errors due to increased light non-uniformity.

The self-reference method largely eliminates uncertainty influences arising due to spectral shift of the halogen lights. Measurements can be improved upon using direct spectral output measurement feedback with a spectroradiometer, which is an entire project in itself and is currently not possible to fit into the current work. This feedback will be needed for measuring multi-junction solar cells as a change in the spectrum of halogen lights changes the junction current balance.

From the uncertainty analysis it is apparent that measurement uncertainties in data acquisition make no significant contribution in high irradiance situations. However, this changes drastically when measuring at low intensity as the DAQ card’s absolute measurement accuracy at the measurement input range becomes the largest contribution with 2% (k=1) in the current on the c-Si device and with an unacceptable 4% on the a-Si device. An

appropriately automated measurement range setting, signal amplification and signal-strength dependent calibration can significantly reduce those uncertainties but has not yet been implemented into the system.

6.7 Conclusions

A method for a complete indoor characterisation of devices has been presented. A G-T-E performance matrix has been measured on a c-Si solar cell and an a-Si mini module using the LED-based solar simulator. Results clearly demonstrate that the measurement apparatus is capable of measuring the device parameters required for an indoor based approach which includes spectral variations. This opens a new dimension for laboratory based PV device characterisation as it is the first time that sunlight spectra with their variability can be reproduced, meaning that spectral effects on devices can be measured in a controlled environment. The concept is a very promising start for a more accurate energy rating and energy yield prediction, especially for thin-film amorphous and multi-junction devices, where spectral effects are known to be an issue.

The a-Si device measured showed significant spectral influences not only on I_{SC} but also in FF, V_{OC}, I_{MP} and V_{MP}. Additionally, temperature coefficients have shown to be dependent on irradiance, spectrum and the device temperature itself and are thus nonlinear in all respects. This is not only an indication that a GTE-matrix can be measured, it shows that measurements at varying spectrum, irradiance and device temperature are highly important to be able to make an accurate prediction of the device performance at a specific location regardless of the material or structure of a PV device of choice.

An uncertainty analysis shows that measurements are robust. Uncertainty is slightly larger compared to that of commercial test houses [93]. However, it also shows that much improvement and optimisation is needed and possible to provide more accurate data for energy yield prediction, especially at low light conditions. Uncertainty contributions have been indentified and will in future be reduced with better calibration accuracies and equipment. In the

current measurement set-up with test device self referencing, multi-junction devices cannot be measured accurately. Nevertheless, the system provides all the functions necessary to measure these more complex devices and initial steps have been taken to make this possible. The planned new version of the solar simulator will further reduce measurement uncertainties and increase measurement speed.

The demonstrated work has implications on the device performance measurements in the energy rating standard that is currently under development by the international electrotechnical commission (IEC) [34], as it could make the standard applicable to multi-junctions. Furthermore, a method for energy yield prediction is currently being work on that includes measurements in a G-T-E performance matrix.

7 Thesis Conclusions

The main aim of this work was to develop a novel indoor measurement system and new measurement approaches that provide a solution for fast and accurate power rating and energy rating of photovoltaic devices. This was achieved through the following main elements of the work:

- A novel LED-based solar simulator prototype was developed that provides variability in measurement conditions as seen outdoors.
- A new automated measurement approach for power rating of single- and multi-junction solar cells was developed that allows the characterisation of these devices without any prior knowledge of device structure and number of junctions.
- The concept of photovoltaic device performance measurements for energy yield predictions of PV devices at varying irradiance spectrum, light intensity and temperature was developed and demonstrated.

The following sections identify the main conclusions within these three areas. Recommendations for future work are given in the last section.

7.1 LED-based solar simulator prototype

Prior to this work, the technology and concept of LED solar simulators was at a very early stage. Solar simulators based on LEDs did not produce enough light intensity to carry out accurate device characterisation and consisted of only a few LED colours, providing only discrete discontinuous spectral output. The LED-based solar simulator prototype developed throughout this work has vastly improved on this. The system provides much higher light intensity and with eight different LED colours and halogen lights delivers a quasi-continuous spectral output. The solar simulator is a class BAA (Spectral match B, Light intensity non-uniformity A, temporal stability A) over an area of

45x45mm^2. This unit was the first of its kind to achieve qualification according to the IEC60904-9 standard by meeting requirements for light intensity and spectral match. It also is the first unit capable of reproducing spectral variations in the fine detail as seen in the real world with variable air mass and weather conditions.

An LED-based solar simulator provides a much higher flexibility in measurements conditions than any other type of solar simulator, the previously unobtainable variability in spectral irradiance makes it an ideal tool for power rating of multi-junction solar cells. Additionally, it provides the base for more detailed performance measurements for energy rating and energy yield prediction of all photovoltaic device types in three dimensions: spectrum, light intensity and device temperature. Thus, it is the first type of solar simulator that allows investigating device characteristics at more realistic outdoor conditions, with the benefits of a repeatable indoor setting. Since such simulators use a large number of different LED colours, it is also useful as a spectral response measurement system, eliminating the need of external measurement equipment. With variable flash speed, LED simulators can be adjusted to cope with any device, slow or fast responding, which previously was only possible to a limited degree. At the same time, such systems can be operated in steady state, combining the advantages of both types of conventional solar simulators and opening possibilities for controlled preconditioning prior to calibration measurements and also allowing detailed investigations of effects such as degradation, thermal annealing and preconditioning. The flexibility in measurement conditions make the system a useful tool to do research in those fields. Furthermore, such a system can be programmed to work automatically and unattended and combines the functionality of several different types of costly equipment which would have been needed to carry out the same tasks.

LED-based solar simulators are currently a hot topic in the area of device characterisation. Without doubt one can say that the concept of an LED-based solar simulator has been proven in this work. With further improvements and enhancements of the technology, such simulators will

outperform conventional solar simulators and will revolutionise photovoltaic device characterisation.

7.2 Automated characterisation of solar cells

Accurate calibration of devices, especially thin film technologies, requires knowledge of the spectral response to select a closely matched reference cell. This requires specialised measurement equipment that, if of the conventional type (filter based or monochromator), could not be utilised in a factory setting, as the measurements take too long. The new automated characterisation method developed within this work has great potential to change this situation. The method developed can detect first of all the device type (single- or multi-junction). It acquires the spectral response of each junction in the device directly in the solar simulator, which eliminates the need for additional equipment. In the last step it measures the I-V curve at standard test conditions or at any other desired condition with possible variations in measurement spectrum, irradiance and device temperature. Furthermore, the method could be extended to carry out spectrometric characterisation on multi-junction solar cells, which is essential for optimisation of the junctions in the device.

The method can be applied in any multi-source solar simulator. Although, it's best use is in LED-based solar simulators as spectral output can be controlled more precisely. The method's greatest potential lies in its unique spectral response measurement and fitting method. This also allows for voltage dependent spectral response measurements within one measurement cycle. Since the solar simulator illuminates the complete device it acquires the correct average response of the complete solar cell or module which eliminates uncertainties introduced when measuring only single cells or small spots of a test device. Additionally, the approach can cope with slow responding devices such as dye sensitised solar cells because light conditions are stable during the measurement. Furthermore, this method takes less time than conventional spectral response measurement systems and thus has potential to be adapted for factory use in

an automated quality control measurement process. Uncertainty in power rating is reduced as spectral response is not estimated, which additionally reduces the risks in photovoltaic system design.

The ability of the method to detect the junctions in the device under test is of advantage when characterising previously unknown devices or new technologies in the laboratory. This, in addition to the automated determination of the spectral response, has potential to reduce characterisation time and cost. Furthermore, it reduces the effects of human error in characterisation and determination of the device type.

The developed measurement approach was demonstrated on simulated and live measurements of a single and a double-junction a-Si device. The accuracy achieved in simulations was within 0.5% of maximum power of the final I-V curve and the spectral response curves acquired were in very good agreement with the input, which is a first verification of the method. Initial measurements on the simulator showed an error of 0.3% in maximum power on the single-junction device and 4.5% on the double-junction mini module. This larger deviation was identified as being due to a lack of measurement feedback of spectral output rather than a problem in the measurement method itself. Using measurement feedback will greatly enhance measurement quality. Nonetheless, estimating spectral response or using a mismatched reference cell leads to larger uncertainties and measurement errors than observed here, even in the non-ideal case without feedback.

7.3 Performance matrix measurements

The unique ability of the developed simulator to reproduce the spectral variability of the sun has opened the possibility to greatly improve the performance measurements for energy yield predictions. A new method has been developed and demonstrated that adds an additional third dimension to the performance characteristic matrix. It measures performance not only at varying irradiance and device temperature, but also under varying spectrum. This can reduce uncertainties in energy yield prediction, especially of spectrally sensitive devices, because the effect does not need to be modelled

or estimated. Improvements in accuracy of short time energy predictions are also expected, since spectral effects have shown a stronger influence over shorter prediction periods. This should positively influence status monitoring and energy output forecasting for large PV systems.

To date, one could only measure spectral effects outdoors, where the environmental factors are strongly correlated and very difficult to separate. Measuring under controlled conditions makes a separation of the underlying effects far easier. Thus, a direct investigation of spectral influences on device performance can be carried out much more precisely. This ultimately leads to a more detailed understanding of behaviour of different photovoltaic devices and can be used to optimise device structures and materials.

In this work, the developed method was applied to a crystalline- and an amorphous silicon single-junction solar cell. It is the first time that the performance of PV devices has been measured to such a detailed degree in such a short measurement cycle. Also, for the first time measurements verified theoretical predictions in the spectrally influenced behaviour of single junction devices. It has been shown that the crystalline silicon device was very stable over varying spectra, which means that a simple spectral match correction is sufficient to correct for spectral effects. However, results show a far larger spectral effect on the amorphous device and it has been shown that the fill factor is additionally affected. Including these effects will prove important for accurate energy prediction of such technologies.

This work has added a new dimension to photovoltaic device research with the ability to directly investigate spectral effects. This is also important for performance tweaking, especially of multi-junction solar cells, for maximum energy yield in the location in which it is put to use. The developed methods and the technology of an LED-based solar simulator provide the basis for fast and automated performance measurements on all device technologies. Furthermore, adding spectral effects to device performance provides a fair base for energy rating of every technology. With this in mind, the results of this work provide a large step in the direction of energy rating becoming the main cost driving factor in the PV industry, reducing financial risk and also easing device comparisons under realistic aspects.

7.4 Proposed future research

Within this work a prototype version of an LED-base solar simulator was built. Future work would be to design and construct an advanced class AAA version of the solar simulator based on the recommendations of improvements given in this thesis. This would greatly enhance measurement quality as well as improve spectral match. The ultimate goal would be to increase the target illumination to accommodate full size modules (e.g. $2x2m^2$).

Within the scope of this work it was possible to prove the working concept of an automated characterisation. The next steps would be to fully validate and optimise the proposed measurement method with different spectral response parameter models used. For this, appropriate measurement feedback is required. Furthermore, measurements of devices made from different materials and with different structures need to be compared to fully assess measurement uncertainty.

This work has delivered the first ever photovoltaic performance characteristic measurements in three dimensions under controlled conditions in a solar simulator. It was not within the scope of this work to validate the performance characteristic measurements for energy yield predictions, as this is a large project on its own. Future work is needed here to assess the gain in accuracy of long term and short term energy yield predictions for different PV device structures and materials. Additionally, angle of incidence effects should be added as additional dimension to the performance matrix.

Finally, the author would like to mention that the LED-based solar simulator designed and constructed throughout this work is a rich platform from which to launch a number of investigative avenues. This thesis concentrated on new concepts in power and energy rating that have been enabled by the enormous flexibility of the measurement system. The system has opened the possibility to a whole range of research areas in PV device performance, such as preconditioning and degradation effects, light soaking and aging factors, validation and development of physical models of PV devices and

energy prediction software, and irradiance and temperature influences on spectral response.

Publications and Achievements

Journal publications

Monokroussos C., Bliss M., Qiu Y.N., Hibberd C.J., Betts T.R., Tiwari A.N., Gottschalg R., *"Effects of spectrum on the power rating of amorphous silicon photovoltaic devices"*, Progress in Photovoltaics: Research and Applications, published online, 2011, doi: 10.1002/pip.1080.

Hibberd C.J., Plyta F., Monokroussos C., Bliss M., Betts T.R., Gottschalg R., *"Voltage-dependent quantum efficiency measurements of amorphous silicon multi-junction mini-modules"*, Solar Energy Materials and Solar Cells, 95 (1), January 2011, pp 123-126, ISSN 0927-0248.

Bliss M., Betts T.R. and Gottschalg R., *"Indoor measurement of photovoltaic device characteristics at varying irradiance, temperature and spectrum for energy rating"*, Measurement Science and Technology, 21 (11), September 2010, doi: 10.1088/0957-0233/21/11/115701

Bliss M., Betts T.R. and Gottschalg R., *"An LED-based Photovoltaic Measurement System with Variable Spectrum and Flash Speed"*, Solar Energy Materials and Solar Cells, 93 (6+7), June 2009, pp 825-830, ISSN 0927 0248.

Conference publications

Bliss M., Betts T.R. and Gottschalg R., *"Performance measurements at varying irradiance spectrum, intensity and module temperature of amorphous silicon solar cells"*, 35th IEEE Photovoltaic Specialists Conference, (IEEE PVSC 35), Honolulu, USA, June 2010, pp 2660-2665, ISBN 978-1-4244-5890-5.

Krawczynski M., Strobel M.B., Goss B., Bristow N., Bliss M., Betts T.R., Gottschalg R., *"Large scale PV system monitoring - modules technology intercomparison"*, 35th IEEE Photovoltaic Specialists Conference, (IEEE PVSC 35), Honolulu, USA, June 2010, pp 2295-2300, ISBN 978-1-4244-5890-5.

Bliss M., Betts T.R. and Gottschalg R., *"Indoor Measurement of GTE-matrix for Energy Rating"*, Proceedings of the 6th Photovoltaic Science Applications and Technology Conference (PVSAT6), Southampton, UK, March 2010, pp 169-172, ISBN 0904963756.

Roy J., Bliss M., Betts T.R. and Gottschalg R., *"Effect of I-V Translations of Irradiance-Temperature on the Energy Yield Prediction of PV Module and Spectral Changes over Irradiance and Temperature"*, Proceedings of the 6th Photovoltaic Science Applications and Technology Conference

(PVSAT6), Southampton, UK, March 2010, pp 149-152, ISBN 0904963756.

Bliss M., Wendlandt S., Betts T.R. and Gottschalg R., *"Towards a High Power, All LED Solar Simulator Closely Matching Realistic Solar Spectra"*, 24th European Photovoltaic Solar Energy Conference, (EU-PVSEC 24), Hamburg, Germany, September 2009, paper 4AV.3.11

Bliss M., Hibberd C.J., Qiu Y., Betts T.R. and Gottschalg, R., *"Automated Characterisation of Multi-Junction Thin Film Silicon Solar Cells"*, 24th European Photovoltaic Solar Energy Conference, (EU-PVSEC 24), Hamburg, Germany, September 2009, paper 3AV.2.32

Goss B., Cradden K., Gwillim R., Bliss M., Strobel M., Gottschalg R., *"Inter-Continental Optimisation of Photovoltaic Technologies in Large Arrays"*, 24th European Photovoltaic Solar Energy Conference, (EU-PVSEC 24), Hamburg, Germany, September 2009, paper 4BO.12.1

Goss B., Benfield C., Gwillim R., Bliss M., Strobel M., Gottschalg R., *"Large Scale Evaluation of Photovoltaic Technologies in Different Climates"*, 34th IEEE Photovoltaic Specialists Conference, (IEEE PVSC 34), Philadelphia, USA, June 2009

Bliss M., Betts T.R. and Gottschalg R., *"Towards an Accurate and Automated Characterisation of Multi-Junction Solar Cells"*, Proceedings of the 5th Photovoltaic Science Applications and Technology Conference, (PVSAT5), Wrexham, UK, April 2009, pp 43-46, ISBN 0904963748.

Goss B., Benfield C., Gwillim R., Bliss M., Strobel M. and Gottschalg R., *"Large Scale Evaluation of Photovoltaic Technologies in Different Climates"*, Proceedings of the 5th Photovoltaic Science Applications and Technology Conference, (PVSAT5), Wrexham, UK, April 2009, pp 65-68, ISBN 0904963748.

Hibberd C.J., Bliss M., Upadhyaya H.M. and Gottschalg R., *"Characterisation of a filter-based external quantum efficiency measurement system"*, Proceedings of the 5th Photovoltaic Science Applications and Technology Conference, (PVSAT5), Wrexham, UK, April 2009, pp 239-242, ISBN 0904963748.

Bliss M., Betts T.R. and Gottschalg R., *"Advantages in using LEDS as the main light source in solar simulators for measuring PV device characteristics"*, Reliability of Photovoltaic Cells, Modules, Components and Systems, 7048, SPIE Optics & Photonics 2008, San Diego, USA, August 2008, pp 07-1 to 07-11, ISBN 9780819472687.

Bliss M., Betts T.R. and Gottschalg R., (Best poster award), *"Initial Solar Cell Characterisation Test and Comparison with A LED-Based Solar Simulator with Variable Flash Speed and Spectrum"*, Proceedings of the 4th Photovoltaic Science Applications and Technology Conference, (PVSAT4), Bath, UK, April 2008, pp 215-218, ISBN 0904963733.

Bliss M., Betts T.R. and Gottschalg R., (Young researcher award), *"An LED-Based Photovoltaic Measurement System with Variable Spectrum and*

Flash Speed", 17th International Photovoltaic Science and Engineering Conference, Fukuoka, Japan, December 2007, pp 447-448.

Awards

Young Researchers Award at the 17th International Photovoltaic Science and Engineering Conference in Fukuoka, Japan, December 2007.

Best Poster Award at the 4th Photovoltaic Science Applications and Technology Conference in Bath, UK, April 2008.

Graduate School Research Student Prize at faculty of engineering Loughborough University 2008/09.

References

[1] IEC 60904-3 2008 Photovoltaic devices - Part 3: Measurement Principles for Terrestrial PV Solar Devices with Reference Spectral Irradiance Data.

[2] S. Williams, R. Gottschalg and D. G. Infield, "PV modules real operating performance in the UK, A temperate maritime climate," in Paris, France, 2004, pp. 2109 - 2112.

[3] J. Merten, J. M. Asensi, C. Voz, A. V. Shah, R. Platz and J. Andreu, "Improved equivalent circuit and analytical model for amorphous silicon solar cells and modules," *Electron Devices, IEEE Transactions on,* vol. 45, pp. 423-429, 1998.

[4] S. R. Wenham, M. A. Green, M. E. Watt and R. Corkish, *Applied Photovoltaics (2nd Edition).* Earthscan, 2007.

[5] W. Shockley and H. J. Queisser, "Detailed Balance Limit of Efficiency of p-n Junction Solar Cells," *J. Appl. Phys.,* vol. 32, pp. 510-519, March 1961, 1961.

[6] A. D. Vos, "Detailed balance limit of the efficiency of tandem solar cells," *J. Phys. D,* vol. 13, pp. 839, 1980.

[7] G. F. Virshup, "Measurement techniques for multijunction solar cells," in *Photovoltaic Specialists Conference, 1990., Conference Record of the Twenty First IEEE,* 1990, pp. 1249-1255 vol.2.

[8] J. Burdick and T. Glatfelter, "Spectral response and I-V measurements of tandem amorphous-silicon alloy solar cells," *Solar Cells,* vol. 18, pp. 301-Oct., 1986.

[9] M. Yamaguchi, T. Takamoto and K. Araki, "Super high-efficiency multi-junction and concentrator solar cells," *Solar Energy Mater. Solar Cells,* vol. 90, pp. 3068-3077, 11/23, 2006.

[10] M. Wolf and H. Rauschenbach, "Series resistance effects on solar cell measurements," *Advanced Energy Conversion,* vol. 3, pp. 455-479, 6, 1963.

[11] H. Müllejans, T. Wagner, F. Merli, A. Jäger-Waldau and E. D. Dunlop, "Changes in spectral response with temperature and irradiance intensity," *Thin Solid Films,* vol. 451-452, pp. 145-151, 3/22, 2004.

[12] M. A. Green, Solar Cells: Operating Principles, Technology, and System Applications. Englewood Cliffs, NJ, Prentice-Hall, Inc., 1982.

[13] K. Emery, J. Burdick, Y. Caiyem, D. Dunlavy, H. Field, B. Kroposki, T. Moriarty, L. Ottoson, S. Rummel, T. Strand and M. W. Wanlass, "Temperature dependence of photovoltaic cells, modules and systems," in *Photovoltaic Specialists Conference, 1996., Conference Record of the Twenty Fifth IEEE,* 1996, pp. 1275-1278.

[14] K. Sriprapha, S. Inthisang, S. Y. Myong, S. Miyajima, A. Yamada, P. Sichanugrist and M. Konagai, "Development of amorphous silicon-based thin-film solar cells with low-temperature coefficient," in 2008, pp. 70450C.

[15] ISO 9488:2000 solar energy - vocabulary.

[16] R. Gottschalg, The Solar Resource and the Fundamentals of Solar Radiation for Renewable Energy Systems. SCI-Notes: Solar Energy (Key Note), 2001.

[17] C. Hu and R. M. White, *Solar Cells: From Basic to Advanced Systems.* Mcgraw-Hill College, 1983.

[18] R. Adelhelm, "Performance and parameter analysis of tandem solar cells using measurements at multiple spectral conditions," *Solar Energy Mater. Solar Cells,* vol. 50, pp. 185-195, 1998.

[19] R. Rüther, G. Kleiss and K. Reiche, "Spectral effects on amorphous silicon solar module fill factors," *Solar Energy Mater. Solar Cells,* vol. 71, pp. 375-385, 2/15, 2002.

[20] R. Gottschalg, T. R. Betts, D. G. Infield and M. J. Kearney, "The effect of spectral variations on the performance parameters of single and double junction amorphous silicon solar cells," *Solar Energy Mater. Solar Cells,* vol. 85, pp. 415-428, 1/31, 2005.

[21] C. Dechthummarong, B. Wiengmoon, D. Chenvidhya, C. Jivacate and K. Kirtikara, "Physical deterioration of encapsulation and electrical insulation properties of PV modules after long-term operation in Thailand," *Solar Energy Mater. Solar Cells,* vol. 94, pp. 1437-1440, 9, 2010.

[22] O. S. Sastry, S. Saurabh, S. K. Shil, P. C. Pant, R. Kumar, A. Kumar and B. Bandopadhyay, "Performance analysis of field exposed single crystalline silicon modules," *Solar Energy Mater. Solar Cells,* vol. 94, pp. 1463-1468, 9, 2010.

[23] C. R. Osterwald, J. Adelstein, J. A. D. Cueto, B. Kroposki, D. Trudell and T. Moriarty, "Comparison of degradation rates of individual modules held at maximum power," in *Photovoltaic Energy Conversion, Conference Record of the 2006 IEEE 4th World Conference on,* 2006, pp. 2085-2088.

[24] J. Zhu, Y. Qiu, T. R. Betts and R. Gottschalg, "Effects of different data collection strategies on outdoor performance measurements and degradation," in *Proceedings of the 24th European Photovoltaic Solar Energy Conference,* Hamburg, Germany, 2009, pp. 3439 - 3445.

[25] D. L. Staebler and C. R. Wronski, "Reversible conductivity changes in discharge-produced amorphous Si," *Appl. Phys. Lett.,* vol. 31, pp. 292-294, August 15, 1977, 1977.

[26] D. L. King, J. A. Kratochvil and W. E. Boyson, "Stabilization and performance characteristics of commercial amorphous-silicon PV modules," in *Photovoltaic Specialists Conference, 2000. Conference Record of the Twenty-Eighth IEEE,* 2000, pp. 1446-1449.

[27] R. Rüther and J. Livingstone, "Seasonal variations in amorphous silicon solar module outputs and thin film characteristics," *Solar Energy Mater. Solar Cells,* vol. 36, pp. 29-43, 1, 1995.

[28] J. A. del Cueto and B. von Roedern, "Temperature-induced changes in the performance of amorphous silicon multi-junction modules in controlled light-soaking," *Prog Photovoltaics Res Appl,* vol. 7, pp. 101-112, 1999.

[29] J. Merten and J. Andreu, "Clear separation of seasonal effects on the performance of amorphous silicon solar modules by outdoor I/V-measurements," *Solar Energy Mater. Solar Cells,* vol. 52, pp. 11-25, 3/16, 1998.

[30] IEC 61215:2005 Crystalline silicon terrestrial photovoltaic (PV) modules — Design qualification and type approval.

[31] C. Riordan and R. Hulstron, "What is an air mass 1.5 spectrum? [solar cell performance calculations]," in *Photovoltaic Specialists Conference, 1990., Conference Record of the Twenty First IEEE,* 1990, pp. 1085-1088 vol.2.

[32] K. Emery, "The rating of photovoltaic performance," *Electron Devices, IEEE Transactions on,* vol. 46, pp. 1928-1931, 1999.

[33] C. A. Gueymard, D. Myers and K. Emery, "Proposed reference irradiance spectra for solar energy systems testing," *Solar Energy,* vol. 73, pp. 443-467, 12, 2002.

[34] IEC 61853 photovoltaic (PV) module performance testing and energy rating (draft standard).

[35] G. Friesen, D. Chianese, I. Pola, A. Realini and A. Bernasconi. Energy rating measurements and predictions at ISAAC. Presented at Proceedings of the 22th European Photovoltaic Solar Energy Conference.

[36] B. Kroposki, K. Emery, D. Myers and L. Mrig, "A comparison of photovoltaic module performance evaluation methodologies for energy ratings," in *Photovoltaic Energy Conversion, 1994., Conference Record of the Twenty Fourth. IEEE Photovoltaic Specialists Conference - 1994, 1994 IEEE First World Conference on,* Waikoloa, HI, 1994, pp. 858 - 862.

[37] R. P. Kenny, E. D. Dunlop, H. A. Ossenbrink and H. Müllejans, "A practical method for the energy rating of c-Si photovoltaic modules based on standard tests," *Prog Photovoltaics Res Appl,* vol. 14, pp. 155-166, 2006.

[38] M. Bliss, R. Gottschalg and D. G. Infield, "Improved outdoor monitoring of photovoltaic modules," in *Proceedings of the 2nd Photovoltaic Science, Applications and Technology Conference,* Loughborough, UK, 2005, pp. 105 - 112.

[39] M. Bliss, "Development of an advanced measurement system for photovoltaic modules," CREST, Electronic and Electrical Engineering, Loughborough University, 2005.

[40] Wacom Electric Co. Ltd. Wacom solar simulator products. *2010(07/27),* Available: www.wacom-ele.co.jp; www.wacom-ele.co.jp/Solar/ENGsolar2.htm.

[41] Pasan SA. Pasan sun simulator IIIb. *2010(07/27),* Available: www.pasan.ch; www.pasan.ch/website/en/products/sun-simulators/pasan-sun-simulator-iiib.

[42] W. Herrmann, W. Wiesner, H. -. Pitzer and R. Wyssada, "Development of an indoor test facility for the qualification of photovoltaic systems and components," TÜV Rheinland Sicherheit und Umweltschutz GmbH, 1995.

[43] Y. Hishikawa and S. Igari, "Characterization of the I-V curves of multi-junction solar Cells/Modules by high-fidelity solar simulators and their irradiance dependence," in *Proceedings of the 19th European Photovoltaic Solar Energy Conference,* Paris, France, 2004, pp. 1340 - 1345.

[44] M. Bennett and R. Podlesny, "Two source simulator for improved solar simulation," in *Photovoltaic Specialists Conference, 1990., Conference Record of the Twenty First IEEE,* 1990, pp. 1438-1442 vol.2.

[45] J. H. Warner, R. J. Walters, S. R. Messenger, J. R. Lorentzen, G. P. Summers, H. L. Cotal and N. H. Karam, "Measurement and characterization of triple junction solar cells using a close matched multizone solar simulator," in 2004, pp. 45-55.

[46] B. L. Sopori, C. Marshall and K. Emery, "Mixing optical beams for solar simulation-a new approach [to solar cell testing]," in *Photovoltaic Specialists Conference, 1990., Conference Record of the Twenty First IEEE,* 1990, pp. 1116-1121 vol.2.

[47] R. J. Matson, K. A. Emery and R. E. Bird, "Terrestrial solar spectra, solar simulation and solar cell short-circuit current calibration: a review," *Solar Cells,* vol. 11, pp. 105-45, 1984.

[48] K. Emery, D. Myers and S. Rummel, "Solar simulation-problems and solutions," in *Photovoltaic Specialists Conference, 1988., Conference Record of the Twentieth IEEE,* 1988, pp. 1087 - 1091.

[49] F. Granek and T. Zdanowicz, "Advanced system for calibration and characterization of solar cells," *Opto-Electronics Review,* vol. 12, pp. 57-67, 2004.

[50] M. Shimotomai, Y. Shinohara and S. Igari, "The development of the I-V measurement by pulsed multi-flash, and the effectivene," in Waikoloa, HI, 2006, pp. 2223.

[51] SPIRE Corporation, *SPIRE SPI-SUN 240A Manual.* 1984.

[52] IEC 60891 2009: Photovoltaic devices - Procedures for temperature and irradiance corrections to measured I-V characteristics.

[53] H. Müllejans, D. Pavanello and A. Virtuani, "New correction procedure for IV curves measured under varying irradiance," in *23rd European Photovoltaic Solar Energy Conference Proceedings,* Valencia, Spain, 2008, pp. 2818-2821.

[54] A. M. Andreas and D. R. Myers, "Pulse analysis spectroradiometer system for measuring the spectral distribution of flash solar

simulators," in *Proc. SPIE: Optical Modeling and Measurements for Solar Energy Systems II,* 2008, pp. 70460I.

[55] J. Kiehl, K. Emery and A. M. Andreas, "Testing concentrator cells: Spectral considerations of a flash lamp system," in *Proceedings of the 19th European Photovoltaic Solar Energy Conference ,* Paris, France, 2004, pp. 2463-2465.

[56] H. A. Ossenbrink, W. Zaaiman and J. Bishop, "Do multi-flash solar simulators measure the wrong fillfactor?" in Louisville, USA, 1993, pp. 1194-1196.

[57] C. Monokroussos, R. Gottschalg, A. N. Tiwari, G. Friesen, D. Chianese and S. Mau, "The effects of solar cell capacitance on calibration accuracy when using a flash simulator," in *Photovoltaic Energy Conversion, Conference Record of the 2006 IEEE 4th World Conference on,* Waikoloa, HI, 2006, pp. 2231-2234.

[58] A. Virtuani, H. Müllejans and E. D. Dunlop, "Comparison of indoor and outdoor performance measurements of recent commercially available solar modules," *Prog Photovoltaics Res Appl,* vol. 9999, 2010.

[59] C. Monokroussos, R. Gottschalg, A. N. Tiwari and D. G. Infield, "Measurement artefacts due to the use of flash simulators," in *Proceedings of the Photovoltaic Science Application and Technology Conference (PVSAT-2),* Loughborough, UK, 2005, pp. 143-151.

[60] K. A. Emery, "Solar simulators and I-V measurement methods," *Solar Cells,* vol. 18, pp. 251-260, 1986.

[61] E. G. Mantingh, W. Zaaiman and H. A. Ossenbrink, "Ultimate transistor electronic load for electrical performance measurement of photovoltaic devices using pulsed solar simulators," in *Conference Record of the Twenty Fourth IEEE Photovoltaic Specialists Conference - 1994,* Waikoloa, HI, 1994, pp. 871 - 873.

[62] N. D. Bristow, "Energy evaluation in outdoor measurements of PV modules," Loughborough University, Tech. Rep. Final MSc report, 2009.

[63] E. Duran, M. Piliougine, M. Sidrach-de-Cardona, J. Galan and J. M. Andujar, "Different methods to obtain the I–V curve of PV modules: A review," in *Photovoltaic Specialists Conference, 2008. PVSC '08. 33rd IEEE,* 2008, pp. 1-6.

[64] D. Willett and S. Kuriyagawa, "The effects of sweep rate, voltage bias and light soaking on the measurement of cis-based solar cell characteristics," in Louisville, USA, 1993, pp. 495-500.

[65] S. Kohraku and K. Kurokawa, "New methods for solar cells measurement by LED solar simulator," in *Proceedings of 3rd World Conference on Photovoltaic Energy Conversion,* Osaka, Japan, 2003, pp. 1977-1980.

[66] D. L. Young, B. Egaas, S. Pinegar and P. Stradins, "A new real-time quantum efficiency measurement system," in *Photovoltaic Specialists Conference, 2008. PVSC '08. 33rd IEEE,* 2008, pp. 1-3.

[67] Philips Lumileds Lighting Company. Luxeon III and luxeon K2 high power LEDs. *2010(08/04),* Available: http://www.philipslumileds.com/.

[68] A. Zukauskas, M. S. Shur and R. Caska, *Introduction to Solid-State Lighting.* Wiley-Interscience, 2002.

[69] Philips Lumileds Lighting Company. (2010, Technology white paper - understanding power LED lifetime analysis. Available: http://www.philipslumileds.com/uploads/165/WP12-pdf;.

[70] IEC 60904-9 2007 photovoltaic devices - part 9: Solar simulator performance requirements.

[71] S. Kohraku and K. Kurokawa, "A fundamental experiment for discrete-wavelength LED solar simulator," *Solar Energy Mater. Solar Cells,* vol. 90, pp. 3364-3370, 2006.

[72] R. Grischke, J. Schmidt, H. Albert, A. Laux, A. Metz, U. Hilsenberg and J. Gentischer, "LED flasher arrays (LFA) for an improved quality control in solar cell production lines," in *Proceedings of the 19th European Photovoltaic Solar Energy Conference,* Paris, France, 2004, pp. 2591-2594.

[73] J. Koyanagi and K. Kurokawa, "A fundamental experiment of solar cell's I-V characteristic measurement using LED solar simulator," in *Proceedings of the Renewable Energy Conference,* Chiba, Japan, 2006, pp. 270-273.

[74] National Instruments. S-series NI DAQ card PCI-6120. *2010(08/02),* Available: www.ni.com; http://sine.ni.com/nips/cds/view/p/lang/en/nid/11943;.

[75] Julabo Labortechnik GmbH. F32 refrigerated / heating circulator. *2010(08/02),* Available: www.julabo.com; http://www.julabo.com/en/p_datasheet.asp?Produkt=F32-EH.

[76] W. Herrmann and W. Wiesner, "Modelling of PV modules: Effects of non-uniformity of irradiance on performance measurements with solar simulators," in *Proceedings of the 16th European Photovoltaic Solar Energy Conference,* Glasgow, UK, 2000, pp. 2338-2341.

[77] IEC 60904-7 2008 Photovoltaic devices - Part 7: Computation of the spectral mismatch correction for measurements of photovoltaic devices.

[78] K. A. Emery, C. R. Osterwald, T. W. Cannon, D. R. Myers, J. Burdick, T. Glatfelter, W. Czubatyj and J. Yang, "Methods for measuring solar cell efficiency independent of reference cell or light source," in *Photovoltaic Specialists Conference, 1985., Conference Record of the Eighteenth IEEE,* Las Vegas, USA, 1985, pp. 623 - 628.

[79] ISO/IEC guide 98-3:2008 uncertainty of measurement - part 3: Guide to the expression of uncertainty in measurement (GUM:1995).

[80] JCGM 200:2008 (Ed. 3) International Vocabulary of Metrology - Basic and general concepts and associated terms.

[81] IEC 60904-4 2009 Photovoltaic devices - Part 4: Reference solar devices — Procedures for establishing calibration traceability.

[82] H. Mullejans, W. Zaaiman and R. Galleano, "Analysis and mitigation of measurement uncertainties in the traceability chain for the calibration of photovoltaic devices," *Meas. Sci. Technol.,* vol. 20, 2009.

[83] K. A. Emery, C. R. Osterwald and C. V. Wells, "Uncertainty analysis of photovoltaic efficiency measurements," in *Conference Record of the Nineteenth IEEE Photovoltaic Specialists Conference,* New Orleans, USA, 1987, pp. 9.

[84] K. Emery, "Photovoltaic efficiency measurements," in *Proceedings of the SPIE:The International Society for Optical Engineering,* 2004, pp. 36-44.

[85] W. Herrmann, "Leistungscharacterisierung und vergleichbarkeit von messergebnissen," in *6. Workshop Photovoltaische Modultechnik,* 2009, .

[86] Kipp & Zonen. SP-lite silicon detector pyranometer. *2010(08/10),* Available: http://www.kippzonen.com/; http://www.kippzonen.com/?product/991/SP+Lite2.aspx.

[87] StellarNet Inc. Stellarnet EPP2000 spectroradiometer. *2010(08/11),* Available: http://www.stellarnet-inc.com/; http://www.stellarnet-inc.com/products_spectrometers_EPP2000HR.htm;.

[88] OSRAM GmbH. Osram ministar halogen light bulb. *2007(03/15),* Available: www.osram.com; http://www.osram.com/products/general/tungsten/contest/facts_figures.html.

[89] Kipp & Zonen. CMP11 thermopile pyranometer. *2010(08/10),* Available: http://www.kippzonen.com/; http://www.kippzonen.com/?product/1371/CMP+11.aspx.

[90] IEC 60904-1 2006 Photovoltaic devices - Part 1: Measurement of photovoltaic current-voltage characteristics.

[91] H. Field and K. Emery, "An uncertainty analysis of the spectral correction factor," in *Photovoltaic Specialists Conference, 1993., Conference Record of the Twenty Third IEEE,* 1993, pp. 1180-1187.

[92] J. L. Balenzategui and F. Chenlo, "Measurement and analysis of angular response of bare and encapsulated silicon solar cells," *Solar Energy Mater. Solar Cells,* vol. 86, pp. 53-83, 2/15, 2005.

[93] R. Haselhuhn, "Modultests aus anwendersicht," in *6. Workshop Photovoltaische Modultechnik,* 2009, .

[94] S. H. Jang and M. W. Shin, "Fabrication and thermal optimization of LED solar cell simulator," *Current Applied Physics,* vol. 10, pp. S537-S539, 5, 2010.

[95] F. C. Krebs, K. O. Sylvester-Hvid and M. Jørgensen, "A self-calibrating led-based solar test platform," *Prog Photovoltaics Res Appl,* vol. 9999, 2010.

[96] Strama MPS GmbH, "Sun simulator for PV modules with integrated annealing function," vol. 2010, .

[97] A. Böttcher, A. Prorok, N. Ferretti, A. Preiss, S. Krauter and P. Grunow, "Flasher tolerances of power measurement on micromorph tandem modules," in *Proceedings of the 25th European Photovoltaic Solar Energy Conference and Exhibition / 5th World Conference on Photovoltaic Energy Conversion,* Valencia, Spain, 2010, pp. 3161-3164.

[98] T. Swonke and U. Hoyer, "Concept for a real AM1.5 simulator based on LED-technology and survey on different types of solar simulators," in *Proceedings of the 24th European Photovoltaic Solar Energy Conference,* Hamburg, Germany, 2009, pp. 3377-3379.

[99] SPIRE Corporation, "Press release: Spire Receives DOE Grant to Develop LED Based Solar Simulator," vol. 2010, 2010.

[100] R. Gottschalg, "Personal discussion on solar simulator calibration in production lines," 2010.

[101] IEC 60904-10 2009 Photovoltaic devices - Part 10: Methods of linearity measurement.

[102] K. Heidler and B. Muller-Bierl, "Measurement of multi-junction solar cells," in *Proceedings of the 10th European Photovoltaic Solar Energy Conference,* Lisbon, Portugal, 1991, pp. 111 - 114.

[103] K. Emery, C. R. Osterwald, T. Glatfelter, J. Burdick and G. Virshup, "A comparison of the errors in determining the conversion efficiency of multijunction solar cells by various methods," *Solar Cells,* vol. 24, pp. 371-380, 8, 1988.

[104] R. Shimokawa, F. Nagamine, M. Nakata, K. Fujisawa and Y. Hamakawa, "Supplementary-Light Method for Measuring the Conversion Efficiency of Multijunction Solar Cells," *Japanese Journal of Applied Physics,* vol. 28, pp. 845-848, 1989.

[105] T. Glatfelter and J. Burdick, "A method for determining the conversion efficiency of multiple-cell photovoltaic devices," in *Photovoltaic Specialists Conference, 1987., Conference Record of the Nineteens IEEE,* New Orleans, Louisiana, 1987, pp. 1187 - 1193.

[106] K. Heidler, A. Schonecker, B. Muller-Bierl and K. Bucher, "Progress in the measurement of multi-junction devices at ISE [solar cell testing]," in *Photovoltaic Specialists Conference, 1991., Conference Record of the Twenty Second IEEE,* 1991, pp. 430-435 vol.1.

[107] M. Meusel, R. Adelhelm, F. Dimroth, A. W. Bett and W. Warta, "Spectral Mismatch Correction and Spectrometric Characterization of Monolithic III-V Multi-junction Solar Cells," *PROGRESS IN PHOTOVOLTAICS,* vol. 10;, pp. 243-256, 2002.

[108] E. F. Zalewski and J. Geist, "Solar cell spectral response characterization," *Appl. Opt.,* vol. 18, pp. 3942-3947, 1979.

[109] O. S. Sastry, A. K. Mukerjee and K. L. Chopra, "Spectral response inhomogeneities in large-area solar cells," *Solid-State Electronics,* vol. 28, pp. 579-585, 6, 1985.

[110] Y. Hishikawa, Y. Tsuno and K. Kurokawa, "Spectral response measurement of PV modules and multi-junction devices," in *Proceedings of the 22th European Photovoltaic Solar Energy Conference,* Milan, Italy, 2007, .

[111] J. Sutterlüti, S. Janki, A. Hügli, J. Meier and F. P. Baumgartner, "Mapping of the local spectral photocurrent of monolithic series connected a-si:H P-I-N thin film solar modules," in *Proceedings of the 21th European Photovoltaic Solar Energy Conference,* Dresden, Germany, 2006, pp. 1749-1752.

[112] P. R. Beljean, J. Roux, Y. Pelet, C. Droz, N. Peguiron and V. Fakhfouri, "Module spectral response measurements using large area flashers," in *Proceedings of the 25th European Photovoltaic Solar Energy Conference and Exhibition / 5th World Conference on Photovoltaic Energy Conversion,* Valencia, Spain, 2010, pp. 4212 - 4214.

[113] IEC 60904-8 1998 photovoltaic devices - part 8: Measurement of spectral response of a photovoltaic (PV) device.

[114] J. Cárabe, "A new approach to measuring spectral responses of non-linear solar cells," *Solar Cells,* vol. 31, pp. 39-46, 2, 1991.

[115] J. S. Hartman and M. A. Lind, "Spectral response measurements for solar cells," *Solar Cells,* vol. 7, pp. 147-157, 11, 1982.

[116] K. Bucher and A. Schonecker, "Spectral response measurements of multi-junction solar cells with a grating monochromator and a fourier spectrometer," in *Proceedings of the Tenth E.C. Photovoltaic Solar Energy Conference,* Lisabon, Potugal, 1991, pp. 107-110.

[117] C. J. Hibberd, M. Bliss, H. M. Upadhyaya and R. Gottschalg, "Characterisation of a filter-based external quantum efficiency measurement system," in *Proceedings of the 5th Photovoltaic Science Application and Technology Conference (PVSAT-5),* Wrexham, UK, 2009, pp. 239 - 242.

[118] Y. Tsuno, K. Kamisako and K. Kurokawa, "New generation of PV module rating by LED solar simulator - A novel approach and its capabilities," in *Photovoltaic Specialists Conference, 2008. PVSC '08. 33rd IEEE,* 2008, pp. 1-5.

[119] C. J. Hibberd, F. Plyta, C. Monokroussos, M. Bliss, T. R. Betts and R. Gottschalg, "Voltage-dependent quantum efficiency measurements of amorphous silicon multi-junction mini-modules," *Solar Energy Mater. Solar Cells,* vol. In Press, Corrected Proof, .

[120] J. Bruns, S. Gall and H. G. Wagemann, "On the bias dependent spectral characteristics of a-Si:H solar cells," *J. Non Cryst. Solids,* vol. 137-138, pp. 1193-1196, 1991.

[121] D. W. Marquardt, "An Algorithm for Least-Squares Estimation of Nonlinear Parameters," *SIAM J Appl Math,* vol. 11, pp. 431-441, June 1963, 1963.

[122] W. H. Press, S. A. Teukolsky, W. T. Vetterling and B. P. Flannery, "Numerical recipes in C: The art of scientific computing," in Anonymous New York, NY, USA: Cambridge University Press, 1992, pp. 683-688.

[123] H. Schade and Z. E. Smith, "Optical-Properties and Quantum Efficiency of a-SI1-xCx-H/a-SI-H Solar Cells," *J. Appl. Phys.,* vol. 57, pp. 568-574, 1985.

[124] S. Nann and K. Emery, "Spectral effects on PV-device rating," *Solar Energy Mater. Solar Cells,* vol. 27, pp. 189-216, 8, 1992.

[125] G. Friesen, S. Dittmann, S. Williams, R. Gottschalg, H. G. Beyer, A. Guérin de Montgareuil, N. J. C. M. Van Der Borg, A. R. Burgers, R. P. Kenny, T. Huld, B. Müller, C. Reise, J. Kurnik and M. Topic, "Intercomparison of different energy prediction methods within the european project "performance" - results on the 2nd round robin," in *Proceedings of the 24th European Photovoltaic Solar Energy Conference,* Hamburg, Germany, 2009, pp. 3189-3197.

[126] R. Gottschalg, J. del Cueto, T. R. Betts, S. R. Williams and D. G. Infield, "Investigating the seasonal performance of amorphous silicon single- and multi-junction modules," in *Proceedings of the 3rd World Conference on Photovoltaic Energy Conversion,* Osaka, Japan, 2003, pp. 2078 - 2081.

[127] T. Minemoto, M. Toda, S. Nagae, M. Gotoh, A. Nakajima, K. Yamamoto, H. Takakura and Y. Hamakawa, "Effect of spectral irradiance distribution on the outdoor performance of amorphous Si//thin-film crystalline Si stacked photovoltaic modules," *Solar Energy Mater. Solar Cells,* vol. 91, pp. 120-122, 1/23, 2007.

[128] G. Friesen, R. Gottschalg, H. G. Beyer, S. Williams, A. Guerin de Montgareuil, N. van der Borg, W. G. J. H. M. van Sark, T. Huld, B. Müller, A. C. de Keizer and Y. Niu, "Intercomparison of different energy prediction methods within the european project "performance" - results on the 1st round robin," in *Proceedings of the 22th European Photovoltaic Solar Energy Conference,* Milan, Italy, 2007, .

[129] R. P. Kenny, T. A. Huld and S. Iglesias, "Energy rating of PV modules an PVGIS irradiance and temperature database," in *Proceedings of the 21st European Photovoltaic Solar Energy Conference,* Dresden, Germany, 2006, pp. 2088-2092.

[130] R. Kröni, S. Stettler, G. Friesen, D. Chianese, R. Kenny and W. Durisch, "Energy rating of solar modules," Swiss Federal Office of Energy SFOE, 2005.

[131] R. P. Kenny, G. Friesen, D. Chianese, A. Bernasconi and E. D. Dunlop, "Energy rating of PV modules: Comparison of methods and approach," in *Photovoltaic Energy Conversion, 2003. Proceedings of 3rd World Conference on,* 2003, pp. 2015-2018.

[132] M. B. Strobel, T. R. Betts, G. Friesen, H. G. Beyer and R. Gottschalg, "Uncertainty in Photovoltaic performance parameters – dependence on location and material," *Solar Energy Mater. Solar Cells,* vol. 93, pp. 1124-1128, 6, 2009.

[133] Y. Hishikawa, "Characterization of the Silicon-Based Thin Film Multi-Junction Solar Cells," *Proceedings Volume 862 Amorphous and Nanocrystalline Silicon Science and Technology—2005,* vol. 862, pp. 579-590, 2005.

[134] A. Nakajima, M. Goto, H. Takata, M. Yoshimi, K. Yamamoto, T. Suezaki, Y. Tawada, T. Meguro, M. Ichikawa, S. Fukuda, K. Hayashi and T. Sawada, "Improvement on actual output power of thin film silicon hybrid module," in *Proceddings of the 3rd World Conference on Photovoltaic Energy Conversion,* Osaka, Japan, 2003, pp. 1915-1918.

[135] C. A. Gueymard, "Parameterized transmittance model for direct beam and circumsolar spectral irradiance," *Solar Energy,* vol. 71, pp. 325-346, 11, 2001.

[136] M. Zehner, M. Hartmann, J. Weizenbeck, T. Gratzl, T. Weigl, B. Mayer, G. Wirth, M. Krawczynski, T. R. Betts, R. Gottschalg, A. Hammer, B. Giesler, G. Becker and O. Mayer, "Systematic analysis of meteorological irradiation effects," in *Proceedings of the 25th European Photovoltaic Solar Energy Conference / 5th World Conference on Photovoltaic Energy Conversion,* Valencia, Spain, 2010, pp. 4545-4548.

[137] K. Emery, S. Winter, S. Pinegar and D. Nalley, "Linearity testing of photovoltaic cells," in *Photovoltaic Energy Conversion, Conference Record of the 2006 IEEE 4th World Conference on,* 2006, pp. 2177-2180.

[138] R. P. Kenny, A. Ioannides, H. Müllejans, W. Zaaiman and E. D. Dunlop, "Performance of thin film PV modules," *Thin Solid Films,* vol. 511-512, pp. 663-672, 7/26, 2006.

[139] A. H. Fanney, M. W. Davis, B. P. Dougherty, D. L. King, W. E. Boyson and J. A. Kratochvil, "Comparison of photovoltaic module performance measurements," *J. Sol. Energy Eng.,* pp. 152-159, 2006.

[140] C. Monokroussos, M. Bliss, Y. N. Qiu, C. J. Hibberd, T. R. Betts, A. N. Tiwari and R. Gottschalg, "Effects of spectrum on the power rating of amorphous silicon photovoltaic devices," *Prog Photovoltaics Res Appl,* pp. published online, 2011.

[141] J. A. Eikelboom and M. J. Jansen. (2000, Characterisation of PV modules of new generations - results of tests and simulations. The Netherlands Energy Research Foundation.

[142] M. Topic, K. Brecl and J. Sites, "Effective efficiency of PV modules under field conditions," *Progress in Photovoltaics: Research and Applications,* vol. 15, pp. 19-26, 2007.

[143] H. Müllejans, H. Bossong and E. D. Dunlop, "Temperature and bias light dependence of spectral response measurements," in *Proceedings of the PV in Europe Conference,* Rome, Italy, 2002, pp. 891-894.

[144] D. E. Carlson, G. Lin and G. Ganguly, "Temperature dependence of amorphous silicon solar cell PV parameters," in *Photovoltaic Specialists Conference, 2000. Conference Record of the Twenty-Eighth IEEE,* 2000, pp. 707-712.

Appendices

Appendix A: LED colour distribution of main centre array

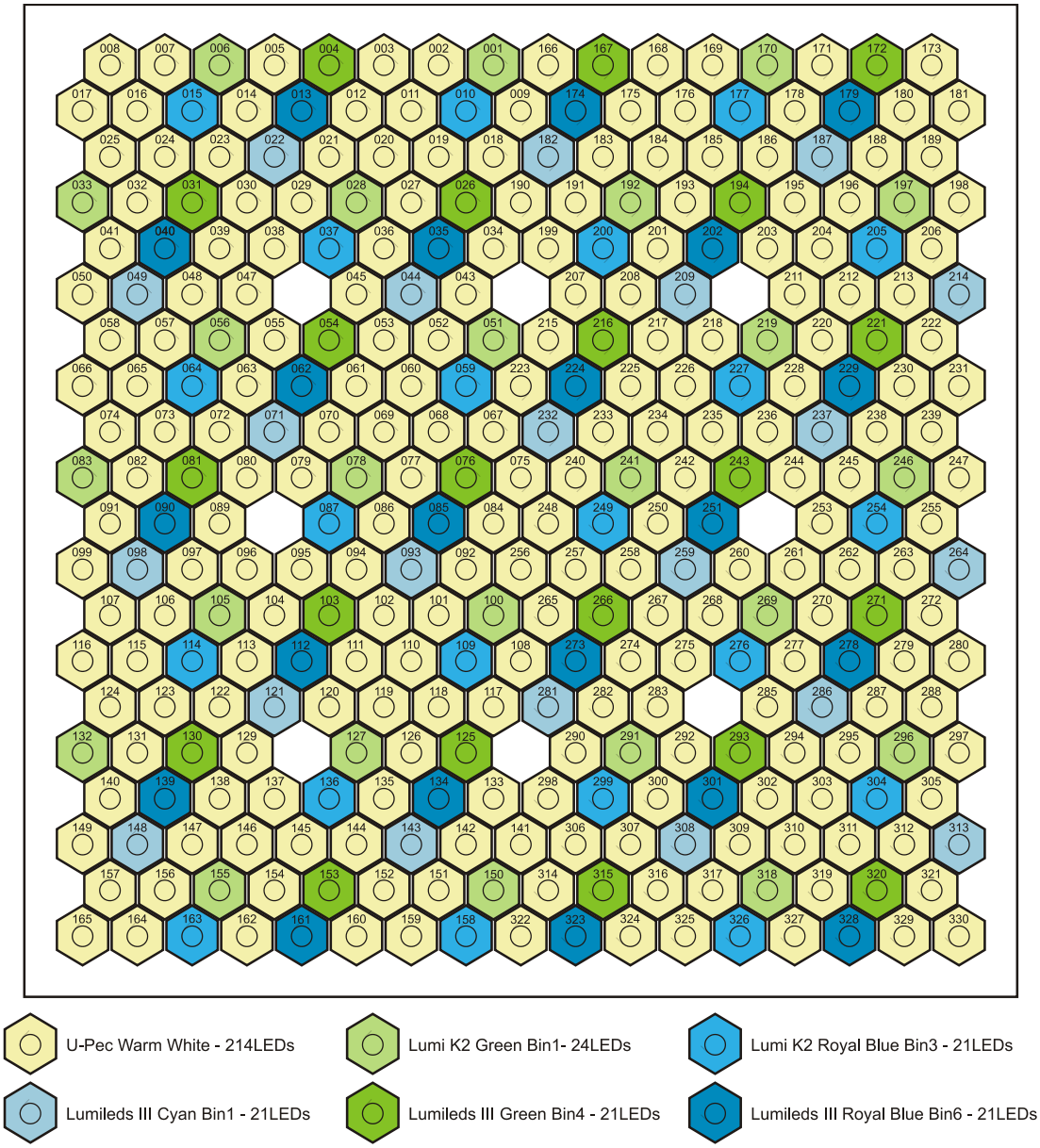

Appendix B: Printed circuit board (PCB) layout of main centre array

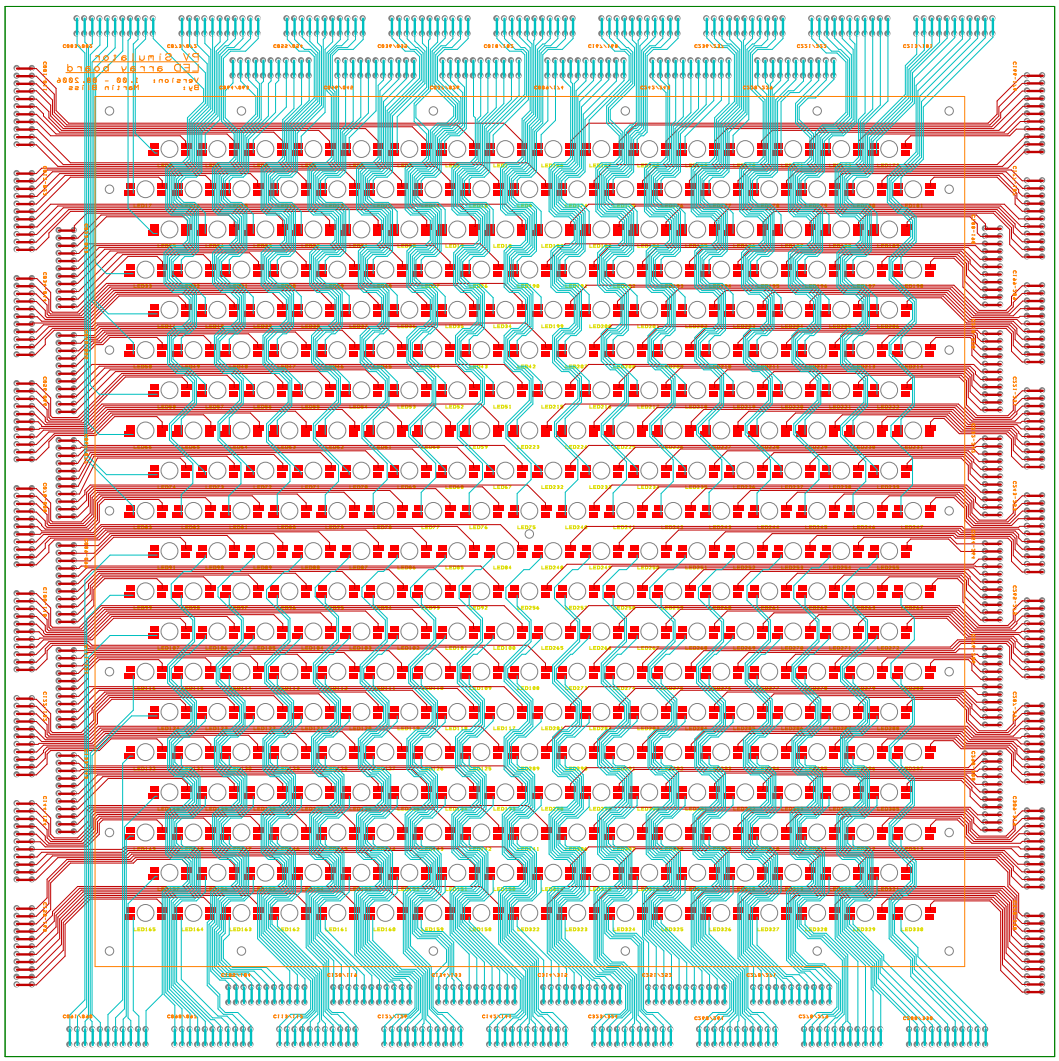

Top silk screen

Top copper

Top and bottom pin pads

Bottom silk screen

Bottom copper

Appendix C: Light source mounting structure on side array

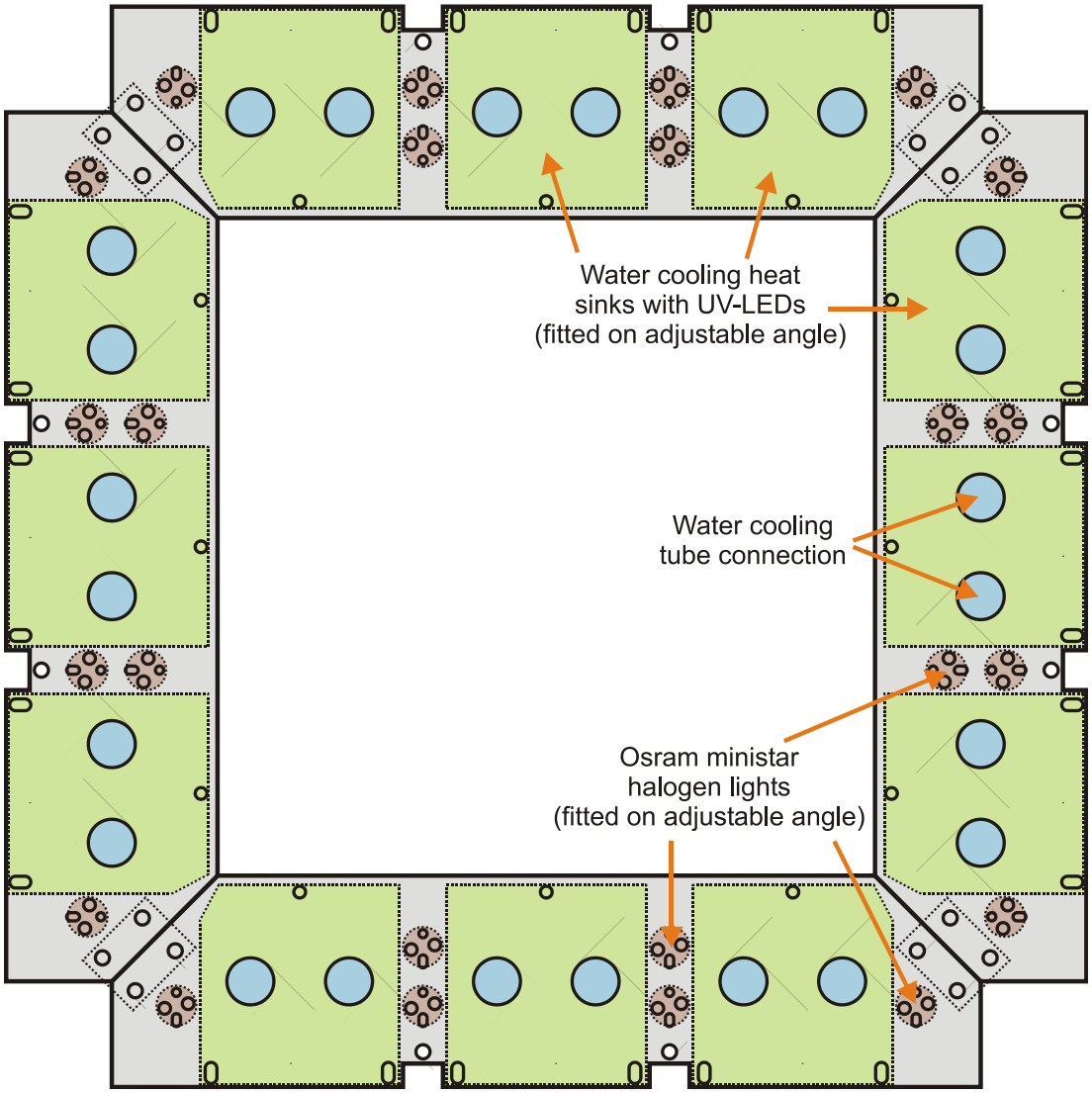

Appendix D: Circuit diagram of the DC power cut-off board

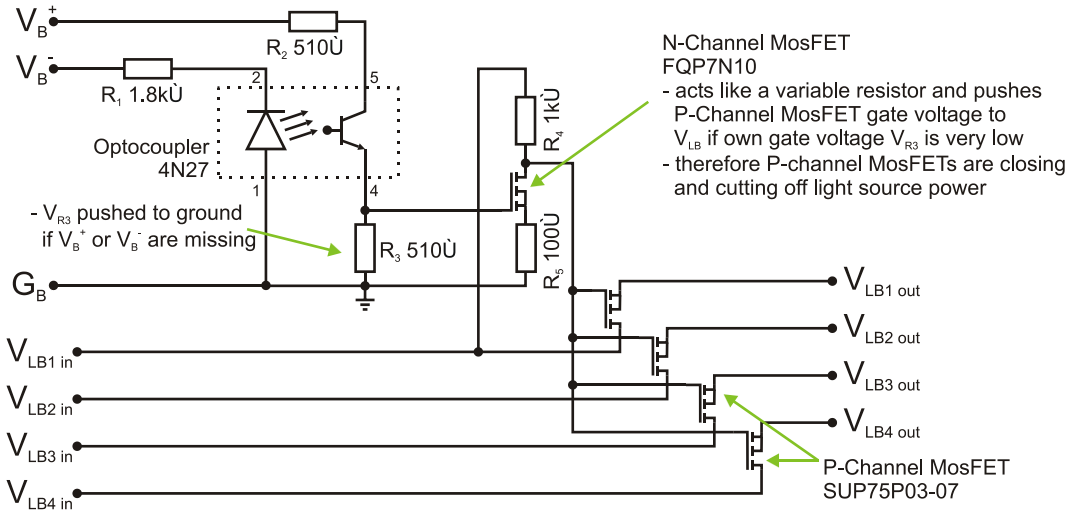

$V_{LBn\ in}$ - light source or relay power input (from power supplys;12V / 24V)
$V_{LBn\ out}$ - light source or relay power output (to current regulation board)
V_B - amplifier power supply sense (from current regulation board; +15V / -15V)

Appendix E: Circuit diagram of main light source control board

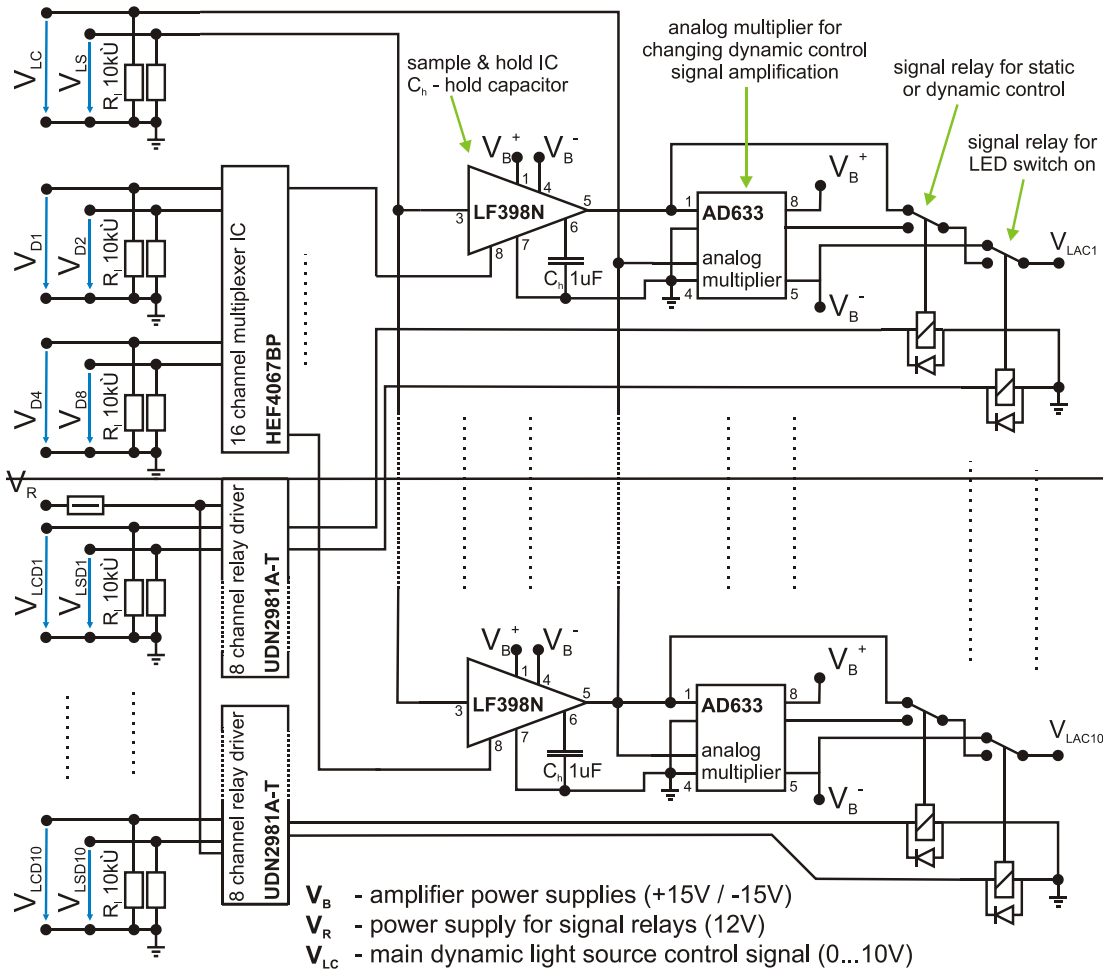

V_B - amplifier power supplies (+15V / -15V)
V_R - power supply for signal relays (12V)
V_{LC} - main dynamic light source control signal (0...10V)
V_{LS} - static control and dynamic amplification signal (0...10V)
V_{Dn} - digital static and dynamic amplification setting control lines
V_{LCDn} - digital light source on/off control
V_{LSDn} - digital light source static/dynamic control
V_{LACn} - analog light source current control signal (0...10V)

Appendix F: Circuit diagram of light source current control board

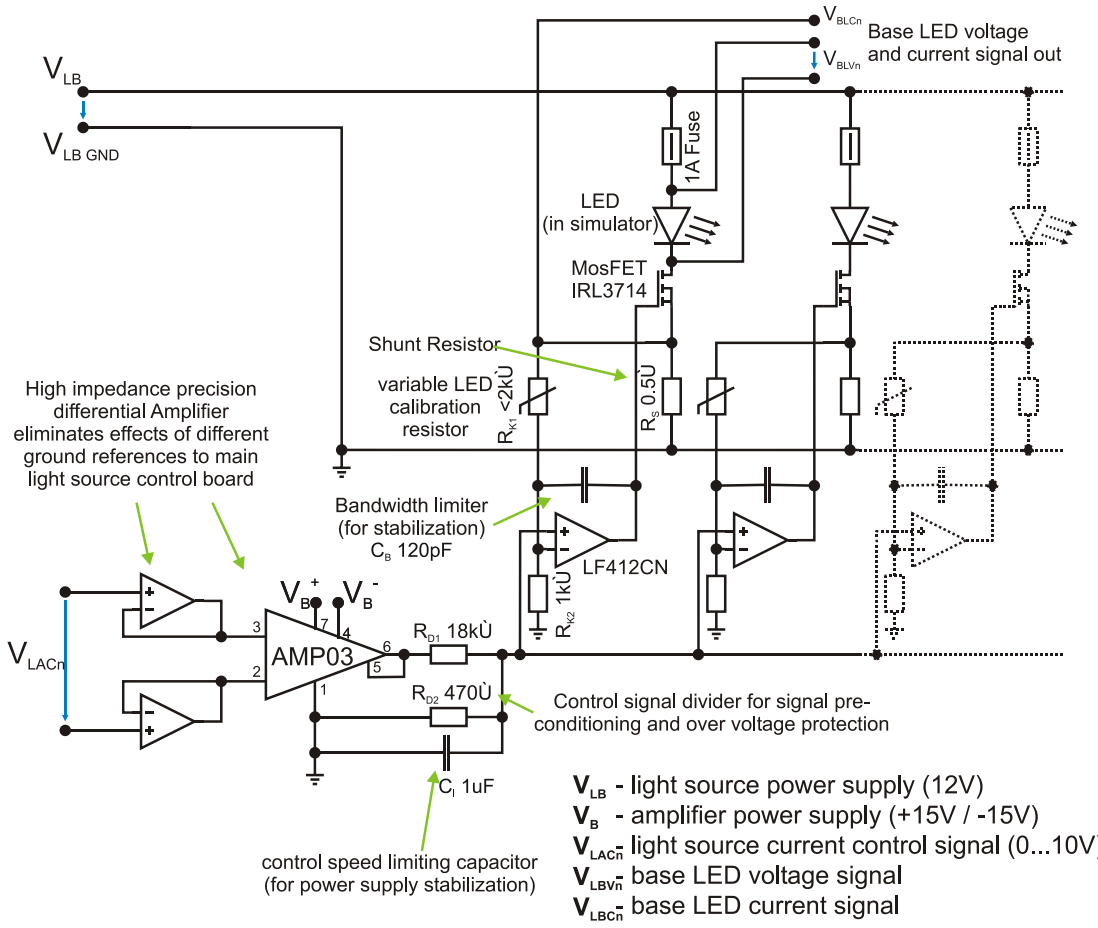

Appendix G: Simplified schematic of the custom build I-V tracer

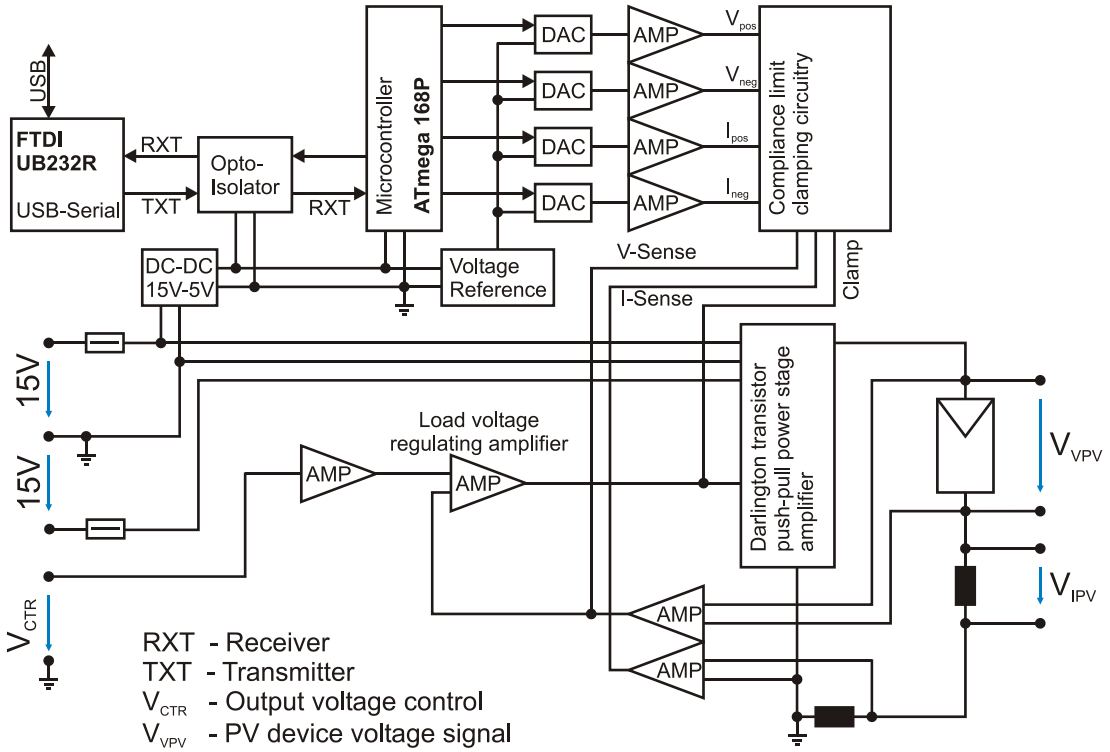

RXT - Receiver
TXT - Transmitter
V_{CTR} - Output voltage control
V_{VPV} - PV device voltage signal
V_{IPV} - PV device current signal
V_{pos} - Positive voltage compliance
V_{neg} - Negative voltage compliance
I_{pos} - Positive current compliance
I_{neg} - Negative current compliance

Appendix H: Simplified schematic of the peltier temperature controller

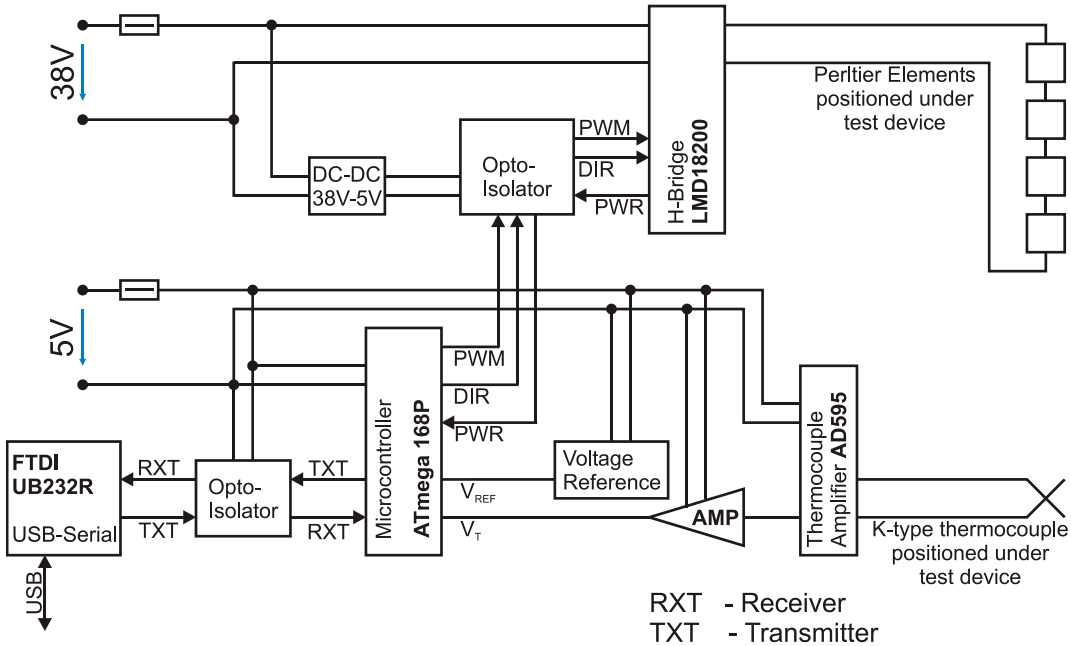

RXT - Receiver
TXT - Transmitter
PWR - Power OK flag
DIR - Heating Cooling control
PWM - Pulse width modulation
V_{REF} - Reference Voltage for ADC
V_T - Temperature signal

Appendix I: Circuit diagram of the power distribution unit

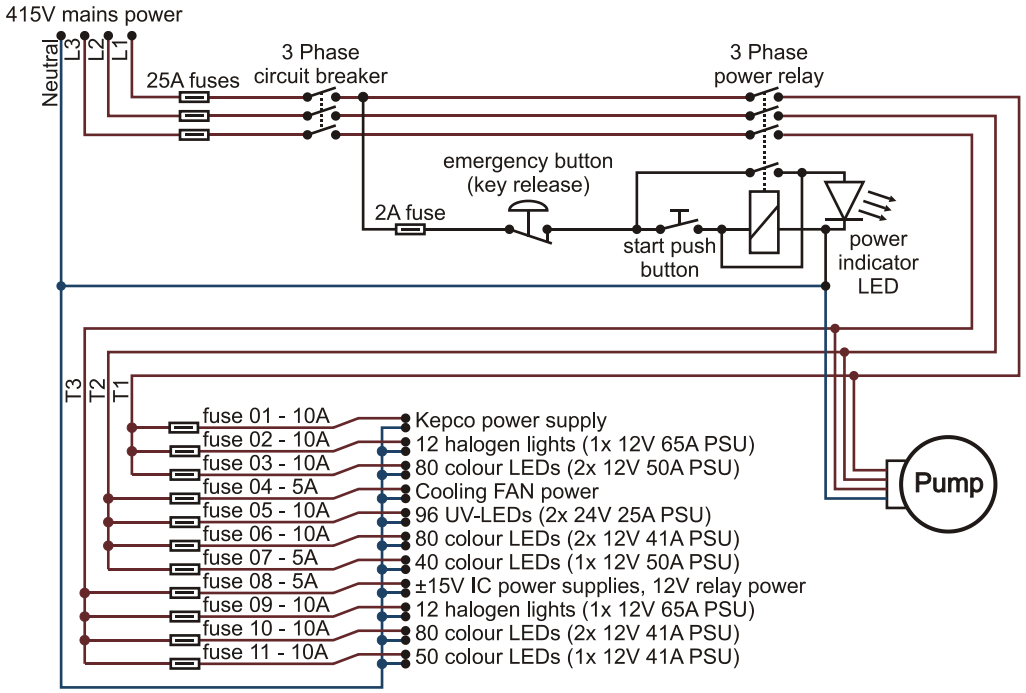

Appendix J: Circuit diagram of main power control board

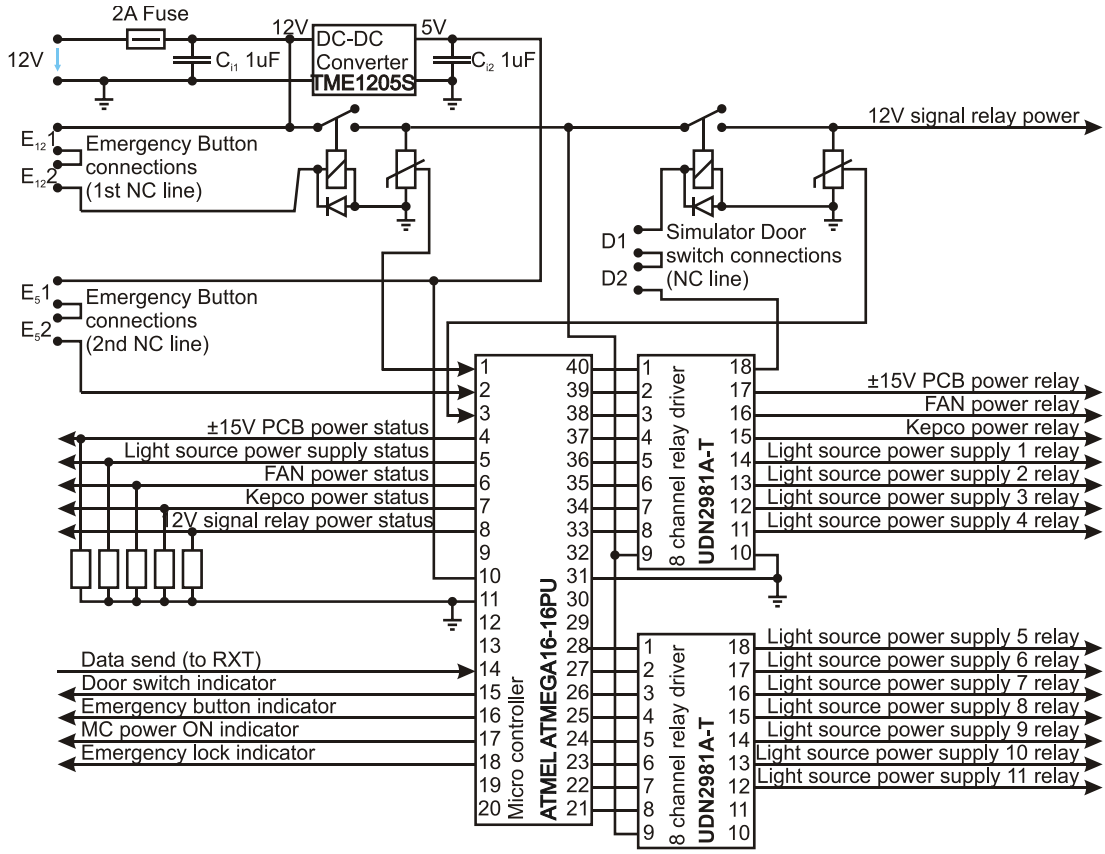

Appendix K: Input and output terminals from DAQ cards

NI 6120 S-series DAQ card I/O configuration:

Terminal	Channel	Input / Output signal usage
AI	0	PV device voltage
AI	1	PV device current
AI	2	Irradiance sensor 1
AI	3	Irradiance sensor 2
AO	0	Main dynamic light source control
AO	1	I-V tracer output control
DI	P0.0	Kepco current limit flag
DI	P0.1	Kepco voltage limit flag
DI	P0.2	Kepco current mode flag
DI	P0.3	Kepco voltage mode flag
DI	P0.4	Kepco tracing mode control
Digital Trigger	PFI 2	Measurement trigger input
Counter Out	CTR 0	Measurement timing output

NI6229 M-series DAQ card I/O configuration:

Terminal	Channel	Input / Output signal usage
AI	0	water temperature sensor ingoing
AI	8	water temperature sensor outgoing
AI	1	PV device temperature
AI	9	PV device cooling block
AI	2 – 10	LED array heat sink temperature sensor
AI	3 – 11	UV LED heat sink temperature sensor
AI	4 – 12	Simulator air temperature sensor
AI	5 – 13	Rack temperature sensor 1 (Top)
AI	6 – 14	Rack temperature sensor 2 (Bottom)
AI	7 – 15	Base light source 1 - halogen
AI	16 – 24	Base light source 2 - warm white
AI	17 – 25	Base light source 3 - UV at 375nm
AI	18 – 26	Base light source 9 - green at 545nm
AI	19 – 27	Base light source 5 - royal blue at 440nm
AI	20 – 28	Base light source 6 - royal blue at 460nm
AI	21 – 29	Base light source 7 - cyan at 490nm
AI	22 – 30	Base light source 8 - green at 520nm
AI	23 – 31	Base light source 4 - UV at 395nm
AO	2	Light source static output control
DI	P0.00	Kepco power status
DI	P0.01	±15V amplifier power status
DI	P0.02	Light source power supply status
DI	P0.03	Fan power status
DI	P0.04	12V signal relay power status
DO	P0.05	PCU serial power control line
DI	P0.06	Simulator door status
DI	P0.07	Emergency button status
DO	P0.08	Sample and hold signal set D1
DO	P0.09	Sample and hold signal set D2
DO	P0.10	Sample and hold signal set D4
DO	P0.11	Sample and hold signal set D8
DO	P0.12	Light source control signal route T1
DO	P0.13	Light source control signal on/off T1
DO	P0.14	Light source control signal route T2

DO	P0.15	Light source control signal on/off T2
DO	P0.16	Light source control route T3
DO	P0.17	Light source control on/off T3
DO	P0.18	Light source control route T4
DO	P0.19	Light source control on/off T4
DO	P0.20	Light source control route T5
DO	P0.21	Light source control on/off T5
DO	P0.22	Light source control route T6
DO	P0.23	Light source control on/off T6
DO	P0.24	Light source control route T7
DO	P0.25	Light source control on/off T7
DO	P0.26	Light source control route T8
DO	P0.27	Light source control on/off T8
DO	P0.28	Light source control route T9
DO	P0.29	Light source control on/off T9
DO	P0.30	Light source control route T10
DO	P0.31	Light source control on/off T10
DI	P1.00	PCU MC power indicator
DI	P1.01	Emergency lock indicator
CTR	PFI 12	Water flow sensor